
The University of Manchester


# DEVELOPMENT OF POLYHIPE CHROMATOGRAPHY AND LANTHANIDE-DOPED LATEX PARTICLES FOR USE IN THE ANALYSIS OF ENGINEERED NANOPARTICLES

A thesis submitted to

**The University of Manchester**

for the degree of

**Doctor of Philosophy**

in the

**Faculty of Engineering and Physical Sciences**

**2013**

**Jonathan Mark Hughes**

**School of Chemistry**

**Table of Contents**

Total Number of Pages 274

Total Word Count 68,066

## List of Figures

## List of Tables

**List of Abbreviations**

| | |
|---|---|
| AUC | Analytical Ultracentrifugation |
| BADE | bisphenol A diglycidyl ether |
| BET | Bruneaur-Emmett-Teller |
| BMA | benzyl methacrylatre |
| BuA | butyl acrylate |
| BuMA | butyl metacrylate |
| CCD | Charged Couple Device |
| CLSM | Confocal Laser Scanning Microscopy |
| DLS | Dynamic Light Scattering |
| DMAEMA | 2-(dimethylamino) ethyl methacrylate |
| DSC | Differential sedimentation Centrigugation |
| DVB | Divinylbenzene |
| EDX | Energy dispersive X-ray spectroscopy |
| EELS | electron energy loss spectroscopy |
| EGDMA | ethyleneglycol dimethacrylate |
| ESEM | Enviromental scanning electron microscopy |
| FFT | Fast Fourier Trasnform |
| GMA | glycidyl methacrylate |
| GPC | Gel Permeation Chromatography |
| HDPE | High density polyethylene |
| HEMA | 2-hydroxyethyl methacrylate |
| HIPE(s) | High Internal Phase Emulsion(s) |
| HLB | Hydrophillic-Lippophillic Balence |
| HPLC | High Presurse Liquid Chromatography |
| HPMA | 2-hydroxypropyl methacrylate |
| i.d. | internal diameter |
| ICP-MS | inductively coupled plasma mass spectrometry |
| KPS | potassium persulphate |
| LIBD | Laser-induced breakdown detection Spectroscopy |
| MIP | mercuray intersion propsymetry |
| MWCO | Molecular Weight Cut-Off |
| NSOM | Near-field Scanning Optical Microscopy |

| | |
|---|---|
| Np(s) | Nanoparticle(s) |
| NTA | Nanoparticle Tracking Analysis |
| PCL | polycapralactone |
| PIT | Phase Inversion Temperature |
| PNP(s) | polymer nanoparticle(s) |
| SAED | Selected Area Electron Diffraction |
| SANS | Small Angle Neutron Scatting |
| SAXS | Small Angle X-ray Scattering |
| SEM | Scanning Electron Microscopy |
| SLS | Static Light Scattering |
| SPM | Scanning Probe Microsocpy |
| STEM | Scanning Transmission electron Microscopy |
| TCE | Trichloroethane |
| TEA | Triethylamine |
| TEM | Transmission electron Microscopy |
| TEOS | Tetra Ethyl Orthosilicate |
| XRD | X-ray diffraction |
| XRM | X-ray microscopy |
| HDC | hydrodynamic chromatography |
| SEC | size exclusuion chromtography |

**ABSTRACT**

The aims of this thesis were twofold: A) To use high internal phase emulsion (HIPE) templated materials to produce a chromatographic stationary phase for the size separation of engendered nanoparticles (NPs). B) To produce well characterised lanthanide doped polymer NPs with a potential use as analytical standards.

Initially, silica materials were prepared from oil-in-water HIPEs by a two stage acid/base catalysed sol gel process. As well as presenting the expected macroporosity typical of HIPE templated materials, it was also found that micro- and meso-porosity could be influenced by surfactant choice and reaction with iron (III) chloride or copper (I) chloride which had been included in the HIPE. However, the resulting silica materials were deemed inappropriate for the desired chromatography.

Monolithic columns were prepared from HIPE templated polymers (polyHIPEs) and incorporated into a HPLC system. Poly(styrene-co-divinylbenzene) and poly(ethylene-glycol dimethacrylate) polyHIPE columns were able to separate sub-micron polystyrene latexes, detected by UV absorption, and dysprosium doped polystyrene latex particles and gold nanoparticles detected by inductively coupled plasma mass spectrometry (ICP-MS).

Dysprosium, gadolinium and neodymium doped polystyrene NPs were prepared by micro-emulsion polymerisation. Particle size was controlled (over a 40 – 160 nm range) by tailoring of surfactant and initiator concentrations. Particles were characterised by dynamic light scattering, differential centrifugal sedimentation, transition electron microscopy and hydrodynamic chromatography (HDC)-ICP-MS. Also, particle surface change, lanthanide content and solids content were analysed. The latter two appear related to particle size.

As far as the author is aware there are no cases of the use of polyHIPE columns size separation in the literature. Nor are there any cases of encapsulation of metals within polymer nanoparticles by micro-emulsion polymerisation reported.

## DECLARATION

No portion of the work referred to in this thesis has been submitted in support of an application for another degree or qualification at this or any other university or other institute of learning.

## COPYRIGHT STATEMENT

**i.** The author of this thesis (including any appendices and/or schedules to this thesis) owns certain copyright or related rights in it (the "Copyright") and s/he has given The University of Manchester certain rights to use such Copyright, including for administrative purposes.

**ii.** Copies of this thesis, either in full or in extracts and whether in hard or electronic copy, may be made **only** in accordance with the Copyright, Designs and Patents Act 1988 (as amended) and regulations issued under it or, where appropriate, in accordance with licensing agreements which the University has from time to time. This page must form part of any such copies made.

**iii.** The ownership of certain Copyright, patents, designs, trademarks and other intellectual property (the "Intellectual Property") and any reproductions of copyright works in the thesis, for example graphs and tables ("Reproductions"), which may be described in this thesis, may not be owned by the author and may be owned by third parties. Such Intellectual Property and Reproductions cannot and must not be made available for use without the prior written permission of the owner(s) of the relevant Intellectual Property and/or Reproductions.

**iv.** Further information on the conditions under which disclosure, publication and commercialisation of this thesis, the Copyright and any Intellectual Property and/or Reproductions described in it may take place is available in the University IP Policy (see http://documents.manchester.ac.uk/DocuInfo.aspx?DocID=487), in any relevant Thesis restriction declarations deposited in the University Library, The University Library's regulations (see http://www.manchester.ac.uk/library/aboutus/regulations) and in The University's policy on Presentation of Theses

**Acknowledgements**

As well as thanking both fera and the EPSRC for funding I would like to express my gratitude to the following people:

- Prof. Peter Budd (University of Manchester, UoM) and Dr. John Lewis (fera), for their supervision, advice and support during this work.
- Dr. Paul Christian (UoM) and Dr. Karen Tiede (fera) for their support as my initial supervisors and for putting together the project in the first place.
- Agnieszka Dudkiewicz (fera/ University of York) for some helpful and enlightening discussions
- Dr. Pranab Dutta (fera) for his help in collecting the DSC data.
- Andrew Coffey (Agilent) of advice on chromatography.
- Kieth Nixon and Rhiana Sung (UoM) for their help in setting up the HPLC system.
- Sam Magee (UoM) for advice, support and supplying the lanthanide chlorides.
- Andrew Grieve and his colleagues in the fera trace metals team for giving instrument time of the ICP-MS and for collecting data of the lanthanide content of the latex particles. Along with numerous other members of fera for various advice
- Prof. Steve Yeates (UoM) for a helpful discussion in the nature of emulsions.
- Michael Faulkner for training of the SEM.
- Dr Nicole Hondow and Dr Zadeada Aslam from the University of Leeds for access to the LENIF facilities and acquiring the TEM images
- All the members of Prof. Budd's research group for multiple pieces of advice.
- All my family and friends who have supported me, particularly my parents Julie and Richard Hughes
- Last but by no means least Stephanie Duensing for her thorough and unyielding support.

# Chapter 1
# Introduction

## 1 Introduction Structure

This introduction will be split into 3 sections. Section 1 will briefly outline the aims and objectives of this thesis as a whole, more specific aims and objectives will be given at the start of each chapter. Section 2 will briefly outline some frequently used methods for the analysis and detection of nanoparticles (NPs) in aqueous media. A particular focus will be placed on the analytical techniques utilised in this work *i.e.*, dynamic light scattering (DLS), scanning and transmission electron microscopy (SEM and TEM), hydrodynamic chromatography (HDC) and differential centrifugal sedimentation (DCS). Finally, section 3 will cover some of the theory and concepts of emulsions, concluding with more specific detail on high internal phase emulsions (HIPEs), which will be used regularly for synthesis throughout this thesis.

## 1.1 Aims and Objectives

There were two primary aims for this thesis. The first aim was to produce a chromatographic column from HIPE templated materials capable of size separating

engineered nanoparticles in aqueous media. The second aim was to produce a series of highly monodisperse polymer nanoparticles, containing a low natural abundance element, over a 40 - 160 nm size range, with a potential use as analytical standards.

These aims were achieved by the following specific objectives:

With respect to the first overall aim:

1. HIPEs were used to produce a variety of materials, both silica and polymer, with a macroporous pore structure.
2. These materials were then characterised by various methods and assessed for their potential as a chromatographic stationary.
3. The most promising materials were prepared inside empty chromatography columns incorporated into a high pressure liquid chromatography (HPLC) system.
4. Commercially obtained latexes of a wide size range (100 nm, 460 nm and 800 nm) were then injected into an eluent flow through the columns.
5. The most promising HIPE templated materials from objective 4 were then further investigated for the ability to separate smaller particles (< 100 nm) which matches the European definition of nano,[1] *i.e.*, gold colloids of 5, 10 and 20 nm and polymer NPs. These polymer particles were produced to stratify the second primary aim.
6. The columns produced for objective 5 were attached to an inductively coupled mass spectrometer (ICP-MS), as an element specific detector, to allow elemental analysis of the particles.

With respect to the second overall aim:

1. A series of test particles were produced by micro-emulsion polymerisation of styrene to establish the synthetic parameters which would yield particles of the desired size.

2. The test particles were also doped with a chromium complex to establish the proof of principle that metal complexes could be encapsulated within particles by micro-emulsion polymerisation.
3. A series of particles were then produced using the conditions established by objective 1 and characterised by a variety of techniques. The particles were also doped with lanthanide complexes which, due to their low natural abundance, would act as markers in element specific detection techniques.

## 1.2 Nanoparticles (NPs)

When compared to the more established scientific disciplines, the areas of nanoscience and nanotechnology are young and still rapidly developing. However, the history of NP usage can be traced back nearly 2,400 years with the first instances of 'soluble' gold (what is now known to be colloidal gold) appearing in Egypt and China in the 4$^{th}$ century BCE. However, for the majority of the time that they have been utilised by humans it has been for aesthetic purposes, exploiting the optical properties of NPs *e.g.* dichroic glass.

The first scientific description of changes in material properties due to particle dimensions on the nanometre scale came in 1857 when Michael Faraday[2] reported the formation of red solutions of colloidal gold (though the term colloid was not coined until 1861 by Thomas Graham)[3] upon the reduction of tetrachloroaurate with phosphorous in carbon disulphide. Despite this long history of use, the true potential of nanoscience has only become understood within the last 50 years.

The term *nanotechnology* was first used in 1974 by Norio Taniguchi[4] to describe the manufacture of materials on the nanometre scale. However, it was not until the advent of new imaging techniques (such as scanning tunnelling microscopy in 1981 and atomic

force microscopy in 1986) that NPs, colloids and atomic clusters *etc.* could been seen and studied in detail. These new developments allowed considerable advances in the field of nanoscience such as the discovery of Buckminsterfullerene ($C_{60}$) in 1985.[5]

The proceeding 20 years have seen significant growth in scientific interest into nanotechnology and NPs leading to an increase in research output (Figure 1.1). The growth in scientific interest has also been mirrored in commercial interest in nanoscience. The global nanotechnology market being worth an estimated US $20.1 billion in 2011, with nanomaterials expected to have sales worth $37.3 billion in 2017 [6]

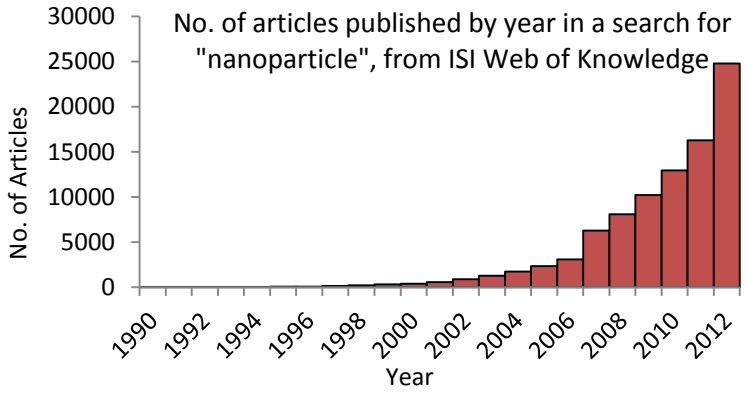


Figure 1.1: Graph showing the increased number of scientific articles published per year containing the topic "nanoparticle". Retrieved from ISI Web of Knowledge (http//www.*isiknowledge.com/*), search performed 26/6/2013.

Because of this relative youth and continued rapid development of the fields of nanoscience and nanotechnology, there is often a lack of full consensus on what constitutes a nanomaterial or NP, with a comprehensive definition yet to be universally adopted. In recent years efforts have been made to produce comprehensive definitions for the myriad aspects of nanoscience with various standardisation organizations such as ASTM International,[7] the British Standards Institution (BSI)[8] and the International Organization for Standardisation (ISO),[9] just to name a few, all developing definitions. The definition that is most commonly applied to nanomaterials is that they must have at least one dimension of $\leq$ 100 nanometres (nm), one nm being equal to $10^{-9}$ m. This is also the

current European legal definition.[1] With the increased scientific research and commercial use of NPs it is becoming increasingly important to be able to accurately detect and categorise engineered NPs.

### 1.2.1 Summary of Techniques for Analysis of Nanoparticles in Aquatic Environments.

The following section will look at analytical techniques that can be used for aqueous NP analysis. Broadly speaking, there are five main categories of analytical techniques for NP analysis.

1. Electromagnetic scattering methods
2. Microscopy methods
3. Centrifugation and filtration techniques
5. Spectroscopic methods
4. Chromatographic and related techniques

There are also several other techniques that do not fit into any of the above groups. However, as none of the techniques were used in this work they will not be covered here. Should more comprehensive summary be required, the reader is directed to reviews by Tiede *et al.*[10], Hasselhöv and Kaegi,[11] and more recently Bandyopadhyay *et al.*[12] and Zänker & Schierz,[13] all of which are referred to here.

#### 1.2.1.1 Electromagnetic (EM) Scattering Methods

##### 1.2.1.1.1 Dynamic Light Scattering

Dynamic light scattering (DLS), also known as photon correlation spectroscopy, is a widely used and useful technique for the sizing of engineered nanoparticles (ENPs) and

can provide fast, *in-situ*, real time sizing. It operates by the principle that a coherent laser will induce an oscillating electric dipole on the particle (provided that the particles are small compared to the wavelength) and this in turn will re-radiate light. Particles experiencing Brownian motion in a medium will be constantly changing position, thus the patterns of constructive and destructive interference will be constantly changing. This will lead to changes in scattering intensity as the particles move. Small particles, being more mobile, create greater changes in scattering intensity when compared to larger, less mobile particles. By measuring these changes over increments of nano- to micro-seconds and then autocorrelating to the initial measurement DLS can produce sizing information. The decay of the autocorrelation function is related to diffusion coefficient of the particles in the medium, by the following equation**:**

$$g^{(2)}(t) - 1 \approx Ae^{(-2q^2Dt)} \qquad \text{(Eq. 1.1)}$$

where: $g^2(t)-1$ is the correlation function,

$D$ is the diffusion coefficient,

$A$ is an instrument constant,

$q$ is the scattering form factor and

$t$ is time.

It is necessary for DLS to be carried out with a dilute sample so as to minimise the particle-particle interactions so the scattering of light can be attributed to the self-diffusion of the particles (their diffusion coefficient), which is itself related to particle hydrodynamic diameter via the Stokes-Einstein equation:[14]

$$d_H = \frac{k_B T}{3\pi\eta D} \qquad \text{(Eq. 1.2)}$$

where: $d_H$ is the hydrodynamic diameter,

$D$ the diffusion coefficient,

$k_B$ is the Boltzmann constant,

*T* is temperature and

$\eta$ is the viscosity of dispersion medium.

Because DLS measures intensity of scattered light and the efficiency of light scattering is dependent on particle size (proportional to $\boldsymbol{d_H^6}$, for particles of less than one-twentieth of the wavelength, and to $\boldsymbol{d_H^2}$ for larger particles) DLS will return an intensity weighted diffusion coefficient. This in turn leads to an intensity weighted z-average particle diameter ($\bar{D}_z$) which will be skewed to larger particle sizes. The z-average diameter is defined as follows:

$$\bar{D}_z = \sum_i n_i d_i^6 \Big/ \sum_i n_i d_i^5 \qquad \text{(Eq. 1. 3)}$$

This is a particular problem if the sample is polydisperse with respect to particle size or identity where more than one diffusion coefficient must be extracted from the autocorrelation leading to be inaccurate results.[15] While it is possible to convert the intensity weighted diameter to a volume or number weighted diameter by use of the Mie theory, this requires additional knowledge of the particles refractive index and density.[16]

Advantages of DLS include the non-destructive nature which leaves samples free for further analysis, the ease of use which has led to it being employed in the field,[17] and the speed of analysis which can allow monitoring of nanoparticle behaviour such as agglomeration[18] and conjugation.[19] The drawbacks include the assumption of spherical particles and unreliability for polydisperse samples (which is ubiquitous for natural samples).

#### 1.2.1.1.2 Static Classical Light Scattering (SLS)

Small particles ($d<\lambda/20$) scatter isotropically perpendicular to the polarization of the incident light. If $\lambda/20 < d < \lambda$, forward scattering is favoured with greater diameters

producing scattering of greater intensity. When $\lambda \approx d$, constructive or destructive interferences are observed at certain angles which relate to size. When $d > \lambda$, the angular dependency becomes complex, displaying minima and maxima and certain angles. By measuring the intensity of variations in the scattering of laser light over wide range of angles, SLS can calculate the molar mass, $M_w$, the second viral coefficient, $A_2$, and root mean squared radius of gyration,$< R_g^2 >$. For NP analysis $< R_g^2 >$ is the most relevant of these terms and relates how the mass of the particle is distributed from its centre of mass. The full scattering theory is complex and beyond the scope of this introduction, with thorough discussions available elsewhere.[20]

The advantages are much the same as DLS, but when used in conjunction with Field Flow Fractionation (FFF) (discussed in 1.2.1.4.3), SLS can also determine particle shape. However, as scattering intensity is inversely proportional to $d^2$ for larger particles and $d^6$ for particles $d < \lambda/20$ (as with DLS)[15] a disproportionally small amount of larger particles can skew results. This means that SLS is a poor technique for the measurement of samples of polydisperse sizes. Size dependency also means smaller particles require a greater detection limit. As such, detection of NPs < 50nm will require high concentrations.[11]

#### 1.2.1.1.3 Laser Diffraction

When a laser interacts with a particle, diffraction patterns are produced with the diffraction patterns described by the Mie theory. This primarily applies to particles sizes above the laser wavelength in the micron size range (the Mie size regions)[21] However, laser diffraction methods can make use of these diffraction patterns to provide sizing for particles in the size range ≈ 0.05-1000 $\mu$m. This is achieved by incorporating backscatter detectors and multiple lasers.[22] Laser diffraction yields an equivalent spherical volume

diameter, which combined with the size range of operation means that laser diffraction is useful in the study of agglomeration processes. However, laser diffraction is limited by poor sensitivity and the required high detection angles for particles on the submicron scale.[23]

#### 1.2.1.1.4 Turbidimetry and Nephelometry

Most commonly used in medicinal and biological sciences for the determination of the concentration of small biological molecules (*e.g.*, proteins[24] and microtubules[25]) turbidimetry and nephelometry have both been used to measure NP concentration. They can also provide estimates of particles size provided the particle refractive index is known.[26,27] However, this is usually only the case for NPs produced in the laboratory and not natural samples. Turbidimetry measures the light transmitted, whereas nephelometry measures scattering intensity (typically perpendicular to the incident laser). It has advantages which make it a useful tool in aquatic environmental studies[28] as it provides rapid measurement and simplicity of operation at an economical price. Measurements also do not perturb the system and accurate results can be achieved with small sample amounts. However, as mentioned before, scattering is concentration dependent and results can become unreliable when the NPs do not have high levels of monodispersity.

#### 1.2.1.1.5 Nanoparticle Tracking Analysis (NTA)

NTA is a technique recently developed by NanoSight Ltd., which tracks NPs in solution in real time. This allows for the production of number based distributions compared to the intensity based distributions measured by DLS.[29] This therefore allows more accurate size measurements of polydisperse NP samples, as results are not skewed by scattering intensity.

An incident laser illuminates individual point scatterers in the sample and the individual Brownian motions are tracked through an optical microscope by a charge coupled device (CCD) camera operating at 30 frames $s^{-1}$. The diffuse motion is captured in two dimensions, so a correction term is used for in the Stokes-Einstein equation to calculate distributions of diffusion coefficients and the hydrodynamic diameters of the particles.[30]

The resolution depends upon the refractive index of the NPs. For high refractive index NPs *e.g.*, gold, NTA can size particles down to ≈10 nm, with the detection of 8 nm for silver colloids being reported.[30] However, as refractive index is decreased the resolution is reduced. This means that for characterising an unknown sample NTA can only be reliably used in the particle range 30-1000 nm. NTA also has a limited operating rage of concentration, typically $10^7$-$10^9$ particles $ml^{-1}$,[31] though this can be improved by increasing data acquisition time.

#### 1.2.1.1.6 Small Angle X-ray Scattering (SAXS) & Small Angle Neutron Scattering (SANS)

SAXS and SANS are able to overcome some of the limitations of light scattering by using the lower wavelengths of X-rays and neutrons respectively. SAXS uses similar principles to DLS but is able to probe much smaller particles due to the smaller wavelength of X-rays[32] (0.1-0.2 nm, with 0.154 nm being the most commonly used[33]). Unlike many of the aforementioned scattering methods, it is capable of the characterisation of both liquid and solid, mono or polydisperse samples. For polydisperse samples only the size distribution can be determined, while for a monodisperse sample the size, shape and structural determination can be obtained.[10]

SANS uses a neutron beam with a typical wavelength of 0.001-3 nm which scatter due to interactions with the atomic nucleus. Due to the mode of scattering it is possible for SANS to distinguish between isotopes, with the greatest distinction between hydrogen and deuterium. This allows SANS to be used to study NP-NP or NP-surfactant interactions.[34] Like SAXS, SANS can be used effectively on both solid and liquid samples. The major drawback of both SAXS and SANS is that they are generally limited to use in large scale facilities which are capable of providing the high photon fluxes for both experiments.

#### 1.2.1.2 Microscopy Techniques

The size of NPs puts them outside of the diffraction limit of visible light ($\lambda/2$) meaning that conventional optical microscopy cannot normally produce images of NPs. However, there are other microscopic methods that can be used to image NPs. These techniques can be separated into two main families: electron microscopy and scanning probe microscopy (SPM). Electron microscopy can be seen as analogous to optical microscopy which uses electrons instead of photons for imaging; SPM forms images of surfaces by using a scanning probe. These techniques can produce good quality information for a wide range of NP properties from shape and size, to agglomeration state and chemical composition. Unfortunately, use of both forms of microscopy is time consuming, limiting the number of particles that can be analysed and potentially limiting the statistical relevance of distributions produced.[10] A further disadvantage means that analysis cannot be done in situ. The samples must be removed from their environment and prepared before analysis can take place. This sample preparation is also often destructive and therefore does not allow analysis of the many NP interactions that take place in aqueous suspension.

#### 1.2.1.2.1 Electron Microscopy

The principle of wave-particle duality dictates that electrons must have an associated de Broglie wavelength. It is this phenomenon that electron microscopes exploit in order to image materials on the atomic level. There are two main families of electron microscopes: scanning electron microscopes (SEM) and transmission electron microscopes (TEM), although it is possible to fit a TEM with a scanning unit leading to the scanning transmission electron microscope (STEM). By measuring signals from the variety of ways in which electrons interact with matter it is possible to obtain a large amount of information about the NPs under study such as shape, size, chemical composition, structure and agglomeration.[35] Depending upon certain features of microscope setup and sample composition, only some of these signals can be detected. Thus, characterisation should ideally be undertaken with both SEM and TEM under different microscope setups so as to ensure a full analysis of NPs. For a more thorough discussion of electron microscopy techniques the reader is directed to the review of Dudkiewicz *et al.*[36]

##### 1.2.1.2.1.1Transmission Electron Microscopy (TEM)

In TEM, a parallel beam of electrons is required to pass through the sample before being detected by either a fluorescent screen or a CCD camera (the most common method as the operator is not required to remain in darkness while using the TEM). For the required electron transparency in TEM, the sample must be very thin. The limits upon sample thickness are determined by the atomic weight of the sample and energy of the electrons (the acceleration voltage). As electrons are diffracted more by heavier nuclei, higher atomic weight decreases the maximum thickness, whereas a greater acceleration voltage increases maximum thickness. The limits of the thickness are also affected by the type of information that is desired. If only morphological information is required then the

thickness of particles can be up to several $\mu$m, whereas analytical and high resolution applications require samples of thickness < 100 nm. As NPs tend to be thin enough, additional thinning of the sample is seldom necessary.[11] Determination of the morphology of a sample only requires the TEM to be operated in conventional imaging mode.

TEM is a useful tool for detecting contaminant NPs containing heavy metals in organic and biological samples as heavy elements have much stronger contrast compared to carbon, oxygen, nitrogen and hydrogen. The NPs show up as dark spots compared to the much lighter organics.[37]

By using Selected Area Electron Diffraction (SAED) to study the diffraction patterns or Fast Fourier Transform (FFT) of high resolution images, information regarding the crystalline and atomic structure of the particle can be revealed.[38,39]

As mentioned above, it is possible to fit a conventional TEM with a scanning unit giving rise to the STEM. With STEM, a focused electron probe is scanned over the sample surface which requires the use of a convergent electron beam. This means that the operational principles of the STEM are in reality closer to those of an SEM.

One way to get an analysis of liquid sample is by the use of a cryo-TEM which enables imaging of frozen samples. This allows structure that could potentially be lost by other sample perpetration methods to be investigated. For example this method was employed to view 2 – 4 nm titania NPs doped with Fe(III) in an aqueous environment.[40]

#### 1.2.1.2.1.2 Scanning Electron Microscopy (SEM)

SEM utilises the scanning of a focused electron probe over the surface of the sample to produce detailed topography which is often complimentary to information obtained by TEM. This is done by the analysis of either the secondary electrons or the backscattered electrons depending upon the type of information required. Secondary

electrons are generated as ionisation products from the bombardment of a sample by the primary electrons; backscattered electrons are primary electrons scattered back towards the detector. One of the disadvantages of SEM is that it conventionally requires high vacuum conditions to prevent charging effect, meaning that analysis cannot be done on liquid samples. As such, sample preparation is often necessary *e.g.*, dehydration or cryofixing. Unfortunately, this can lead to alteration of the sample.[10] For non-conducting particles (*e.g.*, most polymer latexes) it is also necessary to coat the particles with a conducting surface, such as gold.

Some newer devices are capable of working only at low vacuum (a few mbar) to allow the investigation of materials unstable at high vacuum. The environmental SEM (ESEM) can be operated at even higher pressure, ≈20 mbar. This allows the triple point of water to be reached (0.01 $^{o}$C, 6.11 mbar) by cooling the sample. Further, by gas ionisation in the sample chamber the positive negative charge balance is maintained, removing the need for coating and thus allowing the investigation of uncoated aquatic colloids. Unfortunately, gas ionisation in ESEM causes the scattering of electrons before the sample is reached. This means that the secondary electron image can only use the un-scattered portion of the beam to produce an image. Resolution is decreased, particularly for organics, from ≈ 10 nm to ≈100 nm. This decrease is primarily due to the electron optics and sample stability rather than the technique itself. However, as the same sample could not be studied uncoated by conventional SEM, comparisons of ESEM and SEM are therefore not valid.[11] As such, SEM and ESEM should be used as complimentary techniques.[41,42]

SEM is useful for bulk analysis to get a general sample overview, followed by TEM studies to perform the more detailed examination (*e.g.*, an association between cells and micron sized aggregates was shown with SEM, and a full investigation was then performed with TEM).[38] SEM is also useful for investigating NPs that cannot be removed

from substrates. The low voltages that can be used in both SEM and ESEM allow investigations of uncoated NPs reducing the risk of misleading artefacts.

#### 1.2.1.2.1.3 Elemental Analysis and Electron Microscopy

Both SEM and TEM become far more effective analytical tools when combined with elemental analysis. Interaction of electrons with matter results in the emission of X-rays. The nature of the X-rays produced will be characteristic of the chemical composition of the sample. Electron microscopy can utilise this phenomenon by both Energy dispersive X-ray spectroscopy (EDX) and electron energy loss spectroscopy (EELS) for elemental analysis.

Use of EDX usually requires a sample thickness of a few $\mu$m. As this is rarely met for NPs, only qualitative SEM-EDX is possible for NPs.[11]

With TEM-EDX qualitative information can be acquired in a straight forward manner. Consequently, it is these results which are generally found in the literature.[43,44,45] Quantitative analysis is also possible with TEM-EDX provided the electron beam passes completely through the sample (which is usually the case for NPs) and that the beam is only scattered once. If the above criteria are fulfilled by the sample, quantification of the X-ray signal is possible using the Cliff-Lorimer thin film approximation[46] and a correction for atomic number ($Z$). Provided that TEM-EDX is properly calibrated it can produce elemental analysis with an accuracy of ± 5 % for elements heavier than carbon.[47,48]

When an electron interacts with a sample producing an X-ray, it loses energy. This energy loss is characteristic of the individual elements in the sample. Measurement of this energy loss by EELS can provide information on the chemical composition of a sample. However, as EELS requires the electron to pass completely through the sample it can only be utilised with TEM. It can be used qualitatively with samples of a few tens of nm thick,

and useful information can still be obtained up to a thickness of 100nm. EELS has proved useful for characterising engineered NPs *e.g.*, iron oxides[49] and titanium dioxide[50] amongst many others

#### 1.2.1.2.2 Scanning Probe Microscopy (SPM)

SPM is a much more general family of microscopy than electron microscopy. It utilises a probe to scan the sample surface and create and image. Only three of the various types will be briefly discussed below.

##### 1.2.1.2.2.1 Atomic Force Microscopy (AFM)

AFM employs a nanosturctured tip attached to an oscillating cantilever which is scanned over the surface of a sample. Attractive and repulsive forces felt by the tip causes changes in the oscillations which are recorded by measurement of deflections of a laser beam directed at a fixed point upon the cantilever. One of the advantages of AFM is that it can be used in both air and water. Measurements of particle height have a lower limit of 0.1 nm. However, as the tip typically has a curvature of about 10nm, AFM cannot probe close to the particle edge in NPs <10 nm.[51]

##### 1.2.1.2.2.2 Near-field Scanning Optical Microscopy (NSOM)

NSOM is a technique which gives far higher resolution than conventional microscopes. Lateral spatial resolutions as low as 20 nm and vertical resolutions of as low as 2-5 nm are possible.[52] This means that NSOM is useful for studying some lager NPs and NP agglomerates.[53] NSOM operates by illuminating the sample with an optical fibre through a sub-wavelength sized aperture only a few nm from the sample surface. This

allows a spatial resolution approaching the diameter the aperture through the use of the near field evanescent waves that exist only on the object surface.[54]

#### 1.2.1.2.2.3 Confocal Laser Scanning Microscopy (CLSM).

Despite the limitations placed upon confocal microscopy by the diffraction limit of light, horizontal resolutions of 200 nm and vertical resolutions of 500 nm are possible when using CLSM, as well as the ability to produce 3D images.[55] Fluorescent specimens can be located more precisely still. If combined with fluorescence correlation spectroscopy when the colloids are naturally fluorescent or have been treated with fluorescent dyes, CLSM can be used to study colloids in complex systems.[56] CLSM operates by exciting the sample with a laser. The laser then reflects off a dichroic mirror and onto two other motorised mirrors which scan the laser across the sample. The sample then fluoresces and the light follows the same path back as the incident light passing through the dichroic mirror and is then focused on a pin hole, removing all unfocused light. This means only one point of the sample is imaged at any given instant. Therefore, in order to get a full image it must build one pixel at a time.

#### 1.2.1.2.3 X-ray Microscopy (XRM)

XRM is similar to both optical and electron microscopy, but uses X-rays instead of visible light or electrons. Due to the longer wavelength of X-rays compared to electrons the resolution is only down to 30 nm. The major advantage of XRM is that it can be used to view samples in the aqueous phase without the need for sample preparation,[57] as well as be used to view biological samples due to the less destructive nature.[58]

#### 1.2.1.3 Spectroscopic Methods

Many spectroscopic methods have found use in NP characterisation but only a few will be covered here. A more thorough discussion can be found in Tiede *et al.*[10]

##### 1.2.1.3.1 Optical Spectroscopy

Ultraviolet–Visible (UV-VIS) and infrared (IR) spectroscopy can easily be used for measurements of light adsorption in NPs. Concentration can be established using the Beer-Lambert law:

$$-\log_{10} {}^{I}/_{I_0} = \varepsilon c l \qquad \text{(Eq. 1.4)}$$

where: $I$ is intensity of the transmitted beam,

$I_0$ is the intensity of the incident beam,

$\varepsilon$ is the molar extinction coefficient,

$c$ is concentration and

$l$ is path length.

However, as for NPs analysis the molar extinction coefficient can be affected by light scattering. As the NPs and aggregates get larger, or for NPs with a high refractive index, the scattering contribution becomes even more important. There is no simple relationship between the scattering contribution and concentration of the sample. As such, for complex mixtures of NPs the method becomes unreliable.

However, due the minimum perturbation to the sample and ease of operation, optical spectroscopy has found use in NP characterisation.[59] When Fourier-transform-IR (FT-IR) is used, optical spectroscopy has shown to be useful for organic-based nanoparticles such as fullerenes and carbon nanotubes (*e.g.*, comparisons of colloidal suspensions of C60). [60]

Surface plasmon effects also produce absorption bands that are seen with UV-vis spectroscopy in metal NPs that do not show up in larger particles or solutions of metal salts and these bands can be related to both the size and shape of the NPs in the dispersion (*e.g.*, in the study of silver NPs).[61]

#### 1.2.1.3.2 Fluorescence Spectroscopy

Though limited to particles that are either self-fluorescent or dyed fluorescence, spectroscopy can be used for NP analysis. The agglomeration of self-fluorescing semiconductor quantum dots can be studied my monitoring changes in fluorescence spectra *e.g.*, CdSe.[62]

#### 1.2.1.3.3 X-ray Photoelectron Spectroscopy (XPS)

XPS utilizes the photoelectric effect to probe the surface (top 1-10 nm) of particulate substrates. This is done by measuring the kinetic energy and electron flux produced when an X-ray beam is projected onto the sample, as a surface analysis technique XPS can be used to study composition and redox state of NPs.[63]

#### 1.2.1.3.4 X-ray diffraction (XRD)

By measuring the elastic scattering of X-rays by the electron clouds of the individual atoms in the system, XRD can provide crystallographic and elemental composition information on NPs as well as size information.

#### 1.2.1.3.5 Laser-induced breakdown detection Spectroscopy (LIBDS)

LIBDS uses a short laser pulse focused upon the sample surface to create a plasma plume. In the plume, constituent atoms of the sample are excited. As they relax they

produce characteristic spectral emissions. It has the advantage of having very low detection limits; however, it cannot distinguish between different types of particles and requires particle-specific size calibration.[64]

#### 1.2.1.4 Fractionation and Separation Methods

Fractionation can be done on the basis of chemical or physical properties. Fractionation of physical properties is by far the most common with regards to NPs. As such, discussion will focus upon physical methods.

##### 1.2.1.4.1 Filtration

Filtration methods use membranes to separate NPs. The distinction between the different methods is due to the different membrane pore size or membrane molecular weight cut-off (MWCO) being used. MWCO can be defined as the lowest molecular weight of solute (in Daltons) which will be 90% retained by the membrane. Micro-filtration uses a membrane with pore sizes in the region of 0.2-10 $\mu$m whereas ultra-filtration uses membranes with a MWCO of 1000 -100 million Da. A fairly recent form of filtration is nano-filtration; it uses membranes with pore sizes of 0.5-1 nm and can be used to separate small NPs from monovalent ions.[65]

##### 1.2.1.4.2 Centrifugation

The centrifugation techniques of analytical ultracentrifugation (AUC) and differential centrifugal sedimentation (DCS) – also called centrifugal particle sedimentation – are well established methods for size fractioning of NPs. Both AUC and DCS broadly operate on the same principal which relies on the fact that particles will usually have a density greater than the dispersion medium. Therefore, application of

centrifugal force generated by the rapid acceleration of a rotor will induce sedimentation of the particles (Figure 1.2). As the applied force is proportional to the particle mass, larger particles will sediment at a faster rate than smaller ones. Both frictional and buoyant forces will oppose the centrifugal force but once these forces come to equilibrium (≈ $10^{-6}$ s) the particles will reach terminal velocity which is related to the size of the individual particles. Sedimentation of the sample can be monitored in real time by a UV or visible light absorption system, viewing the concentration relative to the applied centrifugal field. As larger mass particles settle with a lower applied field, by using a fluid with a known gradient of viscosity and density it is possible to create a mass profile of the NPs in the sample from the following equation:[66]

$$\ln\left(\frac{x}{x_0}\right) = d_v^2 \frac{2(\rho_{part}-\rho)}{9\eta}(\pi v)^2(t-t_0) \qquad \text{(Eq. 1.5)}$$

where $x_0$ and $x$ are the starting and end positions from the centrifuge centre at time $t_o$ and $t$, $v$ is the centrifuge rotational speed, $\eta$ is the viscosity of the dispersion medium, $\rho_{part}$ is particle density and $d_v$ is the particle volumetric diameter.

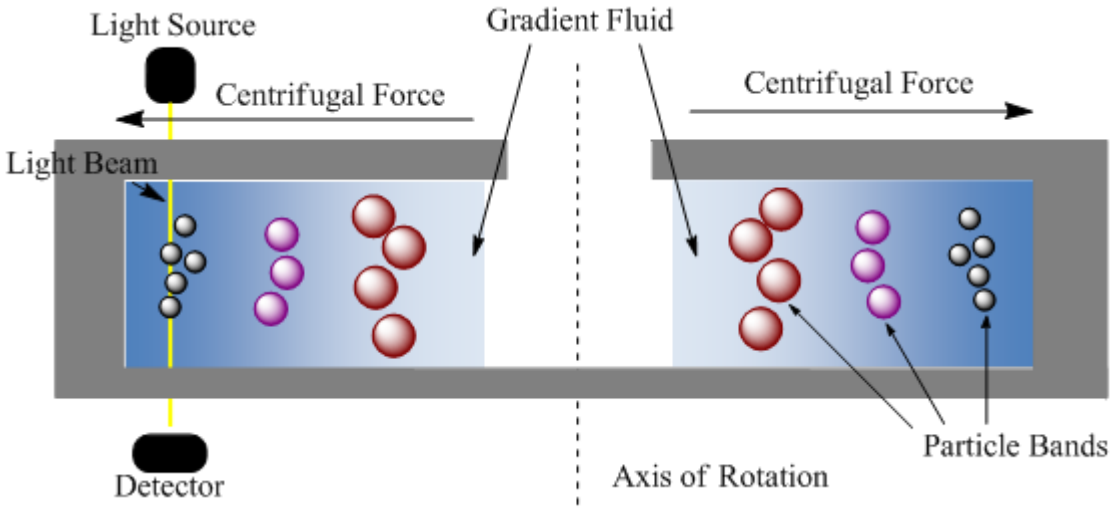


Figure 1.2: Schematic of the operation of differential centrifugal analysis, using a disk and the centrifuge chamber, displaying the basic principal of separation.

Compared to light scattering methods such as DLS, AUC and DCS offer a better size resolution with accurate determination of particles to 2–3 nm. These techniques are also far more effective for analysis of mixtures of sizes.[67] Also, as particles have already been separated before detection, with proper calibration it is possible to quantify the amount of material of a given size passing through the detector at a given interval.[68]

The lower forces used in DCS, while not necessarily a problem for NPs with a high density such as metals, mean that smaller low density particles may sediment very slowly or not at all. This effectively put a limit on detection of certain samples [*e.g.* 20 nm for amorphous silica, 40 nm for polymer latexes (chapter 5 of this thesis)]. This lower size limit is less of an issue for AUC which utilises much greater centrifugal forces (> 100,000 g), however, these forces have been known to induce aggregation.[69] Even with the knowledge of the density of the primary particles, knowledge of the density of the aggregates will be difficult to establish. A variation of DCS allows the analysis of low density particles. The particles are deposited at the bottom of a centrifuge chamber at the start of the analysis instead of at the top. By using fluid which has a greater density than the particles, they will sediment to the top on application of the centrifugal force.[70]

While not as widely cited in the literature,[71] centrifugation techniques have been used to analyse a variety of NPs (*e.g.* silica[72], gold,[73] particles with core/shell morphologies[74] amongst others).

#### 1.2.1.4.3 Field Flow Fractionation (FFF)

FFF is a family of separation techniques that separates particles based upon how they interact with an applied field. The technique has been recently reviewed by Whalund[75] The balance between Brownian motion (diffusion) and an applied field distributes the particles against one of the walls of a thin channel. A laminar flow through the channel at

right angles to the field then transports the particles through the channel.[76] The particle mean height is inversely proportional to particle size and proportional to transport velocity (Figure 1.3). The type of FFF depends upon the field applied, either a hydrodynamic field (Flow FFF) or a centrifugal field (Sedimentation FFF).

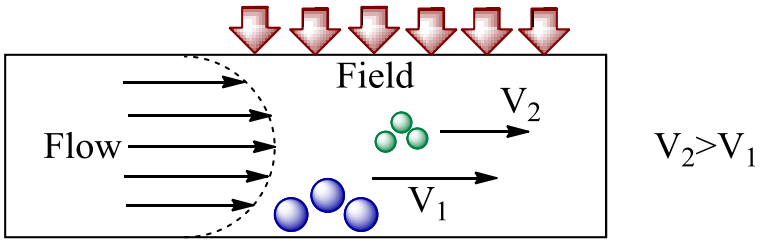


Figure 1.3: Diagram showing the basic principle behind Field Flow Fractionation (FFF).

As well as being able to separate NPs in the over a wide size range (1 nm – 800 nm for Flow-FFF, and 30 – 800 nm for Sedimentation-FFF), the elution time of FFF can be directly related to physical properties such as hydrodynamic volume and diffusion coefficient (Flow-FFF), and buoyant mass and equivalent spherical volume diameter (Sedimentation FFF), making it a versatile analytical tool. The drawback with FFF is that the versatility comes with high complexity.

FFF has been a valuable technique for investigating environmental colloids using both optical detectors and inductively coupled plasma mass spectrometry (ICP-MS)[77,78] (*e.g.*, analysis of carbon nanotubes[79] and metal oxide NP's[80] amongst others). Shape information has also been determined by FFF by combining it with either light scattering or microscopic methods.[81]

### 1.2.1.5 Chromatography Methods

#### 1.2.1.5.1 Size Exclusion Chromatography (SEC)

SEC (also known as gel permeation chromatography (GPC) in the field of polymer science) is a method that was especially developed for the separation of

macromolecules. SEC separates NPs on the basis of size. NPs flow through a column filled with a packing material that has pores in the size range of the particles to be separated. Separation occurs on the basis of the particles' ability to enter the pores, which is defined by the hydrodynamic volume (size and shape) of the NPs. Smaller particles have access to a greater distribution of pores and thus have a greater volume of column to transit (Figure 1.4). Consequently, particles that are unable to enter any pores will elute from the column in the oversized peak. These larger particles are outside of the operating size of the specific column. As such, fractionation is not possible for oversized NPs. After the oversized particles come the fractionated particles, with the largest eluting first and the smallest last. The last to elute is the salt peak containing the dissolved molecules and ions which have passed the complete pore volume. SEC is a versatile technique which has been applied to the study of a variety of NPs both engineered[82] and natural[83] (*e.g.*, separation of CdS, ZnS and sillica colloids (2 – 20 nm),[84] chiral gold clusters[85] and dextran-modified iron oxides).[86] Selection of the mobile phase must be made carefully as the choice may affect the fractionation procedure. For example, the separation of Au/Pd core-shell NPs required the presence of SDS in the eluent to stabilise the particles.[87] A shape separation of rod-like and spherical gold NPs was undertaken using a mobile phase containing SDS and Brij-35.[88] By use of a poly(methyl methacrylate) brush grafted to the surface of the stationary phase, separation of quantum dots and NPs was achieved independently of the surface nature.[89]

A sub type of SEC, recycling GPC, has been applied to separate thiol stabilised gold nanocrystals,[90] the alternate recycling was found to increase the separation efficiency with the square root of the cycle number, allowing separation of particles with a size difference of only 6 Å.

The main drawback with regards to the separation of natural samples is the operating size range of SEC with regards to nanoparticles, though columns are produced which are specifically designed for the separation larger molecules such as proteins and DNA, and have an effective operating size range of up to around 100 nm.

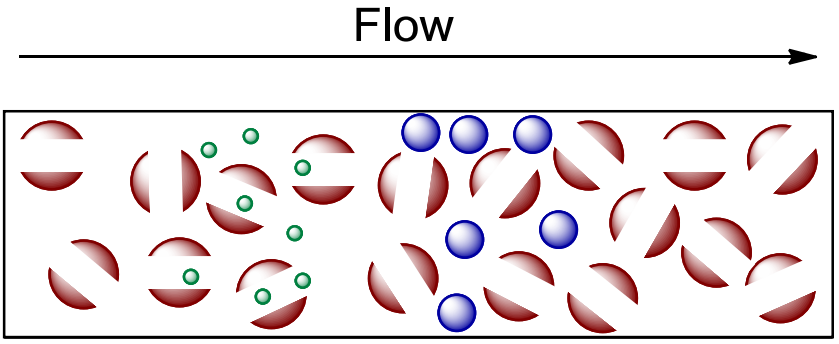


Figure 1.4: A simplified schematic of the separation mechanism of size exclusion chromatography. In reality the packing beads have multiple pores.

#### 1.2.1.5.2 Hydrodynamic Chromatography (HDC)

Originally developed by Small *et al.*[91] at the Dow Chemical Company in the early 1970's, HDC is a size fractionating method that allows the simultaneous determination of the hydrodynamic diameter and granularity distribution of polymers or colloids. The technique has been recently reviewed by Stiegel and Brewer.[92] Separation occurs in either narrow capillary channels or in the voids between non-porous beads which can be considered to act as capillary channels. The separation mechanism of HDC can be described in terms of a parabolic flow profile occurring within narrow channels. The liquid closest to the walls of the channel experiences the highest hydrodynamic drag and consequently elutes slower than the liquid in the centre of the channels. The centre of mass of larger particles has a greater excluded volume compared to smaller particles and cannot approach as close to the wall of the capillary channel, thus will remain in the faster flowing regions of the eluent and will travel thorough the channels quickest eluting first (Figure 1.5).

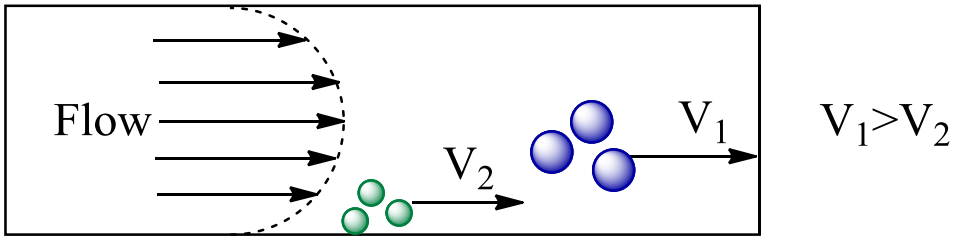


Figure 1.5: Schematic illustration of principle of HDC separation. Larger particles have a greater excluded volume and the centre of mass cannot approach the wall as close as small particles. They therefore so experience a greater average flow velocity leading to their elusion before smaller particles.

A model to express the relationship between retention time and solute size was presented by Brenner and Gaydos[93] in 1977 and can be expressed in the following equation:

$$t_m/t_0 = R = (1 + B\lambda - C\lambda^2)^{-1} \quad \text{(Eq. 1.6)}$$

where: $t_m$ is the retention time of the particle,

$t_0$ is the retention time of a minimum solute,

$R$ is the relative retention time,

$\lambda$ is the ratio of the effective diameter of the particle ($d_p$) to the diameter of the capillary ($d_c$) and

B and C are both constants that relate to the nature of the column. (0.5-5 for a capillary column and 2.7-2.8 for a packed column)[94]

Equation 1.6 is based upon the assumption that particles are rigid and spherical which is not always the case, particularly for natural samples.

While the separating of efficiency of HDC is currently comparatively poor (though this can be improved by the use of narrower capillaries and smaller packing materials) the operational size range is good (5-1200nm),[10] with a low analysis time <10 min.

By coupling a packed HDC column to an ICP-MS, it was shown to be possible to determine both the chemical composition as well as the size of $TiO_2$, $SiO_2$, $Al_2O_3$ and

$Fe_2O_3$ nanoparticles,[95] as well as silver nanoparticles in activated sludge.[96] The capillary tube method has been applied for the separation synthetic polymer particles, biopolymers and liquid nanocapsules.[97] A sub technique of capillary HDC – wide bore HDC – in which the internal diameter of the capillaries is greater than 0.7 mm, has been employed to separate CdS and Au sols over a size range of 3-27 nm.[98]. Recently Pergantis and co-workers[99] developed a single particle HDC-ICP-MS system which allowed the measurement of the number concentrations of gold nanoparticles. It has also been used for the sizing and chemical characterisation of liposome type nanoparticle by coupling to a MALI-TOF mass spectrometer.[100]

### 1.2.2 Summation

The ideal technique for the separation of aqueous dispersions nanoparticles would meet the following criteria;

- High resolution.
- Wide operating size range.
- Minimal perturbation of the sample.
- Separate purely based upon size, with negligible contribution form surface chemistry.
- Be non-destructive
- As well as sizing information it should able to also elucidate data on the elemental composition
- Require minimal prior knowledge to the particle properties to allow analysis of unknown samples.

Table 1.1: Brief summary of the discussed techniques used in the analysis of nanoparticles.

| Technique | Properties Mesured | Operating Size Range | Pros | Cons |
|---|---|---|---|---|
| Dynamic Light Scattering | Size.<br>Size distribution. | 3 nm to micron size | Can measure particles in dispersion<br>Fast and simple<br>Can measure aggregation Processes<br>Non-Destructive | Limited for polydisperse samples<br>Disproportionately influenced by large particles/aggregates |
| Static Classical Light Scattering (SLS) | Molecular weight.<br>Root mean square radius of gyration. | 3 nm – 10 $\mu$m | As with DLS | As with DLS |
| Laser Diffraction | Size | 0.05 – 1000 $\mu$m | Opperating size range.<br>Non-destructive.<br>Can measure particles in dispersion. | Poor sensitivity.<br>High detection angles for submicron particles. |
| Turbidimetry and Nephelometry | Concentration | 50 nm – > 1000 nm | Minimium sample perterbation.<br>Simple equipment.<br>Can perform in situ measurements. | Inaccurate for complex mixtures.<br>Data can be skewed by large particles/aggregates |
| Nanoparticle Tracking Analysis (NTA) | Size | 10 – 1000 NM | Good for polydisperse samples.<br>Provides number based size distributions. | Limited operating range of concentration.<br>Resolution decreases with decreasing refractive index. |
| Small Angle X-ray Scattering (SAXS) & Small Angle Neutron Scattering (SANS) | In monodisperse size, shape and struture, is polydisperse only size distribution | 1 – 1000 nm (SANS) | Analysis of both liquids and solids. | Limited to use in large scale facilaties |

| Technique | Properties Mesured | Operating Size Range | Pros | Cons |
|---|---|---|---|---|
| Transmission Electron Microscopy (TEM) | Size and shape. | > 0.1 nm | High resolution | Destructive.<br>Sample information can be lost due to preperation. |
| Scanning Electron Microscopy (SEM) | Size and shape | > 1 nm | High resolution | Destructive<br>Requires high vacuum<br>Surface charging |
| Elemental Analysis and Electron Microscopy (EELS and EDX) | Chemical composition | n.a. | EELS can be used on lighter elements. | EDX only applicable for heavy elements. |
| Atomic Force Microscopy (AFM) | Size<br>Surface topography.<br>Electrical/mechanical properties. | > 0.1 nm | Ambient environment.<br>Use for both liquid and dry samples | Overestimations of lateral dimensions |
| Near-field Scanning Optical Microscopy (NSOM) | Size<br>Chemical bonding | > 30 nm | Optical imaging | Can not visulis small particles. |
| Confocal Laser Scanning Microscopy (CLSM) | Size<br>Concentration | > 200 nm | Can produce 3D images | Requires fluorescent samples |
| X-ray Microscopy (XRM) | Size<br>Shape | > 30 nm | Can view aqueous samples without preperation | Radiation Damage |
| Optical Spectroscopy | Concentration.<br>Size and shape. | n.a. | Good for imaging organic particles.<br>Minimal sample perturbation | Unreliable for mixtures |
| Fluorescence Spectroscopy | Concentration | n.a. | Dilute samples in small volumes | Limited to fluresent particles. |
| X-ray Spectroscopy (XRS) | Elemental composition<br>Size.<br>Shape. | $\approx 1\mu$m | Highly accurate for surface information.<br>Can identify all but two elements. | Requires high vaccum.<br>Unable to detect hydrogen or helium. |

| Technique | Properties Mesured | Operating Size Range | Pros | Cons |
|---|---|---|---|---|
| X-ray diffraction (XRD) | Crystal strutures.<br>Size.<br>Elemental data. | 0.5 nm – > 1$\mu$m | Can distinquish between the different crystal forms of particles. | High Level of sample perterbation.<br>Can only be used on dry samples. |
| Laser-induced breakdown detection Spectroscopy (LIBD) | Elemental Composition | n.a. | Low detection Limits<br>Solid Phase Analysis | Destrutive<br>Can't distinguish between different particles in a mixture |
| Filtration | Size fractionation | 1 nm – 1 $\mu$m depending on pore size. | Fast.<br>Low cost.<br>High volumes. | Clogging.<br>Broad pore size distribution.<br>Size fractionation is frequently poorly defined. |
| Centrifugation | Size and size distribution for particles of a know density. | 2 nm – 80 $\mu$m Dependant on particle density. | High resolution.<br>Low surface effects. | Requires some prior knowledge of the particles.<br>Can induce aggregation. |
| Field Flow Fractionation (FFF) | Size<br>Size Distribution<br>Buoyant Mass | 1 nm – 1 $\mu$m | Size Range<br>Mild on Analytes<br>Potential for combination with elemental analysis | Complex<br>Membrane Interactions<br>Dilution |
| Size Exclusion Chromatography (SEC) | Size | <100 nm | High Resolution | Interactions with the mobile phase<br>Can only be used for the anlyisis of small paticles |
| Hydrodynamic Chromatography (HDC) | Size | 5 nm – 1200 nm | Non destrutive.<br>Wide size range. | Interactions with the mobile phase<br>Poor resolution at the lower size range |

As can been seen form Table 1.1 and from the following sections currently no one technique meets all these criteria. Indeed for the foreseeable future in is unreasonable to think that any one technique would be able to meet these criteria. Consequently there is always a demand for improvements to existing techniques or the development of novel and complementary analysis techniques. It is the aim of this thesis, therefore, to investigate if HIPE templated materials (discussed in detail in below and in the introductions to chapter 2 and 3) have and potential for the use in the size separation of nanoparticles.

### 1.3 Introduction Emulsions and HIPEs

This section will give some background theory on emulsions and in particular high internal phase emulsions (HIPEs). Throughout this thesis HIPEs will be used to produce a variety of porous materials; however, the relevant introductions to the different types of material will be included in each chapter rather than here.

#### 1.3.1 Emulsions

Emulsions are liquid-in-liquid systems that consist of two immiscible liquids in which one liquid is dispersed within the other creating an interface.[101] They are usually formed by mixing the two liquids together via high shear or sonification.[102] Emulsions are generally categorised as either oil-in-water (o/w) or water-in-oil (w/o), where oil refers to a liquid immiscible with water. The two phases are normally termed the internal (or dispersed) phase, and the external (or continuous) phase. The internal phase will generally take the form of polydisperse droplets with average droplet sizes of several microns.[103] However, special techniques can be applied such as emulsion fractionation which allow the formation of monodisperse emulsions with finely tuned droplet sizes.[104,105,106]

Emulsions are thermodynamically unstable and will therefore not form spontaneously. This instability is due to the large increase in surface free energy upon forming an emulsion that results from the combination of interfacial tension ($\sigma$), the large surface area of the internal phase and the differences in the densities of the two phases.[107] Consequently, without stabilisation the droplets of the internal phase interact and coalesce and the emulsion will phase separate into two layers over time.[108] In order for an emulsion to be considered stable there must be no discernable change in the number, distribution and special arrangement of the droplets of the internal phase over the experimental time period. This time period can vary from as little as several seconds to as much as several years.[109] The primary driving force of the aforementioned coalescence of droplets is the universal Van der Waals attraction. It is this attraction that must be overcome to produce a kinetically stable emulsion. This is achieved by the addition of a stabiliser to the emulsion that prevents break down by creating energy barriers to droplet interaction, thereby preventing coalescence.[110]

### 1.3.2 Surfactants

The most common method of stabilising emulsions is through the use of surface active agents, or surfactants. Surfactants can generally be viewed as having two sections: the head which is hydrophilic, and the tail which is lipophilic (or hydrophobic). This dual nature is a form of amphoterism and it allows surfactants to align themselves at the liquid-liquid interface in the emulsion and prevent coalescence. It does this by lowering the interfacial tension between the two liquids, with the hydrophilic segment sitting in the water phase and the hydrophobic section sitting in the oil phase (Figure 1.6).[111]

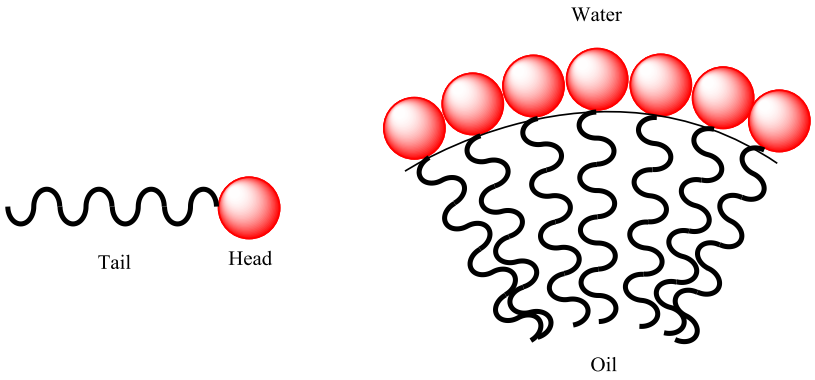


Figure 1.6: Representation of a surfactant stabilised oil in water interface.

There are generally four accepted classifications of surfactants based upon the nature of the head group: anionic, cationic, amphoteric (zwitterionic) and non-ionic.[112] However, as new surfactants are developed and put into use, new methods of classification are also becoming apparent in the literature.[113]

Due to the amphoteric nature of surfactants, once they reach a sufficiently high concentration in a solution they are able to form micelles. These are approximately spherical aggregates of surfactant formed when the heads and tails align with each other. The point at which this occurs for the surfactant/solvent system is known as the critical micelle concentration (cmc).

The nature and concentration of the surfactant is the primary factor in determining the stability of an emulsion. Different surfactants can be used to stabilise different types of emulsions.

The Bancroft Rule states that the phase in which the surfactant in most soluble will be the continuous phase. While there are exceptions, it is a useful rule for a quick selection of a surfactant in most systems.[114] Nevertheless, other more quantitative systems are in use which allows the selection of the surfactant with greater certainty. One such example is the hydrophilic-lipophilic balance (HLB) concept.

### 1.3.2.1. The Hydrophilic-Lipophilic Balance (HLB) Concept

The Hydrophilic-Lipophilic Balance, or HLB, concept was developed by Griffin in the late 1940's[115] to provide an association between the structural properties of a surfactant and its emulsifying properties. It provides a semi-empirical scale which allows the selection of surfactants appropriate for purpose based upon the relative percentage of hydrophobic to hydrophilic groups.[111] The value of the HLB for a given surfactant is representative of the type of emulsion it will form (Table 1.2).

Table 1.2: Applications of surfactants within a given HLB range. (Values from ref. 111)

| HLB Range | Application |
|---|---|
| 3-6 | Water-in-oil emulsion |
| 7-9 | Wetting agent |
| 8-18 | Oil-in-water emulsion |
| 13-15 | Detergent |
| 15-18 | Solubiliser |

Table 1.3: Required HLB Numbers for emulsification of various oils. (Values from refs. 111 & 116)

| Oil Type | Oil-in-Water Emulsion HLB | Water-in-Oil Emulsion HLB |
|---|---|---|
| Mineral Oil | 9-12 | 6 |
| Beeswax | 9 | 5 |
| Kerosene | 12 | 6 |
| Paraffin Oil | 10 | 4 |

Griffin proposed the following formulas for calculating the HLB of several types of non-ionic surfactants. For most polyhydric alcohol fatty acid esters the HLB can be calculated approximately by the following equation:

$$HLB = 20\left(1 - {}^{S}/_{A}\right) \qquad \text{(Eq. 1.7)}$$

where: *S* is saponification value of the ester and

*A* is the acid value of the acid.

When the surfactant contains polyoxyethylene chains and polyhydric alcohols as hydrophilic groups, the following equation can be used:

$$HLB = {}^{E + P}/_{5} \qquad \text{(Eq. 1.8)}$$

where: P is the mass percentage of polyhydric alcohol content.

When polyoxyethylene alkyl ethers and polyoxyethylene esters make up the surfactant the following equation can be used:

$$HLB = {}^{E}/_{5} \quad \text{(Eq. 1.9)}$$

where: E is equivalent to the mass percentage of oxyethylene content.[117,118]

The problem with the above equations is that they only cover a limited variety of surfactants. As mentioned, they cannot be used for ionic surfactants, nor can they be applied to surfactants that contain propylene oxide and butylene oxide, or surfactants containing nitrogen and sulphur.

Davies later developed a method for calculating the HLB of a surfactant from the chemical formula. The method assigns specific chemical groups within the surfactant structure empirically determined values. The HLB can be calculated from the following equation:[119]

$$HLB = 7 + \sum(Hydrophilic\ group\ values) - \sum(lipophilic\ group\ values) \quad \text{(Eq.1.10)}$$

Good agreement was found between HLB values calculated by Davies' method and those obtained by experiment. Table 1.4 below includes a list of the HLB group values of some common structural groups; a more comprehensive list can be found in reference 116.

As well as surfactants, other types of stabilisation are also possible. In Pickering emulsions disperse droplets are stabilised by the absorbance of solid particles at the phase interface.[120,121] Emulsions can also be stabilised by Janus particles, a relatively recent innovation named after the Roman god Janus who possessed two faces. Janus particles are amphiphilic particles in which one hemisphere is hydrophilic and the other is hydrophobic.[122] They can be used to greatly enhance the stability of Pickering emulsions[123] However, this work will only be focusing upon the use of surfactants as stabilisers.

Table 1.4: HLB Group Values for some common groups.

| Structural Group | Group Value |
|---|---|
| Hydrophilic | |
| $-SO_4^-Na^+$ | 38.7 |
| $-COO^-K^+$ | 21.1 |
| $-COO^-Na^+$ | 19.1 |
| -COOH | 2.1 |
| -N (tertiary amine) | 9.4 |
| -O- | 1.3 |
| -OH (free) | 1.9 |
| Lipophilic | |
| $-CH_3$ | 0.475 |
| $-CH_2-$ | 0.475 |
| -CH= | 0.475 |
| $-(CH_2CH_2CH_2O)-$ | 0.15 |

### 1.3.3 High Internal Phase Emulsions (HIPEs)

High Internal Phase Emulsions or HIPEs have been known for some time,[120,124] and though HIPE is the common nomenclature when used for the preparation of porous materials (and shall be used throughout this thesis), they are known under various names. These include names such as aphrons,[125] high internal phase ratio emulsions,[126] gel emulsions (due to exhibiting behaviour similar to gels),[127] hydrocarbon gels,[128] and simply, highly concentrated emulsions.[129] HIPEs are a subcategory of emulsion in which the internal phase ratio ($\phi$) is $\geq$ 0.7405 of the total volume of the emulsion. They can be viewed as consisting of tightly packed liquid droplets with persistent microscopic films or thin films between the droplets.[130] As with traditional emulsions, they require a stabiliser. The value $\phi$ = 0.7405 represents the maximum volume that uniform spheres can occupy in a given volume when packed in the most efficient manner; as such, the droplets of HIPEs are often polydisperse and polyhedral.[131] It had been previously thought that $\phi$ = 0.7405 was the maximum possible value for the internal phase volume fraction before an emulsion would invert.[132] However, by using a surfactant that is completely insoluble in the dispersed phase, emulsions with $\phi$ as high of 0.99 can be formed.[133] As with traditional emulsions, HIPEs can be classified as either o/w or w/o.[134] They can be formed from a

wide variety of oils and organic liquids and the 'water' phase is almost always aqueous. However, the use of polar organic liquids has allowed the formation of HIPEs with a non-aqueous 'water' phase.[135]

### 1.3.3.1 HIPE Formation

HIPEs can be formed by several methods such as concentration by osmotic compression, in which a moderately concentrated emulsion is compressed. By low speed centrifugation, or ultra-centrifugation, 'squeezing' out the external phase.[136] By phase inversion in which a lower concentrated emulsion of the opposite type required is inverted to a highly concentrated emulsion of the desired type by a rapid change in temperature, o/w HIPEs are obtained by a temperature quench in w/o emulsions,[137,138] and w/o HIPEs are formed by a temperature increase in o/w emulsions.[139,140] It is also possible to use variations in the pH and electrolyte concentration to form HIPEs.[141] However, the most common method, and the method used in this work, is formation of HIPEs by mechanical stirring. The internal phase is added slowly with constant stirring of the external phase, which takes the form of a solution of swollen micelles of surfactant. During agitation, a multiple emulsion forms (both o/w and w/o emulsions exist simultaneously). Eventually, the less stable form of the emulsion will give way to the more stable form, resulting in a HIPE.[130]

### 1.3.3.2 HIPE Stability

The stability of HIPEs can range from several hours to under a minute, and though the mechanisms behind the high stability are not fully understood, there are several variables that contribute to HIPE stability. For a HIPE to form, these variables must be sufficiently distant from the balanced state of the corresponding microemulsion.[130]

Of all the factors that affect the stability of HIPEs, the foremost is the nature of the surfactant. However, the concentration of the surfactant as well as the electrolyte concentration of the aqueous phase, the viscosity of the continuous phase, the internal phase ratio, the nature of the two phases and the temperature of the HIPE also contribute to overall stability.[142] As mentioned before, the HLB of a surfactant affects the stability of an emulsion. As this is the same for HIPEs, high HLBs are required to form o/w HIPEs and conversely low HLBs are required for w/o HIPEs. However, other surfactant properties must also be taken into consideration. For two surfactants of identical HLB the surfactant with the highest molecular weight will produce the most stable HIPEs. The bulkier surfactant will produce thin films between droplets with a greater thickness than a surfactant with a lower molecular weight which produces a more stable emulsion.[143,144] The molecular weight is also important when producing HIPEs in mixed surfactant systems. Mixing surfactants of differing molecular weights can cause destabilisation of the HIPE, while mixing surfactants similar in terms of molecular weight has a stabilising effect.[145] It was also found that o/w HIPEs containing aromatic or halogenated oil phases were difficult or impossible to form without the use of ionic surfactants, possibly due to the generally more polar nature of such liquids.[146]

Surfactant concentration can also play a vital role. Below a certain concentration HIPEs are always unstable due to incomplete coverage of the emulsion droplets.

From the study of water-in-xylene HIPEs, Ford and co-workers[147] suggested three necessary properties of a surfactant for it to be successful in forming stable HIPEs: 1) rapid adsorption at the interface, 2) the formation of a rigid interfacial film and 3) a lowering of interfacial tension between the phases. The most important factor is the formation of a rigid film, which results when there is an interaction – either electrostatic or hydrogen bonding – between adjacent surfactant molecules.

The nature of the two phases is also important, as well as it being necessary for the surfactant to be more soluble in the continuous phase (as dictated by the Bancroft rule) HIPEs will be more stable the greater the mutual insolubility of the two phases (*e.g.*, alkane-in-water HIPEs stabilised by Span 80 (sorbitan monoolate) were more stable the longer the alkyl chain of the oil phase).[148] This however does not preclude the formation of HIPEs of two miscible liquids (*e.g.*, water-in-dioxane) which can be achieved with appropriate surfactants.[149,150] The viscosity of the two phases also plays a role; an external phase with a high viscosity prevents efficient mixing of the HIPE which leads to smaller maximum possible volume fraction.[146]

The presence of electrolytes in the aqueous phase has a significant impact upon the stability of w/o HIPEs, with increased stability upon addition of electrolytes to the aqueous phase.[151] However, for o/w HIPEs, electrolyte concentration generally appears to have no stabilising influence.[132] In w/o HIPEs the surfactants adopt a more ordered arrangement at the interface with increasing salt concentration.[152] Salts that decrease the cloud point of non-ionic surfactants provide a greater stabilisation.[153] Kizling and Kronberg[154] proposed that the reason for increased stability in the presence of electrolyte is due to interactions between the hydrophilic portions of the surfactant and the electrolyte, which further increases surfactant solubility in the aqueous phase. Erikson, Kizling and Kronberg[155] have since observed these interactions by IR studies. They also proposed that reduction in refractive index disparity on the addition of electrolyte causes a reduction in the attractive forces between droplets of the dispersed phase. When the refractive indexes of the two phases are matched the attractive forces are at a minimum and the HIPE becomes transparent and exhibits exceptionally high stability.[154,155]

The attractive forces between droplets can be calculated from the following equation:

$$A = a\left(\frac{\varepsilon_w - \varepsilon_0}{\varepsilon_w + \varepsilon_0}\right)^2 + b\frac{\left(n_w^2 - n_0^2\right)^2}{\left(n_w^2 + n_0^2\right)^{3/2}} \quad \text{(Eq. 1.11)}$$

where: $A$ is the attractive force, or Hamaker constant,

$a$ and $b$ are constants and

$\varepsilon$ and $n$ the dielectric constant and refractive index respectively either the oil (o) phase or the water (w) phase.

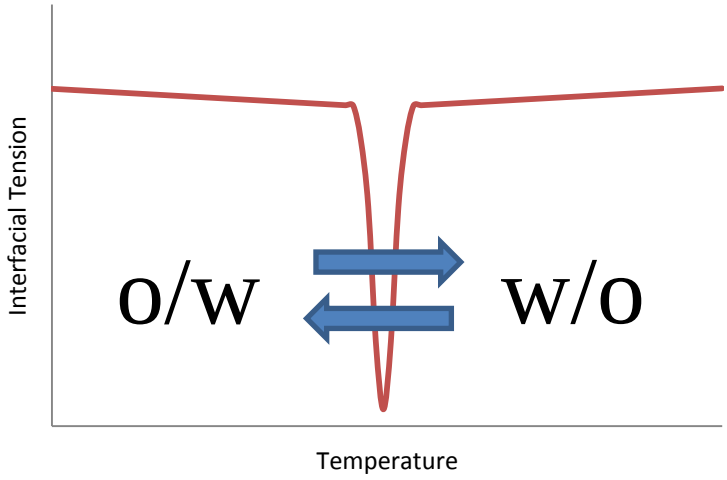


Figure 1.7: Illustration of dramatic drop in interfacial tension at the phase inversion temperature which allows an oil-in-water emulsion to spontaneously turn to a water-in-oil emulsion.

For a HIPE formed with non-ionic surfactants to be stable, it is necessary for them to be formed at ~10-20 $^{o}$C above for o/w, or below for w/o, the phase inversion temperature (PIT), also known as the HLB temperature of the HIPE.[156] The PIT of a given system is the temperature at which the surfactant goes from being water soluble to oil soluble. HIPEs formed within 10-20 $^{o}$C of the PIT are highly unstable due to the large decrease in interfacial tension which increases the probability of thin film rupture (Figure 1.7).[157] Conversely, an excessive increase in interfacial tension will result in a loss of HIPE stability. This is due to increased capillary pressure ($P_c$), which accompanies high interfacial tension and causes decrease in film thickness ($h_f$). When $P_c$ is greater than the steric repulsion between droplets the films will rupture and the HIPE will collapse. This

increase in interfacial tension corresponds to a decrease in $h_f$ which increases the probability of film destabilisation. For an emulsion with droplet sizes of 1-10 $\mu$m an interfacial tension of ~ 0.1-10 mN m$^{-1}$ is most favourable for stability.[130]

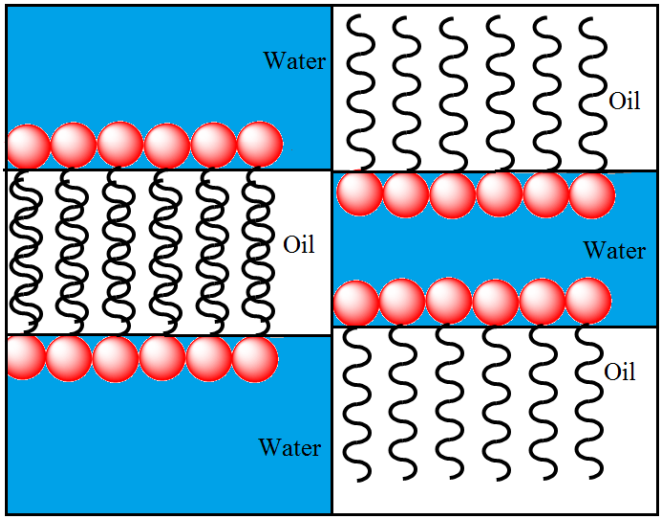


Figure 1.8: Surfactant stabilised w/o/w and o/w/o liquid thin films, resembling bi-layer membranes

As mentioned previously, thin films exist between droplets in a HIPE, and it is the microscopic properties of these films that control the macroscopic properties.[130] These thin films resemble bi-layer membranes (Figure 1.8), and in the thermodynamic equilibrium state the thin film is imagined as an array of holes of varying radii ($r_h$) which will appear and disappear spontaneously according to thermodynamic fluctuations. The film will remain stable unless a hole with $r_h \geq$ the critical radius ($r_h^*$) is formed, at which point the film will rupture and two droplets will coalesce. The probability of hole formation is given by the following equation:

$$P_h = e^{(-W_h/kT)} \qquad \text{(Eq.1.12)}$$

where: $P_h$ is the probability of hole formation,

$W_h$ is the energy penalty due to hole formation,

k is the Boltzmann constant and

T, is the temperature.

Consequently, as equation (Eq. 1.12) shows, the probability of hole formation is proportional to temperature, with higher temperatures increasing the chances of a hole forming in the film. Thus, HIPEs will be more stable at lower temperature, provided the temperature is kept above the PIT.[130]

### 1.3.3.3 HIPE Rheology

The rheological properties of HIPEs are affected by several variables such as droplet radius ($R$), interfacial tension ($\sigma$), the internal phase volume fraction, the nature of the stabilising surfactant, temperature, and the viscosity of the external phase ,$\eta_e$.[130] The viscosity of the internal phase, $\eta_i$, provided it is sufficiently high, can also have an effect upon the final viscosity of the HIPE, $\eta_{HIPE}$.[158]

The high levels of interfacial tension found within HIPEs give rise to a high viscosity that is characterised by a high yield stress, which is the shear stress required to induce flow. HIPEs therefore behave as non-Newtonian fluids.[132] Below the yield stress HIPEs act as viscoelastic solids due to the attraction between liquid droplets. Above the yield stress the viscosity will vary inversely to shear. The shear elasticity modulus, $G'$, of HIPEs is given by the following semi-empirical formula of Princen:[159]

$$G' = C\left(\frac{\sigma_0}{R}\right)\phi_v^{1/3}(\phi_v - \phi_c) \qquad \phi_c < \phi_v < 1 \qquad \text{(Eq. 1.13)}$$

where: $C$=1.77,

$\phi_c$ = 0.74,

$\phi_v$ the volume fraction of the HIPE,

$\sigma_0$ is the interfacial tension

and $R$ is the droplet radius.

Eq. 1.13 has been experimentally verified for the limit of $G'_{max} \cong 0.5\ (\sigma_o/R)$,[160,161] however, the dependence of $G'$ upon $\sigma_i$ has been the subject of some debate.[162,163]

Increasing surfactant concentration will lead to an associated increase in viscosity. The nature of the surfactant will also have an effect, with those that produce rigid interfacial films usually producing HIPEs with higher viscosities.[164] The nature of the surfactants becomes more pronounced with smaller average droplet sizes.[165] Increasing the internal phase volume also causes an increase in viscosity;[166] this is due to the higher energy requirements to efficiently mix the emulsion.

By decreasing the average droplet radii the total interfacial area increases, as a consequence so does the total interfacial tension which corresponds to an increase in viscosity.[167]

#### 1.3.3.4 HIPE Geometry

As mentioned, $\phi$ = 0.7405 represents the most efficient packing of uniform spheres. Consequently, the droplets of the internal phase in a HIPE are either polydisperse or deformed polyhedral, and can be both.[142,131] Though both polydisperse and monodisperse deformed systems can be formed, theoretical calculations suggest that a deformed monodisperse system is more favourable.[168] Lissant[124] calculated that for $\phi$ = 0.74 – 0.94 uniform emulsion droplets would take the form of rhomboidal dodecahedra, further deforming to tetrakaidecahedra if $\phi$ is increased to >94%. Lissant and Mayham later observed this polyhedral structure by means of SEM, as did Cameron and co-workers[169] by using cryo-SEM. Lissant and co-workers[170] noticed that the more stable emulsions showed the highest degree of monodispersity, with polydisperse droplets being observed in the early stages mixing or after some coalescence. Das and Ghosh[171] noted that initially droplets of the internal phase will be polydisperse spheres gradually transforming into a system of monodisperse polyhedral droplets. This is due to a greater efficiency of emulsification, which sees a reduction in radius of the larger droplets, which leads to an

increase in the total interfacial area. It has also been noted that when increasing external phase viscosity, the average droplet size will decrease.[172]

Though HIPEs tend to favour monodisperse geometry, they are rarely truly monodisperse and some degree of polydispersity, which is dependent upon the physical properties of the HIPE and the experimental conditions, is almost always observed.[132] Though a novel method for the production of truly monodisperse HIPEs has been developed by Bibette.[173]

## 1.4 References


1. J. Potočnik, *Off. J. Euro. Comm*., 2011, **L275**, 38-40
2. M. Faraday, *Phil. Trans. R. Soc. Lond.*, 1857, **147**, 145-181
3. T. Graham, *Philos. Trans. R. Soc. Lond.*,1861, **151**, 183-224
4. N. Taniguchi**,** Proceedings of the International Conference on Production Engineering, Tokyo, 1974
5. H. Kroto, H.W. Heath, S.C. O'Brien, R.F. Curl, R.E. Smalley, *Nature*, 1985, **318**, 162-163
6**.** BCC Research, *Nanotechnology: A Realistic Market Assessment*, 2012, Report Code: NAN031E
7. ASTM International (2006) E 2456-06
8. British Standards Institute, (2007), PAS 136:2007
9. International Organization for Standardization, (2008), ISO/TS 27687:2008
10. K. Tiede, A. B. A. Boxall, S.P. Tear, Steven, J. Lewis, H. David, M. Hassellov, *Food, Addit., Contam.*, 2008, **25**, 795-821
11. M. Hassellöv, R. Kaegi, in Enviromental and Human Health Impacts of Nanotechnology, ed J. R. Lead, E. Smith, Wiley-Blackwell, Chichester, 2009, ch. 6, pp. 211-266
12. S. Bandyopadhyay, J. R. Peralta-Videa, J. L. Gardea-Torresdey, *Environ. Eng. Sci.*, 2013, **30**, 118-125
13. H. Zänker, A. Schierz, *Annu. Rev. Anal. Chem.*, 2012, 5, 107–32
14.H. K. Mercus, in Particle Size Measurements, Springer, 2009, ch. 12, pp. 299-317
15. M. Filella, J. Zhang, M. E. Newman, J. Buffle, *Colloid. Surface. A.*, 1997, **120**, 27-46
16. Malvern Instruments Ltd. *DYNAMIC LIGHT SCATTERING COMMON TERMS DEFINED*, 2011
17. A. Ledin, S. Karlsson, A. Duker, B. Allard, *Water. Res.*, 1994, **28**, 1539-1545
18. J. Jiang, G. Oberdörster, P. Biswas, *J. Nanopart. Res.*, 2009, **11**, 77-89
19. H. Jans, X. Liu, L. Austin, G. Maes and Q. Huo, *Anal. Chem.*, 2009, **81**, 9425–9432
20. R. Xu in *Particle Characterization: Light Scattering Methods*, Kluwer Academic, Dordrecht, 2000, ch.2, pp. 56-110
21. F. Mallamace, N. Macali in *Light Scattering: Principles and Development* ed. W. Brown, Monographs on the physics and chemistry of materials, vol. 53 Oxford University Press, Oxford, 2002, 1st edn., ch.12, pp.381-438
22. Laser Diffraction Particle Sizing, Malvern Isntuments Ltd., UK., From Malvern Instruments Ltd. Website; http://tinyurl.com/k694gfa, accessed 24/7/2013.
23. S. A. Kübert, C. M. Keck, *J. Pharm. Technol. Drug. Res.*, 2013, http://dx.doi.org/10.7243/2050-120X-2-17
24. H. Suzuki, H. Onishi, K. Takahashi, S. Watanabe, *J. Biochem.*, 1978, **84**, 1529-1542
25. F. Gaskin, C. R. Cantor, *J. Mol. Biol.*, 1974, **89**, 737-758
26. J. M. Irache, C. Duuer, G. Ponchel, D. Duchene, *Int. J. Pharm.*, 1993, **90**, R9-R12
27. V. Guschin, W. Becker, N. Eisenreich, A. Bendfeld, *Chem. Eng. Technol.*, 2012, **35**, 317-322
28. F. Peng, D. L. Johnson, S. W. Effler, *J. Am. Water Ressor. As.*, 2002, **38**, 1453-65
29. *M110B Application Review NTA, Applications of Nanoparticle Tracking Analysis (NTA) in Nanoparticle Research*, 2009, NanoSlight Ltd., Technical Note
30.A. Malloy, B. Carr, *Part. Part. Syst. Charact.*, 2006, **23**, 197–204
31. V. Filipe, A. Hawe, W. Jiskoot, *Phram. Res.*, 2010, **27**, 796-810
32. Y. Mori, M. Furukawa, T. Hayashi, K. Nakamura, *Particul. Sci. Technol.*, 2006, **24**, 97-103
33. O. Kratky in *Small Angle X-ray Scattering* ed. O. Glatter, O. Kratky, Academic Press, London, 1st edn., 1982, ch. 1, pp. 3-13
34. H. Wang, W. Zhou, D. L. Ho, K. I. Winey, J. E. Fischer, C. J. Glinka, E. K. Hobbie, *Nano. Lett.*, 2004, **4**, 1789-1793
35. D. Mavrocordatos, W. Pronk, M. Boller, *Water Sci. Technol.*, 2004, **50**, 9–18
36. A. Dudkiewicz, K. Tiede, K. Loeschner, L. H. S. Jensen, E. Jensen, R. Wierzbicki, A. B. A. Boxall, K. Molhave, *TrAC-Trend. Anal. Chem*, 2011, **30**, 28–43
37. A. Taylor, K. M. Wilson, P. Murray, D. G. Fernig, R. Levy, *Chem. Soc. Rev.*, 2012, **41**, 2707-2717

38. M. Labrenz, G. K. Druschel, T. Thomsen-Ebert, B. Gilbert, S. A. Welch, K. M. Kemner, G. A. Logan, R. E. Summons, G. De Stasio, P. L. Bond, B. Lai, S. D. Kelly, J. F. Banfield, *Science*, 2000, **290**, 1744-1747
39. F. Zhang, Q. Jin, S. Chan, *J. Appl. Phys.*, 2004, **95**, 4319-4326
40. C. Y. Wang, C. Bottcher, D. W. Bahnemann, J. K. Dohrmann, *J. Nanoparticle Res.*, 2004, **6**, 119–122.
41. F. J. Doucet, J. R. Lead, L. Maguire, E.P. Achterberg, G. E. Millward. *J Environ Monit.*, 2005, **7**, 115–121
42. P. S. Redwood, J. R. Lead, R.M Harrison, I. P. Jones, S, Stoll, *Environ. Sci. Technol.*, 2005, **39**, 1962–1966
43. S. M. Webb, G. G. Leppard, J. F. Gaillard, *Environ. Sci. Technol.*, 2000, **34**, 1926-1933
44. C. Mondi, K. Leifer, D Mavroordatos, D. Perret, *J. Microsc-Oxford*, 2002, **207**, 180-190
45. D. Perret, J. F. Gaillard, J. Dominik, O. Atteia, *Environ. Sci. Technol.*, 2000,**34**, 3540-3546
46. G. Cliff, G. W. Lorimer, *J. Microsc-Oxford*, 1975, **103**, 203-207
47. R. Brydson in *Nanocharacterization* ed. A. I. Kirkland, J. L. Hutchinson, RSC Publishing, Cambridge, 1st edn., 2007, RSC nanoscience & nanotechnology vol. 3, ch.4, pp. 94-137
48. J. Buffle, R. R. Devite, D. Perret, G. G. Lappard, *Geochim. Cosmochim. Ac.*,1989, **53**, 399-408
49. D. Mavrocordatos, D. R. Kaegi, V. Schmatloch, *Atmos. Environ.*, 2002, **34**, 5653-5660
50. D. H. Anjum, N. K. Memon, S. Ho Chung, *Mater Lett.*, 2013, **108**, 134-138
51. E. Balinos, G. Papastavrou, K. J. Wilkinson in *Environmental Colloids and Particles: Behaviour, Structure and Characterization*, ed. K. J. Wilkinson, J. R. Lead, John Wiley and Sons, Chichester, 2007, ch. 9, pp. 405-468
52. Y. Oshikane, T. Kataoka, M. Okuda, S. Hara, H. Inoue, M. Nakano, *Sci. Technol. Adv. Mat.*, 2007, **8**,181-185
53. A. D. Maynard, *Philos. Trans. R. Soc. Lond. A.*, 2000, **358**, 2593–2609.
54. E. Betzig, J.K. Trautman, T.D. Harris, J.S. Weiner, R.L. Kostelak, *Science*, 1991, **251**, 1468-1470
55. V.Prasad, D. Semwogerere, E. R. Weeks, *J. Phys. Condens. Mat.*, 2007, **19**, 113102
56. J. R. Lead, K. J. Wilkinson, K. Starchev, S. Canonica, J. Buffle, *Environ. Sci. Technol.* 2000, **34**, 1365–1369
57. J. Thieme , I. McNulty, S. Vogt, D. Paterson, *Environ. Sci. Technol.*, 2007, **41**, 6885–6889
58. C-C. Chien, C-C. Cheng,H. H. Chen, Y. Hwu, Y. S. Chu, C. Petibois, A. Chen, Y-T.Ching, G. Margaritondo, *Anal. Bioanal. Chem.*, 2012, **404**, 1287-1296
59.W. W. Yu, L. Qu, W. Guo, X. Peng, *Chem. Mater.*, 2003, **15**, 2854-2860
60. G. V. Andrievsky, V. K. Klochkov, A. B. Bordyuh, G. I. Dovbeshko, *Chem. Phys. Lett.*, 2002, **364**, 8–17
61. A. Panácek, L. Kvítek, R. Prucek, M. Kolář, R. Veceřová, N. Pizúrová, V. K. Sharma, T. Nevěcná, R. Zbořil, *J. Phys. Chem. B.*, 2006, **110**, 16248-16253
62. R. E. Bailey, A. M. Smith, S. Nie, *Physica. E.*, 2004, **25**, 1-12
63. G. Zhang, D. Yang, E. Sacher, *J. Phys. Chem. C*, 2007, **111**, 565–570
64. Maria Sovago, E-J, Buis, M. Sandtke, *Spectrochim. Acta B, 2013,*In press, http://dx.doi.org/10.1016/j.sab.2013.05.033.
65. S. Y. Lee, H. J. Kim, R. Patel, S. J. Im, J. H. Kim, B. R. Min, *Polym. Adv. Technol.*, 2007, **18**, 562-568
66. H. Coflen, S. Tirosh, A. Zaban, *Langmuir*, 2003, **19**, 10654-10659
67. W. Anderson, D, Kozak, V. A. Coleman, Å K. Jämting, M. Trau, *J. Colloid. Interf. Sci.*,2013, **405**, 322–330
68. R. P.Carney, J. Y. Kim, H. Qian, R. Jin, H. Mehenni, F. Stellacci, O. M. Bakr, *Nat. Commun.*, 2011 **2**, 335
69. L. J. Gimbert, J. F. Banfield, *Rev. Mineral. Geochem.*, 2005, **58**, 109-155
70 .S. T. Fitzpatrick, in *Particle Size Distribution III*, ed. T. Prover, American Chemical Society, Washington D. C.,1998, ch. 19, pp 285–294
71. L. Calzolai, D. Gilliland, F. Rossi, *Food Addit Contam.*2012, **29**, 1183-1193

72. A. Braun, O. Couteau, K. Franks, V. Kestens, G. Roebben, A. Lamberty, T.P.J. Linsinger, *Adv. Powder Technol.*, 2011, **22**, 766–770
73. W. Jiang, D. B. Hibbert, G. Moran, J. Herrmann, Å. K. Jämting, V. A. Coleman, *RSC Adv.*, 2013,**3**, 7367-7374
74. L.A. Fielding, O. O. Mykhaylyk, S. P. Armes, P. W. Fowler, V. Mittal, S. Fitzpatrick, *Langmuir*, 2012, **28**, 2536-3544
75.K-G. Whalund, *J. Chromatogor.A.*, 2013, **1287**,97–112
76. J. C. Giddings, *Science*, 1993, **260**, 1906-1920
77. K. Tiede, A. B.A. Boxall, S. P. Tear, J. Lewis, H. David, M. Hassellöv, *Food Addit. Contam.*, 2008, **25**, 795-821
78. M. E. Hoque, K. Khosravi, K. Newman, C. D. Metcalfe, *J. Chromatagor. A.*, 2012, 1233, 109-115
79. M. H. Moon, D. J. Kang, J. H. Jung, J. M. Kim, *J. Sep. Sci.*, 2004, **27**, 710-717
80. L. J. Gimbert, R. E. Hamon, P. S. Casey, P. J. Worsfold, *Environ. Chem.*, 2007, **4**, 8-10
81. M. Baalousha, J. R. Lead, *Environ. Sci. Technol.*, 2007, **41**, 1111-1117
82. G. S. Duesberg, M. Burghard, J. Muster, G. Philpp, S. Roth, *Chem. Comm.*, 1998, **3**, 435-436
83. I.V. Perminova, F. H. Frimmel, A. V. Kudryavtsev, N. A. Kulikova, G. Abbt-Braun, S. Hesse, V. S. Petrosyan, *Environ. Sci. Technol*,. 2003, **37**, 2477-2485
84. Z. Asparnut, T. Yamada, L. W. Lim, T. Takeuchi, *Anal. Bioanal. Chem.*, 2008, **391**, 353-359
85. C. Gautier, R. Taras, S. Galdiali, T. Burgi, *Chirality*, 2008, **20**, 486-493
86. J. Hradila, A. Pisareva, M. Babica, D. Horak, *China Particuol.* 2007, **5**, 162–168
87. F. K. Liu, *Chromatographia*, 2009, **70,** 7–13
88. G. T. Wei, F. K. Liu, C. R. C. Wang, *Anal. Chem.*, 1999, **71,** 2085–2091
89. T. Arita, T. Yoshimura, T. Adschiri, *Nanoscale,* 2010, **2**, 1467–1473
90. A. M. Al-Somali, K. M. Krueger, J. C. Falkner, V. L. Colvin, *Anal. Chem.*, 2004, **76,** 5903–5910
91. H. Small, *J. Colloid Interface Sci*., 1974, **48,** 147–161
92. A. M. Striegel, A. K. Brewer, *Annu. Rev. Anal. Chem*., 2012, **5**, 15-34
93. H. Brenner, H. Gaydos, *J. Colloid Interf. Sci.*, 1977, **58**, 312-356
94. E. Venema, J. C. Kraak, H. Poppe, R. Tijssen, *J. Chromatogr. A.*,1996, **740**, 159-167
95. K. Tiede, A. B. A. Boxall, D. Tiede, S. P. Tear, H. David, J. Lewis, J. Anal. At. Spectrom., 2009, 24, 964–972
96. K. Tiede, A. B. A. Boxall, X. Wang, D. Gore, D. Tiede, M. Baxter, H. David, S. P. Tear, J. Lewis, *J. Anal. At. Spectrom.*, 2010, **25**, 1149-1154
97. T. Takeuchi, Z. S. Aspanut, L. W. Lim, *Anal. Sci.* 2009, **25**, 301–306
98. C. H. Fischer, M. Giersig, *J. Chromatogr. A*, 1994, **688,** 97–105
99. S. A. Pergantis, T. L. Jones-Lepp, E. M. Heithmar, *Anal Chem*, 2012, **84**,6454-6462
100. J. P.F. G. Helsper, R.J. B. Peters, L. Brouwer, S. Weigel, *Anal. Bioanal. Chem.*, **2013**. 405, 1181-1189
101. F. Leal-Calderon, V. Schmitt, J. Bibette in *Emulsion Science: Basic Principles*, Springer, New York, 2nd edn., 2007, ch. 1, pp. 5-51
102. P. Ghosh *Colloid and Interface Science*, PHI Learning, New Delhi, 2009,1st edn., ch. 3, pp. 69-94
103. H. Zhang, A. Cooper, Soft Matter, 2005, **1**, 107-113
104. P. B. Umbanhowar, V. Prasad, D. A. Weitz, *Langmuir*, 2000, **16**, 347-351
105. A. S. Utada, E. Lorenceau, D. R. Link, P. D. Kaplan, H. A. Stone, D. A. Weitz, *Science*, 2005, **308**, 537-541
106. K. Westesen, T. Wehler, *J. Pharmaceut. Sci.*, 1993, **82**, 1237-1244
107. M. M. Crowley in *Remington : the science and practice of pharmacy*, ed. D. B. Troy, Lippincott, Williams & Wilkins, Philadelphia, 2006, 21st edn., ch. 39 pp. 745-775.
108. I. Capek in *Emulsion Science and Technology,* ed. T. F. Tadros, Wiley-VCH, Weinheim, 2009, 1st edn., ch. 13, pp. 243-309
109. B. P. Binks in *Modern Aspects of Emulsion Science*, ed. B. P. Binks, Royal Society of Chemisty, Camberidge, 1998, 1st edn., ch. 1, pp. 1-55

110. T. F. Tadros, *Applied surfactants: principles and applications*, Wiley-VCH, Weinheim, 2005, 1st edn., ch. 13, pp. 433-502
111. T. F. Tadros in *Emulsion Science and Technology*, ed. T. F. Tadros, Wiley-VCH, Weinheim, 2009, 1st edn., Ch. 1, pp. 1-56
112. D. Myers in *Surfactant science and technology*, John Wiley & Sons, Hoboken, 2006, 3rd edn., ch. 2, pp. 29-79
113. D. ganguli, M. ganguli in *Inorganic Particle Synthesis via Macro and Microemulsions: A Micrometer to Nanometer Landscape*, Kluwer Academic/Plenum Publishers, New York, 2003, 1st edn., ch. 2, pp. 21-42
114. E. Ruckenstein, *Langmuir*, 1996, **12**, 6351-6353
115. W. C. Griffin, *J. Soc. Cosmet, Chem.*,1949, **1**, 311-326
116. Akzo Nobel Surface Chemistry LLC, Porduct, Emulisfication & HLB, 2008, Publication SC-08-06.
117. W. C. Griffin, *J. Soc. Cosmet, Chem.*,1954, **5**, 249-256
118. R. C. Pasquali, M. P. Taurozi, C. Bregni, *Inter. J. Pharm.*, 2008, **356**, 44-51
119. J. T. Davies, *Gas/Liquid and Liquid/Liquid Interfaces.Proceedings of 2nd International Conferacne on Surface Activity*, Butterworths, London, 1957, 426-438
120. S.U. Pickering, *J. Chem. Soc., Trans.*, 1907, **91**, 2001-2021
121. W. Ramsden, *Proc. R. Soc. Lond.*, 1903, **72**, 477-486
122. C. Casagrande, P. Fabre, M. Veyssie, E. Raphael, *Europhys. Lett.*, 1989, **9**, 251-255
123. B. P. Binks, P. D. I. Fletcher, *Langmuir*, 2001, **17**, 4707-4710
124. K. J. Lissant, *J. Coll. Interf. Sci.*, 1966, **22**, 462-468
125. G.J. Lye, D.C. Stuckey, *Colloids. Surf, A Physicochem. Eng. Asp.*, 1998, **131,** 119-136
126. J.M. Williams, *Langmuir*, 1991, **7**, 1370-1377
127. P. A. Reynolds, E. P. Gilbert, J. W. White, *J. Phys. Chem., B.*, 2000, **104**, 7012-7022
128. H. Hoffmann, *Adv. Coll. Interf. Sci.* 1990, **32**, 123-150
129. K. Kovalchuk, I. Masalova, A. Ya. Malkin, *Colloid J.*, 2010, **72**, 806-814
130. V. G. Babak, M. Stébé, *J. Disper. Sci. Technol.*, 2002, **23**, 1-22
131. G. Calderó, A. Patti, M. Llinàs, M. J. García-Celma, *Curr. Opin. Colloid In.*, 2012, **17**, 255–260
132. N. R. Cameron, D. C. Sherrington, *Adv. Polym. Sci.* 1996, **126**, 163-214
133. E. Ruckentein, J. S. Park, *Polymer*, 1992, **33**, 406-417
134. N. Brun, S. Ungereanu, H. Deleuze, R. Backov, *Chem. Soc. Rev.*, 2011, **40**, 771-788
135. N. R. Cameron, D. C. Sherrington, *J. Chem. Soc. Frarady Trans.*, 1996, **92**, 1543-1547
136. T. G. Mason, M. D. Lacasse, G. S. Grest, D. Levine, J. Bibette, D. A. Weitz, *Phys. Rev. E*, 1997, **56**, 3150-3166
137. K. Ozawa, C. Solans, H. Kunieda, *J. Coll. Interf. Sci.*, 1997, **188**, 275-281
138. L. Taisne, B. Cabane, *Langmuir*, 1998, **14**, 4744-4752
139. H. Maekawa, J. Esquena, S. Bishop, C. Solans, B. F. Chemlka, *Adv. Mater.*, 2003, **15**, 591-596
140. T. Förster, W. Von Rybinski, A. Wade, *Adv. Coll. Interf. Sci.*, 1995, **58**, 119-149
141. S. Sun, Z. Li, T. Nagi, *Angew. Chem.*, 2010, **122**, 2209-2212
142. N. R. Cameron, in Monolithic *Materials: Preparation, Properties and Applications Journal of Chromatography Library Vol. 67* ed. F. Švec, T. B. Tennikova, Z. Deyl, Elsevier, Amsterdam, 2003, Ch. 12, pp. 255-276
143. C. T. Lee, Jr., P. A. Psathas, K. P. Johnston, *Langmuir,* 1999, **15**, 6781-6791
144. P. A. Reynolds, E. P. Gilbert, M. J. Henderson, J. W. White, *J. Phys. Chem. B,* 2009, **113**, 12231-12242
145. P. A. Reynolds, E. P. Gilbert, M. J. Henderson, J. W. White, *J. Phys. Chem. B,* 2009, **113**, 12243-12256
146. H. H. Chen, E. Ruckenstein, *J. Coll. Interf. Sci*, 1991, **145**, 260-269
147. R. E. Ford, C. G. L. Furmidge, *J. Colloid Interf. Sci.*, 1966, **22**, 331-341
148. M. Capdevila, A. Maestro, M. Porras, J. M. Gutiérrez, *J. Coll. Interf. Sci.,* 2010, **345**, 27-33
149. J. Yang, G. Yang, H. Liu, L. Bai, Q. Zhang, *J. Appl. Polym. Sci.*, 2010, **119**, 412-418

150. S. Kovačič, D. Stefanec, P. Krajnc, *Macromolecules*, 2007, **40**, 8056-*8060*
151. R. Pons, C. Solans, M. J. Stébé, P. Erra, J-C. Ravey, *Prog. Coll. Polym. Sci.*, 1992, **89**, 110-113
152. V. Rajagopalan, C. Solans, H. Kunieda, *Coll. Polym. Sci.*, 1994, **272**, 1166-1173
153. H. Kunieda, N. Yano, C. Solans, *Coll. Surf.*, 1989, **36**, 313-322
154. J. Kizling, B. Kronberg, *Coll.Surf.*, 1990, **50**, 131-140
155. J. Kizling, B. Kronberg, J. Eriksson, *Adv. Colloid Interfac.*, 2006, **123-126**, 295-302
156. H. Kunieda, C. Solans, N. Shida, J. L. Parra, *Colloid. Surface.* 1987, **24**, 225-237
157. H. Wennerstrom, O. Soderman, U. Olsson, B. Lindman, *Colloid. Surface. A.*, 1997, **123-124**, 13-26
158. C. F. Welch, G. D. Rose, D. Malotky, S. T. Eckersley, *Langmuir*, 2006, **22**, 1544-1550
159. H. M. Princen, IlangmuirI, 1986, **2**, 519-524
160. R. Pons, P. Taylor, T. F. Tadros, *Colloid Polym. Sci.*, 1997, **275, 796-776**
161. N. Jager-Lézer, J.-F. Tranchant, V. Alard, C. Vu, P. C. Tchoreoff, J.-L. Gtossiord, *Rheol. Acta*, 1998, **37**, 129-138
162. Y. Hemar, D. S. Horne, *Langmuir*, 2000, **16**, 3050-3057
163. T. G. Mason, *Coll. Interf. Sci.*, 1999, **14**, 231-238
164. R. E. Ford, C. G. L. Fumbridge, *J. Sci. Food Agric.*, 1967, **18**, 419-428
165. I. Masalova, R. Foundazi, A. Ya. Malkin, *Colloid. Surface. A.*, 2011, **375**, 76-86
166. R. Pal, E. Rhodes, *J. Coll. Interf. Sci.*, 1985, **107**, 301-307
167. Y. Otsubo, P. K. Prund'homme, *Rheol. Acta*, 1994, **33**, 303-306
168. K. J. Lissant, *J Soc. Cosmet. Chem.*, 1970, **21**, 141-154
169. N. R Cameron, D. C. Sherrington, L. Albiston, D. P. Gregory, *Colloid. Polym. Sci.* 1996, **274**, 592-595
170. K. J. Lissant, K. G. Mayhan, *J. Coll. Interf. Sci*., 1973, **42**, 201-208
171. A. K. Das, P. K. Ghosh, *Langmuir*, 1990, **6**, 1668-1675
172. S. J. Lee, *Korea-Aust. Rheol. J*., 2006, **18**, 183-189
173. J. Bibette, *J. Coll. Interf. Sci.*, 1991, **147,** 474-478

# Chapter 2

# Silica Materials Produced from High Internal Phase Emulsions, SiHIPEs

## 2.1 Introduction

This chapter presents an investigation into the potential of porous silica materials (produced from high internal phase emulsions and termed SiHIPEs) to be applied as a chromatographic stationary phase for the separation of nanoparticles. HIPEs containing an inorganic precursor (frequently an alkoxide) have been used to produce a variety of 3D inorganic oxides,[1] with SiHIPEs appearing the most frequently in the literature. As well as SiHIPEs, the natural creaming of emulsions in the presence of a surfactant has also been used to produce macroporosity in silica.[2] Monoliths have been formed from regular o/w emulsions,[3,4] and there are also examples where porous silica materials have been produced from Pickering HIPEs stabilised with nano-sized silica particles.[5]

### 2.1.1 Aims and Objectives

The aim of the work carried out in this chapter was to investigate whether SiHIPE materials could be suitable for application as a chromatographic stationary phase for the separation of nanoparticles.

Sol-gel methods can frequently take up to a week.[3] To reduce synthesis time, the acid/base catalysis method initially presented by Hu and co-workers[6] was employed. Production of both SiHIPE beads and monoliths was investigated as potential materials to form as a packed column and a monolithic column, respectively. As SiHIPEs generally are less open than polyHIPEs, a particular focus was to improve the porosity of the resulting SiHIPE materials.

### 2.1.2 HIPEs as a Route to Porous Materials

As mentioned in chapter 1, HIPEs are a class of emulsions with an internal volume phase ($\phi$) of greater than 74.05 %.[7] In the context of porous solids they provide a flexible synthetic route to a variety of materials. This is achieved by including a polymerisable species within the external phase and then undertaking a polymerisation. Once polymerisation has been completed, the internal phase is removed and the result is a porous structure templated by the emulsion droplets. At this point, it is worth noting that though this work will only focus upon HIPEs as a route to porous materials, they can be used for various other synthetic purposes [*e.g.*, polymerisation of both phases produces a composite material (Figure 2.1)].

Porous materials produced from HIPEs typically exhibit a distinctive pore structure consisting of large macroporous cages (typically of the size range 1 - 100 $\mu$m) interconnected by smaller cage windows (Figure 2.2). These larger pores have assorted names in the literature (*e.g.*, cages, voids, cells or simply pores, with the smaller pores having variously been termed windows, interconnects and pore throats). Throughout this work the terms cage and window will be used.

As $\phi$ is decreased, the pore structure of the resultant templated material becomes increasingly closed,[8] though open structures can still be produced with $\phi$ as low as 0.6.[9]

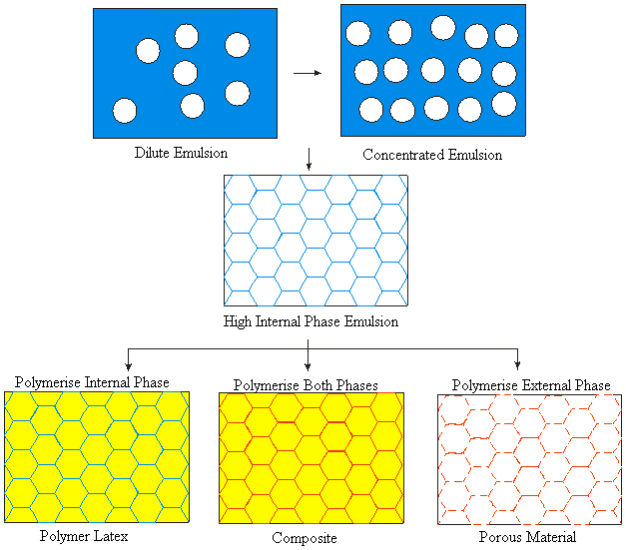


Figure 2.1: Schematic representation of the materials that can be formed from high internal phase emulsion templating

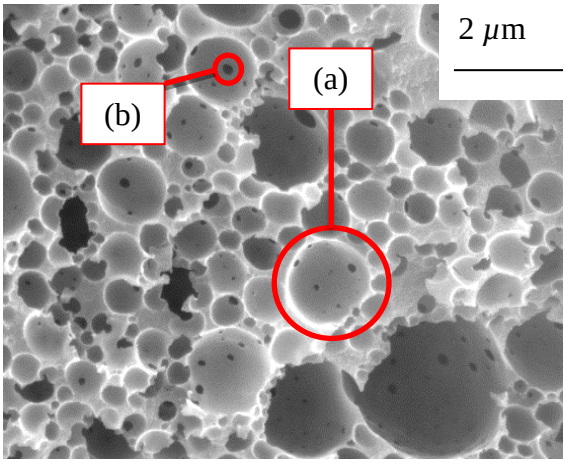


Figure 2.2: SEM image of a SiHIPE, illustrating (a): the larger cages and (b): the smaller windows. The image was obtained by the author at the University Of Manchester School Of Materials.

In their review, Zhang and Cooper[10] grouped HIPE templated porous materials into five categories:

1. Hydrophobic Polymers
2. Hydrophilic Polymers
3. Inorganic Oxides
4. Metals and Carbons
5. Organic-Inorganic Hybrids

As inorganic oxides (and SiHIPE in particular) are the only category relevant to this chapter, only these will be discussed here. Should information on other types of HIPE templated porous materials be required the reader is directed to the aforementioned review.

### 2.1.3 SiHIPE

Silica structures are by far the most widely studied HIPE templated inorganic materials. The most common system consists of an o/w HIPE, with an aqueous phase containing a silicon alkoxide as a precursor, of which tetraethyl orthosilicate (TEOS) is by far the most common.[3,11] The continuous phase is typically converted to a silica network by application of a sol-gel process which can take as long as a week.[11] Often, a small amount of either acid or base is present in the external phase – often referred to as the sol – to catalyse the reaction. The result is a porous silica structure which has been termed SiHIPE. Once the materials have been washed to remove the internal phase and then dried, they are usually calcined at ≈ 600 $^{o}$C.[11,12] The resultant materials can have BET surface areas up to 830 $m^2$ $g^{-1}$.[3] This is typically much higher than observed for polyHIPEs, due to inherent microporosity in the silica walls resulting from the sol-gel process.

An alternative method was developed by Hu and co-workers[6] that used both acid and base catalysis. A sol of TEOS, Triton X-405, hydrochloric acid and water was aged for 24 hours, after which an o/w HIPE was formed and then rapidly converted to a silica structure (or set) by immersion of droplets of the HIPE in diethylamine. The resulting materials displayed a similar macropore structure compared to SiHIPE materials previously produced by Carn *et al.*[3] (Fig. 4 d from reference 6 and Fig. 2 b from reference 3 respectively). However, the BET surface area was reduced (140 $m^2$ $g^{-1}$ compared to 830 $m^2$ $g^{-1}$). Comparison of the $N_2$ sorption isotherms suggests this was due to reduced

microporosity in the silica walls (Fig. 4 from reference 6 and Fig. 5 and Fig. 6 from reference 3, respectively).

The macrostructures of silica materials produced from both o/w and w/o HIPEs emulsions were investigated in detail by Yi and Yang.[13] They found that in o/w HIPEs the droplets would migrate and self-assemble in mobile, local regions that deteriorated the uniformity of the macropore structure**.**

Though o/w HIPEs are *de rigueur* for production of SiHIPE silica, Imhof and Pine used an oil-in-formaldehyde emulsion to synthesise ordered macroporous silica.[14] Sols of tetramethyl orthosilicate (TEOS) were added to an acidified (pH=2) mixture of water and formaldehyde, after which an emulsion with isooctane was formed. The emulsion was then concentrated by centrifugation and used as a template to produce macroporous silica.

Zhang and co-workers have used an aqueous/TEOS/monomer sol to form an o/w HIPE which was then polymerized by o/w/o sedimentation polymerisation, to form hybrid silica/polymer beads. Calcination of the beads subsequently removed the polymer producing hierarchically porous silica.[15]

### 2.1.4 Other Inorganic Oxides

Unlike silica alkoxides, other metal alkoxides are generally so reactive to water and even atmospheric moisture, that the use of an aqueous phase for emulsion templating becomes essentially prohibited. This can be overcome by reducing the reactivity of the precursor by reacting it with a chelating agent. Such an approach was used to prepare macroporous titania and zirconia.[16] Another method to overcome this problem is to use particulate precursors rather than molecular ones. Porous alumina was produced by use of a polymerisable w/o emulsion containing alumina powders. By increasing the water content of the emulsion, the porosity could also be increased.[17] Another technique that has

been used with considerable success is the use of a sacrificial polymer scaffold which prevents the inorganic precursors coming into direct contact with water. This has been used by Maekawa and co-workers[18] to prepare meso/macroporous materials of silica, titania and zirconia. Polystyrene polyHIPE monoliths were prepared from either a w/o or an o/w HIPE. A monomer/sol-gel mixture was then imbibed into the polyHIPE and the organic template was then removed by calcination or solvent extraction. A similar process has also been used by Zhang *et al.*[19] in which polyHIPE beads of poly(acrylamide) were submerged in an inorganic precursor solution. Subsequent sol-gel condensation in air was followed by calcination resulting in porous structures of silica, alumina, titania and zirconia.

Brun and co-workers[20] prepared SiHIPE monoliths with supported ionic liquid layers of 6 to 12 nm in thickness by impregnation with organic solvents. By subsequent entrapping of palladium ions within the ionic liquids, these hybrid foams were used as catalysts for the Heck coupling reaction of iodobenzene and cyclohexyl acrylate.

### 2.1.5 Organic-Silica Composites

This project does not deal with organic-inorganic composites experimentally, so only a brief overview will be given.

Polysiloxanes and polysilsesquioxanes are the most commonly studied variety of hybrids. Polysiloxanes are inorganic-organic polymers with the general chemical formula $[R_2SiO]_n$ in which the polymer backbone consists of -Si-O-Si- polymer chains. The strength and flexibility of these chains contributes to the elasticity of these materials which also have a high thermal stability and high permeability to gasses.[21,22] Silsesquioxanes contain siloxane groups ($R_2SiO$) in a random ladder or cage arrangement (Figure 2.3) and it is known that incorporating these materials either as a blend or via grafting into polymers can enhance thermal resistance, mechanical stability and oxidative resistance.[23]

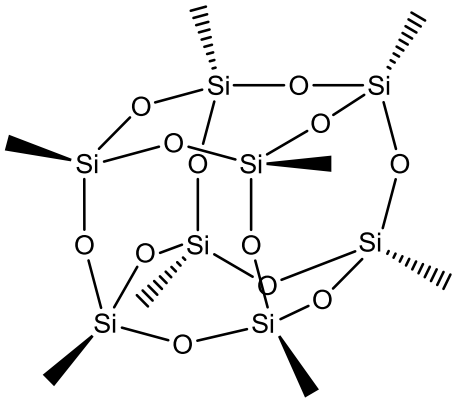


Figure 2.3: Silsesquioxane cage structure

Zhang *et al.* used a hydrolysed TEOS sol mixed with an aqueous monomer solution as the external phase of an o/w HIPE from which beads were produced by o/w/o sedimentation polymerisation.[19] They also reported a method in which poly(acrylamide) polyHIPE beads were produced and modified post-synthesis to create polymer-silica and polymer-metal oxide beads.[18,19]

Grosse *et al.*[24] have prepared organic-inorganic hybrids from polysiloxanes. Siloxanes formed part of the external phase of a w/o HIPE stabilised by a siloxane based surfactant. The siloxanes were then crosslinked by means of vinyl groups present. Ungureanu and co-workers[25] used o/w HIPEs to form "organo-Si(HIPE)" from an acidified and partially aqueous TEOS sol. Alkyl or phenyl trialkoxysilanes were also present in the sol which, after condensation, yielded an organic-inorganic hybrid. They have also formed mercapto- and amino-silane materials by post synthesis modification of a SiHIPE.[26] They further developed this work by using both the mercapto- and amino- SiHIPEs as supports for palladium nanoparticles which would catalyse the Mizoroki–Heck coupling reaction.[27]

Silverstein *et al.* [28,29,30] produced organic-inorganic hybrids by means of co-polymerisation of vinyl functionalised silsesquioxanes in an o/w HIPE. They also formed organic-inorganic hybrids from w/o HIPEs by radical co-polymerisation of styrene and

divinylbenzene with 3-methacryloxypropyl-trimethoxysilane in which the trimethoxysilyl groups subsequently underwent hydrolytic condensation to form a polysilsesquioxne network.[31]

### 2.1.6 Silica Sol-Gel

As mentioned, the majority of SiHIPE materials exploit a sol-gel process in the external phase to form silica materials. Sol-gel is a wet technique that can be used to form both glassy and ceramic materials at low temperatures and can be applied to form homogeneous silica materials with highly tailored properties. For SiHIPE production the sol-gel makes use of a silicon alkoxide precursor contained within the aqueous phase, this precursor reacts readily with the water and acid or base catalyst to form a colloidal suspensions of silica particles (the sol). The particles subsequently grow, forming chains which will ultimately form an interlinking network, turning the continuous phase into an inorganic silica gel.[32] Three reactions are generally used to describe the sol-gel process:

1. Hydrolysis (Figure 2.4)
2. Alcohol condensation
3. Water condensation (Figure 2.5)

The final characteristics of the sol-gel products are related to a number of factors which influence the rates of hydrolysis and condensation reactions, *e.g.*, temperature, pH, reagent concentrations, catalyst nature and concentration, water/Si molar ratio, and drying.[33]

Though the hydrolysis reaction can occur in the presence of water alone, a catalyst, (typically a mineral acid or amine) is commonly employed. The use of a catalyst greatly enhances the rate and completeness of hydrolysis.[34]

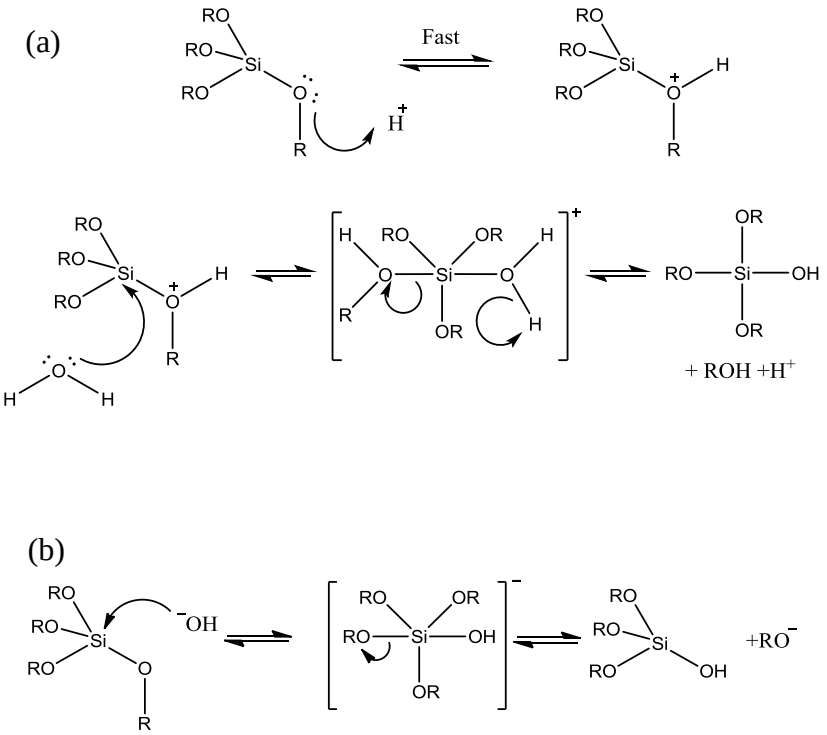


Figure 2.4: Mechanism of (a) acid catalysed and (b) base catalysed hydrolysis of a silicon alkoxide.

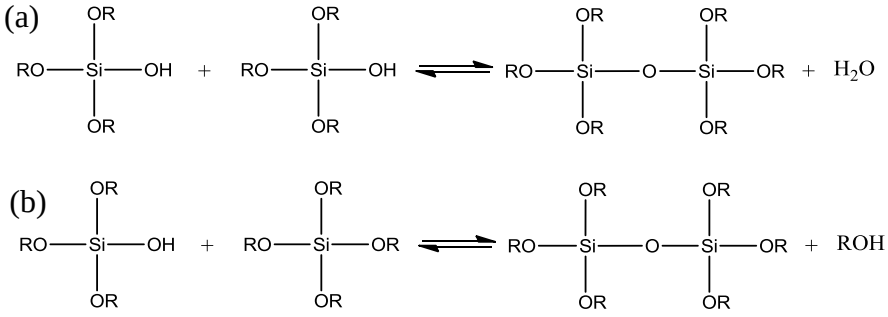


Figure 2.5: The (a) water condensation and (b) alcohol condensation reaction of the sol-gel process.

The silicon alkoxide effectively acts an inorganic monomer which polymerises to form a silica network in three stages:

1. Polymerisation of silicon alkoxide to form colloidal silica particles.
2. Growth of particles.
3. Particles link to form chains which extended throughout the dispersed phase, turning the sol into a gel.

The nature of the catalytic conditions influences the nature of the resulting silica chains. Under acid catalysed conditions, chains are primarily linear and randomly branched; they then entangle forming additional branches, resulting in gelling. Under basic catalysis, chains have a greater degree of branching which act as discrete clusters which do not interpenetrate prior to gelling.[35]

In this chapter, the sol-gel process developed by Hu and co-workers[6] will be used to produce SiHIPE materials from o/w HIPEs containing TEOS as a precursor in the aqueous phase.

## 2.2 Experimental

### 2.2.1 Preparation of SiHIPE Materials.

#### 2.2.1.1 Materials

Copper (I) chloride (CuCl; 97 % Sigma-Aldrich), heavy mineral oil (Sigma-Aldrich), n-hexane (Sigma-Aldrich), hydrochloric acid (Fisher, ~36 %), iron (III) chloride hexahydrate ($FeCl_3 \cdot 6H_2O$; Aldrich, 98 %), silicon dioxide nanopowder (15 nm; Aldrich, 99.5 %), tetraethyl orthosilicate (TEOS; Aldrich, 98 %), toluene (Sigma-Aldrich), trichloroethane (TCE; Fisher), triethylamine (TEA; Sigma-Aldrich, ≥99 %), Triton X-405 (octylphenol ethoxylate; Sigma-Aldrich, 70% in $H_2O$) and Tween 80 (polysorbate 80; Fluka) were all used as received.

#### 2.2.1.2 Preparation of Sols

TEOS (3 ml, 2.8 g), Triton X-405 (1.74 g)[i] or Tween 80 (1.1 g) and deionised water (1ml if Triton X-405 was being used or 1.5 ml if Tween 80 was being used) were mixed

[i] Triton X-405 was only used in Sols/HIPEs prepared for the experiments with accelerated aging of the sol. All other SiHIPEs reported in this chapter were prepared from HIPEs stabilised using Tween 80.

until homogeneous in a 25 ml glass sample vial. If either of the transition metal salts, $FeCl_3 \cdot 6H_2O$ (1 mmol, 0.27 g) or CuCl (1 mmol, 0.1 g), was required they were also added at this stage. Hydrochloric acid (70 $\mu$l) was then added with further stirring after which the sample vial was loosely sealed to prevent evaporation. For sols prepared using Triton X-405 the sol was either placed in a preheated oil bath for either up to 2 hours (60 $^{o}$C) or for up to 30 minutes (72 $^{o}$C), depending upon the aging conditions required. For sols prepared using Tween 80 they were then left to age for 24 hours at room temperature.

#### 2.2.1.3 Formation of HIPEs

Once aging of the sols was complete, a portion of the sol was transferred to a second 25 ml sample vial (1 ml or 0.75 ml for HIPEs of internal volume fractions of 0.80 or 0.85 respectively). For sols aged in an oil bath the samples were taken at the required time intervals (15 minutes, 30 minutes, 1 hour, 1 hour 30 minutes or 2 hours) and transferred to a second 25 ml sample vial in ice and cooled for 5 minutes.

To form the HIPE a PTFE 9 mm cross stirrer bar was placed in the vial with the sample of sol and stirred at the maximum speed of a magnetic stirrer plate. Heavy mineral oil (4.00 ml or 4.25 ml for HIPEs of internal volume fractions of 0.80 or 0.85 respectively) was then added at a rate of approximately 2 drops $s^{-1}$ to the sol from an addition funnel suspended directly above the centre of the stirrer bar.

#### 2.2.1.4 Formation of Beads from HIPEs

If a HIPE formed, it was packed into a 5 ml syringe and manually extruded drop-wise into a 25 ml sample vial half filled with TEA. The beads were then left to set (4 hours). After this, the TEA was decanted and replaced with n-hexane to remove the

mineral oil (4 hours or 30 minutes). After washing, the breads were left until they visually appeared dry (no more the 24 hours) and then calcined (See section 2.2.1.8).

If the beads had been prepared from a sol containing either CuCl or $FeCl_3 \cdot 6H_2O$ they were washed, post calcination, in hydrochloric acid (24 hours, with at least four changes of acid) and then deionised water (18 hours, three changes of water) after which they were dried in an oven at 65 $^oC$.

### 2.2.1.5 Toluene Reservoir

HIPEs with an oil fraction of 0.8 were prepared from a sol aged for 1 hour at 60$^oC$ via the methods detailed in sections 2.2.1.2 and 2.2.1.3. The HIPE was then placed in a 100 ml beaker containing toluene (50 ml) and stirred at 600 rpm with an IKA RW20.n overhead mechanical stirrer to fully disperse the HIPE. After 30 minutes, TEA (5 ml) was added to the mixture and stirring was continued for a further 30 seconds. The beads were left in the toluene to set (4 hours) and then removed using filter paper. They were then washed in n-hexane (4 hours) after which they were left to air dry (<12 hours, judged by observation) and then calcined (See section 2.2.1.8).

### 2.2.1.6 Formation SiHIPE monoliths

To form monolithic structures, a tubular mould was fashioned from a 2.5 ml polypropylene syringe with the top and bottom removed. The mould was perforated on four equally spaced planes along the length. Each plane consisted of four holes at 90 $^o$ to each other round the circumference. Once the HIPE had been formed by the methods detailed in sections 2.2.1.2 and 2.2.1.3, it was transferred to the mould and submerged in TEA and sealed. The HIPE was left in the amine for the designated time (overnight or 2 hours). For HIPEs which contained CuCl, the mould was submerged in heavy mineral oil,

instead of TEA, and left to cure at room temperature for a week. The oil was then replaced with TEA and the monolith left until it had turned from green to blue (< 2 hours). Once the monoliths had been set, the TEA was replaced with TCE and the monoliths were left for the allotted wash time (4 hours or 2 hours). After washing in TCE the monolith was left to air dry (judged by inspection, usually 1-2 days), and then removed from the mould and calcined (See section 2.2.1.8).

### 2.2.1.7 Monoliths from Sols Containing $SiO_2$ Nanopowder

The exact compositions of the sols are listed in Table 2.1, the following method takes Si53 as the example. $SiO_2$ nanopowder (0.44 g) and TEOS (1.12 g) were placed in a 25 ml sample vial and mixed together into a paste. Tween 80 (1.10 g) along with deionised water (0.60 ml) was then added to the paste and mixed. Lastly, HCl (70 $\mu$l) was added and all components were thoroughly mixed. The sol was then left to age at room temperature (18 hours) with mild stirring. After aging, a HIPE was formed by the methods detailed in section 2.2.1.2 and 2.2.1.3 and a monolith was then produced, set, washed and calcined as detailed in section 2.2.1.6 and section 2.2.1.8.

Table 2.1: Composition of sols containing both TEOS and $SiO_2$.

| Sample | $SiO_2$ Nanopowder (g/mmol) | TEOS (g/mmol) | Water (ml) | Tween 80 (g) | Hydrochloric Acid ($\mu$l) |
|---|---|---|---|---|---|
| Si53 | 0.44/7.32 | 1.20/5.37 | 0.60 | 1.06 | 70 |
| Si60 | 0.59/9.82 | 0.56/2.69 | 0.45 | 1.06 | 70 |
| Si62 | 0.44/7.32 | 1.20/5.37 | 0.60 | 1.06 | 70 |
| Si71 | 0.51/8.49 | 0.84/4.03 | 0.45 | 1.06 | 70 |

### 2.2.1.8 Calcination

Calcination was performed in an air atmosphere in a tube furnace (Carbolite GHC 12/450 fitted with a Eurotherm 2132 controller) at 650 $^{o}$C (2 hours). The temperature was raised via a staged heating process in which the temperature was increased in steps of 100

$^{o}$C (starting at 100 $^{o}$C), at a ramp rate of 5 $^{o}$C min$^{-1}$. After each 100 $^{o}$C increase, the furnace would dwell at the temperature for 1 hour, after which the temperature would again rise by 100 $^{o}$C. The process repeated until the maximum temperature was reached, at which point the furnace would dwell for 2 hours before naturally cooling to ambient temperature.

### 2.2.2 Measurements

#### 2.2.2.1 Surface Area

Surface areas were determined using a Beckman Coulter SA(TM) 3100 Surface Area and Pore Size Analyser. Samples were outgassed at a maximum temperature of 360 $^{o}$C for 240 minutes and the analysis was then run using nitrogen as the adsorbate at 77 K. Surface area calculations were obtained from the Brunauer-Emmett-Teller (BET) model of adsorption using a 10 point analysis.

#### 2.2.2.2 Scanning Electron Microscopy (SEM)

SEM at the University Of Manchester School Of Materials on a Phillips XL30 FEG SEM, all samples had previously been sputter coated with gold/palladium.

The cage and cage-window diameters were calculated from SEM by manual measurement (of around ≈ 100 entities for both windows and cages) with software designed for the measurement of nanoparticles. From this raw data, size distributions were produced for both the cages and windows. The raw data was also used to produce average diameters for the cages and windows (number, $D_n$ , area, $D_a$, and volume, $D_v$, diameters were produced for the cages and number, $d_n$, and area, $d_a$, averages were produced for the windows). Once the average diameter had been determined a statistical correction was applied by multiplying the average value measured from SEM by $2/(3^{1/2})$. (The explanation for the statistical correction is given in reference 36 and in section A1.1 of appendix 1).

The openness of the SiHIPE materials was, when possible, calculated from SEM by the calculation proposed by Pulko and Krajnc[37] which is detailed in section A1.2 of appendix 1.

## 2.3 Results and discussion

### 2.3.1 Effect of Temperature upon Sol Aging

Hu and co-workers, who first presented the method utilised for production of the SiHIPE materials in this chapter, required the sol to be aged for 24 hours at room temperature. This was attributed to the need for at least partial progression of the sol-gel process. Hydrolysis of silica will form small nano sized $Si_x(OEt)_y(OH)_z$ particles, which then grow into clusters, which eventually interlink and gel the sol. However, before gelling the sol they will cause an increase in the viscosity of the sol. This increase in viscosity was believed to be crucial in giving the HIPE kinetic stability.[6] To reduce aging time and thus reduce the time of the overall production process of SiHIPE materials, the aging of the sols was accelerated by heating under various conditions. These conditions and whether the sol would form 80% internal phase HIPE are shown in Table 2.2.

Before heating all sols appeared identical; clear liquids with a yellow coloration. However, after aging, despite having the same visual appearance, those that had been aged at elevated temperatures had undergone a marked increase in viscosity when compared to sols aged for the same time at ambient temperature. This can be attributed to the fact that as temperature increases so does reaction rate (all other factors being equal), thus the rate of the reactions in sol-gel process increase. This increases the rate of silica particle growth which, as particles form chains and begin to entangle, increases viscosity. It was also observed that if heating was extended much beyond 2 hours (at 60 $^{o}$C) then sols would gel making HIPE formation impossible. As expected, the sols which had been heated – even

for as little as ten minutes (Si-2B) – would form HIPEs, whereas the sols aged for equivalent times at room temperature did not. This was attributed to insufficient formation and interlinking of silica chains**.**

Table 2.2: Summary of aging conditions of silica sols and the result of subsequent formation of an 80% oil phase HIPE.

| Sample | Heating Time (min) | Temperature ($^{o}$C) | HIPE formed |
|---|---|---|---|
| Si-2B | 10 | 73 | Yes |
| Si-1E | 30 | 60 | Yes |
| Si-1F | 60 | 60 | Yes |
| Si-1G | 90 | 60 | Yes |
| Si-1H | 120 | 60 | Yes |
| Si-3A | 30 | Room Temp. | No |
| Si-3B | 60 | Room Temp. | No |
| Si-3C | 90 | Room Temp. | No |
| Si-3D | 120 | Room Temp. | No |

The HIPEs once formed, presented as white liquids with very high viscosity, such that it allowed the HIPE to remain in the sample vial when inverted. Post calcination the beads had the appearance of a glassy phase material (due to fusing of the silica particles) with a diameter ≈ 3 mm, and shapes between spherical and tear dropped (Figure 2.6). Comparison of the nitrogen sorption isotherms (Figure 2.6) of the beads produced from sols aged for 10 minutes at 72 $^{o}$C (Si-2B) and 60 minutes at 60 $^{o}$C (Si-1F) show similar internal pore structures. Porosity is, as expected, almost exclusively macroporous (> 50 nm). Mesoporosity (2 nm to 50 nm) is minimal, as evidenced by the lack of significant hysteresis. The trivial uptake at very low relative pressure indicates only small amounts of microporosity (< 2 nm). The small amount of microporosity observed is likely to be as a result of the inherent microporosity in the silica walls, which results from the sol gel process, or from removal of the surfactant head during calcination from the silica walls.

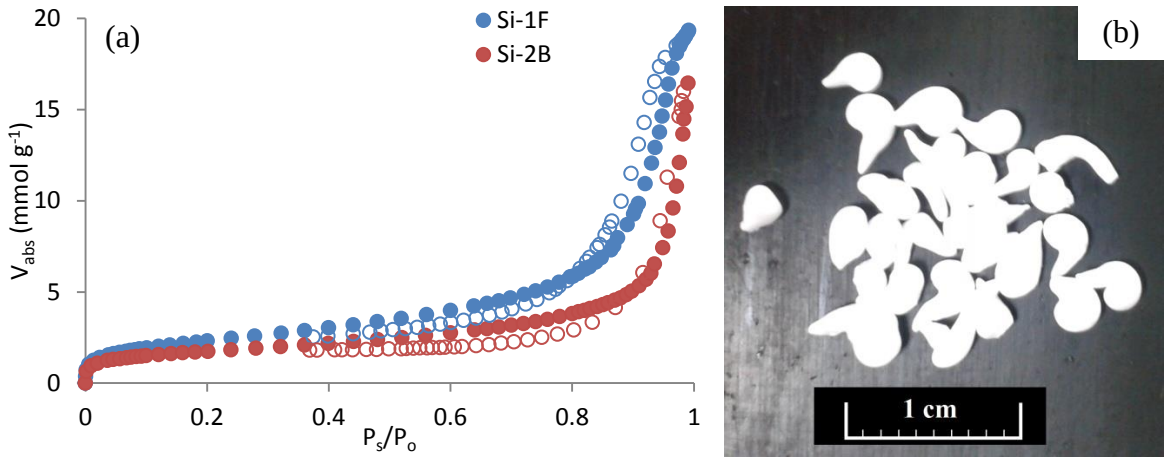


Figure 2.6: (a) BET isotherms showing adsorption (●) and desorption (○) for Silica beads produced from sols aged for 1hr at 60°C (red) and 10 minutes at 73 °C (blue). (b) Images of beads produced from a sol aged at 60 °C of 1 hour (Si-1F)

The internal pore structure, of the sample Si-1F, was further elucidated by SEM, revealing the expected two tier macroporous structure of large cages interconnected by smaller windows (Table 2.3). This is the classic hierarchical pore structure observed in materials produced from HIPEs, be they organic or inorganic. The large pores are cages templated by the emulsion droplets, with the cage windows most likely forming during the polymerisation process due to density differences between the silica gel phase silica sol. These density differences result in shrinkage of the interfacial film separating the droplets causing rupture at the thinnest point forming the windows.[38,39]

Table 2.3: Average cage and cage window diameters obtained from SEM of the SiHIPE sample Si-1F

| Sample | Average Cage Diameter ($\mu$m) | | Average Window Diameter ($\mu$m) | | Openness (%) |
|---|---|---|---|---|---|
| | $D_n$ / %RSD [a] | $D_v$ / %RSD [b] | $d_n$ / %RSD [c] | $d_a$ / %RSD [d] | |
| Si-1F | 2.9 / 81 | 4.5 / 156 | 0.3 / 56 | 0.4/109 | 8 |

[a] $D_n$ = number average diameter of the cages.
[b] $D_v$ = volume average diameter of the cages.
[c] $d_n$ = number average diameter of the windows.
[d] $d_a$ = area average diameter of the windows.

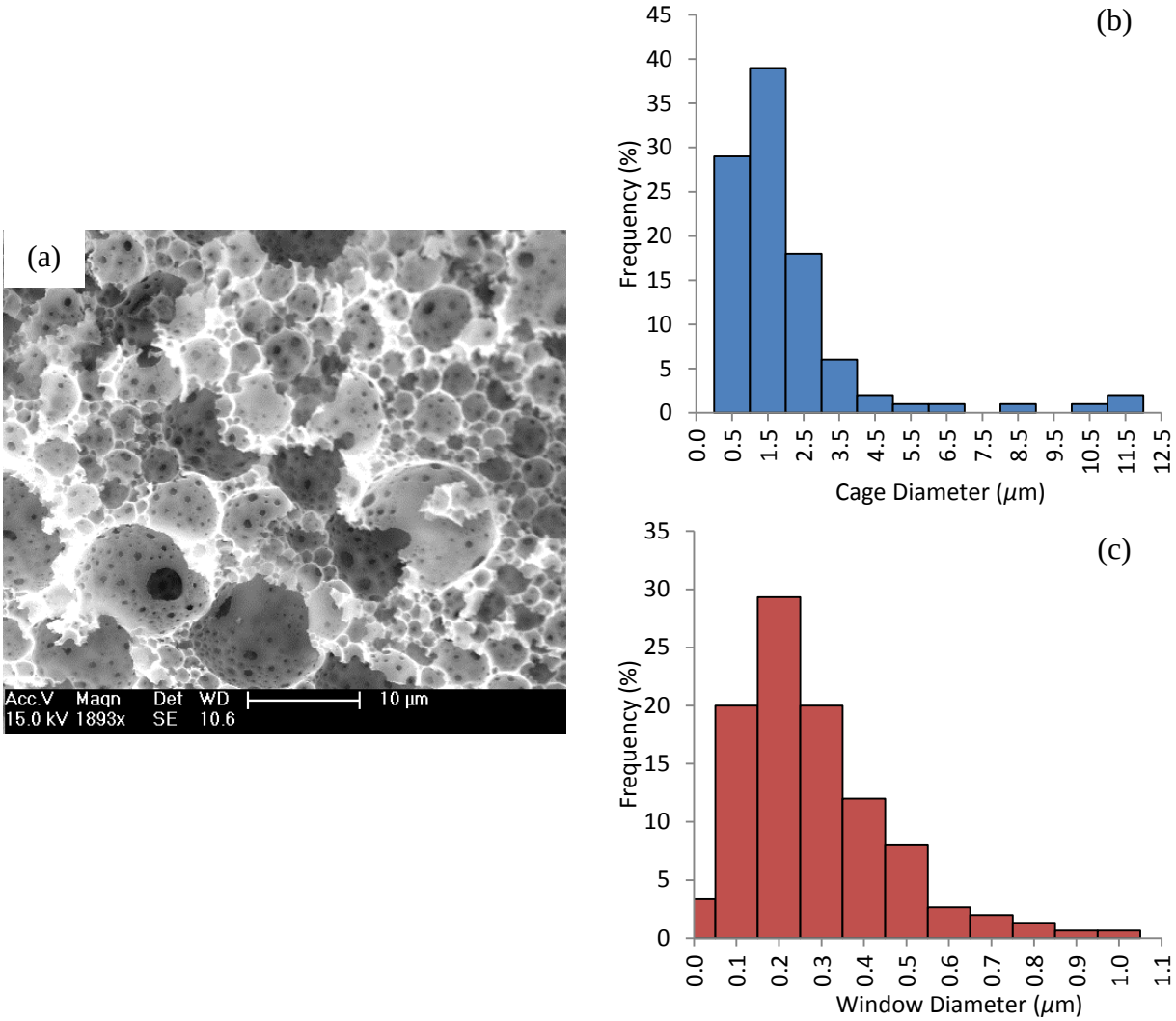


Figure 2.7: SEM image (a) and size distributions of (b) the cages and (c) the windows of the SiHIPE Si-1F produced from an 80% internal volume HIPE from a sol aged for 1 hour at 60 °C.

Table 2.4: Comparison of BET surface areas and absorption volumes of SiHIPE beads produced from HIPEs with a 0.8 oil fraction and from sols aged under different conditions. Both HIPEs were stabilised by the surfactant Triton X-405.

| Sample | Sol Aging Conditions | BET Surface Area ($m^2$ $g^{-1}$) | Maximum Absorbance (mmol $g^{-1}$) |
|---|---|---|---|
| Si-2B | 10 min @ 72 °C | 130 | 19.3 @ $P_s/P_o$ = 0.9914 |
| Si-1F | 30 min @ 60 °C | 160 | 16.5 @ $P_s/P_o$ = 0.9905 |

Pore size distributions created from the SEM micrographs, (Figure 2.7) show little overlap between the diameters of the cages and of the windows. The windows also had a narrower size distribution, likely due to the fact that the emulsion droplets which template

the cages will be subject to coalescence and Ostwald ripening before gelling of the silica network which will increase the size distribution of the droplets. The sizes and distribution of the cages is consistent with those of SiHIPE beads previously produced by acid/amine catalysis,[6] suggesting that thermally accelerating sol aging does not affect the subsequent HIPE.

The BET surface areas and maximum absorbed volume of the beads (Table 2.4) are comparable (Si-2B), or slightly greater (Si-1F by ≈ 20 $m^2$ $g^{-1}$) to similar beads previously produced from HIPEs of an 80% oil content,[6] but without accelerated aging of the sol. Further suggesting that heating the sol does not negatively affect HIPE formation or the sol-gel process utilised to produce the beads.

When Tween 80 was used as the surfactant in place of Triton X-405, the HIPEs, and the resulting beads, visually appeared identical. However, interestingly, the BET surface area of the beads more than doubled (Table 2.5). Comparison of the BET sorption isotherms (Figure 2.8 for the SiHIPE beads produced using Tween 80 and Figure 2.6 for the beads produced using Triton X-405) show that the while the macroporosity and mesoporosity, as well as the volume of $N_2$ adsorbed is similar irrespective of surfactant used, there was greater microporosity in the beads produced using Tween 80. It is this greater microporosity that is responsible for the greater surface area.

Table 2.5: BET surface areas and absorption volumes of SiHIPE beads produced from HIPEs stabilised by Tween 80.

| Sample | HIPE Oil Volume Fraction | BET Surface Area ($m^2$ $g^{-1}$) | Maximum Adsorbance (mmol $g^{-1}$) |
|---|---|---|---|
| Si40b | 0.80 | 340 | 17.4 @ $P_s/P_o$ = 0.9935 |
| Si85 | 0.85 | 380 | 15.7 @ $P_s/P_o$ = 0.9884 |

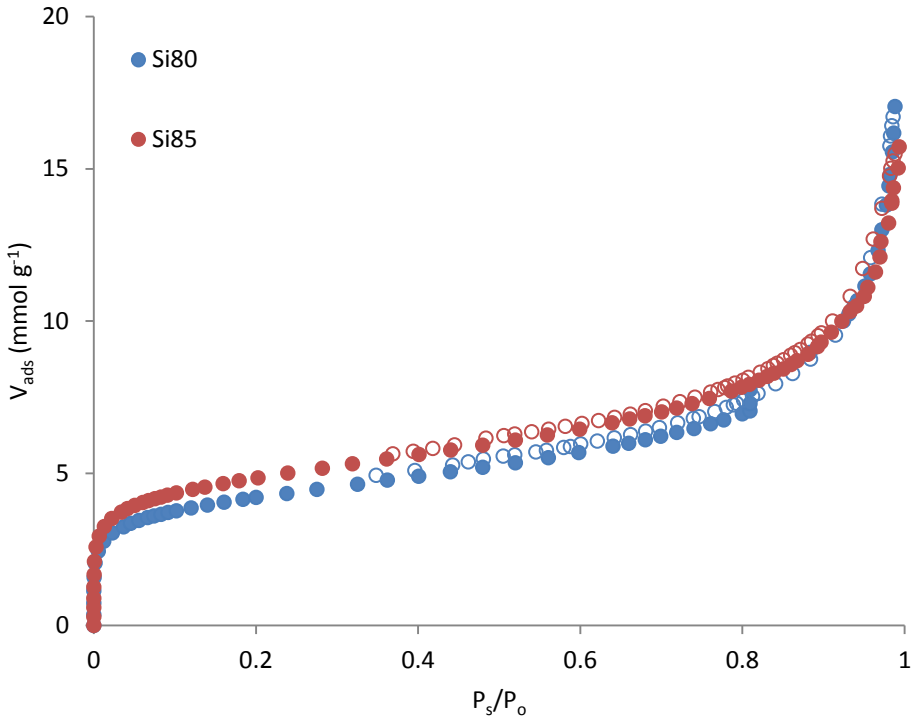


Figure 2.8: BET sorption isotherms showing adsorption (●) and desorption (○), of silica beads produced from HIPEs stabilised by Tween 80

Table 2.6: Average cage and average window diameters obtained from SEM of the SiHIPE sample Si-40b which was produced from a HIPE stabilised by Tween 80.

| Sample | Average Cage Diameter ($\mu$m) | | Average Window Diameter ($\mu$m) | | Openness (%) |
|---|---|---|---|---|---|
| | $D_n$ / %RSD [a] | $D_v$ / %RSD [b] | $d_n$ / %RSD [c] | $d_a$ / %RSD [d] | |
| Si-40b | 0.8 / 66 | 1.1 / 150 | 0.1 / 64 | 0.1/132 | 5 |

[a] $D_n$ = number average diameter of the cages.
[b] $D_v$ = volume average diameter of the cages.
[c] $d_n$ = number average diameter of the windows.
[d] $d_a$ = area average diameter of the windows

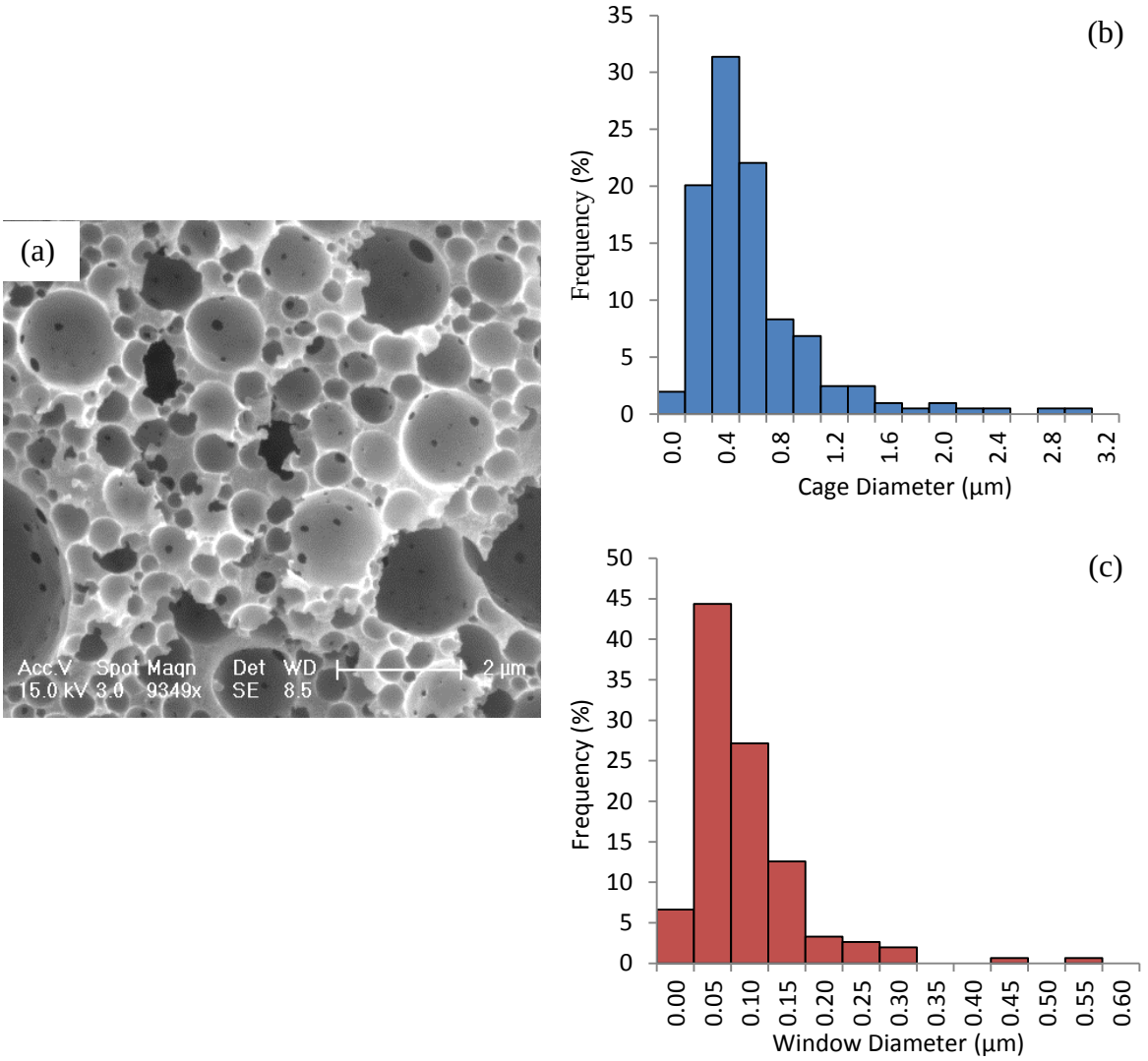


Figure 2.9: SEM (a) of the SiHIPE sample Si40b (produced from a HIPE stabilised by Tween 80) and the (b) cage and (c) window size distributions obtained from the SEM.

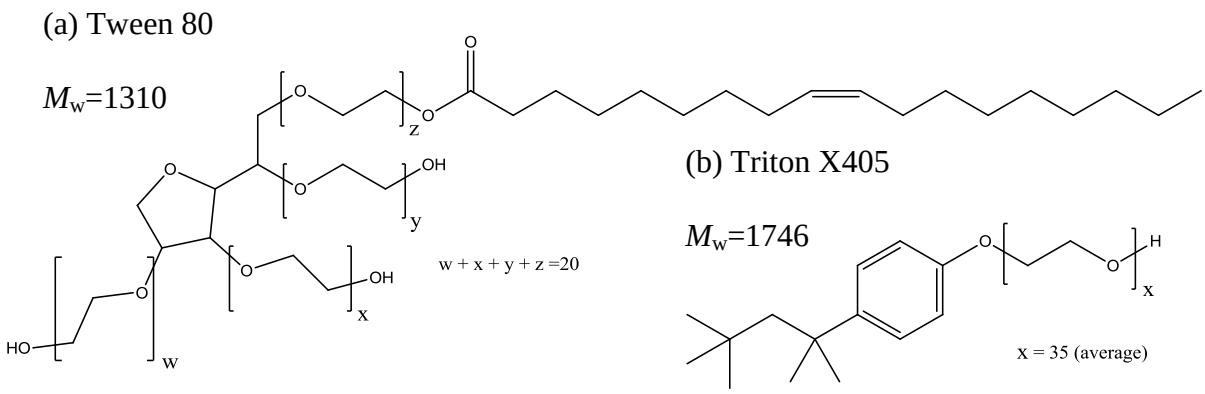


Figure 2.10: Structure of the surfactants (a) Tween 80 and (b) Triton X-405. Tween 80 hydrophile $M_w$ = 1044 and Triton X-405 hydrophile $M_w$ = 1557 (average)

It is probable that the change of surfactant was the cause of the increased microporosity. The surfactant sits at the oil-water interface, with the hydrophilic head located within the external (aqueous) phase of the HIPE. When the external phase gels the surfactant becomes entrapped and is not likely to be removed by washing. However, calcination thermally decomposes the surfactant resulting in pores in the silica network (this has been demonstrated by using high molecular weight surfactants to direct mesoporosity into silica[40,41]). While the hydrophiles of Tween 80 and Triton X-405 are chemically similar (both are composed of poly(ethylene oxide) (PEO) chains) they are structurally different. The PEO chains take the form of a single, linear chain in Triton X-405, whereas in Tween 80 they form four branches (Figure 2.10). It is tentatively suggested that this branched structure which, despite the lower molecular weight of the hydrophile, may be more efficient at templating the micropores.

SEM showed that both cages and cage windows of Si40b were smaller than those of Si-1F (Figure 2.9). Cage windows were also less numerous (Table 2.6) resulting in a less open structure (openness of 5 % compared to 8 %).

### 2.3.2 Reservoir dispersion of the HIPE to control bead formation.

The high viscosity of the HIPEs meant that the manual extrusion method, discussed in the previous section, frequently produced beads that were oblate or teardrop shaped (rather than spherical) and it was also not possible to form beads smaller than 2 mm. These sizes and shapes would prevent efficient packing and would result in large interstitial voids between beads which would severely limit, if not completely negate, any potential chromatography performance as a packing material.

In an attempt to produce smaller spherical beads, a HIPE with oil fraction of 0.80 was dispersed with rapid stirring in a toluene reservoir, forming an o/w/o emulsion. The

hope was that the stirring would form small, polydisperse HIPE droplets which could be gelled by addition of TEA to the reaction. Initially, it was thought the HIPE had collapsed after setting as no beads were visually apparent. However, due to the similar refractive indexes of silica (n=1.46)[42] and toluene (n=1.50)[43] it was not possible to observe them visually until the toluene had been decanted. The resultant beads were much smaller (some <1 mm) and more uniform in shape than beads produced by manual extrusion; however, they were still too large to make an effective packing material (Figure 2.11).

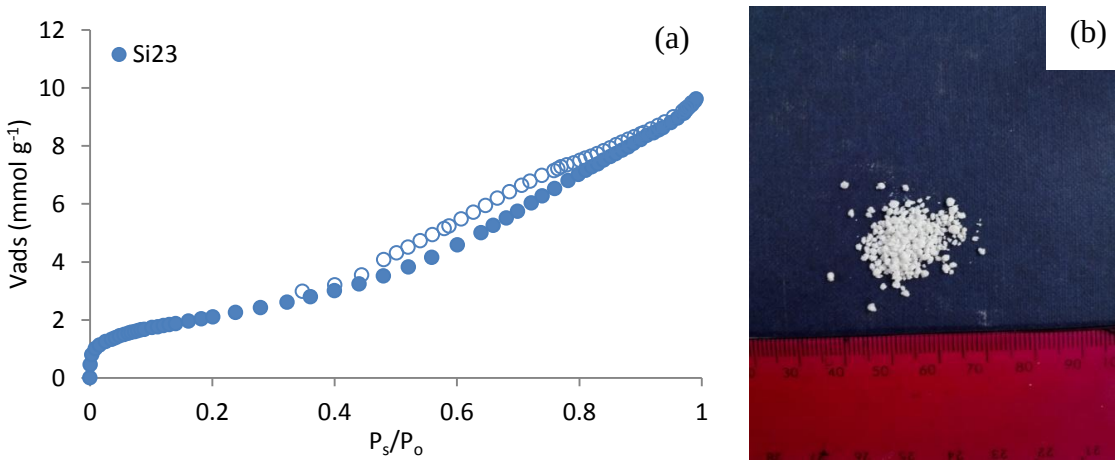


Figure 2.11: (a) BET Isotherm of porous silica beads produced from a HIPE dispersed in toluene showing adsorption (●) and desorption (○), and (b) image of beads produced from HIPE dispersed in toluene.

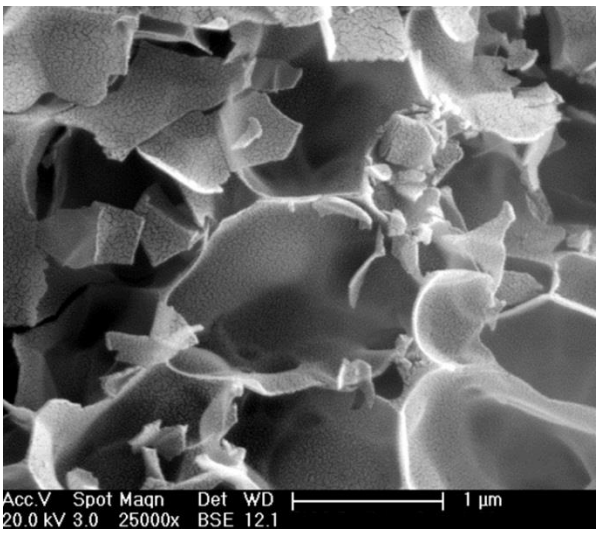


Figure 2.12: SEM micrograph of the internal structure of silica beads prepared by dispersion of a HIPE in a toluene reservoir.

The BET surface area of 150 $m^2$ $g^{-1}$ was comparable to other beads produced using Triton X-405 as the surfactant; however, the $N_2$ volume adsorbed was considerably less. The BET isotherm (Figure 2.11) shows that, as expected, the majority of the porosity is in the form of macropores, with negligible microporosity present. The small hysteresis present on the isotherm indicates the appearance of a small amount of mesoporosity. SEM micrographs of the beads internal structure (Figure 2.12) shows the expected macroporous cages templated by the emulsion droplets which visually appear smaller than in the previous beads; however, the interconnecting windows are no longer present. This closed pore structure is often observed when materials are produced from emulsions with internal volume fractions below the HIPEs threshold.[8] Since no secondary stabiliser was present in the toluene, it is possible that prior to the introduction of TEA a portion of the HIPE oil phase was washed away by the toluene resulting in a less concentrated emulsion. This would account for both the closed pore structure and the reduced size of the cages.

### 2.3.3 Transition Metal Salts as Additional Porogens

Transition metal compounds have previously been used to increase meso and microporosity in silica materials,[44,45] thus in an attempt to increase the porosity of the SiHIPE beads the transition metal salts $FeCl_3 \cdot 6H_2O$ and CuCl were dissolved in the sol prior to HIPE formation. It was theorised that when the HIPE was exposed to the TEA, the salts would react with the amine forming precipitated species within the silica network. Once these had been removed by washing with hydrochloric acid, porosity would be increased.

$FeCl_3 \cdot 6H_2O$ dissolved readily in the sol resulting in an orange sol which formed a yellow HIPE. CuCl was only soluble in the sol once TEOS, water and acid had been

added, and would not dissolve in any binary mixtures of the two, both the sol and the resulting HIPE appeared green (Figure 2.13).

When submerged in TEA, both sets of HIPEs displayed a clear and monitorable colour change as the TEA diffused through the aqueous phase of the HIPE. HIPEs which contained CuCl changed from green to light blue, whereas HIPEs containing $FeCl_3$ changed from yellow to orange/brown. The colour of the beads did not change after drying and calcination, however it did darken as water and sol-gel products were removed, concentrating the metal species. Once the metal species had been removed by washing with HCl, the result was white silica beads (Figure 2.13) similar in appearance to those previously produced and displayed in Figure 2.6.

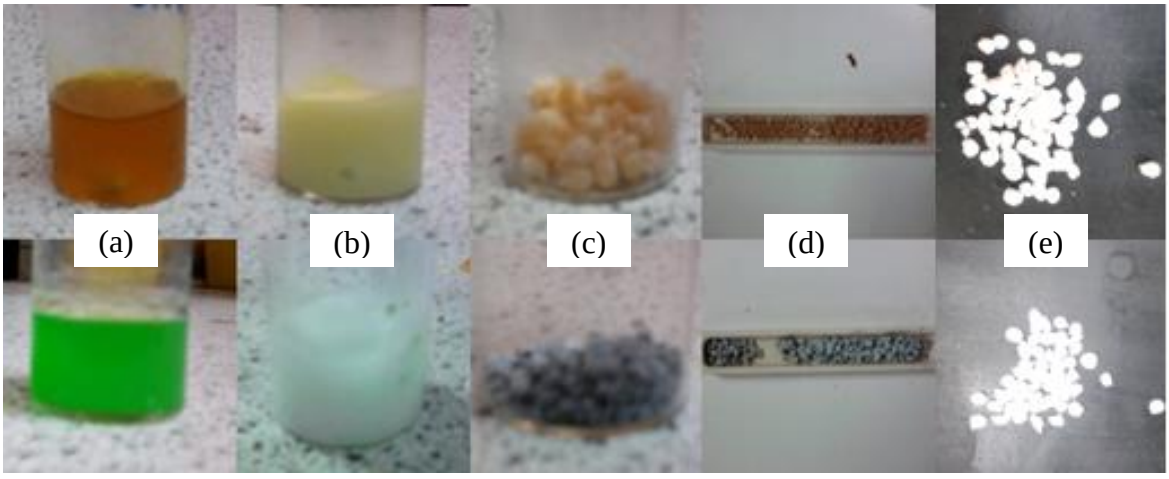


Figure 2.13: Images of (a) the Sols, (b) HIPEs, (c) beads after setting in TEA, (d) beads after calcination and (e) the beads after washing in conc. HCl then water. The samples displayed in top row contained $FeCl_3 \cdot H_2O$ in the sol and bottom row contained CuCl the sol.

Analysis by $N_2$ sorption showed a significant increase in the BET surface area of the beads (Table 2.7) compared to the SiHIPE beads detailed in section 2.3.1. SiCu2a had a surface area of double the largest so far measured (Si85) and approaching the levels possible with slow curing of the HIPE.3 Similar surface areas were produced with both metal salts, and as expected, the surface area was larger when the oil fraction of the initial

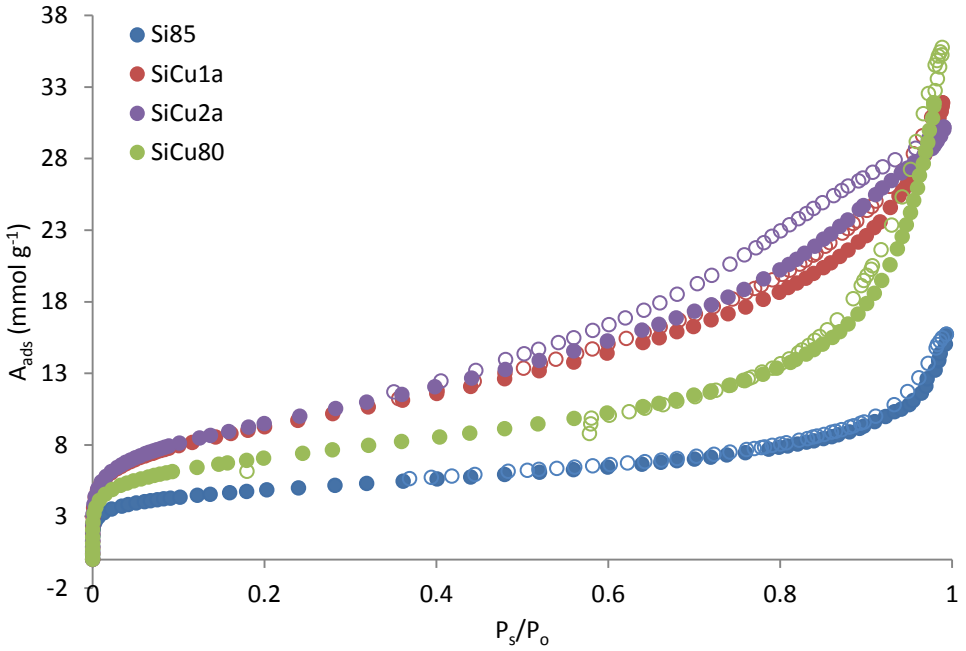


Figure 2.14: $N_2$ sorption isotherms of SiHIPE beads prepared from a sol containing 1 mmol of CuCl, showing adsorption (●) and desorption (○).The isotherm of the SiHIPE beads with the highest surface area (prepared with a transition metal salt and an internal phase volume fraction 0.85) is also included for comparison

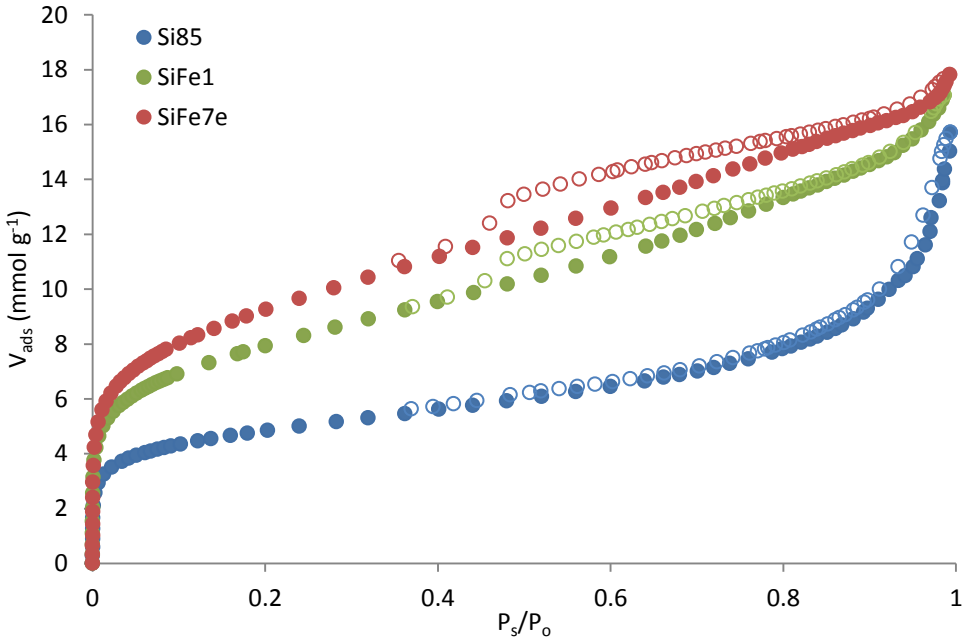


Figure 2.15: $N_2$ sorption isotherms of SiHIPE beads prepared from a sol containing 1 mmol of $FeCl_3 \cdot 6H_2O$, showing adsorption (●) and desorption (○).The isotherm of the SiHIPE beads with the highest surface area (prepared with a transition metal salt and an internal phase volume fraction 0.85) is also included for comparison.

HIPE was greater. While the absorbed volume of the beads did not increase much from previous values when $FeCl_3$ was included in the sol, this was not the case with CuCl. A significant increase in adsorbed volume being recorded, with all samples having values greater than 30 mmol $g^{-1}$, more than 10 mmol $g^{-1}$ greater than the largest value up to this point.

The $N_2$ sorption isotherms (Figure 2.14 and Figure 2.15) show that the cause of the high surface area was significantly increased microporosity compared to beads prepared previously. Hysteresis was present to varying degrees in the desorption isotherms of most samples, indicating the emergence of non-trivial mesoporosity.

Table 2.7: Surface areas and maximum adsorbed volumes of SiHIPE beads produced from sols containing transition metal salts.

| Sample | Transition Metal Salt in Sol | Internal Phase Volume Fraction | BET Surface area ($m^2$ $g^{-1}$) | Maximum Absorbance (mmol $g^{-1}$) |
|---|---|---|---|---|
| SiFe7e | $FeCl_3 \cdot 6H_2O$ | 0.85 | 750 | 17.8 ($P_s/P_o$ = 0.9925) |
| SiFe1 | $FeCl_3 \cdot 6H_2O$ | 0.80 | 640 | 17.1 ($P_s/P_o$ = 0.9862) |
| SiCu80 | CuCl | 0.80 | 570 | 35.8 ($P_s/P_o$ = 0.9889) |
| SiCu1a | CuCl | 0.85 | 750 | 31.9 ($P_s/P_o$ = 0.9890) |
| SiCu2a | CuCl | 0.85 | 770 | 30.2 ($P_s/P_o$ = 0.9906) |
| Si85 | None | 0.85 | 380 | 15.7 ($P_s/P_o$ = 0.9935) |

The pore structure of the beads was further investigated by SEM of the samples SiFe7e (Figure 2.16) and SiCu1a (Figure 2.17). By comparison with Si-1F in Figure 2.7 it can be seen that the metal salts have significantly influenced the pore structure of the beads. The hierarchical pore structure that one would expect of SiHIPE materials is still present; however, the pore structure now appears tri-modal, in contrast to the typical bi-modal structure. The three sizes of pore can be described as follows:

1. Large cages: these are considerably larger than the cages previously observed and are separated by silica walls formed by

2. Small cages: these, appearing similar to and are of a similar diameter to the cages previously observed in this work in the SiHIPE beads produced using Tween 80. They are interconnected by,
3. Windows: these are the smallest pores. Again they appear similar to and are of a similar size to those measured in the SiHIPE beads produced using Tween 80 previously described in this chapter. They do however occur considerably less frequently than in the previous samples.

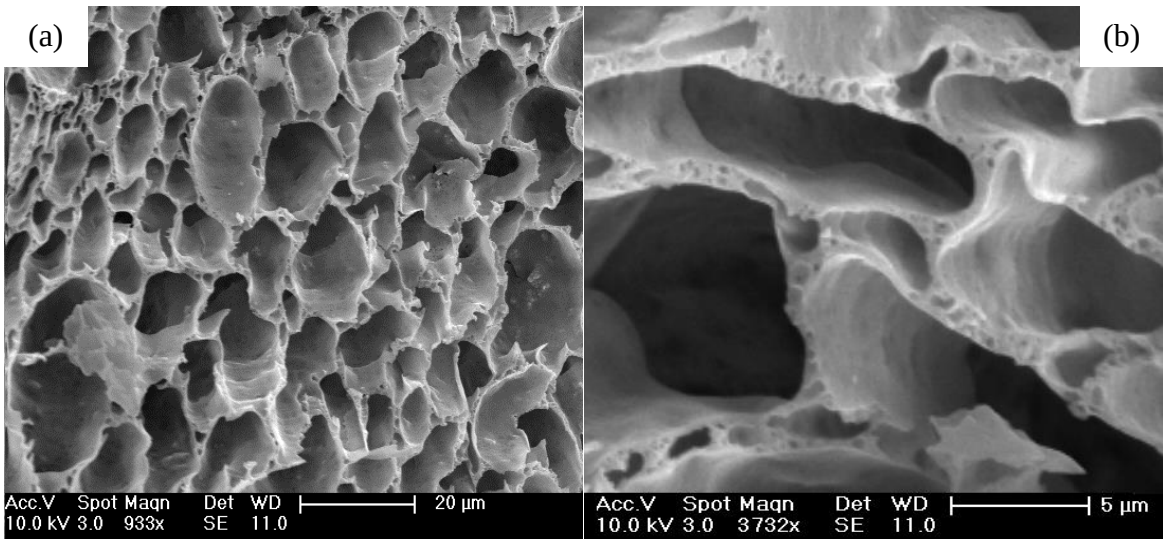


Figure 2.16: SEM Micrographs of SiFe7e, showing (a) the large cages and (b) the separating walls between, consisting of the smaller cages and windows.

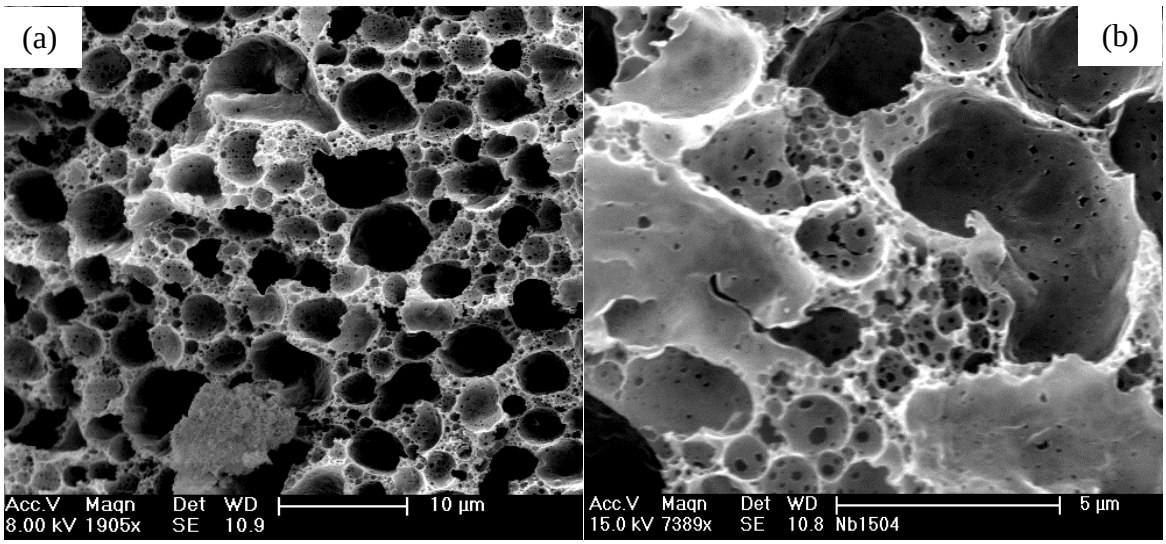


Figure 2.17: SEM Micrographs of SiCu1a, showing (a) the large cages and (b) the separating walls between, consisting of the smaller cages and windows.

Table 2.8: Average diameter of the large and small cages, determined by SEM, of SiHIPE materials additionally templated by transition metal salts

| Sample | Diameter of Large Cages ($\mu$m) | | Diameter of Small Cages ($\mu$m) | |
|---|---|---|---|---|
| | $D_n$ / %RSD [a] | $D_v$ / %RSD [b] | $D_n$ / %RSD [a] | $D_v$ / %RSD [b] |
| SiFe7e | 15.1 / 35 | 16.7 / 100 | 0.6 / 54 | 0.7 / 112 |
| SiCu1a | 4.4 / 26 | 4.7 / 95 | 0.7 / 41 | 0.8 / 107 |

[a] $D_n$ = number average diameter of the cages. [b] $D_v$ = volume average diameter of the cages.

Table 2.9: Average diameter of the windows, determined by SEM, of SiHIPE materials additionally templated by transition metal salts

| Sample | Diameter of Windows ($\mu$m) | |
|---|---|---|
| | $d_n$ / %RSD [a] | $d_a$ / %RSD [b] |
| SiFe7e | 0.2 / 53 | 0.3 / 113 |
| SiCu1a | 0.2 / 52 | 0.2 / 136 |

[a] $d_n$ = number average diameter of the windows. [b] $d_a$ = area average diameter of the windows

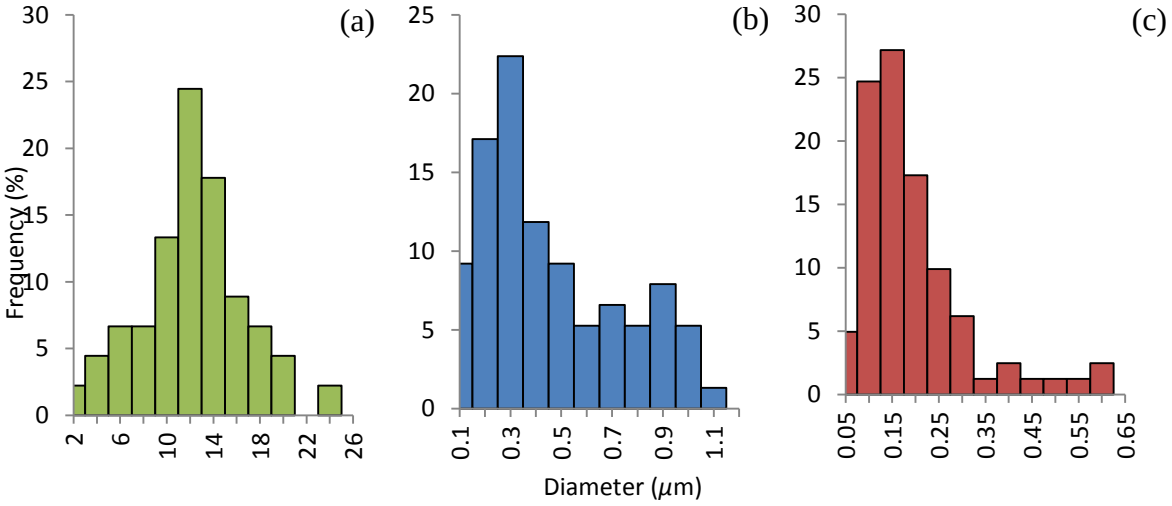


Figure 2.18: Pore size distributions of (a) large cages, (b) small cages and (c) cage windows, determined by SEM, of the SiHIPE sample SiFe7e

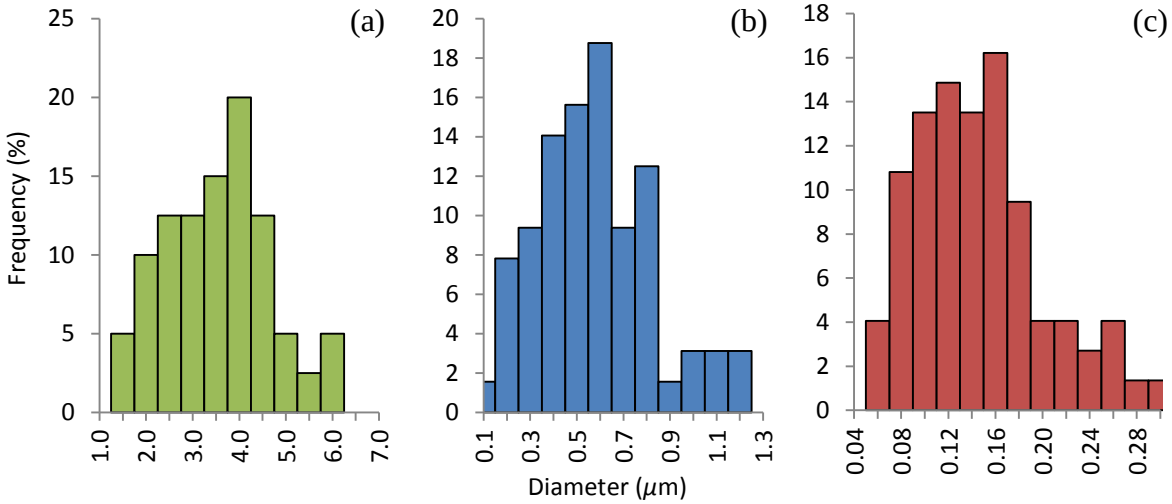


Figure 2.19: Pore size distributions of (a) large cages, (b) small cages and (c) cage windows, determined by, SEM of the sample SiCu1a

The average diameter of the large and small cages is shown in Table 2.8 and the average diameter of the cages is shown in Table 2.9. Size distributions for the samples SiFe7e and SiCu1a are presented in Figure 2.18 and Figure 2.19, respectively.

The increase in microporosity and the emergence of mesoporosity was attributed to the metal salts and their reaction with the TEA. The iron(III) chloride in the aqueous phase of the HIPE takes the form of the acidic iron(III)hexaaqua ion, $[Fe(H_2O)_6]^{3+}$, giving the sol and HIPE the yellow colouration. When the HIPE was submerged in the TEA (which acts as base), the TEA would diffuse into the aqueous phase reacting with $[Fe(H_2O)_6]^{3+}$ yielding the orange-brown precipitate iron (III) hydroxide by the following equation:

$$[Fe(H_2O)_6]^{3+}_{(aq)} + 3N(CH_2CH_3)_{3(aq)} \rightarrow [Fe(OH)_3\ (H_2O)_3]_{(s)} + 3HN(CH_2CH_3)^{3+}_{(aq)}$$

This reaction could be observed by the colour change of the HIPE from yellow to brown. While often referred to as iron(III) hydroxide, and denoted as $Fe(OH)_3(H_2O)_3$, it is not a true hydroxide and it is more accurately described as iron(III) oxide-hydride, $FeO(OH)\cdot 4H_2O$.[46] This orange-brown gelatinous precipitate will dehydrate to form the iron oxide $Fe_2O_3$ when heated above 200 $^oC$.[47] Exposure to TEA rapidly converted the silica particles into a silica network, gelling the sol around the iron precipitate. This will prevent aggregation such that only small particles of precipitate will form within the silica network. When these are removed by the acid wash they will template small pores throughout the network. The presence of hysteresis with a defined hump in the $N_2$ sorption isotherms (near $P_s/P_o$ =0.4), as well as increased microporosity, indicates that particles of iron hydroxide precipitate over the 0 – 2 nm range micropore range as well as the lower end of the 2 – 50 nm mesopore range.

The green coloration of sol containing CuCl results from the formation of $[CuCl_4]^{2-}$ in equilibrium with the copper hexaaqua ion in the presence of chloride ions by the following reaction:

$$[Cu(H_2O)_6]^{2+} + 4Cl^- \rightleftharpoons [CuCl_4]^{2-} + 6H_2O$$

Although copper in CuCl is in the form $Cu^+$ it is quickly oxidized to $Cu^{2+}$ in the presence of moisture and oxygen, which allows the formation of $[CuCl_4]^{2-}$.[48]

The behaviour of the copper ion when exposed to TEA is not quite as clear and requires further investigation to be fully understood. However, two possible actions are more likely than others: on exposure to TEA $[Cu(H_2O)]^{2+}$ in equilibrium with $[CuCl_4]^{2-}$, it will form either the precipitate $Cu(OH)_2(H_2O)_4$ or, if the TEA concentration is high enough, the complex $[Cu(TEA)_4(H_2O)]^{2+}$ and dissolve back into the aqueous phase. Both mechanisms will shift the equilibrium in favour of $[Cu(H_2O)]^{2+}$ allowing further reaction with TEA depleting $[CuCl_4]^{2-}$. Since both results would yield a blue compound the product of the reaction could not be elucidated qualitatively from the colour. However, the fact that the beads remained blue after calcination instead of turning black, due to decomposition of $Cu(OH)_2(H_2O)_4$ to copper(II)oxide (which occurs readily at around 185 $^oC$[49]), suggests the complex was formed. However, it is also possible that both copper hydroxide and the complex with TEA would form sequentially, copper hydroxide forming initially templating the silica, and then as more TEA diffused through the silica, the hydroxide would convert into the amine complex.

A rationale for the persistence of the blue colouration of the silica was proposed by Karakassides *et al.*[44] as a result of electron spin resonance studies. During calcination, the copper amine complex decomposes and the ligand nitrogen on the copper is replaced by oxygen atoms in the silica framework.

The reason the large cages were observed in the SiHIPE beads produced with $FeCl_3$ and CuCl and not in SiHIPE beads produced earlier in this work can probably be related indirectly to the presence of the transition metal salt. From the SEM images (Figure 2.16 and Figure 2.17) it can be seen that the volume of the large cages is too great to have been

templated by the small amount of transition metal salt in the sol forming a hydroxide/amine complex (0.22 mmol $ml^{-1}$ in the sol). However, as mentioned earlier, the iron and copper both form heaxaaqua ions in the sol. As with all transition metal hexaaqua ions the copper(II) hexaaqua ion and iron(III) hexaaqua ion are both acidic. As a result they would have acted as additional catalysts for the sol-gel process. Over the same aging period this would have lead and increased viscosity compared to sols produced without the presence of the hexaaqua ions. As a consequence of the increased viscosity, a greater energy is required for comparable levels efficiency in the mixing of the HIPEs. As mixing was not particularly high shear (the stirrer bar driven by a magnetic stirrer plate rather than a mechanical paddle stirrer) the large cages in the SiHIPE beads produced using transition metal salts likely result from inefficient mixing, which left behind large, unmixed droplets, arising from the increased viscosity of the sol. The reason for the different sizes of the large cages between the SiHIPEs produced with $FeCl_3$ and CuCl may be as a result of the greater acidity of the iron(III) hexaaqua ion which would have produced a more vicious sol after aging than the Cu(II) hexaaqua ion. At this this time this hypothesis is only speculative and ideally, further investigation would be undertaken (*e.g.*, rheological studies on the sols and HIPEs to show the effect of the transition metal salts on viscosity).

While this method of porosity directing is novel for SiHIPEs, it is of little use to the aim of this particular project. Templating results in porosity in the micro and mesoporous regions and pores size of these dimensions will not aid in nanoparticle separation over the desired size range, particularly when capping agents and the hydrodynamic diameter of the particles is considered.

### 2.3.4 SiHIPE Monoliths

Since it had not been possible to produce beads with properties appropriate for column packing either by the manual extrusion method or reservoir dispersion in toluene, it was decided to investigate the production of SiHIPE monoliths, which could be fixed inside a column where they would act as the stationary phase. The monoliths were initially prepared by a similar method used for the SiHIPE beads. However, none survived the calcination process as a result of excessive cracking attributed to the considerable shrinking, at times by greater that 50 %, of the wet monolith.

To reduce shrinkage and improve the mechanical properties of the silica monoliths, $SiO_2$ nanopowder (15 nm) was included in the sol as well as TEOS. The amount of nanopowder and TEOS was varied but the molar content of Si in the sol was kept constant. Initially, the sols were a thick paste, but on addition of acid the sol immediately underwent a raise in temperature and turned from a thick paste to viscous liquid. Despite the lower volume of the sols the HCl volume was not reduced, as the higher relative volume of acid in sols containing higher percentages of $SiO_2$ prevented the sol becoming too viscous to stir. Once HIPEs had been formed, viscosity appeared considerably greater than previous HIPEs.

Two batches of monoliths were prepared; one batch was set in TEA for 2 hours while the second batch was cured for three days in air before being submerged in TEA for 1 hour to set. Washing the resultant HIPEs in trichloroethane (TCE) was found to reduce the cracking and was therefore used instead of n-hexane. All the monoliths survived the calcination process producing white chalky materials with a rough surface (Figure 2.20), the shrinkage and BET surface area measurements are summarized in Table 2.10.

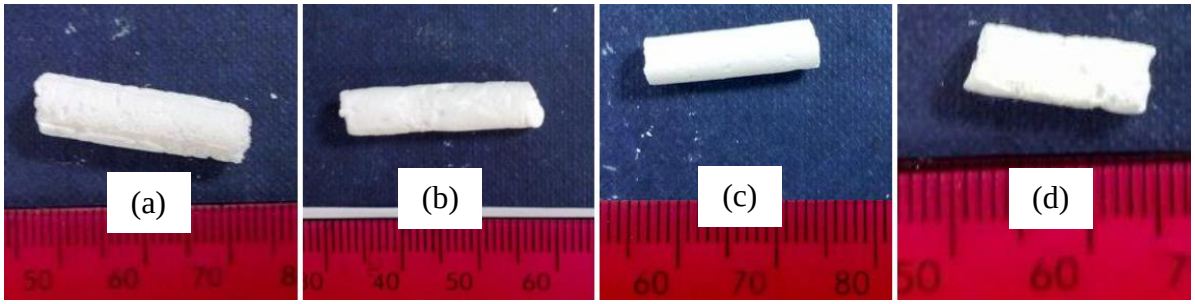


Figure 2.20: Images of the silica monoliths, from left to right, (a) Si53, (b) Si60, (c) Si62 and (d) Si71, scale in mm.

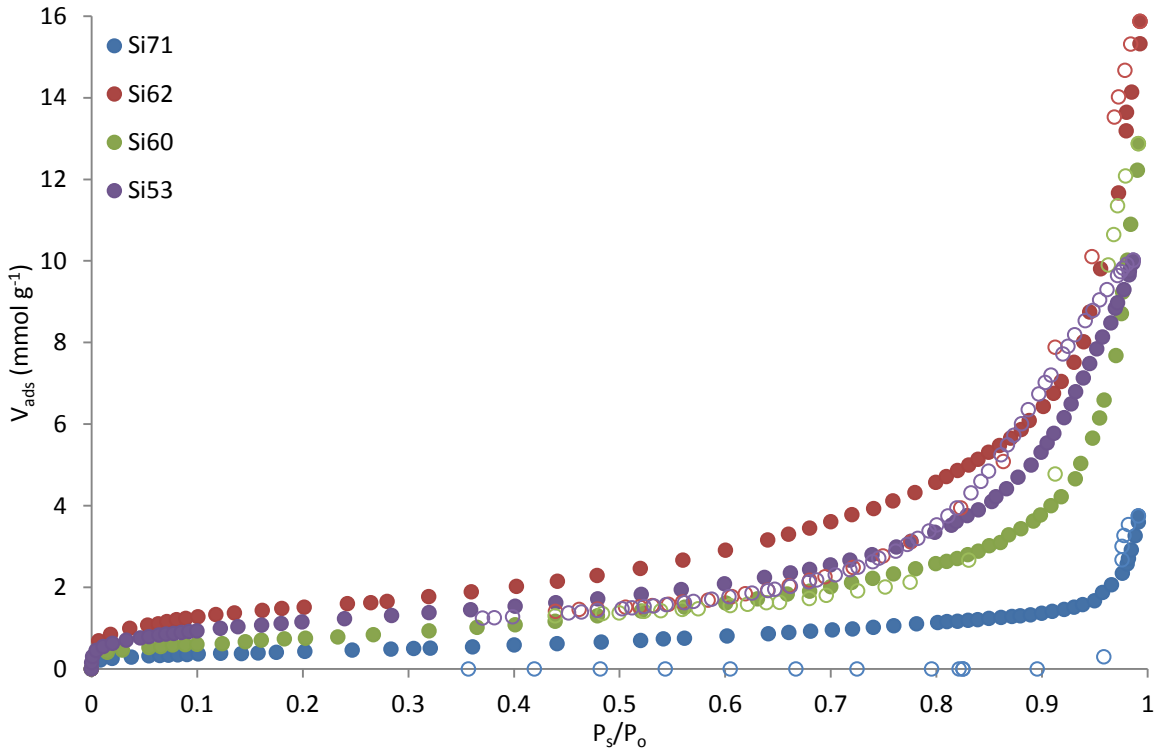


Figure 2.21: $N_2$ sorption isotherms, showing adsorption (●) and desorption (○), of SiHIPE monoliths prepared from sols containing $SiO_2$ nanopowder.

The BET isotherms (Figure 2.21) show the internal pore structure is composed almost exclusively of large macropores with negligible micro and mesoporosity. The desorption isotherms where the hysteresis is observed to drop below adsorption curve, particularly for Si71, can probably be attributed to machine error resulting from the low mass of the samples analysed. The surface areas were considerably lower than those of the beads and generally, the greater the amount of $SiO_2$ nanopowder the lower the surface area. Microporosity, and consequently the high surface area of sol-gel materials, occurs when

the silica gels around the solvents within the sol (usually water and the condensation products). The subsequent removal of these solvents leaves behind a porous network.[50] By reducing the volume of solvent in the gel and replacing it with solid $SiO_2$ (which is not removed by drying) the total void space is reduced and, as such, so is the microporosity. This is reflected by the low surface areas. This would explain why Si60 has a greater surface area than Si71, despite having a greater $SiO_2$ content in the sol, as the water content of the sol was greater allowing solvent templating

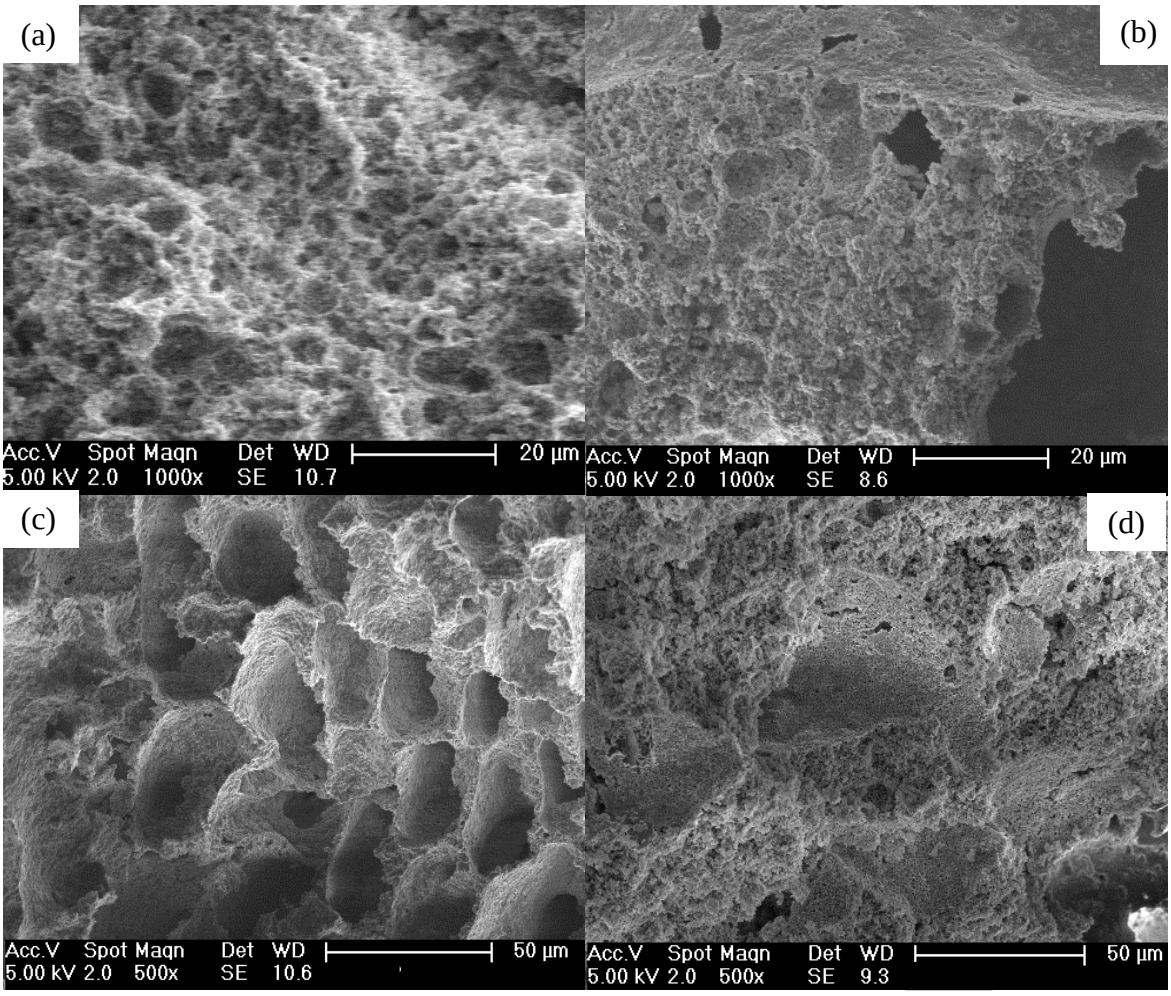


Figure 2.22: SEM images of SiHIPE monoliths, (a) Si53, (b) Si60, (c) Si62 and (c) Si71, formed from sols containing varying amounts of $SiO_2$ nanopowder.

Table 2.10: Surface areas and shrinkage of monoliths produced with varying amounts of $SiO_2$ nanopowder for 80% and 85% HIPES, set with TEA and DEA, respectively

| Sample | $SiO_2$ as % of Total Si | TEOS as % of Total Si | Oil Fraction of HIPE | TEOS:$SiO_2$:Water Mass Ratio | BET Measurements | | Monolith Diameter | | |
|---|---|---|---|---|---|---|---|---|---|
| | | | | | Surface Area ($m^2 g^{-1}$) | Maximum Adsorbance (mmol $g^{-1}$) | Pre drying (mm)[c] | Post calcination (mm)[c] | % Change |
| Si53 | 57.67 | 42.33 | 0.80 [a] | 1.00:0.39:0.54 | 80 | 10.0 | 9 | 5 | 44.4 |
| Si60 | 78.51 | 21.49 | 0.80 [b] | 1.00:1.05:0.80 | 50 | 12.9 | 9 | 7.5 | 16.7 |
| Si62 | 57.67 | 42.33 | 0.80 [b] | 1.00:0.39:0.54 | 100 | 15.9 | 9 | 6 | 33.3 |
| Si71 | 67.80 | 32.20 | 0.85 [b] | 1.00:0.61:0.54 | 30 | 3.8 | 9 | 5 | 44.4 |

[a] set in air for three days followed by 1 hour in TEA
[b] set in TEA for 2 hrs.
[c] Measurements accurate to ± 0.5 mm

SEM images of the monoliths (Figure 2.22) show either a porous structure dominated by macropores or highly textured surface, with clearly defined pores decreasing in prevalence as the $SiO_2$ content of the sol increases. There is a complete absence of any connecting windows, which effectively rules these monoliths out as a possible nanoparticle separation material.

### 2.3.5 Copper Containing SiHIPE Monoliths

CuCl was incorporated into the precursor sol of a SiHIPE monolith, as had been done with the SiHIPE beads in section 2.3.3. However, as rapid gelling of the HIPE with TEA had not been able to produce intact monoliths and the use of $SiO_2$ nanopowder resulted in a closed pore structure, the HIPE was cured for a week before exposure to TEA. The monolith survived the drying and calcination process and had a white chalky appearance similar to those detailed in section 2.3.4. The $N_2$ adsorption isotherm (Figure 2.23) shows the presence of both micro and mesoporosity (also as observed with the SiHIPE beads produced using CuCl) along with a comparable BET surface area, although the maximum adsorbed volume (19.40 mmol $g^{-1}$ at $P_s/P_o$ = 0.9926) had decreased (Table 2.11).

SEM of SiCuMO showed cages of a similar size (Table 2.12) and distribution (Figure 2.24) to the large cages observed for SiHIPE beads prepared using CuCl. Interestingly, the walls between these cages, which in the SiHIPE beads had their own porous structure, were no longer present. Also, while cage windows were present and larger than in the corresponding SiHIPE beads, they were infrequent, resulting in a more closed pore structure. This will limit any possible application as a chromatographic stationary phase. The reduced size of the cage windows is likely an effect of the curing

process, which reduces the shrinkage of the final SiHIPE and as discussed, there is evidence that the shrinkage allows formation of the windows.[38,51]

Table 2.11: BET surface area and absorption volume of the SiHIPE monolith SiCuMO.

| Sample | BET Surface Area ($m^2$ $g^{-1}$) | Maximum Volume Adsorbed (mmol $g^{-1}$) |
|---|---|---|
| SiCuMO | 730 | 19.40 @ 0.9926 |

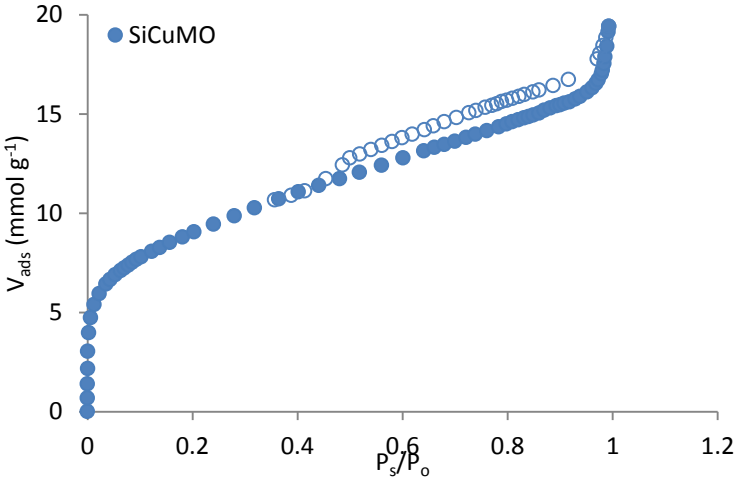


Figure 2.23: $N_2$ sorption isotherm, showing adsorption (●) and desorption (○), of the SiHIPE monolith SiCuMO which was prepared from a HIPE containing CuCl.

Table 2.12: Average cage and average window diameters, obtained from SEM, of the SiHIPE monolith SiCuMO.

| Sample | Cage Diameter | | Cage Window Diameter | | Openess |
|---|---|---|---|---|---|
| | $D_n$ / %RSD | $D_v$ / %RSD | *dn* / %RSD | $d_a$ / %RSD | (%) |
| SiCuMO | 3.8 / 43 | 4.4 / 105 | 0.4 / 62 | 0.5 / 124 | 2 |

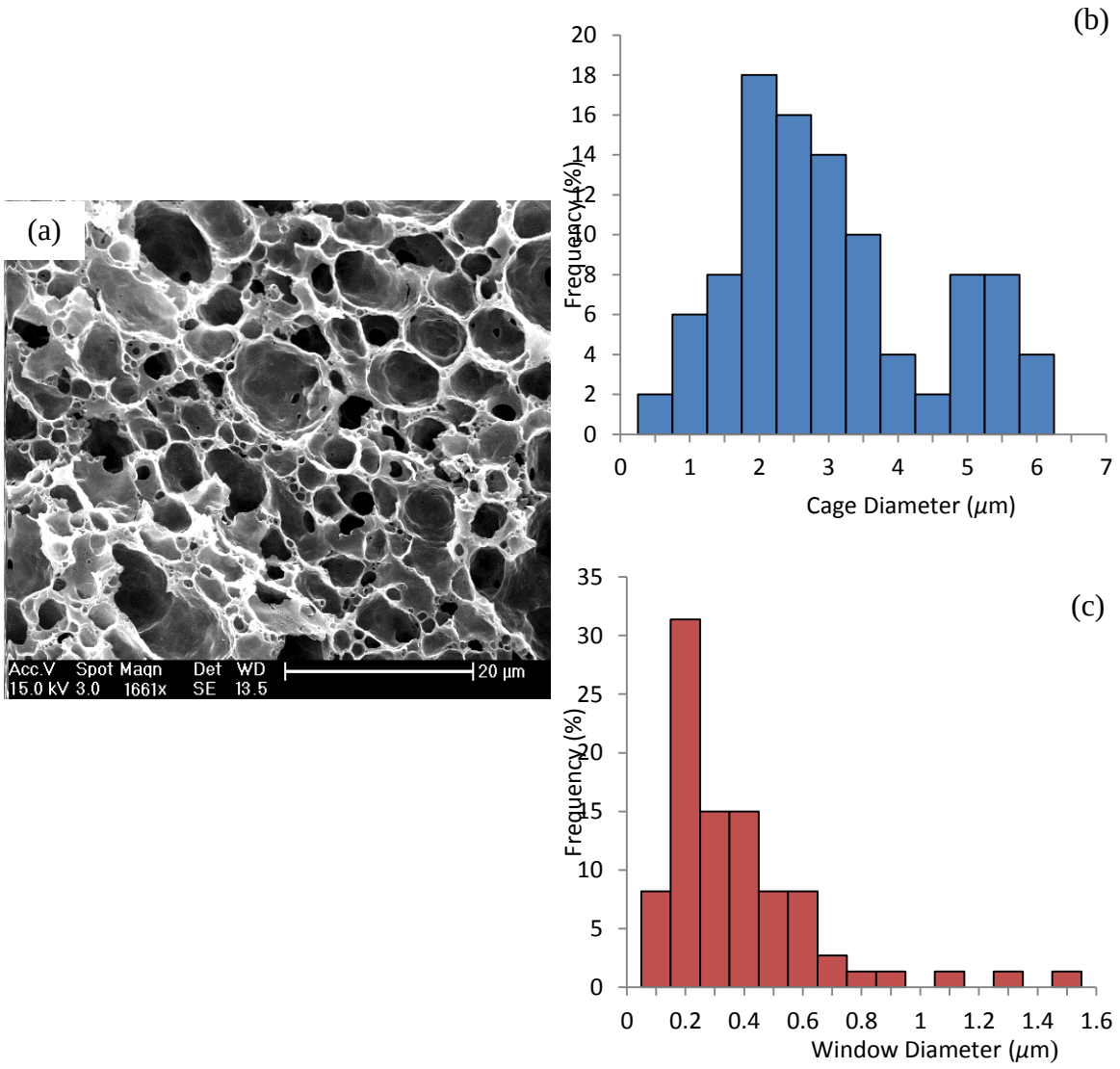


Figure 2.24: Left, SEM image and size distributions of (a) the cages and (b) the cage windows of the SiHIPE monolith SiCuMO, produced a sol aged containing CuCl.

## 2.4 Conclusions

Several interesting insights into the production of SiHIPE materials have been demonstrated in this chapter. It has been shown that the overall production time of SiHIPE materials when using a sol-gel process can be reduced by combining the acid/base technique of Hu *et al.*[6] with thermally accelerated aging of the sol. This accelerated aging produced no noticeable effects upon either the surface area or the final macropore structure of the resulting SiHIPE.

It was shown that the surface area of the SiHIPE could be influenced surfactant choice. By using Tween 80 instead of Triton X-405 to form the HIPE, the microporosity of the resultant SiHIPE beads was found to increase. Though it was not investigated in this work, it is likely that other surfactants could also be utilised in a similar manner. The transition metal salts $FeCl_3 \cdot 6H_2O$ and CuCl were also able to direct porosity in both SiHIPE beads and monoliths by their reaction with the TEA. Their presence resulted in the introduction of mesoporosity as well as significantly increasing the microporosity and surface area. When combined with the effect of Tween 80, this resulted in an almost six fold increase of the BET surface area when compared to beads produced initially.

The aim of this chapter was to investigate SiHIPE materials as a potential chromatographic stationary phase and it was decided that these SiHIPE materials are not appropriate for such a use. Therefore, they will not be investigated further, with attention being turned to polyHIPE materials. It was not possible to produce beads of an appropriate size for use in a packed column while monoliths were brittle and would shrink on drying and calcination. While it was possible to reduce shrinkage by introducing silica nanopowder into the sol, the resulting closed pore structure discounted them as a potential stationary phase. While novel, the ability to template porosity in the meso and micropore range will be a little use for separation over the desired nanoparticle size range. It is for this reason that the mechanisms at play in directing porosity were not fully investigated as they were beyond the scope of this chapter.

## 2.5 References


1. A. Araya, *US Pat. Appl*., 1989, 4 888 309.
2. T. Sen, G. J. T. Tiddy, J. L. Casci, M. W. Anderson, *Chem. Commun*., 2003, 2182–2183
3. F. Carn, A. Colin, M.-F. Achard, H. Deleuze, E. Sellier, M. Birot, R. Backov, *J. Mater. Chem*., 2004, 14, 1370–1376.
4. N. Brun, S. R. S. Prabaharan, M. Morcrette, C. Sanchez, G. Pécastaings, A. Derré, A. Soum, H. Deleuze, M. Birot, R. Backov, *Adv. Funct. Mater.*, 2009, **19**, 3136-3145
5. B. P. Binks, *Adv. Mater*., 2002, **14**, 1824–1827.
6. Y. Hu, M. Nareen, A. Humphries, P. Christian, *J. Sol-Gel Sci. Technol.*, 2010, **53**, 300–306
7. N. R. Cameron, D. C. Sherrington, *Adv. Polym. Sci.* 1996, **126**, 163-213
8. S. S. Manly, N. Graeber, Z. Grof, A. Menner, G. F. Hewitt, F. Stepanek, A. Bismarck, *Soft Matter***,** 2009, **5**, 4780 - 4787
9. A. Menner, R. Powell, A. Bismark, *Macromolecules*, 2006, **39**, 2034-2035
10. H. Xhang, A. I. Cooper, *Soft Mater*, 2005, **1**, 107-113
11. N. Brun, S. R. S. Prabaharan, M. Morcrette, C. Sanchez, G. Pécastaings, A. Derré, A. Soum, H. Deluze, M. Birot, R. Backov, *Adv. Funct. Mater.*, 2009, **19**, 3136-3145
12.T. Sen, G. J. T. Tiddy, J. L. Casci, M. W. Anderson, *Micropor. Mesopor. Mat.*, 2005, **78**, 255-263
13. G.-R. Yi, S.-M. Yang, *Chem. Mater*., 1999, **11**, 2322–2325
14. A. Imhof, D. J. Pine, *Nature*, 1997, **389**, 948–951
15. H. Zhang, G. C. Hardy, M. J. Rosseinsky, A. I. Cooper, *Adv. Mater.*, 2003, **15**, 78–81
16. A. Imhof, D. J. Pine, *Adv. Mater.*, 1998, **10**, 697–700
17. S. Otoishi, Y. Tange, H. Matsuda, *J. Ceram. Soc. Jpn.*, 2000, **108**, 487–491
18. H. Maekawa, J. Esquena, S. Bishop, C. Solans, B. F. Chmelka, *Adv. Mater*., 2003, **15**, 591–596
19. H. Zhang, G. C. Hardy, Y. Z. Khimyak, M. J. Rosseinsky, A. I. Cooper, *Chem. Mater*., 2004, **16**, 4245–4256
20. N. Brun, P. Hesemann, G. Laurent, C. Sanchez, M. Birot, H. Deleuze, R Backov, *New J. Chem.*, 2013, **37**, 157-168
21. A. Rahimi, P. Shokrolahi, *Int. J. Inorg. Mater.*, 2001, **3**, 843-847
22. V. Chandrasekhar in Inorganic and Organometallic Polymers, Springer-Verlang, Berlin Heidelberg, 1st edn., 2005, ch. 6, pp. 209-248
23. R. H. Baney, M. Itoh, A. Sakakibara, T. Suzuki, *Chem. Rev.*, 1995, **95**, 1409-1430
24. M. T. Grosse, M. Lamotte, M. Birot, H. Deleuze, *J. Polym. Sci., Part A: Polym. Chem.* 2008, **46**, 21-32
25. S. Ungureanu, M. Birot, G. Laurent, H. Deleuze, O. Babot, B. Julian-Lopez, M. F. Achard, M. I. Popa, C. Sanchez, R. Backov, *Chem. Mater.* 2007, **19**, 5786-5796
26. S. Ungureanu, H. Deleuze, C. Sanchez, M. I. Popa, R. Backov, *Chem. Mater.* 2008, **20**, 6494-6500
27. S. Ungureanu, H. Deleuze, O. Babot, M. –F. Achard, C. Sanchez, M. I. Popa, R. Backov, *Appl. Catal. A-Gen.*, 2010, **390**, 51-58
28. J. Normatov, M. S. Silverstein, *Macromolecules*,2007, **40**, 8329-8335
29. J. Normatov, M. S. Silverstein, *J. Polym. Sci., Part A: Polym. Chem.* 2008, **46**, 2357-2366
30. J. Normatov, M. S. Silverstein, *Chem. Mater.* 2008, **20**, 1571-1577
31. H. Tai, A. Sergienko, M. S. Silverstein, *Polymer*, 2001, **42**, 4473-4482
32. O. Lev, M. Tsionsky, L. Rabinovich, V. Glezer, S. Sampath, I. Pankratov, J. Gun *Anal. Chem.*, 1995, **67**, 22A–30A
33. C.J**.** Brinker, *J. Non-Cryst. Solids*. 1988, **100**, 31-50.
34. R. Aelion, A. Loebel, F. Eirich, *J. Am. Chem. Soc.*, 1950, **72**, 5705-5712
35. R. K. Iler, *The Chemistry of Silica*, Wiley, New York, 1979, ch.3, pp. 172-304.
36. A. Barbette, N. R. Cameron, *Macromolecules*, 2004, **37**, 3188-3204
37. I. Pulko, P. Krajnc, *Macromol. Rapid Commun.*, 2012, **33**, 1731-1746
38. N. R. Cameron, D. C. Sherrington, L. Albiston, D. P. Gregory, *Colloid. Polym. Sci.*, 1996, **274**, 592-595

39. H. Zhang, in *Hierarchically Structured Porous Materials*, ed. B. L. Su, C. Sanchez, X. Y. Yang, Wiley-VCH, Weinheim, 2012, ch.7, p 209-239
40. C. E. Tattershall, S. J. Aslam, P. M. Budd, *J. Mater. Chem.*, 2002, **12**, 2286-2291
41. C. E. Tattershall, N. P. Jerome, P. M. Budd, *J. Mater. Chem.*, 2001, **11**, 2979-2984
42. J. Zubia, M. Lormer in *Handbook of Optical Fibre Sensing Technology*, ed. J. M. López-Higuera, Wiley, Chichester, 2002, ch. 4, p 58-80
43. Toluene Physical Properties, *Sigma-Aldrich website*, Accsessed 16th July 2013 http://www.sigmaaldrich.com/chemistry/solvents/toluene-center.html
44. M. A. Karakassides, K. G. Fournaris, A. Travlos, D. Petridis, *Adv. Mater.*, 1998, **10**, 483-486
45. X. Dong, W. Shen, Y. Zhu, L. Xiong, J. Shi, *Adv. Funct. Mater.*2005, **15**, 955-960
46. G. Rayner-Canham, in *Descriprtive Inorganic Chemistry*, Freeman, New York, 1996, ch 19, pp. 411-452
47. F. A. Cotton, G. Wilkinson, P. L. Gaus, in *Basic Inorganic Chemistry*, Wiley, New York, 3rd edn., 1995, ch. 24, pp. 545-586
48. F. A. Cotton, G. Wilkinson, in *Advanced Inorganic Chemistry*, Wiley, London, 1966, ch. 29, pp.796-908
49. Digitalfire Ceramic Materials Database, http://tinyurl.com/kzwgrvx, Accessed on 23rd July 2013
50. C. J. Brinker, G. W. Scherrer, in *Sol-Gel Science: The Physics and Chemistry of Sol-Gel Processing*, Elsevier, San Diego, 1990, ch. 9, p. 515-616
51. A. Menner, A. Bismarck, Macromol. Symp. 2006, **242**, 19–24

# Chapter 3

# Synthesis and Characterisation of PolyHIPE Monoliths as Potential Stationary Phases for Chromatographic Separation.

## 3.1 Introduction

Since it was concluded in chapter 2 that SiHIPE materials were not appropriate candidates for the production of a chromatographic stationary phase, attention was turned to polyHIPE materials. This chapter details the synthesis and characterisation of several potential polyHIPE materials with the intention of assessing their chromatographic potential.

### 3.1.1 Aims and Objectives

The aim of this chapter was to discover if polyHIPE monoliths might possibly be applied as chromatographic stationary phases. To this end, this chapter details the synthesis and characterisation of several polyHIPE monoliths, all formed from emulsions with an internal phase fraction $\geq$ 75 %. The polyHIPEs were produced both as freestanding structures and within stainless steel HPLC columns. This allowed characterisation of both the polyHIPE physical properties and, most importantly, by attaching the columns to a high pressure liquid chromatography system, to assess the potential for chromatographic

flow. The primary focus was upon polyHIPEs synthesised from acrylate and methacrylate monomers, as the documented mechanical properties of the resulting polymers would appear to make them suitable candidates for a monolithic chromatographic stationary phase. Though the styrene/divinylbenzene (DVB) system would not initially appear to be ideal for monolithic aqueous chromatography due to the low mechanical stability, they were also investigated due to the large amount of literature available.[1,2,3,4]

### 3.1.2 HIPEs as a Route to Porous Materials

By including a monomer in either the external, internal or both phases of a HIPE and subsequently undertaking a polymerisation of the monomer, a variety of materials can be produced (Figure 2.1).[5] Of these only porous polymeric materials are relevant to this chapter (porous silica from HIPEs was discussed in chapter 2) and, as such, will be the only ones covered here.

For porous polymers to be synthesised from HIPEs the external phase must contain, or be wholly composed, of monomer. Once the monomer phase has been polymerised and the internal phase removed, the resultant material, termed a polyHIPE, will possess an open porous internal structure. SEM images of polyHIPEs typically reveal the pore structure is hierarchical, consisting of two levels of macropores. The first level is made up of larger pores, in the range of 1-100 $\mu$m,[6] which are templated by the emulsion droplets. These are interconnected by a series of smaller pores, typically in the size range of 0.1-5 $\mu$m, forming an open porous network (Figure 3.1). The larger pores have been given several names in the literature, such as cages, voids, cells or pores, while the smaller pores have variously been termed windows, interconnect or pore throats. Throughout this work the terms cages and windows will be used.

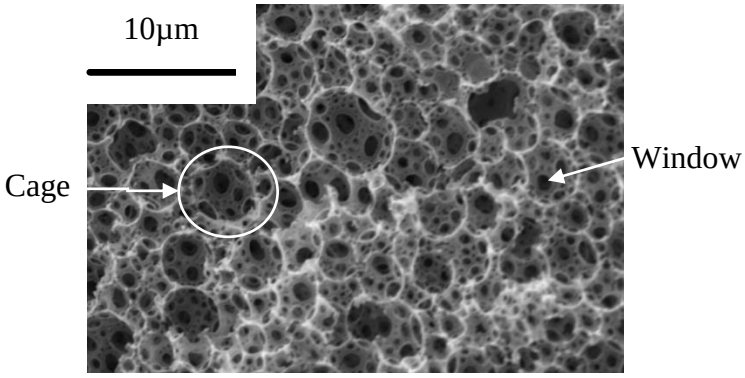


Figure 3.1: SEM image illustrating the typical polyHIPE structure. The image was obtained by the author at the University of Manchester School of Materials.

Two separate theories of the formation of polyHIPE windows have been proposed in the literature. Cameron *et al.*[7] proposed that the windows are formed during polymerisation because of density differences between the monomer external phase and the polymer gel external phase which arise during polymerisation. These differences result in shrinkage and rupture of the interfacial film. Their theory was supported by cryo-SEM imaging which revealed that windows had formed before polymerisation was complete. Menner and Bismarck[8] proposed that the windows form post polymerisation during the washing and drying phase, arguing that rupture as a result of shrinkage would be unlikely to produce consistently round windows. However, there are several reports in the literature of polyHIPEs produced with irregular windows, as well as reports of monolithic columns which allow fluid flow before washing.[9,10] These, along with environmental SEM of wet PolyHIPEs showing an open structure,[11] would appear to support the hypothesis of Cameron and co-workers.

The two most prominent factors influencing the openness of polyHIPEs are the amount/type of surfactant and the volume fraction of the internal phase ($\phi$) in the precursor HIPE. Increasing the amount of surfactant in the HIPE results in a corresponding decrease in the film thickness between droplets, this increases the chances of film rupture leading to a more open stucture.[6] The nature of stabiliser also affects the cage size and openness of

the final polyHIPEs, *e.g.* for similar styrene/DVB systems a change of surfactant from Span 80 to a Span 80/Span 85 mix resulted in considerably decreased cage size.[12] The degree of openness of a polyHIPE is also directly related to the $\phi$ value of the precursor HIPE. As $\phi$ is increased the final polyHIPE possesses a more open structure, and, conversely, as $\phi$ is decreased the resulting polyHIPE structure becomes increasingly closed.[13] It is thought than an increase in $\phi$ results in a transition in droplet shape from spherical to polyhedral. This will cause a redistribution of monomer/polymer mass resulting in an inter-droplet film with greater variation in thickness. Larger areas of the film will therefore be of reduced thickness with an increased probability of rupture, allowing the formation of larger windows and a more open structure.[6]

To produce open porous structures it is usually necessary for $\phi$ to be above the HIPE threshold of 0.7405. However this is not exclusively the case and open porous polymer structures can still be produced from a HIPE with a $\phi$ value of lower than 0.74.[14,15,16] Kovačič and co-workers[17] were able to produce poly(dicyclopentadiene) materials, with structures resembling those of a polyHIPE, from emulsions with $\phi$ as low as 0.5.

When particles, rather than surfactant, are used to stabilise HIPEs (Pickering HIPEs) the resultant polymer will usually display a structure with mostly closed cages.[18,19,20]

Zhang and Cooper[5] split polyHIPEs into two categories; hydrophobic polymers and hydrophilic polymers, the following two sections will briefly discuss each in turn. Should the reader require a more detailed review they are directed to reviews by Pulko and Krajnc6 and by Kimmins and Cameron.[21]

### 3.1.2.1 Hydrophobic Polymers

Generally a hydrophobic polymer will be synthesised from hydrophobic monomers, as such most hydrophobic polyHIPEs require a water-in-oil (w/o) HIPE for synthesis. This was the case with the polyHIPE systems developed by Unilever and disclosed in a series of patents in the early 1980s.[22,23] It was within these patents that these materials were first were termed polyHIPE. The process involved the polymerisation of the continuous phase of a w/o HIPE ($\phi \geq 0.9$) of styrene/DVB with an aqueous phase containing a salt acting as a stabiliser. Both water soluble (potassium persulphate) and oil soluble (2, 2'-azo-bis-isobutyronitrile) initiators were employed and the polymerisation was carried out, typically for 24 hours, in a heated and sealed vessel. After exhaustive washing with ethanol, by Soxhlet extraction, and drying, a solid monolith of cross-linked polystyrene was produced with a permanent interconnected macroporous structure. It should be noted that the use of HIPEs for the production of porous materials had been known for some 20 years before the polyHIPE patents came out of Unilever. Bartl and von Bonin[24] reported the polymerisation of vinyl monomers in w/o HIPEs in 1962, however, the materials they produced had closed pore structures.

Styrene/DVB is the archetypal polyHIPE system and as such has become the most extensively studied. Williams and co-workers[25] in several extensive studies found that the variation of the surfactant/oil ratio greatly influences the openness of the pore system and that the cage size can be tailored by the addition of 4-vinylbenzyl chloride (VBC) to the HIPE. It was also found that varying the salt concentration in the aqueous phase could also influence the cage size of the polyHIPE, with smaller cages being produced for both higher VBC and salt concentrations.[26,27]

PolyHIPEs usually have surface areas in the low tens of $m^2\ g^{-1}$, but by addition of a porogenic solvent to the HIPE system and/or by use of high levels of cross-linking (often

referred to as hyper cross-linking) a third level of porosity, often existing in the mesopore (2-50 nm) range, can be introduced to the polyHIPE. This third level of porosity is found within the walls of the polyHIPE and is evidenced by SEM imaging and by much higher BET surface areas than is seen in the exclusively macroporous systems.[28] Examples in the literature have seen Cameron and Barbetta[29] use mixtures of porogens, to produce styrene/DVB polyHIPEs with surface areas of 550 $m^2$ $g^{-1}$, as well as combing porogenic solvents with high levels of cross-linking (DVB content of 80 %) to produce surface areas of 830 $m^2$ $g^{-1}$. Surface areas of over 1000 $m^2$ $g^{-1}$ have also been achieved; Pulko *et. al*[30] produced styrene/VBC polyHIPEs with a surface area of 1100 $m^2$ $g^{-1}$ by hyper cross-linking followed by reaction with iron (III) chloride. Schwab *et al.*[31] produced polyHIPEs with surface areas of 1210 $m^2$ $g^{-1}$ by swelling a preformed polyHIPE and further cross-linking in the swollen state.

Though styrene/DVB containing HIPE systems are by far the most common in the literature, synthesis of hydrophobic polyHIPEs from many other systems have been reported. By combining styrene with other active monomers, other polyHIPE systems can be prepared (*e. g.*, poly(styrene-*co*-alkylmaleimide[32] and poly(aryl ether sulfone)).[33] With an eye on the potential use of polyHIPEs as scaffolds for tissue engineering, several biodegradable polyHIPEs have been prepared. Addition of poly(ε-caprolactone) (PCL) macromolecules to either a styrene or methyl methacrylate system followed by polymerisation leads to polyHIPEs containing polyPCL.[34,35] A similar procedure allowed the synthesis of polyHIPEs containing poly(lactic acid).[36] Biodegradable polyHIPEs based upon poly(propylene fumarate) have also be synthesised from a w/o HIPE.[37]

Elastomeric polymers have been prepared by the addition of varying amounts of 2-ethylhexyl acrylate to the styrene/DVB phase,[38] and porous polymers have been prepared from HIPEs of both 4-nitrophenyl acrylate/styrene and 2,4,6-trichlorophenyl

acrylate/styrene.[39] There are also various reports of hydrophobic polymers prepared from HIPEs that do not contain styrene. These include PolyHIPEs of poly(VBC-*co*-DVB),[40] poly(2-ethylhexyl acrylate) (this time without styrene),[41] and poly(vinyl ester) resin crosslinked with ethyleneglycol dimethacrylate (EGDMA)[42] amongst others. By crosslinking with DVB, Barbetta *et al.* [43] produced hydrophobic polyHIPEs of glycidyl methacrylate (GMA), usually a relatively hydrophilic monomer. By use of stearyl acrylate which possesses crystallisable side groups, semi-crystaline polyHIPEs have been produced, with the synthesis requiring the initiator to be in the internal phase of the HIPE.[44,45]

PolyHIPEs with magnetic properties have recently been prepared by Kovačič and co-workers[46] by inclusion of maghemite/magnetite nanoparticles in the external phase of a styrene/DVB HIPE. Magnetic poluHIPEs were also prepared by Kovačič and co-workers,[47] by inclusion of the same magnetic nanoparticles into polyHIPEs of poly(dicyclopentadiene), prepared by ring opening metathesis polymerisation. Deleuze *et al.* used ring opening metathesis polymerisation of a norbornene derivative using a Grubbs catalyst to produce polyHIPEs. The reaction allowed the metal-carbene chain of the catalyst to remain active at the end of preparation, meaning that further modification could potentially be possible.[48] Ring opening has also been used to prepare polyHIPEs of poly(dicyclopentadiene).[49]

Conducting polyHIPEs have also been prepared by the coating the surface of a poly(styrene-*co*-DVB) polyHIPE support with a thin film of polypyrole.[50]

### 3.1.2.2 Hydrophilic Polymers

Until recently, little work had been done on the production of hydrophilic polyHIPEs from hydrophilic monomers. Production of hydrophilic polyHIPEs usually

involved the use of polymers with polar or ionic groups[51] or the functionalisation of an already synthesised hydrophobic polyHIPE *e.g.*, nitration[52] or sulphonation[53] of styrene/DVB polyHIPEs. Hydrophilic polyHIPEs have also been produced by the grafting of poly(N-isopropylacrylamide)[54] and polypepetides[55]

Recently the range of monomers from which HIPEs have been produced has been expanded considerably, with many of these new monomers being applicable to the production of hydrophilic polymers. GMA cross-linked with EGDMA polyHIPEs were prepared from w/o HIPEs.[56,57] Use of a monomer with non-trivial hydrophilicity required the use of a tri-block copolymer of poly(ethylene oxide) and poly(propylene oxide) surfactant with a low hydrophilic-lipophillic balance (HLB) to stabilise the o/w HIPE.

As hydrophilic polymers usually require hydrophilic monomers, oil-in-water (o/w) HIPEs are often required to produce hydrophilic polyHIPEs. Poly(2-hydroxethyl methacrylate) (polyHEMA) polyHIPEs were synthesised from o/w HIPEs by Kulygin and co-workers[58] as well as separately by Kovačič *et al.* [59] (who used w/o HIPEs as well). In both cases the water soluble cross-linker methylene bisacrylamide (MBA) was used and the HIPEs required a high HLB number surfactant for stabilisation, Triton X-405 (HLB = 17.6)[58] and Pluronic F68 (HLB = >24) respectively. Interestingly the walls of the cages in the polyHIPEs prepared with Trion X-405 displayed an unusual nanoscale porous structure

Kulygin and co-workers initiated polymerisation by means of the redox pair ammonium persulphate (APS) and N,N,N',N'-tetramethylethylenediamine (TMEDA) which produces a rapid polymerisation process at ambient temperature. By allowing controlled coalescence before initiation it was possible to tune the average cage diameter (scheme 2 in reference 59).

Recently Paljevac and co-workers[11] prepared polyHIPEs form HEMA and by use of different cross-linkers were able to alter the morphology and cage and window size of the polyHIPE.

Poly(N-isopropylacrylamide) polyHIPEs were prepared from an o/w HIPE,[60] also using the initiation system of ammonium persulphate and tetramethylethylenediamine at 60 $^{o}$C. By using poly(N-isopropyacrylamide), a thermoresponsive polymer which undergoes a lower critical solution temperature transition in water at around 31 $^{o}$C, it was possible to produce a stimuli responsive polyHIPE. With removal of the internal phase, oil red nanoparticles dispersed within would adhere to the polyHIPE surface. Then by altering the temperature of the immediate aqueous environment from 18 to 45 $^{o}$C it was possible to 'pump' the nanoparticles into the surroundings.[61]

Hydrophilic polyHIPEs have also been prepared from gelatin and dextran via o/w HIPEs. Polymerisation was performed by radical initiation of vinyl moieties which had been grafted onto the gelatin and dextran.[62] It was also possible to prepare gelatin polyHIPEs without the need for functionalisation by use of enzymatic cross-linking of unfunctionalised gelatin with microbial tranglutaminase.[63] PolyHIPEs based on poly(ethyleneglycol methacrylate) have also been prepared from o/w HIPEs using ammonium persulphate as an initiator and sodium dodecyl sulphate as a surfactant. Tetramethylethylenediamine was added as secondary initiator once the oil phase had been added.[64]

One of the main disadvantages to the formation of hydrophilic polyHIPEs is that since an o/w HIPE is usually used, large amounts of organic solvents are required. Butler and co-workers[65] removed the need for this by the development of HIPEs of supercritical $CO_2$-in-water, which they termed c/w emulsions. They used a perfluoropolyether ammonium carboxylate surfactant and poly(vinyl alcohol) as a co-surfactant to form

polyHIPEs of polyacrylamide (cross-linked with MBA). The $CO_2$ internal phase was simple to remove by pressure reduction. Later development of this technique allowed for a far cheaper surfactant (Tween 40) to be used as well as lowered pressure (20 bar compared to 300 bar). Additionally, poly(hydroxyethyl acrylate) and polyHEMA polyHIPEs were also synthesised.[66]

Recently Forgacz and co-workers[67] used a wood pulp by-product to produce porous materials from waste organic biomass. The external phase consisted of a cellulosic chemical pulp from wood and lignin as a cross-linker. This was emulsified with castor oil using a hydrophilic surfactant to form a HIPE, which was then thermally cross-linked to form a solid monolith.

#### 3.1.2.3 PolyHIPE Beads

PolyHIPEs are mainly synthesised in the monolithic form and take the shape of the reaction vessel in which the polymerisation took place. However, there have been various reported syntheses in the literature of polyHIPE beads. Zhang and Cooper[68] reported the production of monodisperse hydrophilic polyHIPE beads (~ 2 mm diameter) of polyacrylamide (PAM) by sedimentation polymerisation. A conventional o/w or w/o HIPE was formed and droplets of the HIPE are then injected into the top of a column of hot aqueous or hot oil phase as appropriate, forming either a w/o/w or o/w/o double emulsion. Provided the hot medium had density of less than the HIPE, the droplets will sediment to the bottom and the temperature of the medium would initiate polymerisation during the sedimentation process.

Another method that utilises a double emulsion is suspension polymerisation. As before, a conventional HIPE (either w/o or o/w) is prepared and then dispersed in an oil phase or aqueous phase after which polymerisation is then initiated. This allows the

production of much smaller beads than the sedimentation method (diameters as low as 60 $\mu$m) but with a high polydispersity. The method, originally disclosed in series of patents[69] and subsequently commercialized by Biopore, has been used to prepare poly(4-nitrophenyl acrylate) and poly(2,4,6-trichlorophenyl acrylate),[70] beads as well as polyVBC[71] and poly(styrene/DVB)[72] polyHIPE beads.

Gokmen *et al.*[73] developed a technique that allows the formation of small monodisperse beads (down to 400 $\mu$m in diameter) of poly(2-ethylhexyl acrylate). This was achieved by using a microfluidic setup, droplets of a w/o HIPE were generated within a narrow channel experiencing flow, creating a w/o/w emulsion within the narrow channel. This was done by means of two syringe pumps set at vastly different flows. The HIPE droplets were polymerised in the channel via photopolymerisation. By variation of the flow rates it was possible to alter the size and morphology of the beads (Figure 2 and Figure 3 in reference 73). This method also had the further advantage of producing beads without the non-porous skin that is commonly observed on beads prepared by multiple emulsion techniques.

## 3.2 Experimental

### 3.2.1 Synthesis

#### 3.2.1.1 Chemicals

Styrene (Sigma-Aldrich) and divinyl benzene (DVB; Aldrich) were distilled under reduced pressure to remove inhibitors and then stored at –20 $^{o}$C until use. *N,N'*-methylenebisacrylamide (MBA; Sigma-Aldrich) was re-crystallised from methanol and stored at 5 $^{o}$C before use. Benzyl methacrylate (BMA; Aldrich), butyl acrylate (BuA; Aldrich), butyl methacrylate (BuMA; Aldrich), 2-(dimethylamino) ethyl methacrylate (DMAEMA; Acros Organics), ethyleneglycol dimethacrylate (EGDMA; Alfa Aesar)

glycidyl methacrylate (GMA; Aldrich), 2-hydroxyethyl methacrylate (HEMA; Aldrich), 2-hydroxypropyl methacrylate (HPMA; Acros Organics), methyl methacrylate (MMA; Aldrich) were all passed through an alumina column (Brockmann activity I), to remove inhibitors, and then through a 0.45 $\mu$m HDPE filter (Millipore) and used immediately. Bisphenol A diglycidyl ether (BADE; Sigma), calcium chloride (anhydrous; Fisher), cyclohexane (Fisher), 1,4-dioxane (Acros Organics), ethanol (Sigma-Aldrich), methacrylic acid (Aldirch), Pluronic® F-68 (Poly(ethyleneglycol)-*block*-poly(propylene glycol)-*block*-poly(ethyleneglycol) average $M_n$ ~8,350; Sigma), Pluronic® L-121 (*Poly*(ethyleneglycol)-*block*-poly(propylene glycol)-*block*-poly(ethyleneglycol), average $M_n$ ~4,400; Aldrich), potassium persulphate (KPS; Fisher), sodium azide (Aldrich), SPAN™ 80 (sorbitane monooleate; Fluka), tetrabutylammonium bromide (Fluka), and N,N,N',N'-tetramethylethylenediamine (TMEDA; Sigma-Aldrich) were all used as received.

### 3.2.1.2 Synthesis of the VE Resin.

The vinyl ester (VE) resin was prepared via a method previously detailed in the literature[74,75] as follows; BADE (10 g) and tetrabutylammonium bromide (0.20 g) were dissolved in 1,4-dioxane (10 ml) in a round-bottomed flask. The flask was then heated to 90 $^{o}$C and methacrylic acid (2.30 ml) was added. The reaction was then left to proceed (4.5 hours at 90 $^{o}$C). The reaction scheme is displayed Figure 3.2 and a mechanism is proposed in Figure 3.3. Once the reaction was complete the flask was allowed to cool and the VE-resin was used as produced for the synthesis of polyHIPEs by the procedure outlined in section 2.2.1.3.

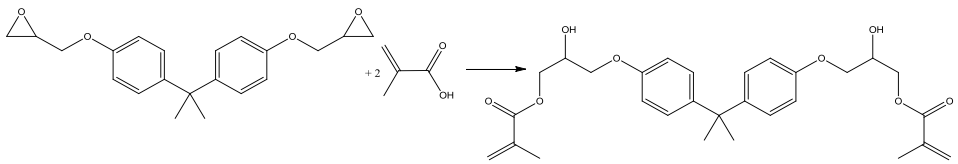

Figure 3.2: Equation for the synthesis of the vinyl ester resin

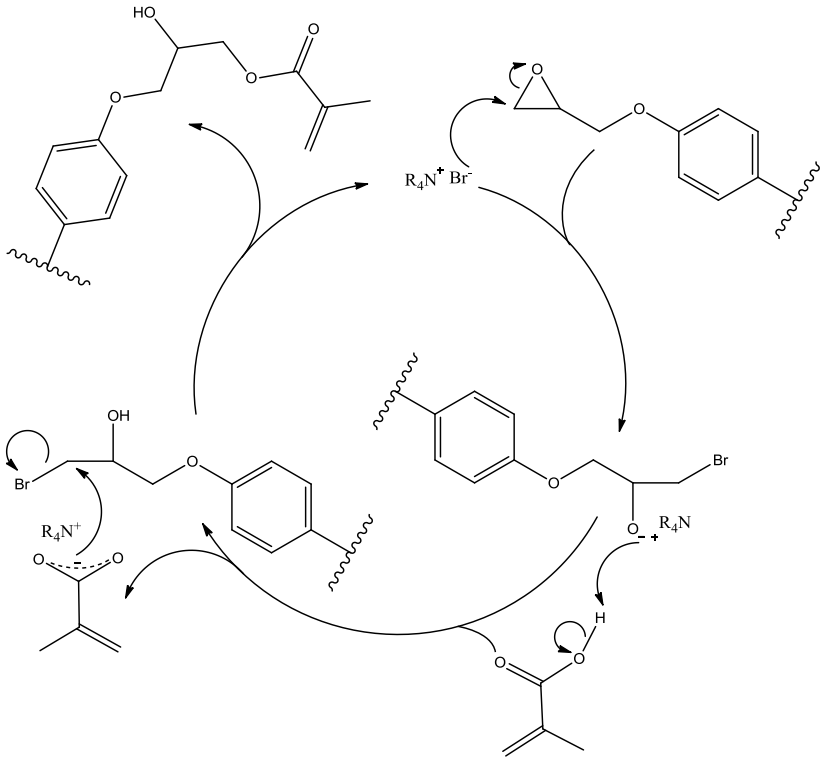


Figure 3.3: Proposed mechanism for the synthesis of the vinyl ester resin, based upon a mechanism Proposed by Fogassey *et al.*[76] for the of the reaction of an epoxide with acetic anhydride, catalysed by a quaternary ammonium salt. *N.b.* only half of bisphenyl A diglycidyl ether is shown in the reaction mechanism.

### 3.2.1.3 Polymerisations

Table 3.1 lists the emulsion compositions and conditions of polymerisation of the HIPE systems discussed in this chapter. The HEMA/MBA polyHIPEs were produced following a method detailed in the literature by Kovačič *et al.*[77] whereas VE-resin polymerisation and polyHIPE formation was adapted from that of Yang *et al.*[78].

The general polyHIPE synthesis procedure was as follows: Monomer, cross-linker, surfactant and any other components that made up the external phase were placed together in a three-neck round-bottom flask. The flask was then fitted with an overhead paddle

stirrer (IKA RW20.n), through the central neck, which was used to mix together the components of the external phase. An addition funnel was then fitted to one of the side necks of the round-bottom flask into which were placed the components of the internal phase. The addition funnel and the remaining side neck of the round-bottom flask where then sealed, by use of a Suba seal, and both phases where purged with nitrogen (30 minutes) by means of a stainless steel needle through the Suba seal. Once purging was complete the needles were removed from the two phases but the nitrogen flow was left active to create a nitrogen atmosphere. The internal phase was then added drop-wise to the monomer phase under constant stirring (450 rpm). Once addition was complete, stirring was continued (30 minutes) to ensure complete mixing of the HIPE. At this point, depending on the method of initiation used, the HIPE was either:

A. For the styrene/DVB, styrene/HEMA/DVB and VE-resin/EGDMA HIPEs. Removed from the round-bottom flask and transferred to either a glass or high density polypropylene (HDPE) mould if a freestanding monolith was being produced, or into an empty stainless steel HPLC column (Supelco, Germany) if a monolithic column was being produced (column length and i.d. are detailed in Table 3.1). It was then placed in an oven at a temperature of $\geq$ 55 $^{o}$C. This generates a sulphate radical by homolytic thermolysis of the KPS, initiating polymerisation (Figure 3.7). Precise conditions are defined in Table 3.1. Or,
B. For all other HIPEs. TMEDA (0.08 ml) was introduced to the HIPE through the Suba seal and stirring continued for a further 3 minutes. This leads to the redox generation of a sulphate radical at ambient temperatures initiating polymerisation (Figure 3.8). After this, the HIPE was removed from the round-bottom flask and transferred to either a glass or HDPE mould, if a freestanding monolith was being

Table 3.1: Emulsion compositions and polymerisation procedures for representative samples of both monoliths and columns.

| Sample [a] | Column or Monolith | Column Type | External Phase | | | Internal Phase | | | Initiator | Polymerization Procedure (Time and Temperature) |
|---|---|---|---|---|---|---|---|---|---|---|
| | | | Monomers | Crosslinker | Additional Components | Surfactant | Oil or Water | Approx. $\phi$ | | |
| PS-1 | Monolith | n.a. | Styrene (0.9 ml) | DVB (0.1 ml) | n.a.. | Span 80 (0.21 g) | Water | 0.9 | KPS | 48 hrs @ 60 °C |
| PS-2 | Monolith | n.a. | Styrene (0.5 ml) | DVB (0.5 ml) | n.a. | Span 80 (0.30 g) | Water (9 ml) | 0.9 | KPS | 48 hrs @ 65 °C |
| PS-3 | Monolith | n.a. | Styrene (0.75 ml) | DVB (0.25 ml) | n.a. | Span 80 (0.30g) | Water (9 ml) | 0.9 | KPS | 48 hrs @ 65 °C |
| PS-5 | Monolith | n.a. | Styrene (0.8 ml) | DVB (0.2 ml) | n.a.. | Span 80 (0.31 g) | Water (9 ml) | 0.9 | KPS | 168 hrs @ 65 °C |
| PS-1C | Column | 4.6 x 150 mm stainless steel | Styrene (1.4 ml) | DVB (0.6 ml) | n.a.. | Span 80 (0.8 g) | Water (15 ml) | 0.9 | KPS | 72 hrs @ 65 °C |
| PS-2C | Column | 4.6 x 150 mm stainless steel | Styrene (1.5 ml) | DVB (0.5 ml) | N.A. | Span 80 (0.6 g) | Water (15 ml) | 0.9 | KPS | 48 hrs @ 65 °C |
| PS-3C | Column | 7.8 x 300 mm stainless steel | Styrene (1.5 ml) | DVB (0.5 ml) | N.A. | Span 80 (0.6 g) | Water (15 ml) | 0.9 | KPS | 48 hrs @ 65 °C |
| StHe | Monolith | n.a. | Styrene (1 ml) & HEMA (1 ml) | DVB (1 ml) | N.A. | Pluronic L121 (0.5 g) | Water (9 ml) | 0.75 | KPS/ TMEDA (0.08 ml) | 24 hrs @ 65 °C |
| HEMA75 | Monolith | n.a. | HEMA (2.2 g) | MBA (0.4 g) | Deionized Water (5.2 ml) & potassium persulphate (0.084 g) | Pluronic F68 (1.5 g) | Cyclohexane (24 ml) | 0.75 | KPS/ TMEDA (0.08 ml) | ≈ 22 hrs @ ambient temp |

| Sample [a] | Column or Monolith | Column Type | External Phase | | | Internal Phase | | | Initiator | Polymerization Procedure (Time and Temperature) |
|---|---|---|---|---|---|---|---|---|---|---|
| | | | Monomers | Crosslinker | Additional Components | Surfactant | Oil or Water | Approx. $\phi$ | | |
| HEMA85 | Monolith | n.a. | HEMA (2.2 g) | MBA (0.4 g) | Deionized Water (5.2 ml) & potassium persulphate (0.084 g) | Pluronic F68 (1.5 g) | Cyclohexane (46 ml) | 0.85 | KPS/ TMEDA (0.08 ml) | ≈ 22 hrs @ ambient temp |
| HEMA90 | Monolith | n.a. | MEHA (2.2 g) | MBA (0.4 g) | Deionized Water (5.2 ml) & potassium persulphate (0.084 g) | Pluronic F68 (1.5 g) | Cyclohexane (72 ml) | 0.90 | KPS/ TMEDA (0.08 ml) | ≈ 22 hrs @ ambient temp |
| HEMA75-C | Column | 4.6 x 150 mm stainless steel | HEMA (2.2 g) | MBA (0.4 g) | Deionized Water (5.2 ml) | Pluronic F68 (1.5 g) | Cyclohexane (24 ml) | 0.75 | KPS/ TMEDA (0.08 ml) | ≈ 22 hrs @ ambient temp |
| HEMA85-C | Column | 4.6 x 150 mm stainless steel | HEMA (2.2 g) | MBA (0.4 g) | Deionized Water (5.2 ml) | Pluronic F68 (1.5 g) | Cyclohexane (46 ml) | 0.85 | KPS/ TMEDA (0.08 ml) | ≈ 22 hrs @ ambient temp |
| HEMA90A-C & HEMA90B-C & HEMA90C-C | Column | 4.6 x 150 mm stainless steel | HEMA (2.2 g) | MBA (0.4 g) | Deionized Water (5.2 ml) potassium persulphate (0.084 g) | Pluronic F68 (1.5 g) | Cyclohexane (72 ml) | 0.90 | KPS/ TMEDA (0.08 ml) | ≈ 22 hrs @ ambient temp |
| HEMA90D-C | Column | 7.8 x 300 mm stainless steel | HEMA (2.2 g) | MBA (0.4 g) | Deionized Water& potassium persulphate (0.084 g) (5.2 ml) | Pluronic F68 (1.5 g) | Cyclohexane (72 ml) | 0.90 | KPS/ TMEDA (0.08 ml) | ≈ 22 hrs @ ambient temp |

| Sample [a] | Column or Monolith | Column Type | External Phase | | | Internal Phase | | | Initiator | Polymerization Procedure (Time and Temperature) |
|---|---|---|---|---|---|---|---|---|---|---|
| | | | Monomers | Crosslinker | Additional Components | Surfactant | Oil or Water | Approx. $\phi$ | | |
| EGDMA1 & EGDMA1C | Monolith (EGDMA1) & Column (EGDMA1C) from the Same HIPE | 4.6 x 150 mm stainless steel | EGDMA (4 ml) | n.a. | n.a. | Pluronic L121 (1.2 ml) | Water (36 ml) | 0.90 | KPS/ TMEDA (0.08 ml) | 2 hrs @ 50 $^{o}$C then 15 hrs at ambient in ethanol |
| MMA1 & MMA1C | Monolith (MMA1) & Column (MMA1C) from the Same HIPE | 4.6 x 150 mm stainless steel | MMA (2.70 ml) | EGDMA (1.3 ml) | n.a. | Pluronic L121 (1.2 ml) | Water (36 ml) | 0.90 | KPS/ TMEDA (0.08 ml) | 2 hrs @ 50 $^{o}$C then 15 hrs at ambient in ethanol |
| MMA2 & MMA2C | Monolith (MMA2) & Column (MMA2C) from the Same HIPE | 4.6 x 150 mm stainless steel | MMA (2.70 ml) | EGDMA (1.3 ml) | n.a. | Pluronic L121 (1.2 ml) | Water (36 ml) | 0.90 | KPS/ TMEDA (0.08 ml) | 2 hrs @ 50 $^{o}$C then 15 hrs at ambient in ethanol |
| GMA 1 & GMA 1C | Monolith (GMA 1) & Column (GMA 1C) from the Same HIPE | 4.6 x 150 mm stainless steel | GMA (2.70 ml) | EGDMA (1.3 ml) | n.a. | Pluronic L121 (1.2 ml) | Water (36 ml) | 0.90 | KPS/ TMEDA (0.08 ml) | 2 hrs @ 50 $^{o}$C then 15 hrs at ambient in ethanol |
| GMA 2 | Monolith | n.a. | GMA (2.70 ml) | EGDMA (1.3 ml) | n.a. | Pluronic L121 (1.2 ml) | Water (36 ml) | 0.90 | KPS/ TMEDA (0.08 ml) | 2 hrs @ 50 $^{o}$C then 15 hrs at ambient in ethanol |
| BuA 1 | Monolith | n.a. | Butyl Acrylate (1.6 ml) | EGDMA (0.4 ml) | n.a. | Pluronic L121 (0.5 g) | Water (10 ml) | 0.90 | KPS/ TMEDA (0.08 ml) | 24 hrs @ 55 $^{o}$C |

| Sample [a] | Column or Monolith | Column Type | External Phase | | | Internal Phase | | | Initiator | Polymerization Procedure (Time and Temperature) |
|---|---|---|---|---|---|---|---|---|---|---|
| | | | Monomers | Crosslinker | Additional Components | Surfactant | Oil or Water | Approx. $\phi$ | | |
| BuA 2 & BuA 2C | Monolith (BuA2) & Column (BuA2C) from the Same HIPE | 4.6 x 150 mm stainless steel | Butyl Acrylate (2.7 ml) | EGDMA (1.3 ml) | n.a. | Pluronic L121 (1.2 ml) | Water (36 ml) | 0.90 | KPS/ TMEDA(0.08 ml) | 2 hrs @ 50 $^{o}$C then 15 hrs at ambient in ethanol |
| HPMA1 & HPMA 1C | Monolith (HPMA1)& Column (HPMA1C) from the Same HIPE | 4.6 x 150 mm stainless steel | HPMA (2.7 ml) | EGDMA (1.3 ml) | n.a. | Pluronic L121 (1.2 ml) | Water (36 ml) | 0.9 | KPS/ TMEDA (0.08 ml) | 2 hrs @ 50 $^{o}$C then 15 hrs at ambient in ethanol |
| VE-1C | Monolith (VE-1)& Column (VE-1C) from the Same HIPE | 4.6 x 150 mm stainless steel | Vinyl Ester Resin (1 g) (ref) | EGDMA (1.2 g) | n.a. | Pluronic L121 (0.5 g) | Water (10 ml) | 0.83 | KPS | 48 hrs @ 65 $^{o}$C |
| VE-2C | Column | 4.6 x 150 mm stainless steel | Vinyl Ester Resin (1 g) (ref) | EGDMA (1.2 g) | n.a. | Pluronic L121 (0.5 g) | Water (10 ml) | 0.83 | KPS | 48 hrs @ 65 $^{o}$C |
| DEAMA1 | No HIPE formed | n.a. | 2-(Dimethyl-amino) ethyl methacrylate (2.7ml) | EGDMA (1.2 ml) | n.a. | Pluronic L121 (1.2 ml) | Water (36 ml) | 0.9 | HIPE did not form | HIPE did not form |

[a]. With respect to the sample identifier if the identifier ends with C then this indicates a column was prepared and the first 3 or 4 letters of the identifier indicate the main monomer present in the external phase

[b.] When water was used as the internal phase it also contained calcium chloride 10 g $l^{-1}$) and potassium persulphate (2.5 g $l^{-1}$).

produced, or, if a monolithic column was being produced the HIPE was transferred into an empty stainless steel HPLC column (Supelco, Germany) (column length and i.d. are detailed in Table 3.1). The glass moulds were then sealed air tight with a small amount of external phase at the surface (to prevent monomer evaporation). The columns were sealed tightly with the supplied end fittings.[i] Once the moulds/columns had been sealed polyHIPEs were allowed to polymerise under the conditions detailed in Table 3.1. Once polymerisation was complete, if a free standing monolith was being produced, the resulting polyHIPE was removed from the mould and washed via Soxhlet extraction with ethanol (24 hours) and then dried under vacuum at 50 $^{o}$C. If a monolithic column was produced, the column was opened up and a thin slice of the polyHIPE was cut from each end of the column with a razor blade to open up the internal pore structure. Columns were then re-sealed with the supplied end fittings and connected to a pump (Model 305, Gilson UK) and manometric module (Model 805, Gilson UK). The back pressure limit of the pump was set at 15 MPa and a 50:50 mixture of ethanol and water was then pumped through the column at a flow rate of 0.10 ml min$^{-1}$ for a minimum of 4 hours. If flow was possible with the ethanol/water mixture, the eluent was changed to deionised water (with 0.01 % w/v sodium azide as a biocide) which was pumped at 0.10 ml min$^{-1}$ for a further 2 hours.

### 3.2.2 Structural Characterisation of PolyHIPE Monoliths

#### 3.2.2.1 Shrinkage of PolyHIPEs upon Washing/Drying.

The amount of shrinkage from the original dimensions was determined as follows; the average diameter of the polyHIPE monolith was calculated from five measurements at different points along its length. This was then subtracted from the original diameter,

[i] Columns were sealed without the supplied frits to avoid the larger particles, which were separated in chapter 4, being retained on the column. The end fittingness supplied with the column were described as zero dead volume so it was believed that omitting the frits would not negatively influence the dead volume of the column.

which was assumed to be the internal diameter of the mould, to determine the diameter change. This change in diameter was then expressed as a percentage of the original diameter.

### 3.2.2.2 Porosity With Respect To Water

To establish the porosity with respect to water, the mass and volume of a dry section of polyHIPE monolith were measured. This was then submerged in deionised water for approximately 36 hours at room temperature (≈ 20 $^{o}$C), after which the wet mass and wet volume were established. The porosity was then calculated from the following equations:

$$\varepsilon = \frac{\left(\Delta m/\rho\right) - \Delta V}{V_d} \quad \text{(Eq. 3.1)}$$

$$\Delta V = V_{\mathrm{W}} - V_{\mathrm{d}} \quad \text{(Eq. 3.2)}$$

where: ε is porosity (%)

$\Delta m$ is the mass difference between the wet and dry samples

$V_{\mathrm{w}}$ the volume of the wet monolith

$V_{\mathrm{d}}$ the volume of the wet monolith

$\rho$ density of the wetting liquid which = 1.00 g ml$^{-3}$ for deionised water (at 20 $^{o}$C).

### 3.2.2.3 Determination of polyHIPE Cages and Windows Size

Samples were first sputter coated with gold/palladium and scanning electron microscopy (SEM) was carried out on a Phillips XL30 FEG SEM or a Zeiss EVO 60 ESEM at the School of Materials at the University of Manchester.

The cage and window diameters were measured manually with software designed for the measurement of nanoparticles. This procedure involved an element of judgement

upon the author's part, but by taking a large number of measurements (between 250 and 300 in each case) from several regions of a sample comparative data could be obtained. Once the various average diameters (number, area and volume for the cages and number and area averages for the windows) had been determined, a statistical correction was applied by multiplying the average value measured from SEM by $2/(3^{1/2})$. (The explanation for the statistical correction is given in reference 79 and in section A1.1 of the appendix 1)

The measurements from SEM were also used to calculate the openness of the PolyHIPEs by the calculation proposed by Pulko and Krajnc6 which is detailed in the section A1.2 of appendix 1.

## 3.3 Results and Discussion

### 3.3.1 Formation and Polymerisation of HIPEs

As with most classes of emulsion, HIPEs are thermodynamically unstable (micro-emulsions, see chapter 5, are an exception to this rule). Therefore, if they are to exist for any extended lifetime they require stabilisation, which is usually is in the form of a surfactant. The majority of polyHIPE materials in the literature utilise highly hydrophobic monomers to form w/o HIPEs which can readily be stabilised by surfactants with a HLB (see Chapter 1 section 1.3.2.1 for an explanation of the HLB concept) of around 4. This was the case with the styrene/DVB HIPEs (the water solubilities of styrene and DVB are 0.031 %[80] and 0.0052 %[81] at 25 $^{o}$C respectively) reported in this work, which were efficiently stabilised by Span 80 (HLB=4.3). However, when monomers with a greater hydrophilicity were used, *i.e.*, MMA (1.5% at 25 $^{o}$C)[82] and GMA (2.3 %),[83] greater stabilisation was necessary and a surfactant with a lower HLB was required. To stabilise these HIPEs, following the work of Krajnc *et al.*,[9] Pluronic L121 (HLB=2-5) was used. As Pluronic L121 also proved to be appropriate for stabilisation of w/o HIPEs of the

hydrophobic acrylates, BuMA, BuA, BMA and EGDMA, as well HIPEs formed from VE-resin/EGDMA it was used for the stabilisation of all the w/o HIPEs described in this chapter, with the exception of the styrene/DVB systems.

Examples in the literature of o/w HIPEs containing HEMA required a surfactant with a high HLB such as Pluronic F68 (HLB > 24)[59] or Triton X-405 (HLB = 17.6)[84] for stabilisation. The polyHIPEs produced by Kovacic *et al.*[59] using Pluronic F68 visually had a more open structure with a greater number of windows than those produced using Triton X-405 by Kluygin *et al.*.[84] It is believed that a more open pore structure will produce a more effective chromatographic stationary phase. Therefore, Pluronic F68 was chosen as the surfactant for the production of the polyHEMA polyHIPEs produced in this work.

All systems, with the exception of DEAMA/EGDMA, formed stable HIPEs which presented as highly viscous white liquids with an oily appearance. While an emulsion did form from DEAMA/EGDMA with a similar appearance to the other systems, the HIPE would rapidly collapse when mixing was ceased. This instability can probably be attributed to the relatively high solubility of DEAMA in water (10.6 %)[85] which, even in the presence of the surfactant, would still diffuse across the o/w interface collapsing the emulsion.

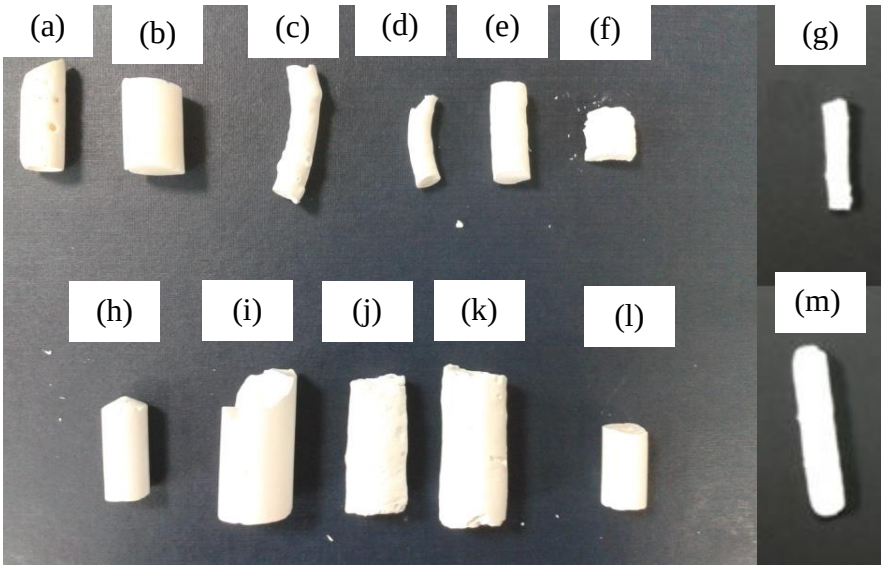


Figure 3.4: Images of the washed and dried polyHIPE monoliths showing (a) PS-3, (b) HEMA75, (c) HEMA85, (d) BuA1, (d) MMA1, (e) HPMA1, (f) EGDMA1, (g) StHE, (h) GMA3, (i) BMA3 and (j) BuMA1 and (m) VE-1

Table 3.2: Post synthesis textural appearance of polyHIPE monoliths

| Sample | Texture (Brittle or Crumbly) |
|---|---|
| PS-3 | Crumbly |
| VE1 | Crumbly |
| HEMA75 | Brittle |
| HEMA85 | Brittle |
| HEMA90 | Brittle |
| StHE | Crumbly |
| BuA1 | Brittle |
| MMA1 | Crumbly |
| HPMA1 | Brittle |
| EGDMA1 | Brittle |
| GMA3 | Brittle |
| BMA3 | Brittle |
| BuMA1 | Brittle |

Table 3.3: Summary of the measured physical properties of the polyHIPEs produced in this chapter. Full data sets can be found in appendix 2.

| Sample | Internal Phase Volume (%) | Porosity To Water (%) | Mean Cage Diameter[a] ($\mu$m) | Mean Window Diameter[b] ($\mu$m) | Openness[c] (%) |
|---|---|---|---|---|---|
| PS-3 | 90 | 67 | 13.0 | 2.0 | 37 |
| VE1 | 82 | 34 | – | – | – |
| HEMA75 | 75 | 80 | 3.3 | 0.9 | 14 |
| HEMA85 | 85 | 93 | 3.1 | 1.3 | 57 |
| HEMA90 | 90 | – | – | 1.1 | – |
| StHE | 90 | 52 | – | – | – |
| BuA1 | 90 | 5 | 9.1 | 1.1 | 8 |
| MMA1 | 90 | 86 | – | 0.2 | – |
| HPMA1 | 90 | 58 | 2.1 | 0.5 | 34 |
| EGDMA1 | 90 | 61 | 2.2 | 0.3 | 35 |
| GMA3 | 90 | 85 | – | 0.4 | – |
| BMA3 | 90 | 9 | 4.3 | 0.4 | – |
| BuMA1 | 90 | 25 | 3.6 | 0.5 | 24 |

[a] Number average cage diameter, $\overline{D_n}$.
[b] Number average window diameter, $\overline{d_n}$.
[c] Calculated from the respective area average diameters, listed in Table 3.5.

Systems that formed stable HIPEs were all successfully polymerised, producing solid polyHIPE monoliths with low densities (Figure 3.4). The textures of monoliths could qualitatively be divided visually into two groups; brittle or crumbly (Table 3.2). Crumbly monoliths were very delicate and would easily disintegrate if not handled with care and chalky residue would also be left behind when touching or placed on most surfaces. Brittle

samples were far more mechanically robust and would snap with a clean fracture when broken, instead of crumbling.

### 3.3.2 Characterisation of PolyHIPE Monoliths

The polyHIPEs produced were characterised by a variety of methods, the results of which are summarised in Table 3.3.

#### 3.3.2.1 Shrinkage of the PolyHIPEs

Table 3.4, below, shows the degree to which the polyHIPE monoliths shrunk upon drying. For polyHIPEs produced from HEMA the final shrinkage was related to the internal phase volume fraction of the original HIPE, higher volume fractions producing a greater shrinkage. This was particularly noticeable for HEMA85 and HEMA90 (Figure 3.4 c and d) both of which, due the extent of the shrinkage, resulted in highly deformed monoliths (this deformation likely makes the value calculated for shrinkage unreliable). The significant level of shrinkage of the polyHEMA/MBA polyHIPEs can probably be attributed to the presence of the water in the external phase of the HIPE. During polymerisation this extra solvent would have become trapped within the polymer matrix, resulting in a swollen monolith. Drying the polyHIPE under vacuum will remove the trapped water, resulting in shrinkage of the monolith. Deformation may have resulted from local areas of anisotropy within the polyHIPE structure which would direct the contraction of the polyHIPE. This would explain why HEMA 90 deformed and shrunk to a greater extent than HEMA 85, which itself deformed more than HEMA 75. This could also potentially explain the shrinkage of the VE-1 monolith, which also contained a significant volume of dioxane in the external phase of the HIPE.

Table 3.4: Shrinkage of the polyHIPE monoliths after post synthesis washing and drying. The diameter of the mould was taken to be the original the diameter mould as the original diameter.

| Monolith | Shrinkage (%) |
|---|---|
| PS-3 | 7 |
| VE1 | 12 |
| HEMA75 | 11 |
| HEMA85 | 28 |
| HEMA90 | 45 |
| StHE | 47 |
| BuA1 | 0 |
| MMA1 | 28 |
| HPMA1 | 9 |
| EGDMA1 | 0 |
| GMA3 | 17 |
| BMA3 | 4 |
| BuMA1 | 0 |

With the exception of VE-1 all the w/o systems had an external phase wholly composed of monomer. For these polyHIPEs as no non-polymerisable solvent was present to form a swollen polymer matrix minimal shrinkage of the bulk monolith was expected. However, some of the polyHIPE systems did display non-trivial shrinkage which is greater than the error of the measurements *i.e.*, MMA1 (28 %) and GMA3 (17 %) and PS-3 (7 %). The reasons for this may be different depending on the monolith. As mentioned earlier PS-3 was a chalky monolith which would easily crumble and left a residue behind of surfaces. The shrinkage could easily be as a result of physical loss of polymer which was observed during handling and washing. The monoliths GMA3 and MMA1 as well as nontrivial shrinkage both also displayed a poorly defined final internal polyHIPE structure (Figure 3.5). This lack of definition in the internal structure may have been caused by significant shrinkage distorting the final structure. A speculative explanation may be; because of the higher hydrophilicity of GMA and MMA compared to the other monomers (octanol/water partition coefficients, log $P_{ow}$, of 0.96 and 0.73 respectively) some small amount of the aqueous internal phase was able to diffuse across the oil water interface (and vice versa).

This will partially destabilise the HIPE resulting in a less continuous polymer structure which would be less rigid to contraction upon drying.

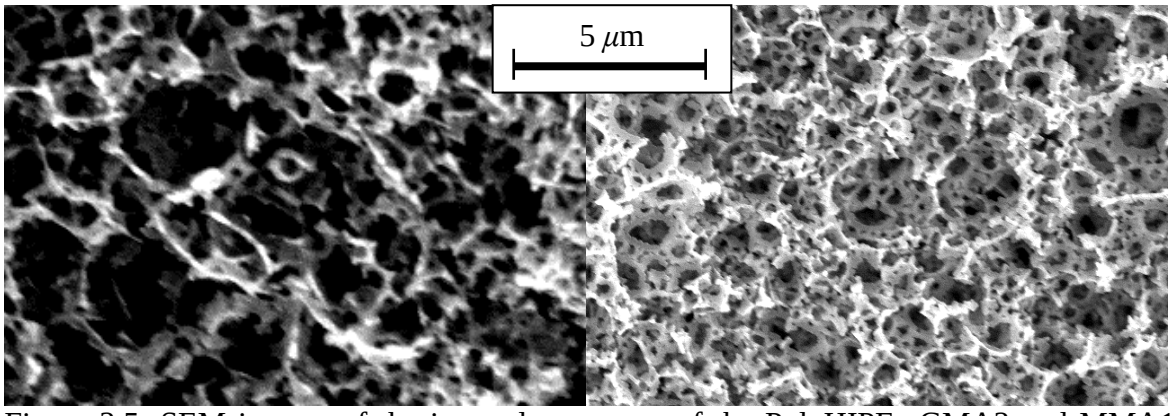


Figure 3.5: SEM images of the internal structures of the PolyHIPEs GMA3 and MMA1 showing a polyHIPE structure but one which is distorted and poorly defined.

### 3.3.2.2 Porosity With Respect To Water

Figure 3.6 shows an apparent correlation between the openness of the polyHIPEs and their porosity to water. While all polyHIPEs would in theory take up the volume of water corresponding to the internal volume due to capillary forces, in reality not all volume will be equally accessible to water. A greater degree of openness would permit a greater uptake as less volume would be excluded to the water. The presence of air bubbles in the polyHIPE will prevent water uptake particularly in small closed cages. Ideally the water uptake would have been performed with degassed water and performed under vacuum which would remove air from the polyHIPE and dissolved gasses from the water. Under such conditions each polyHIPE would be expected to take up a volume close to the nominal porosity of the polyHIPE.

The ability of polyHEMA to form a hydrogel with water, resulting in a significant swelling of the polymer matrix, explains why both HEMA75 and HEMA85 were able to take up a greater volume of water than the internal phase volume of the precursor HIPE. It also explains why HEMA75 had a significant porosity to water despite a low openness (14 %).

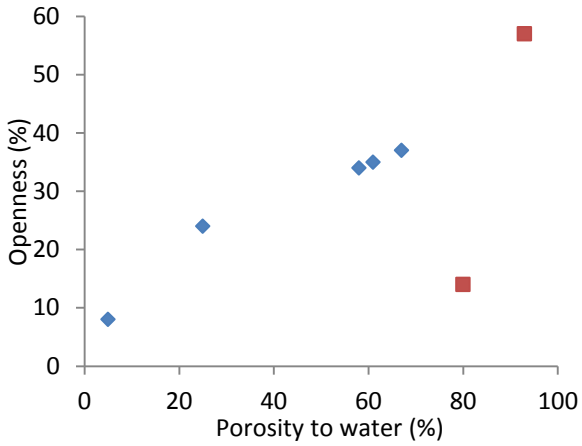


Figure 3.6: Plot of the openness of the polyHIPEs vs. porosity to water as a % of the total monolith volume. The points represented by ◆ correspond to polyHIPEs produced from hydrophobic monomers from w/o HIPEs, whereas the points represented by ■ correspond to the hydrophilic polyHEMA monoliths produced from o/w HIPEs.

### 3.3.2.3 SEM Characterisation of PolyHIPEs

Typically porous materials are characterised by either $N_2$ sorption or by mercury intrusion porosimetry (MIP), both of which allow the production of a pore size distributions. However for the polyHIPE materials discussed in this chapter, neither method was considered appropriate. $N_2$ sorption performs best for smaller pores in the micro- to meso-pore range (<50 nm) which a polyHIPE material will only have minimal amounts. [86] MIP, while useful for characterising the windows, does not return information on the cages. Instead SEM was employed to determine the cage and window sizes and the respective size distributions. Though the results produced from SEM will be of a smaller data set which can increase the random error of the measurements compared to MIP, it gave information on both the cages and the windows. SEM also allowed for the calculation of various metrics such as the number average ($D_n$ and $d_n$ respectively) and surface area average ($D_a$ and $d_a$ respectively) diameters of the cages and windows, as well as the volume average diameter ($D_v$) of the cages. These values allow for a more accurate determination of the openness of the polyHIPE. It has also previously been shown by

Wang *et al.*[53] that SEM and mercury intrusion porosimetry produce a good agreement for the window size distribution.

Table 3.5 contains the calculated average cage and average window diameters as well as openness of the polyHIPEs. SEM images and size distributions of both the cages and windows (determined from SEM) are displayed in Figure 3.9 through Figure 3.16.

Table 3.5: Average diameters of the cages and windows in the PolyHIPEs, determined by SEM.A complete data set can be found in Appendix 2 Section A2.1

| Sample | Average Cage Diameter ($\mu$m) | | | Average Window Diameter ($\mu$m) | | Openness (%) |
|---|---|---|---|---|---|---|
| | $D_n$ | $D_a$ | $D_v$ | $d_n$ | $d_a$ | |
| PS-3 | 13.0 | 13.1 | 14.2 | 2.0 | 2.3 | 37 |
| HEMA75 | 3.3 | 3.4 | 3.5 | 0.9 | 1.1 | 14 |
| HEMA85 | 3.1 | 3.2 | 3.3 | 1.3 | 1.5 | 57 |
| HEMA90 | —[a] | —[a] | —[a] | 1.1 | 1.4 | —[b] |
| BuA1 | 9.1 | 9.5 | 9.9 | 1.1 | 1.4 | 8 |
| MMA1 | —[a] | —[a] | —[a] | 0.2 | 0.2 | —[b] |
| HPMA1 | 2.1 | 2.3 | 2.4 | 0.5 | 0.6 | 34 |
| EGDMA1 | 2.2 | 2.3 | 2.4 | 0.3 | 0.4 | 35 |
| GMA3 | —[a] | —[a] | —[a] | 0.4 | 0.5 | —[b] |
| BMA3 | 4.3 | 4.4 | 5.0 | 0.4 | 0.6 | —[b] |
| BuMA1 | 3.6 | 3.7 | 3.8 | 0.5 | 0.6 | 24 |

[a] cages were to0 poorly defined for an average value to be calculated
[b] The windows of BuMA were not discrete and ran into each other. It was still possible to determine an average size and distribution, but, due to the interconnected nature of the windows, openness would be inaccurate.

As can been seen from Table 3.5 and Figure 3.9, both the cages and windows of PS-3 were significantly larger than those of the other polyHIPEs. This can most likely be attributed to the difference in the method of polymerisation. PS-3 was initiated by homolytic thermolysis of the persulphate into two sulphate radicals (Figure 3.7), which happens above 50 $^{o}$C. This resulted in a much slower polymerisation than the TEMEDA/KPS redox-couple (Figure 3.8) employed for initiation in the other HIPE systems[87] (except for VE-1 but it was not possible to characterise the internal pore structure of that monolith as is discussed later). The slower polymerisation of PS-3 will have allowed coalescence of the HIPE resulting in larger droplets which will template larger cages.

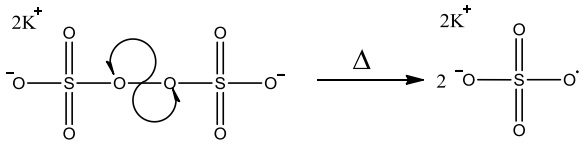

Figure 3.7: Homolytic fission of potassium persulphate by thermolysis under nitrogen at temperatures ≥ 55 °C

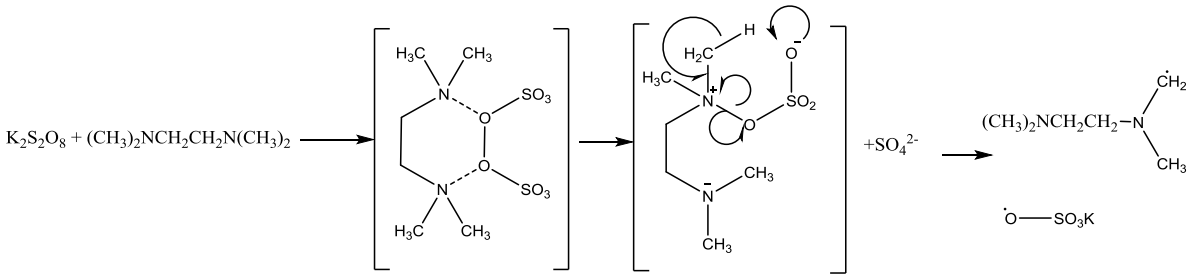

Figure 3.8: Redox generation of the sulphate radical and TMEDA radical, as proposed by Feng *et al.*[88]

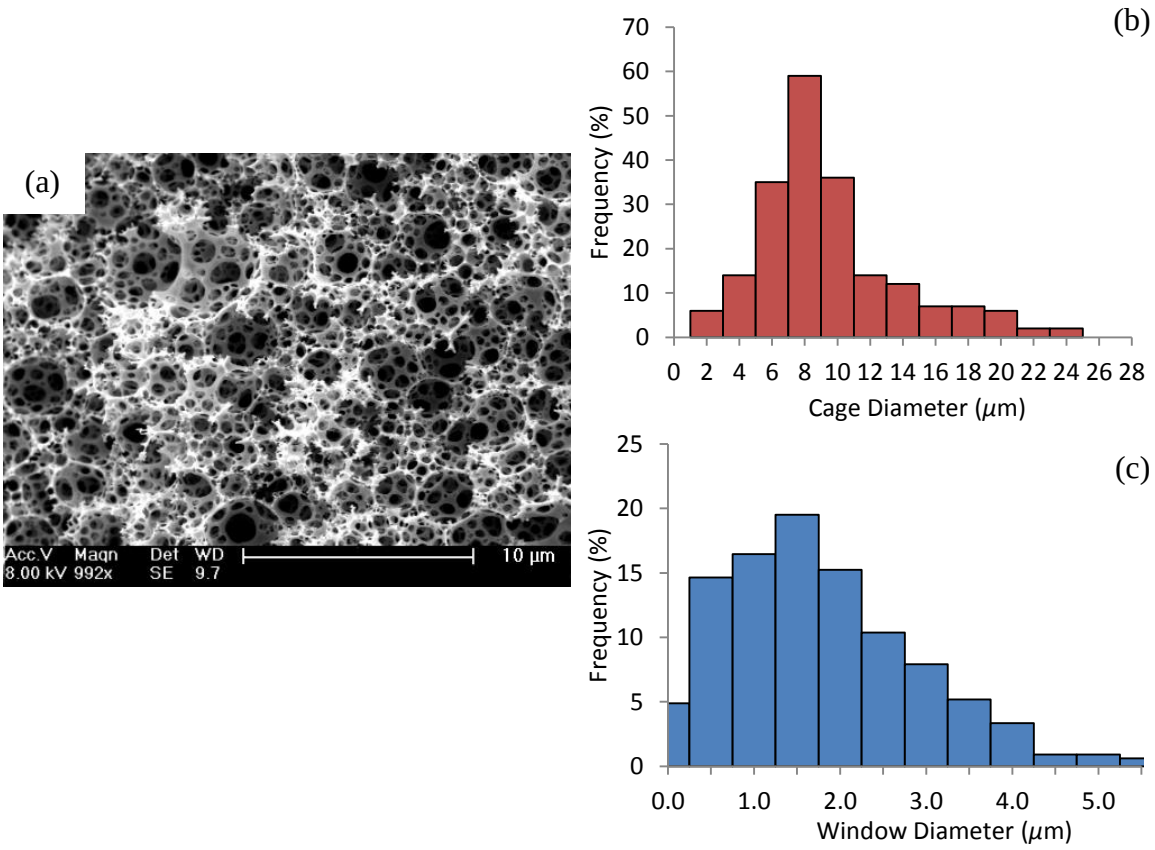


Figure 3.9: (a) SEM micrograph of the polyHIPE monolith PS-3, along with (b) the cage and (c) window size distributions calculated from SEM.

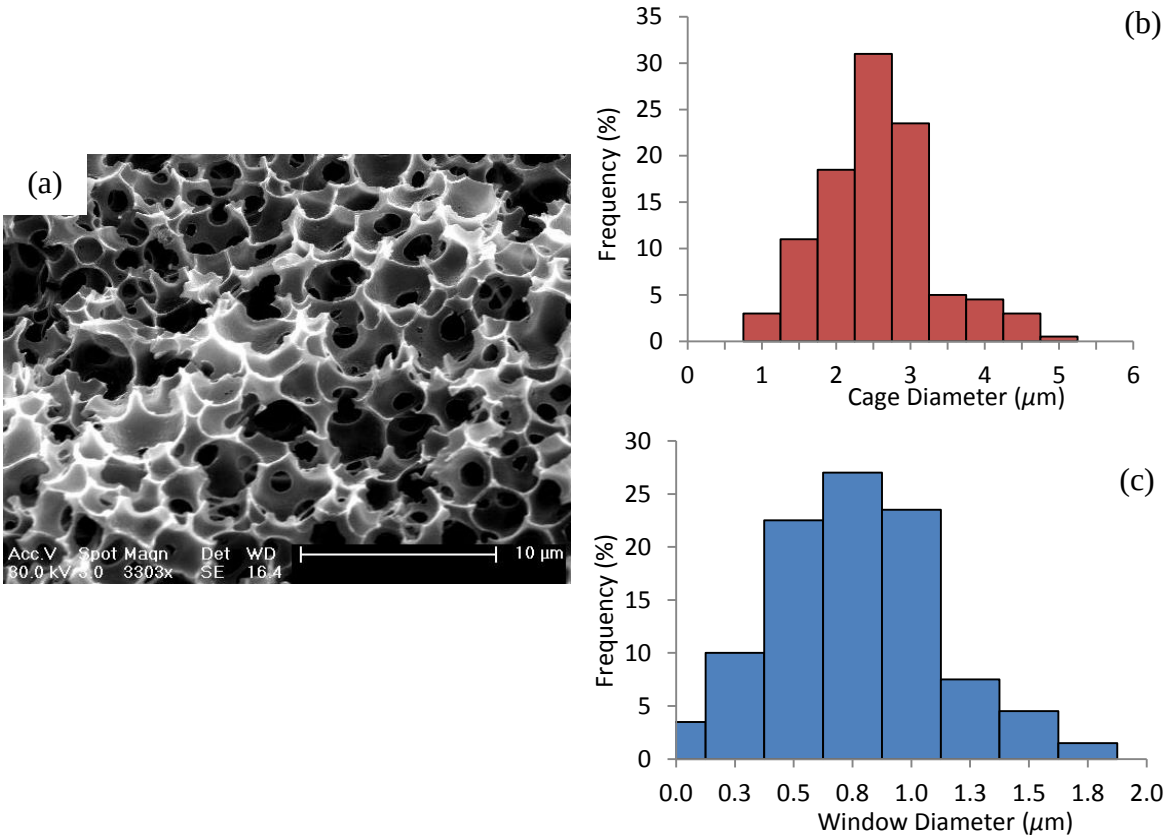


Figure 3.10: (a) SEM micrograph of the polyHIPE monolith HEMA75, along with (b) the cage and (c) window size distributions calculated from SEM.

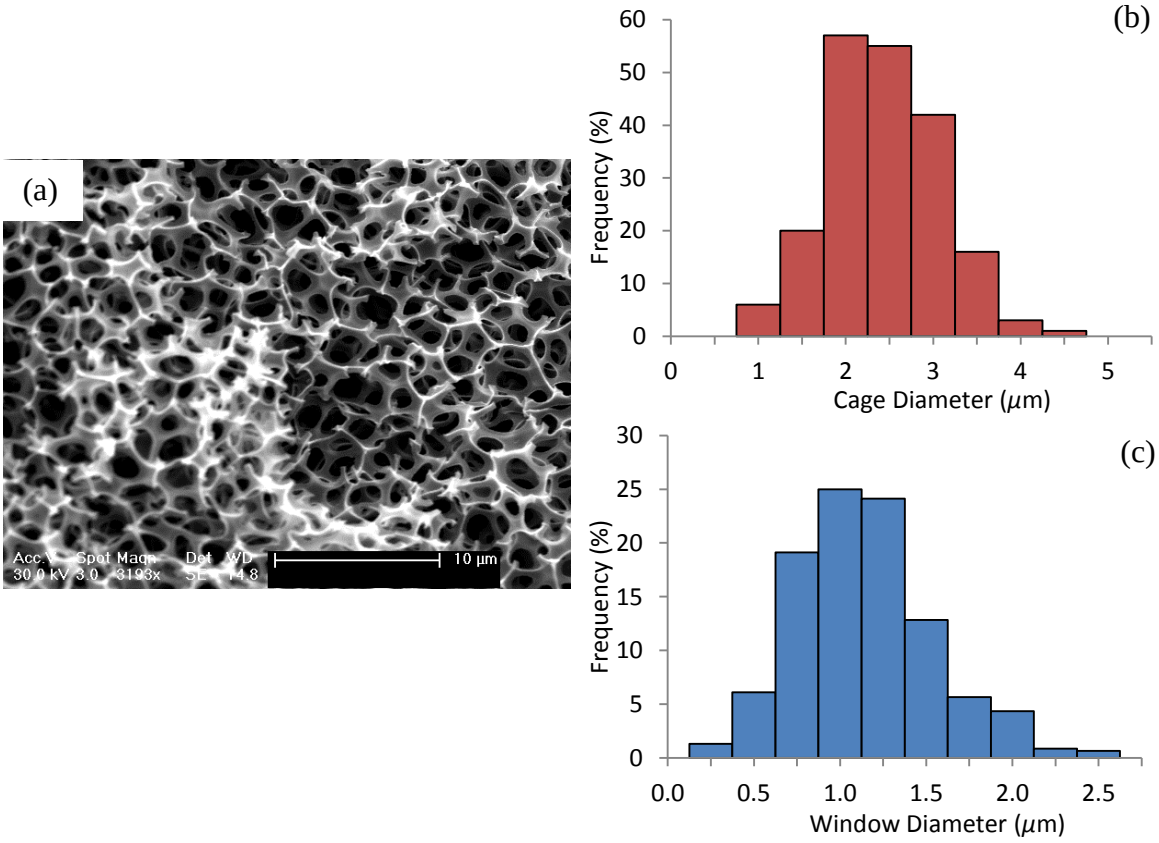


Figure 3.11: (a) SEM micrograph of the polyHIPE monolith HEMA85, along with (b) the cage and (c) window size distributions calculated from SEM.

(b)

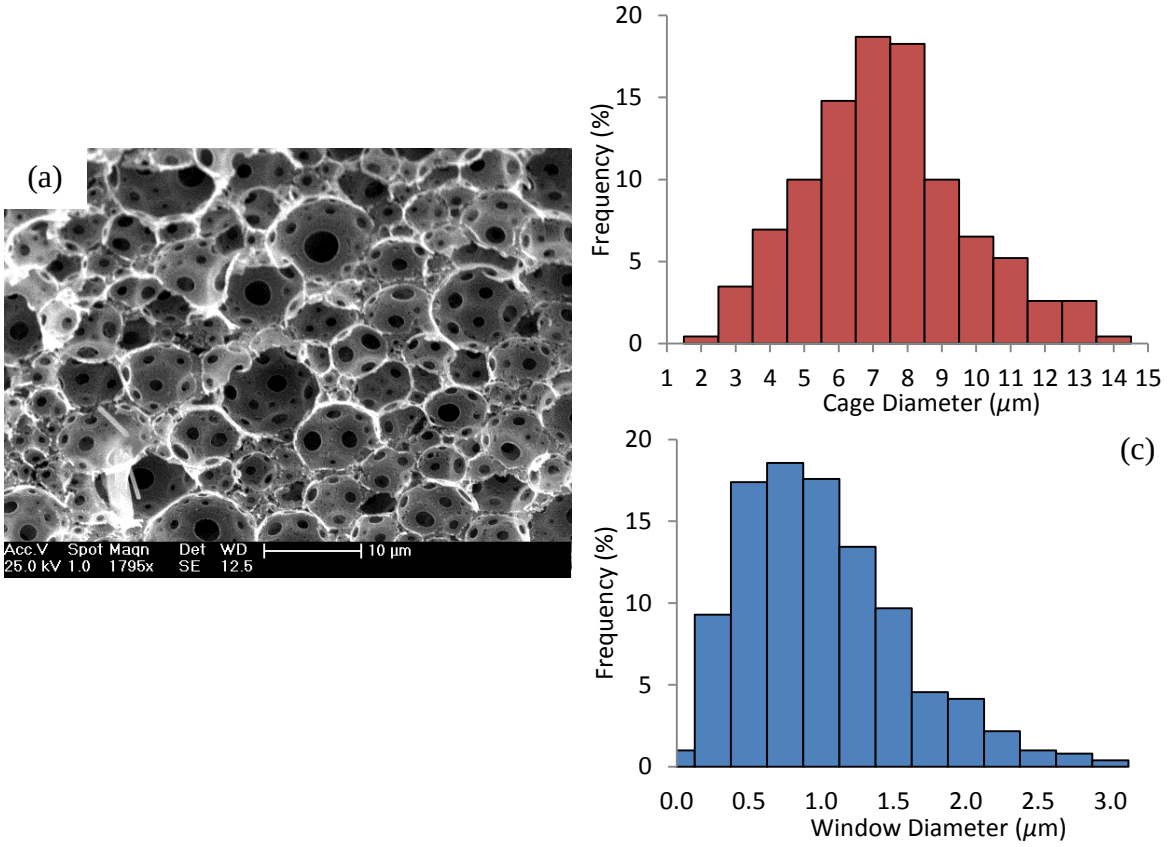


Figure 3.12: (a) SEM micrograph of the polyHIPE monolith BuA1, along with (b) the cage and (c) window size distributions calculated from SEM.

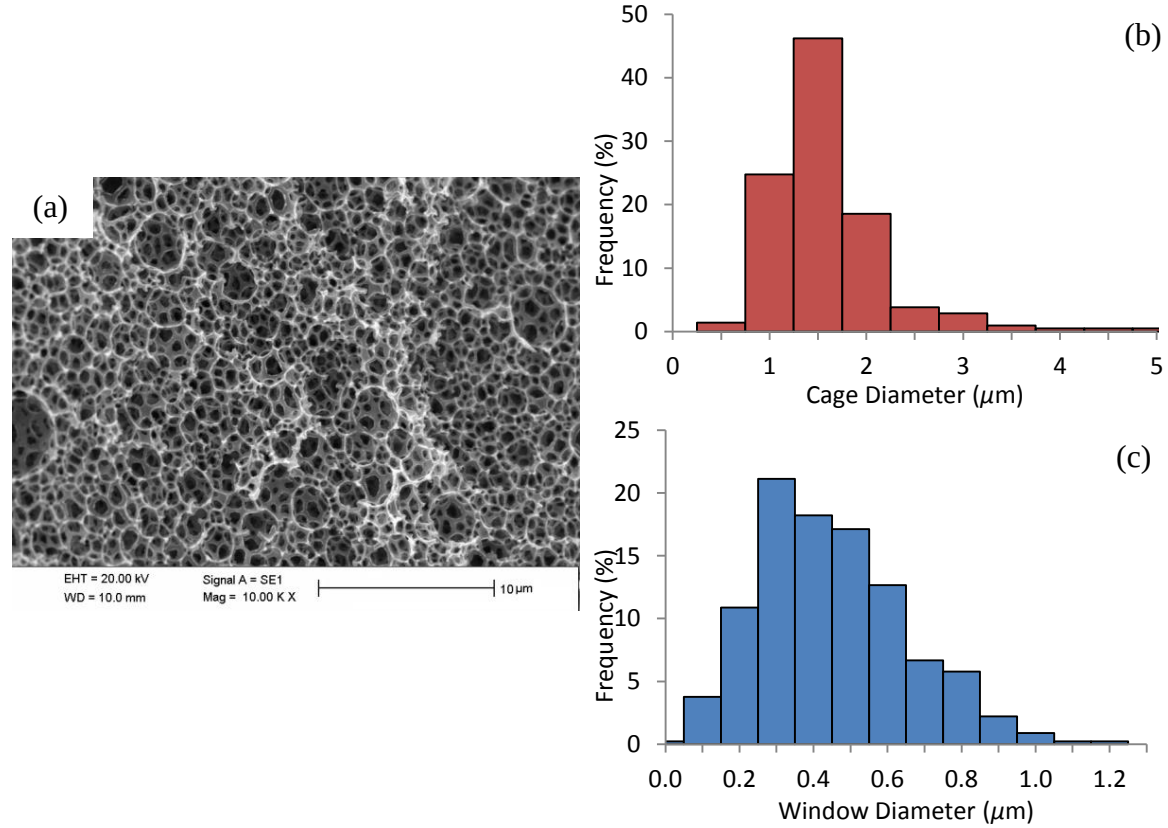


Figure 3.13: (a) SEM micrograph of the polyHIPE monolith HPMA1, along with (b) the cage and (c) window size distributions calculated from SEM.

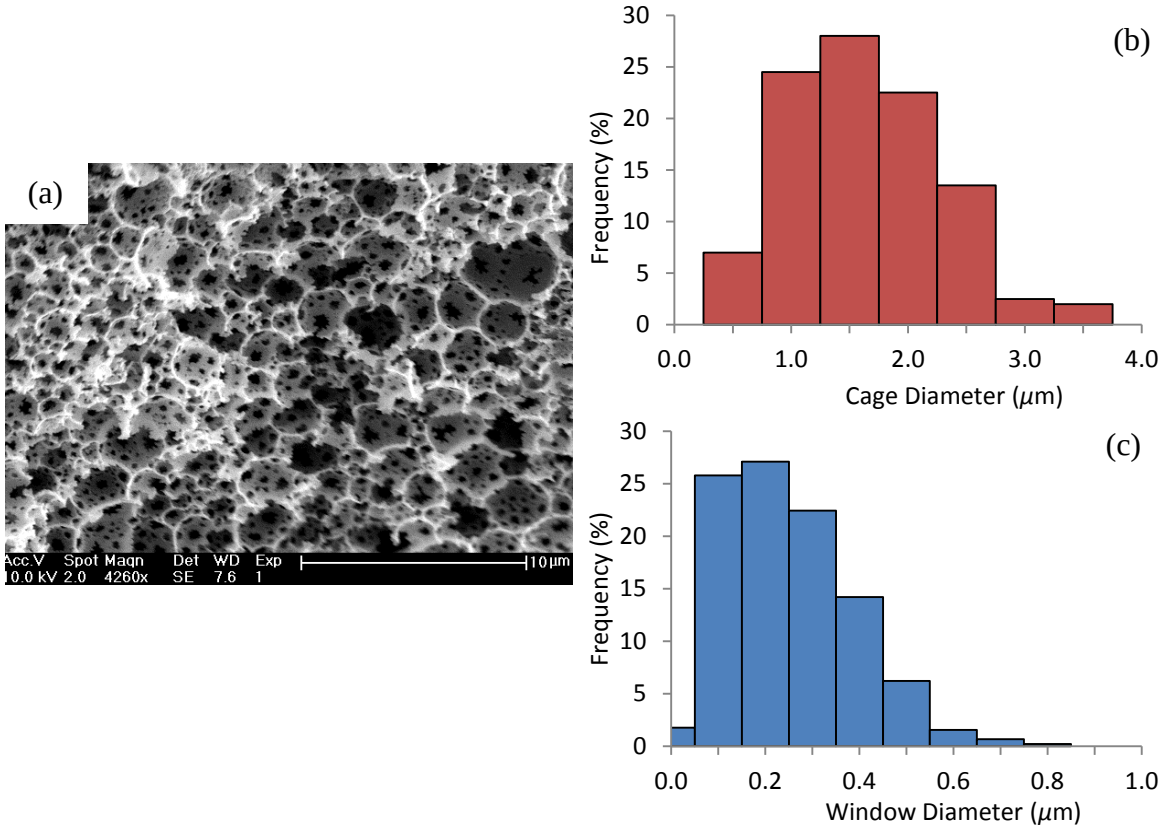


Figure 3.14: (a) SEM micrograph of the polyHIPE monolith EGDMA1, along with (b) the cage and (c) window size distributions calculated from SEM.

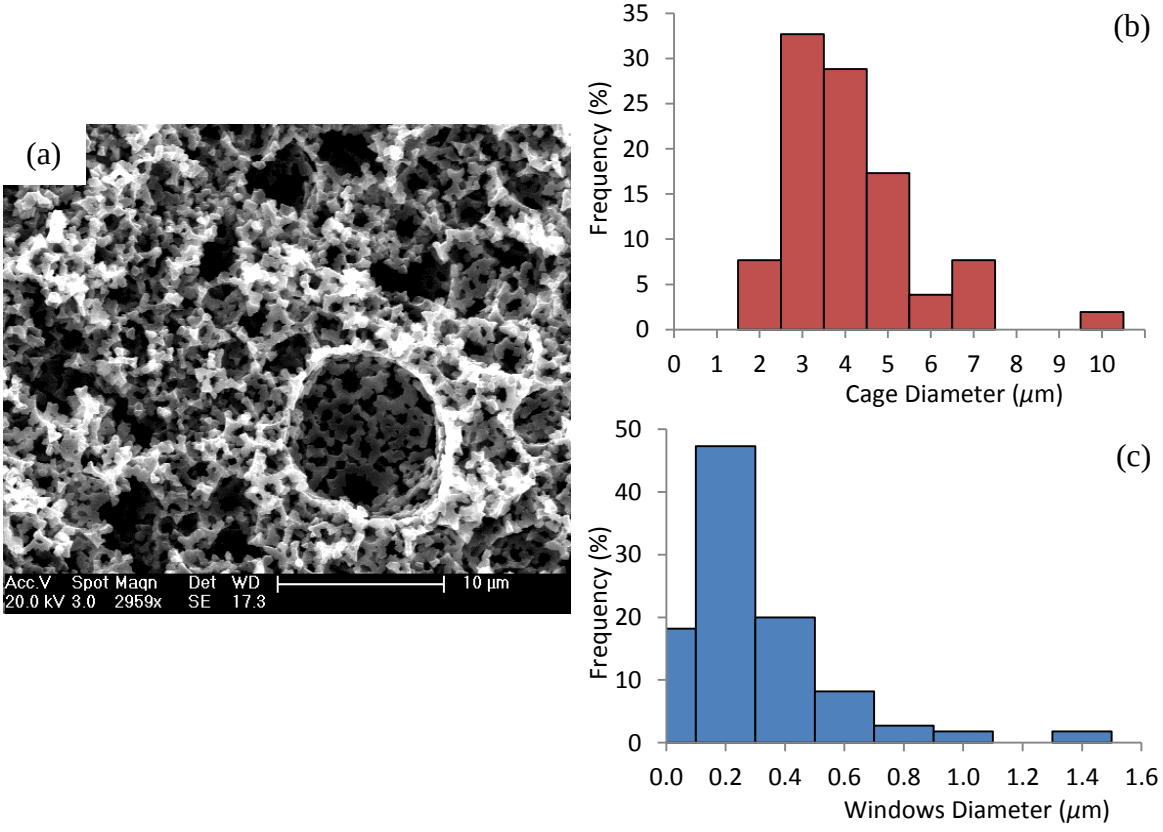


Figure 3.15: (a) SEM micrograph of the polyHIPE monolith BMA3, along with (b) the cage and (c) window size distributions calculated from SEM.

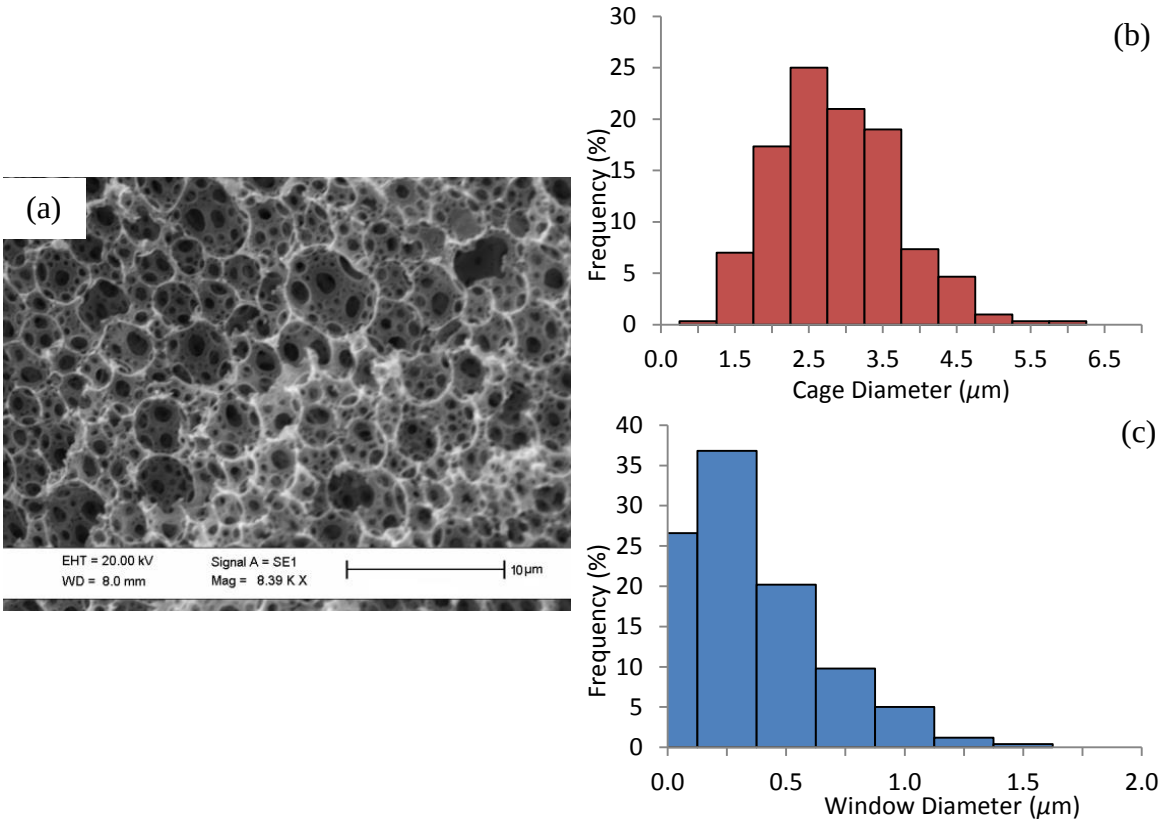


Figure 3.16: (a) SEM micrograph of the polyHIPE monolith BuMA1, along with (b) the cage and (c) window size distributions calculated from SEM.

The SEM also revealed that several of the polyHIPEs, EGDMA1 (Figure 3.14), BMA3 (

Figure **3.15**) and GMA3 (Figure 3.17), in this work possess irregular windows, which further supports that theory of Cameron *et al.*[7] that the windows are formed during polymerisation.

For three of the polyHIPEs, GMA3, MMA1 and HEMA90, it was only possible to determine the window size distribution, and not the cage sizes (Figure 3.17 to Figure 3.19). This was due to the poorly defined internal structure of the polyHIPEs. While cages were still visible, they were frequently distorted and only partially defined, meaning that it was not possible to measure an adequate number to produce an average size or size distribution. Two of the three, GMA3 and MMA1, were produced from w/o HIPES with non-trivial

water solubility (MMA 1.5% and GMA 2.3 %). This will have resulted in lower stability of the HIPE compared to those produced with highly hydrophobic monomers. This may have

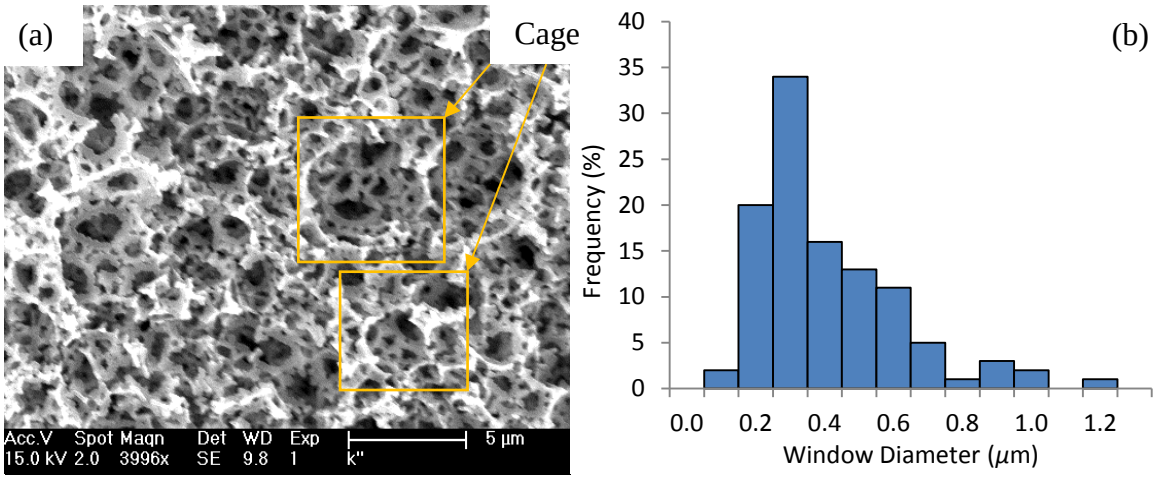


Figure 3.17: (a) SEM micrograph of the polyHIPE GMA3 with the outline of the cages emphasized and (b) the widow size distribution determined from SEM.

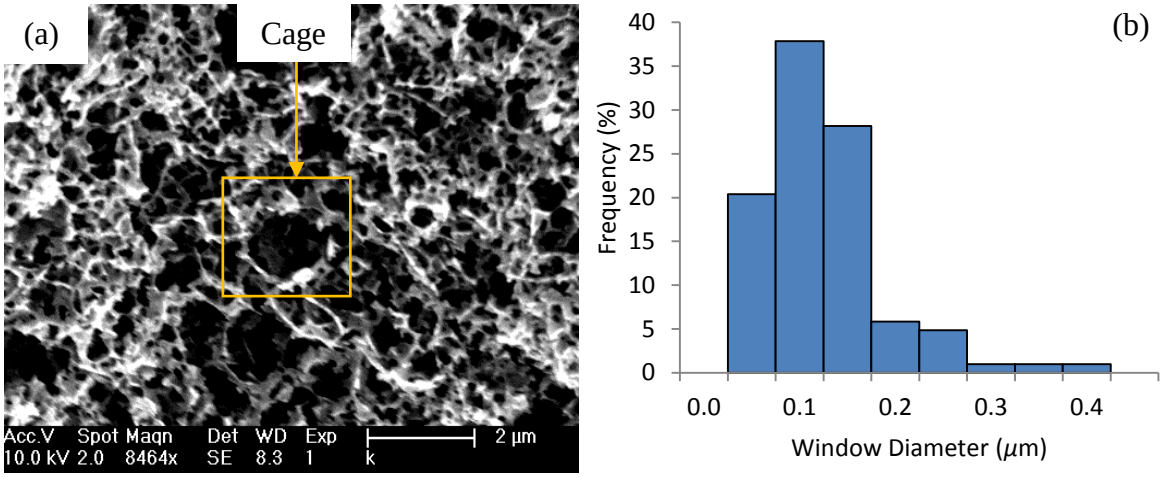


Figure 3.18: (a) SEM micrograph of the polyHIPE MMA1 with the outline of one of the cages emphasized and (b) the widow size distribution determined from SEM.

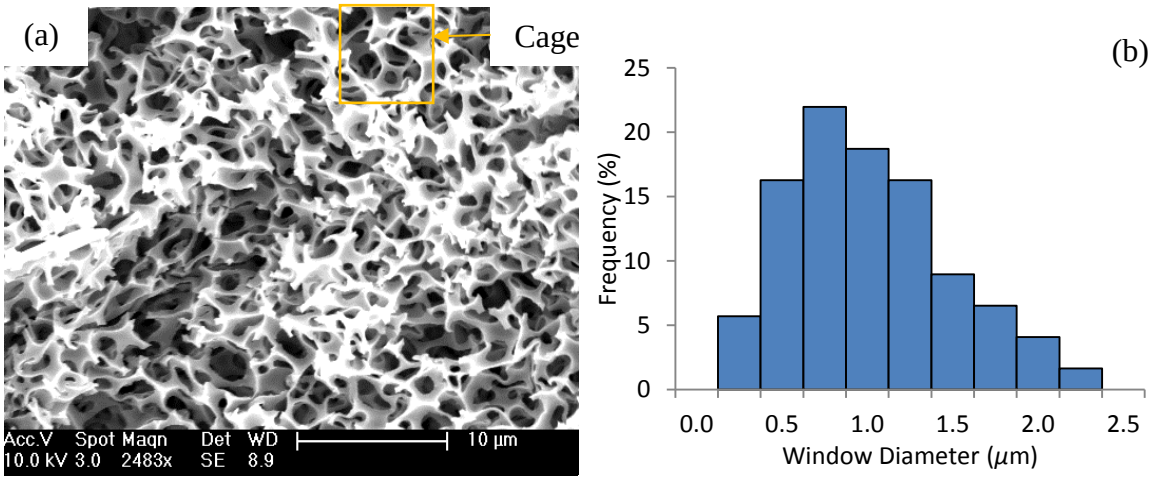


Figure 3.19: (a) SEM micrograph of the polyHIPE HEMA90, with the outline of one of the poorly defined cages outlined and (b) the widow size distribution determined from SEM.

resulted in some degradation of the HIPE structure before the polymerisation was complete, which resulted in a less defined structure in the final polyHIPE.

HEMA 90 was the polyHIPE monolith with the second greatest amount of shrinkage upon polymerisation/drying, which resulted in considerable macroscopic deformation of the resulting monolith. SEM indicates that the deformation also distorted the internal structure on the microscopic level, resulting in a poorly defined cage structure.

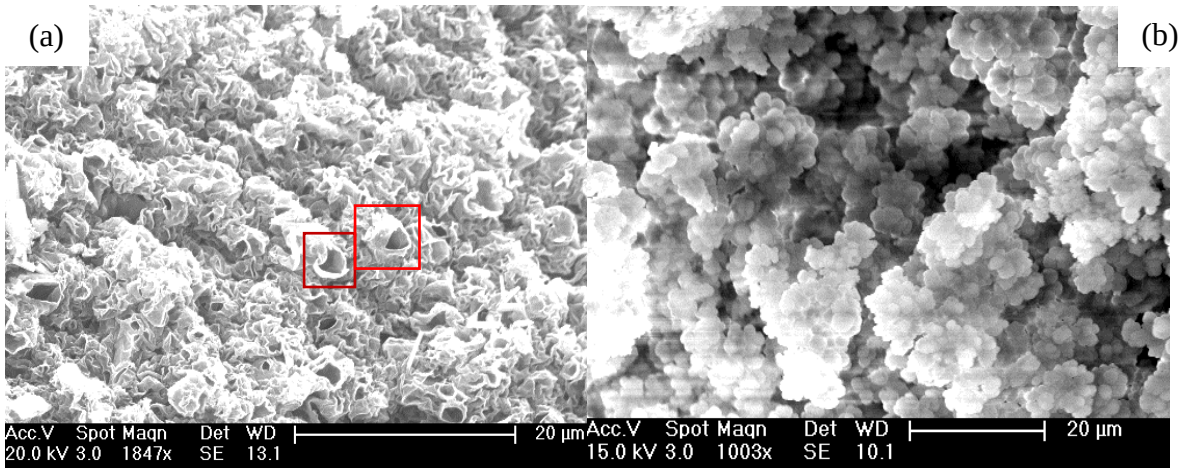


Figure 3.20: (a) SEM image of the sample StHE and (b) the sample VE-1 In image (a) two of the features which may have been templated by the emulsion droplets but did not result in interconnected cages are indicated in the red squares.

SEM of StHE, Figure 3.20 (a), and VE-1, Figure 3.20 (b), revealed that neither monolith possessed the desired open pore structure typical of polyHIPEs. StHE had an almost completely closed internal structure and VE-1 displayed an apparent nodular aggregate structure. The structure of VE-1 is similar to that of a monolithic column prepared from the same vinyl ester resin, but without HIPE templating.[75] This suggests that the HIPE may have collapsed before polymerisation. Visually the HIPE appeared stable and may have collapsed un-observed in the oven due the high temperature of polymerisation. In the work of Yang *et al.*,[78] which acted as an inspiration for this work, a vinyl-ester resin was produced by the same method. From this it was possible to produce a polyHIPE with the expected hierarchical pore structure. However in their work the choice of surfactant, PF 127 (HLB = 22), was different to the work described here.

There were features of the StHE structure that appear to have been templated by emulsion droplets, but with no interconnecting pores present. As mentioned previously, StHE was the monolith which shrunk the most upon polymerisation; this shrinkage could have prevented rupture of the inter-droplet film resulting in the closed structure.

### 3.3.2.4 Chromatographic Flow Properties of PolyHIPEs.

Before investigation into whether it was possible to produce separation with a polyHIPE stationary phase, it was necessary that they could fulfil two criteria;

1. The polyHIPE monolith had to allow a pumped flow of aqueous eluent, as the overall aim of this work was the separation of aqueous dispersions of particles.
2. If eluent flow is forthcoming, the flow must be steady and the polyHIPE must be mechanically robust enough to withstand the back pressures it will experience.

Monolithic polyHIPE stationary phases prepared in columns were produced from the same HIPE as the corresponding monolith (*e.g.*, MMA1 and MMA1c were produced from the same HIPE). This allowed association of the physical properties determined previously in the chapter with the polyHIPE in the column. Eluent was pumped through in two stages, firstly an ethanol/water mix (50:50) to remove any the internal phase as well as any unreacted monomer/surfactant and secondly deionised water. Table 3.6 summarises the results of each of the polyHIPE monolithic columns.

For polyHIPEs that would permit flow, the initial eluent (ethanol:water) would first elute cloudy but after a few hours would appear clear. PolyHIPEs which would not permit flow were extruding out of the end of the column as the backpressure increased. It had been expected that the polyHIPEs which had a greater porosity to water such as those produced from GMA, MMA or HEMA, would be more liable to permit flow, and polyHIPEs with low porosity to water (hydrophobicity) would be more likely to have

restricted flow. However, this was not the case as MMA1c, (the corresponding polyHIPE monolith MMA1 had a porosity to water of 86 %) collapsed readily under flow whereas BMA3c (the corresponding polyHIPE monolith BMA3 had a porosity to water of 9 %) would permit an eluent flow of both ethanol/water and water. So it would appear that the principal factor in determining flow through the polyHIPE columns is the robustness of the polyHIPE to the pressures of flow.

Table 3.6: Results of eluent flow testing, showing if eluent flow was possible through columns containing polyHIPE monolithic stationary phases. All had previously formed freestanding monoliths.

| PolyHIPE | Eluent Flow (yes/no) | Additional Comments |
|---|---|---|
| PS-2C | yes | |
| PS-3C | yes | |
| VE1c | yes | Only with water/ethanol; column collapsed with water alone |
| HEMA1-75c | no | |
| HEMA1-85c | no | |
| HEMA1-90c | no | |
| BuAc | no | |
| MMA1c | no | |
| EGDMA1c | yes | A low flow rate of 0.25 ml $min^{-1}$ was necessary to keep back pressure below 10 MPa |
| GMA1c | yes | |
| GMA3c | yes | |
| BMA1c | yes | |
| BMA3c | yes | |
| BuMA1c | yes | A low flow rate of 0.25 ml $min^{-1}$ was necessary to keep back pressure below 10 MPa |
| HPMA1c | no | |
| HPMA2c | no | |

It had been expected that HEMA polyHIPE columns due to their high hydrophilicity would be able to produce flow, and initially there did appear to be flow with the ethanol:water eluent, however after a while flow would cease and the backpressure on the column would increase until the polyHIPE was extruded out of the column. It may be that as the cyclohexane internal phase was removed and replaced by water containing

eluent the water would be absorbed by the polyHEMA. This would swell the polyHIPE compressing the cages resulting in a closed pore structure blocking the column.

The polyHIPE columns that permitted eluent flow were then investigated further as potential stationary phases for separation of polystyrene latexes, detailed in chapter 4, and lanthanides doped polystyrene particles as well as gold nanoparticles, detailed in chapter 6.

### 3.4 Conclusions

Several polyHIPE materials were successfully prepared and characterised, with Pluronic L121 proving to be a versatile surfactant for the production of polyHIPEs from acrylate monomers, even if the monomer displayed non-trivial water solubility. As far as the author is aware, there are no reported cases of polyHIPEs prepared from benzyl methacrylate, butyl methacrylate or hydroxypropyl methacrylate in the literature. If this is the case then this represents an expansion of the catalogue of monomers from which polyHIPEs can be prepared.

Several of the polyHIPEs, including two of the systems so far not reported in the literature (BuMA1c and BMA3c), could be prepared as monolith columns which would permit an aqueous eluent flow. These materials will be further investigated in chapter 4 and chapter 6 for potential chromatographic size separation of nanoparticles. Even if this is not forthcoming, the fact that several polyHIPEs could be prepared as columns and allow an eluent flow presents the opportunity to investigate then for other types of aqueous chromatography, not just size based.

Porosity to water of the final polyHIPE was appeared to be related to the openness. with a greater openness resulting in a greater uptake of water. The exceptions to this were the polyHEMA polyHIPE materials which took up larger volumes of water due to the ability of polyHEMA to form a hydrogel with water. However, there was no apparent

correlation between the porosity to water and the ability of the polyHIPE to permit eluent flow. The ability of the polyHIPE to withstand the pressures associated with chromatographic flow appeared to be the determining factor in permitting eluent flow.

## 3.5 References


1. P. Hainey, I. M. Huxham, B. Rowatt, D. C. Sherrington, L. Tetley, *Macromolecules*, 1991, **24**, 117–121
2. N. R. Cameron, D. C. Sherrington, *J. Mater. Chem*., 1997, **7**, 2209–2212
3. D. Wang, N. L. Smith, P. M. Budd, *Polym. Int.*, 2005, **54**, 297-203
4. Z. Abbasian, M. R. Moghbeli, *J. Appl. Polym. Sci.*, 2010, **116**, 986-994
5. H. Zhang, A. Cooper, *Soft Matter*, 2005, **1**, 107-113
6. I. Pulko, P. Krajnc, *Macromol. Rapid. Commun.*, 2012, **33**, 1731-1746
7. N. R. Cameron, D. C. Sherrinnton, L. Albiston, D. P. Gregory, *Colloid. Polym. Sci.*, 1996, **274**, 592-595
8. A. Menner, A. Bismarck, *Macromol. Symp.*, 2006, **242**, 19-24
9. P. Krajnc, N. Leber, D. Štefanec, S. Kontrec, A. Podgornik, *J. Chromatgor. A.*, 2011, **1218,** 2396-2401
10. I. Junkar, T. Koloini, P. Krajnc, D. Nemec, A. Podgornik, A. Strancar, *J. Chrmomatagor. A.*, 2007, **1144**, 48-54
11. M. Paljevac, K. Jeřabek, P. Krajnc, *J. Polym. Environ.*, 2012, **20**, 1095-1102
12. P. Krajnc, *Polimery*, 2002**, 47**, 180-183
13**.** S. S. Manly, N. Graeber, Z. Grof, A. Menner, G. F. Hewitt, F. Stepanek, A. Bismarck, *Soft Matter***,** 2009, **5**, 4780 - 4787
14. A. Menner, R. Powell, A. Bismark, *Macromolecules*, 2006, **39**, 2034-2035
15. K. Haibach, A. Menner, R. Powell, A. Bismarck, *Polymer, 2006*, **47**, 4513-4519
16. A. Menner, R. Powell, A. Bismarck, *Soft Matter*, 2006, **2**, 337-342
17. S. Kovačič, K. Jerabek, P. Krajnc, C. Slugovc, *Polym. Chem.*, 2012,**3**, 325-328
18. A. Menner, V. Ikem, M. Salgueiro, M. S. P. Shaffer, A. Bismarck, *Chem. Commun.*, 2007, 4274-4276
19. V. O. Ikem, A. Menner, A. Bismarck, *Langmuir*, 2010, **26**, 8836-8841
20. V. O. Ikem, A. Menner, T. S. Horozov, A. Bismarck, *Adv. Mater.*, 2010, **22**, 3588-3592
21. S. D. Kimmins, N. R. Cameron, *Adv. Funct. Mater.*, 2011, **21**, 211-225
22. D. Barby, Z. Haq, *EU Pat. Appl.*, 1982 601 138
23. Z. Haq, *Eu Pat. Appl.*, 1984, 105 634
24. H. Bartl, W. Von Bonin, *Makromol. Chem.*1962, **57,** 74-95
25. J. M. Williams, D. A. Wrobleski, *Langmuir*, 1988, **4**, 656–662.
26. J. M. Williams, *Langmuir*, 1991, **7**, 1370–1377
27. J. M. Williams, A. J. Gray, M. H. Wilkerson, *Langmuir*, 1990, **6**, 437–444
28. P. Hainey, I. M. Huxham, B. Rowatt, D. C. Sherrington, *Macromolecules*, 1991, **24**, 117–121.
29. N. R. Cameron, A. Barbetta, *J. Mater. Chem*., 2000, **10**, 2466–2471.
30. I. Pulko, J. Wall, P. Krajnc, N. R. Cameron, *Chem.-Eur. J*., 2010, **16**, 2350-2354
31. M. G. Schwab, I. Senkovska, M. Rose, N. Klein, M. Koch, J. Pahnke, G. Jonschker, B. Schmitz, M. Hirscher, S. Kaskel, *Soft Matter*, 2009, **5**, 1055-1059
32. J. R. Duke, M. A. Heisington, D. A. Langlois, B. C. Benicewicz, *Polymer*, 1998, **39**, 4369–4378
33. N. R. Cameron, D. C. Sherrington, *Macromolecules*, 1997, **30**, 5860–5869
34. W. Busby, N. R. Cameron, C. A. B. Jahoda, *Biomacromolecules*, 2001, **2**, 154–164.
35. Y. Lumelsky, M. S. Silverstein, *Macromolecules*, 2009, **42**, 1627-1633
36. W. Busby, N. R. Cameron, C. A. B. Jahoda, *Polym. Int.*, 2002, **51**, 871–881.
37. E. M. Christenson, W. Soofi, J. L. Holm, N. R. Cameron, A. G. Mikos, *Biomacromolecules*, 2007, **8**, 3806-3814
38. N. R. Cameron, D. C. Sherrington, *J. Mater. Chem*., 1997, **7**, 2209–2212
39. P. Krajnc, D, Štefanec, J. F. Brown, N. R. Cameron, *J. Polym. Sci. A.*, 2004, **43**, 296-303
40. S. Kovačič, P. Krajnc, *J. Polym. Sci. A.*, 2009, **47**, 6726-6734
41. I. Gurevitch, M. S. Silverstein, *J. Polym. Sci. A.*, 2010, **48**, 1516-1525
42. J. Yang, G. Yang, H. Liu, L. Bai, Q. Zhang, *J. Appl. Polym. Sci.*, 2011, **119**, 412-418

43. A. Barbetta, M. Dentini, L. Leandri, G. Ferraris, A. Coletta, M. Bernabei, *React. Funct. Polym*. 2009, **69**, 724-736
44. S. Livshin, M. S. Silverstein, *Macromolecules*, 2007, **40**, 6349-6354
45. S. Livshin, M. S. Silverstein, *Macromolecules* 2008, **41**, 3930-3938
46. S. Kovacic, G. Ferk, M. Drofenik, P. Krajnc, *React. Funct. Polym.*, 2012, **72**, 955–961
47. S. Kovačič, N. B. Matsko, G. Ferk, C. Slugovc, *J. Mater. Chem. A*, 2013, **1**, 7971-7978
48. H. Deleuze, R. Faivre, V. Herroguez, *Chem. Comm*., 2002, 2822–2823.
49. S. Kovačič*a*, P. Krajnc, C. Slugovc, *Chem. Commun.*, 2010, **46**, 7504-7506
50. H. Karimian, M. R. Moghbeli, *J. Appl. Polym. Sci*., 2013, **127**, 804-811
51. K. Jomes, B. R. Lothian, A. Martin, G. Taylor, Z. Haq, *US Pat. Appl*., 1986, 4 611 014.
52. N.R. Cameron, D.C. Sherrington, I. Ando, H. Kurosu, *J. Mater. Chem.*, 1996, **6**, 719-726
53. D. Wang, N.L. Smith, P.M. Budd, *Polym. Internat.*, 2005, **54**, 297-30
54. Fabrice Audouin, A. Heise, *Eur. Polym. J*., 2013, **49**, 1073–1079
55. F. Audouin, M. Fox, R. Larragy, P. Clarke, J. Huang, B. O'Connor, A. Heise, *Macromolecules*, 2012, **45**, 6127–6135
56. P. Krajnc, N. Leber, D. Stefanec, *Š*. Kontrec, A. Podgornik, *J. Chromatogr. A*, 2005, **1065**, 69-73
57. C. H. Yao, L. Qi, H. Y. Jia, P. Y. Xin, G. L. *Yang, Y. Chen, J. Mater. Chem.* 2009, **19**, 767-772
58. O. Kulygin, M. S. Silverstein, *Soft Matter*, 2007, **3**, 1525-1529
59. S. Kovačič, D. Stefanec, P. Krajnc, *Macromolecules*, 2007, **40**, 8056-*8060*
60. S. Fujishige, K. Kubota, I. Ando, *J. Phys. Chem*. 1989, **93**, 3311-3313
61. H. F. Zhang, A. I. Cooper, *Adv. Mater*. 2007, **19**, 2439-2444
62. A. Barbetta, M. Dentini, M. S. De Vecchis, P. Filippini, G. Formisano, S. Caiazza, *Adv. Funct. Mater*. 2005, **15**, 118-*124*
63. A. Barbetta, M. Massimi, L. C. Devirgiliis, M. Dentini, *Biomacromolecules* 2006, **7**, 3059-3068
64. F. Fernandez-Trillo, J. C. M. van Hest, J. C. Thies, T. Michon, R. Weberskirch, N. R. Cameron, *Adv. Mater*. 2009, **21**, 55-59
65. R. Butler, C. M. Davies, A. I. Cooper, *Adv. Mater.*, 2001, **13**, 1456–1463
66. R. Butler, I. Hopkinson, A. I. Cooper, *J. Am. Chem. Soc*., 2003, **125**, 14473–81.
67. C. Forgacz, M. Birot, H. Deleuze, *J. Appl. Polym. Sci.*, 2013, **129**, 2606-2013
68. H. Zhang, A. Cooper, *Chem. Mater*. 2002**, 14**, 4017-4020
69. N. H. Li, J. R. Benson, N. Kitagawa, *US Pat. Appl.*, 1997, 5 653 922
70. D. Stefanec, P. Krajnc, *Polym. Int*. 2007, **56**, 1313-1319
71. D. Stefanec, P. Krajnc, *React. Funct. Polym*. 2005, **65**, 37– 45
72. A. Desforges, M. Arpontet, H. Deleuze, O. Mondain-Monval, *React. Funct. Polym*. 2002, **53**, 183-192
73. M. T. Gokmen, W. Van Camp, P. J. Colver, S. A. F. Bon, F. E. Du Prez, *Macromolecules* 2009, **42**, 9289-9294
74. J. G. Gao, H. L. Du, H. N. Sun, *Chin J Catal*,1989, **10**, 422-428
75. G. L. Yang, H. Y. Liu, L. G. Bai, M. M. Jang, T. Zhu, *Microporous Mesoporous Mater.* 2008, **112**, 351-356
76. G. Fogassy, C. Pinel, G. Gelbard, *Catal. Commun*. 2009, **10**, 557-560
77. S. Kovačič, D. Štefanec, P. Kranjnc, *Macromolecules*, 2007, **40**, 8056-8060
78. J. Yang, G. Yang, H. Liu, L. Bai, Q. Zhang, *Chinese J. Chem.*, 2010, **28**, 229-234
79. A. Barbette, N. R. Cameron, *Macromolecules*, 2004, **37**, 3188-3204
80. United States Environmental Protection Agency, *OPPT Chemical Fact Sheets (Styrene) Fact Sheet: Support Document*, 1994, **EPA 749-F-95-019a**
81. Dow Chemical Company, *Divinylbenzene*, 2003, Form No. **503-00002-0103AMS**
82. United States Environmental Protection Agency, OPPT Chemical Fact Sheets (Methyl Methacrylate) Fact Sheet: Support Document, 1994, **EPA 749-F-94-014a**
83. Dow Chemical Company, Glycidyl Methacrylate (GMA), Form No**. 296-01330-1205X-IK**
84. O. Kulygin, M. S. Silverstein, *Soft Matter*, 2007, **3**, 1525-1529
85. W. M. Meylan, P. H. Howard, R. S. Boethling, *Environ. Toxicol. Chem.* 1996, **15**, 100-106

86. S. Lowell, J. E. Shields, M. A. Thomas, M. Thommes in *Characterization of Porous Solids and Powders: Surface Area, Pore Size and Density*, Kluwer, Drodrecht, 2004, ch. 8, pp. 101-128
87. G. Moad, D. H. Solomon in *The Chemistry of Radical Polymerization*, Elsevier, Amsterdam, 2006, ch. 3, pp.319-168
88. X. D. Feng, X. Q. Guo, K. Y. Qiu, *Makromol. Chem.*,1988, **189**, 77-83

# Chapter 4

# Application of PolyHIPE Chromatography with UV detection for the Separation of Polystyrene Latexes.

## 4.1 Introduction

As was known from chapter 3, the five polyHIPE columns BMA3c, BuMA1c, EGDMA1c, GMA3c and PS-3c would all allow a pumped eluent flow of deionised water to transit through. To investigate if these polyHIPE monolithic columns could be employed for size separation they were incorporated into a high pressure liquid chromatography (HPLC) system and different sized analytes injected into the flow.

### 4.1.1 Aims and Objectives

The aim of the work undertaken in this chapter was to use polyHIPE chromatography to separate commercially obtained polystyrene latexes.

A HPLC system was constructed and polyHIPE columns were fitted into the system. To give the best chance of a resolution of the individual particles the latexes were selected covering a wide size range (latex particles with advertised diameters of 100 nm, 460 nm and 800 nm were used) and detection was by means of a UV-VIS detector.

In an effort to minimise electrostatic interactions between the particles and the column, the mobile phase was based on one previously described in the literature, which

had been developed to minimise the electrostatic interactions between latex particles and the column bed in hydrodynamic chromatography (HDC).[1]

### 4.1.2 List of relevant abbreviations from Chapter 3

BMA – benzyl methacrylate

BuMA – butyl methacrylate

EGDMA – ethyleneglycol dimethacrylate

GMA – glycidyl methacrylate

KPS – Potassium persulphate

PS – polystyrene

TEMDA – N,N,N',N'-tetramethylethylenediamine

### 4.1.3 Size Separation

As mentioned in Chapter 1, the chromatographic methods of size exclusion chromatography (SEC) and hydrodynamic chromatography (HDC) have been used successfully in the size separation of nanoparticles. As with all analytical techniques they both have advantages and disadvantages. While SEC has good separation efficiency the operating size range is poor,[2] and unwanted column interactions can sometimes occur.[3] While HDC has a very good operational size range (5-1200 nm)[2] the separating efficiency is currently comparatively poor, although this can be improved by the use of narrower diameter capillaries and smaller packing materials. Though polyHIPEs as monolithic separation media are a relatively new concept, there are several reports in the literature of successful separations using a polyHIPE as a stationary phase (see section 4.1.4).

However, as far as the author is aware, there have, to date, been no reported instances of size-based separation using polyHIPEs.

Conceptually the interconnected pores of a polyHIPE can be viewed as an inverse packed HDC column (Figure 4.1), in which flow will occur in the cages. In HDC flow can only occur in the interstitial volume between beads; this would mean that flow in polyHIPEs would have the advantage of less redundant volume which is inactive during separation. It is hoped that by using analytes of similar chemical identity but different sizes, *i.e.*, polystyrene latex particles, that a size separation, can be achieved with polyHIPE columns.

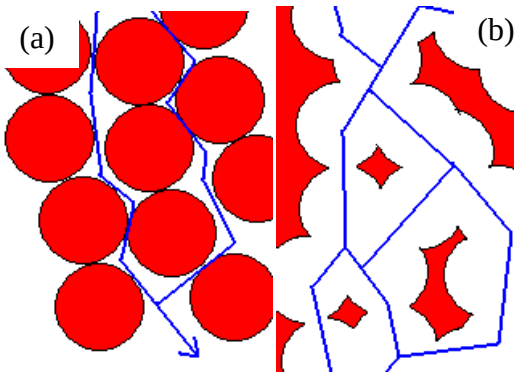


Figure 4.1: Representations of the possible particle path through a HDC column packed with solid beads (a) and through a polyHIPE structure (b)**.**

### 4.1.4 Use of HIPE Templated Materials for Separation and Filtration

Due to the very high porosity of polyHIPEs they have attracted some interest as a potential medium for separation and chromatography. As well as patents disclosing methods of separation with polyHIPEs,[4,5] there are also several cases documented in the literature where researchers have used polyHIPEs for a variety of separations.

Benicewicz and co-workers[6] produced poly(styrene-*co*-vinylbenzylchloride) polyHIPE monoliths which had been functionalised by graft polymerisation of vinylpyridine creating ion exchange properties. These were then used for the separation of

heavy metals, displaying good uptake of both iron and plutonium from aqueous solutions. Tripp and co-workers[7] prepared poly(styrene-*co*-DVB) polyHIPEs to which they grafted the polymer poly(*N*-vinylacetamide). Amide cleavage of the poly(*N*-vinylacetamide) produced a polyHIPE monolithic column containing primary amine groups. This column was then utilised for efficient continuous-flow scavenging of isocyanates.

Bhumgara[8] created a cross-flow filtration module from a poly(styrene-*co*-DVB) polyHIPE which was then used to completely clean a 1 % (by volume) aqueous suspension of aragonite (mean particle diameter 11 $\mu$m). The system proved less successful for the filtration of a solution of cationic surfactant, which was attributed to the formation of a gel on the polyHIPE surface leading to higher rejection. This was partially resolved by use of a sulphonated polyHIPE, but this led to a decrease in permeate flow rate.

Tunç and co-workers have used both poly(isodecylacrylate-*co*-DVB)[9] and poly(styrene-*co*-DVB)[10] polyHIPE columns for the separation of alkylbenzenes by capillary electrochromatography obtaining good resolution. In both cases the polyHIPE columns showed strong electroosmotic flow without the need for an electroosmotic flow generating monomer.

Junkar and co-workers[11] have done work into investigating the pressure drop characteristics of polyHIPE monoliths, which suggests that from a hydrodynamic viewpoint polyHIPEs have some similarities to foam structures, though the results are far from conclusive.

The most common use for polyHIPEs as separation media has been in the separation of proteins and recent years have seen a fair amount of work published on this topic. Yang and co-workers[12] prepared polyHIPE from a novel vinylester resin cross-linked with EDGMA. The polymerisation of the HIPE was performed within a HPLC column and, after washing the polyHIPE with a flow of methanol, they were able to

separate immunoglobulin from an aqueous solution of human plasma and chicken egg yolk, as well as separating interleukin-18 and lysine. The column showed a low back pressure and high column efficiency. Yao and co-workers[13] converted poly(GMA-*co*-EDGMA) monolithic columns into polyHIPEs with weak anion-exchange properties by ring-opening of the epoxy groups present on GMA. These columns were then used in the separation of a protein mixture of lysozyme, BSA, ovalbumin and pepsin A, with an almost complete separation being achieved at a flow rate of 6 ml $min^{-1}$. Krajnc and co-workers[14] also functionalised the epoxy groups of poly(GMA-*co*-EDGMA) monolithic polyHIPE columns. These were used for the separation of moyoglobin, conalbumine and trypsin inhibitor, with good separation being achieved over a short time scale. Pulko and co-workers[15] cast polyHIPE membranes of poly(GMA-*co*-EDGMA-*co*-ethylhexyl methacrylate) which they then modified to form ion-exchange membranes which were then used for the purification of bovine serum albumin.

## 4.2 Experimental

The synthesis of the polyHIPE columns investigated in this chapter is detailed in section 3.2 of chapter 3. Of all the polyHIPEs produced in chapter 3, only those which would permit a flow of water were further investigated in this chapter. A brief summary of the columns is provided here and in Table 4.1 for convenience. All polyHIPE columns were prepared from w/o oil HIPEs of 90 % internal phase volume. Once formed, the HIPEs were injected into blank stainless steel HPLC columns (column length and internal diameter (i.d.) 150 mm x 4.6 mm) and polymerised under the appropriate conditions. Columns were first washed with an eluent flow of ethanol and water (50:50 mixture). After washing was complete the flow was replaced with one of deionised water.

Table 4.1: Summary of the synthesis conditions of the polyHIPE columns discussed in this chapter. For full synthetic details see chapter 3.2

| Column | Monomers | Surfactant | Initiator | Polymerisation Conditions |
|---|---|---|---|---|
| BMA3 | BMA/EGDMA | Pluronic L121 | KPS/TMEDA | 2 hrs @ 50 $^{o}$C |
| BuMA1c | BuMA/EGDMA | Pluronic L121 | KPS/TMEDA | 2 hrs @ 50 $^{o}$C |
| PS-3c | Styrene/DVB | Span 80 | KPS | 72 hrs @ 65 $^{o}$C |
| EGDMA1c | EGDMA | Pluronic L121 | KPS/TMEDA | 2 hrs @ 50 $^{o}$C |
| GMA3c | GMA/EGDMA | Pluronic L121 | KPS/TMEDA | 2 hrs @ 50 $^{o}$C |

### 4.2.1 Equipment

Chromatography experiments were performed on a HPLC system built from a constant flow pump (model 305 Gilson, USA), a manometric module (model 805 Gilson, USA), a manually driven injector valve with an appropriate sample loop (Table 4.2) (model 7125 Rheodyne, USA). Detection was by means of a UV/Vis detector (model 151 Gilson, USA) set at 280 nm, with a sensitivity of 0.005 aufs and a peak width of 10 seconds. Data was acquired by means of a data logger (ADC-11 Pico Technologies, UK) and plotted using PicoLog recorder software (Pico Technologies, UK).

Table 4.2: Parameters of the chromatography set-up specific to the individual the polyHIPE monolithic columns investigated in this chapter.

| Column | Injection Loop (μl) | Flow Rate (ml min$^{-1}$) | Latex Concentration (% w/v) |
|---|---|---|---|
| BMA3 | 50 | 1.00 | 0.01 |
| BuMA1c | 1000 | 0.25 | 0.05 |
| PS-3c | 50 | 1.00 | 0.1 |
| EGDMA1c | 1000 | 0.25 | 0.1 |
| GMA3c | 50 | 0.10 | 0.1 |

### 4.2.2 Chemicals

Actetone (Sigma-Aldrich), sodium azide (Aldrich), sodium dodecyl sulphate (SDS, ≥ 99 %; Sigma-Aldrich), sodium hydrogen phosphate (Alfa Aesar) and TWEEN® 80 **(**sorbitan monooleate; Fluka) were all used as received.

### 4.2.3 Preparation of the Mobile Phase

The mobile phase was based on one described in the literature by McGowan and Langhorst,[1] which had been previously used for the separation of polystyrene latexes in a HDC column. In a large conical flask sodium azide (0.2 g), Tween 80 (2 g), SDS (0.5 g) and sodium hydrogen phosphate, as a buffer, (0.02 g) were all dissolved in deionised water (1 l) which had previously been degassed under vacuum. The flask was then sealed and before each use a low flow of nitrogen was bubbled through the mobile phase for 30 minutes.

### 4.2.4 Separations

Separations were performed on commercial latexes of three sizes, 100 nm, 460 nm and 800 nm (solid content 10 % w/v; Aldrich). The latexes were diluted with mobile phase before use (see Table 4.2 for details of the dilutions used with each column) and then sonicated for 10 minutes to ensure the highest possible monodispersity. Acetone was diluted to 1 % v/v in mobile phase and used as a low molecular weight marker. The flow rate of the pump was tailored for each column to keep the back pressure below 10 MPa (Table 4.2). Injection was undertaken manually and data acquisition was also started manually as rapidly as possible after injection (≈ 1 second). Injections were repeated in duplicate or triplicate. Data and chromatographs reported are averages of triplicate injections.

Table 4.3: Comparison of the advertised with the measured diameter of the latex particles with the diameter measured by DLS. All samples were diluted in mobile phase before measurement.

| Advertised Latex Diameter (nm) | $D_z$ (nm) | PDI |
|---|---|---|
| 100 | 105 | 0.03 |
| 460 | 489 | 0.03 |
| 800 | 830 | 0.01 |

The sizes of the latex particles were confirmed by diluting the particles in mobile phase and measuring the hydrodynamic diameter (the relevant size for chromatography) by dynamic light scattering (DLS) (Table 4.3 and Figure 4.2). DLS was performed on a Zetasizer Nano ZS (Malvern Instruments, UK) with a maximum 5 mW He-Ne laser, of 633 nm wavelength, at 25 $^{o}$C.

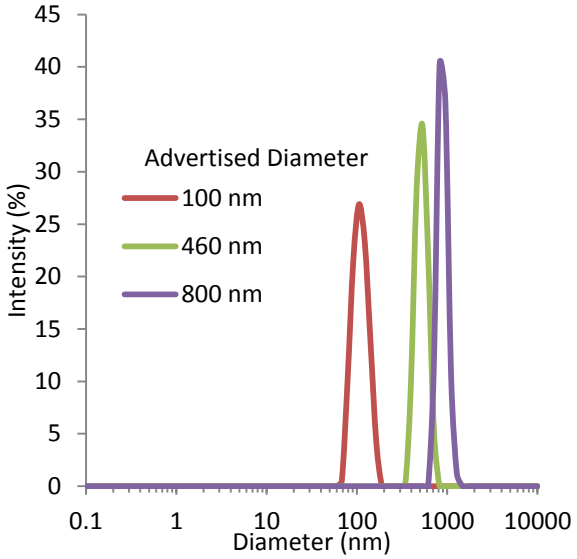


Figure 4.2: Intensity size distributions, measured by DLS, of the commercial polystyrene latex particles used to test the chromatographic properties of the polyHIPE columns described in this chapter.

### 4.2.5 Analysis of the Chromatograms

Resolution of the column and the peak asymmetry factor was calculated from the chromatographs by the equations in sections A1.3 and A1.4 Appendix 1 of this thesis.

## 4.3 Results and Discussion

As mention in chapter 3 all of the polyHIPE columns also had a corresponding freestanding polyHIPE monolith which had been produced from the same HIPE. Since it was not possible to examine the internal pore structure of the polyHIPE columns, SEM

analysis of the corresponding polyHIPE monolith allowed an assumption to be made about the internal pore structure of the polyHIPE columns (chapter 3 Table 3.5). However this assumption is very limited as the monolithic polyHIPE columns were never allowed to dry and as it was unknown fully what effect drying, washing and accompanying shrinkage would have upon the internal structure of the polyHIPE. Formation of the final polyHIPE structure is a complex process with Cameron *et. a.l.*[16] haveing shown that the polyHIPE structure is primarily developed during polymerisation whereas work by Menner and Bismark[17] have shown that the final polyHIPE structure is also brought about by the drying process.

As well as a flow of water (which was established in chapter 3) all the columns permitted flow of the mobile phase, and, when attached to the UV-VIS detector, returned a stable baseline. As mentioned the mobile phase was based on one detailed by McGowen and Langhorst1 which they used for the separation of polystyrene latexes by HDC. It is known that in HDC the effects of electrostatic interactions between the column bed and the transiting particles can be limited if the mobile phase has a suitable ionic strength.[18,19,20] It was for this reason, as an attempt to minimise electrostatic interactions between the polyHIPE and the particles, that this mobile phase was chosen rather just using deionised water. All materials will acquire a surface charge when brought into contact with a polar liquid (such as water) by a variety of mechanisms *i.e.*, electron affinity differences of two phases, ionisation of surface groups, differential ion adsorption from electrolyte solution, differential ion dissolution from a crystal lattice, surface anisotropy, isomorphous substitution.[21] The second of these, ionisation of surface groups, was considered to be particularly prevalent for the polyHIPE columns due to the presence of anionic sulphate groups on the polyHIPE surface. These would be as a result using potassium persulphate as the initiator for the precursor HIPE. Potassium persulphate initiates polymerisation by

means of the sulphate radical anion, which leads to the formation of polymer chains terminated with the sulphate anion. In HIPE polymerisation where the monomer is located in the external phase and the initiator is located in the internal phase, initiation will likely happen by reaction of small amounts of dissolved monomer with a sulphate radical in the internal phase. This species then reacts with more monomer becoming increasing insoluble in the internal aqueous phase. It will then diffuse across the water-oil interface into the external phase. At this point it is reasonable to assume the terminal anionic sulphate of the propagating polymer chain will locate at the interface leading to a charged surface on polymerisation.

### 4.3.1 BuMA1c, Poly(BuMA-*co*-EGDMA) PolyHIPE Column

While all polyHIPE columns permitted flow of the mobile phase this did not necessarily translate into passage of all three sizes of latex particle (100 nm, 460 nm, and 800 nm) through the column. Injection of the 100 nm latex onto BuMA1c (which required a low flow rate of 0.25 ml $min^{-1}$ to prevent the back pressure exceeding the 10 MPa) did produce a chromatograph (Figure 4.3), however injection of the 460 nm latex resulted in the column blocking and the back pressure increasing up to the high pressure limit (10 MPa). Even by reducing the flow rate the back pressure could not be brought down. In an attempt to clear the blockage, acetone was injected onto the column, it was hoped the acetone would dissolve the polystyrene particles clearing the blockage. Unfortunately this was not successful and no further injections of the latex particles were possible.

The latex concentration of the only injection that was possible was such that it produced a detector response above the maximum the data logger could record, manifesting as a plateau at the peak maximum (Figure 4.3). This meant that retention time had to be estimated. To do this the equations of the two linear sections of the peak adjacent

to the plateau were determined and solved as simultaneous equations. This gave an estimated retention time of 342 seconds.

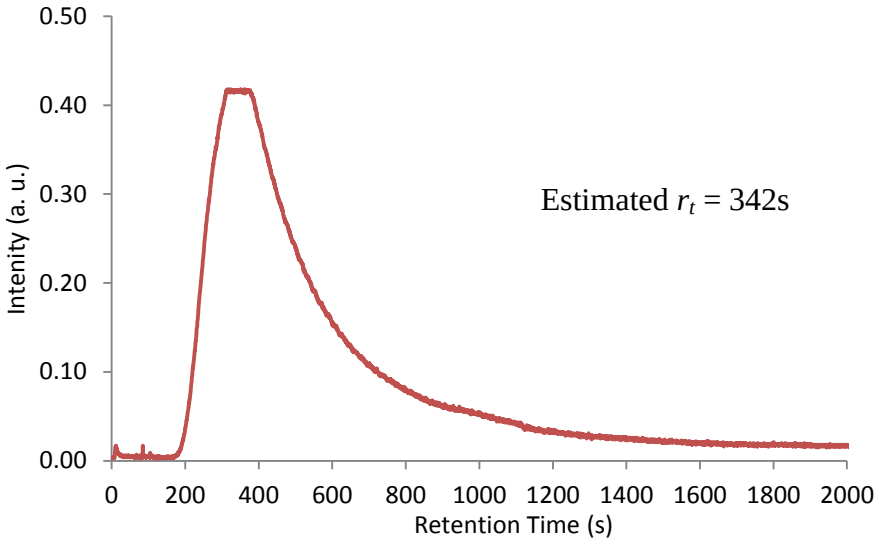


Figure 4.3: Chromatograph of an injection of the 100 nm polystyrene latex onto the polyHIPE columns BuMA1c. As a result of blockage of the column after this injection, no further separation experiments could be carried out on this column.

The cause of the column blockage is unclear. Ideally the column could have been investigated by SEM after chromatographic testing, however in an attempt to restore flow the high pressure limit on the pump was raised and the column subsequently collapsed. It is not believed to be as a result of the size of the polyHIPE windows. SEM of the monolith BuMA1 (chapter 3, Figure 3.16), which was produced from the same HIPE as the polyHIPE column BuMA1c, revealed an average window diameter of 0.54 $\mu$m (or 540 nm) which is 80 nm larger than the 460 nm latex particles. The columns EGDMA1c and BMA3c did allow flow of the 460 nm particles as well as 800 nm latex particles without blockage and SEM of their corresponding monoliths revealed windows of a smaller diameter than BuMA (BMA3 windows 0.47 $\mu$m and EGDMA1 windows 0.35 $\mu$m, chapter 3 Table 3.5). It should be mentioned here that this is highly speculative as it is not known if

the windows are the same size in the processed and unprocessed form of the polyHIPEs, or if they are affected by the pressures of flow to the HIPE.

### 4.3.2 GMA3c, Poly(GMA-*co*-EDGMA) PolyHIPE column

Initially GMA3c produced a stable base line with the mobile phase, but after an injection of the 100 nm latex the detector response would not stabilise and did not return to the baseline after the initial detection. Repeat injections were attempted but the detector response was continuously rising, with frequent spikes such that production of a meaningful chromatograph was impossible. Several injections of acetone, in an attempt to remove any adsorbed latex particles, were unable to restore a stable baseline and it was therefore decided that no further injections would be attempted. As a final investigation to examine the operating size range potential of the column, the 460 nm and 800 nm latex particles were injected on to the column. Both were able to pass through the column without affecting the back pressure suggesting that, had a stable signal been established, the column could operate over wide size range.

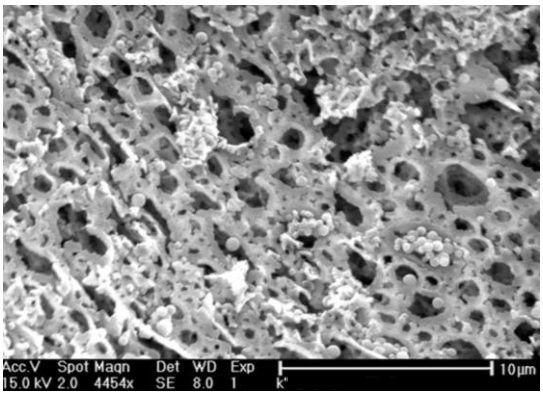


Figure 4.4: SEM of the polyHIPE column GMA3c after injection of all three sizes of latex particles, showing the apparent adsorption of the polystyrene latex particles onto the column surface.

The instability of the baseline, along with the frequent signal spikes, was attributed to the adsorption of latex particles onto the surface of the column, which would

periodically desorb resulting in the detector spikes. SEM of a small fragment of GMA3c, taken after several injections of different sized latex particles, appears to supports this hypothesis, revealing what would what appear to be latex particles present on the polyHIPE surface (Figure 4.4).

### 4.3.3 BMA3c, EGDMA1c and PS-3C PolyHIPE Columns

For three of the polyHIPE columns, BMA3c (poly(BMA-*co*-EGDMA), EGDMA1c (polyEGDMA) and PS-3C (poly(styrene-*co*-DVB)), all three sizes of latex were able to pass through individually, resulting in a separation on each column (Figure 4.5 to Figure 4.9). With the exception of the 100 nm latexes on EGDMA1c (RSD = 4.7 %) each of the columns produced consistent retention times over duplicate or triplicate injections with the highest RSD being 1.6 % (Table 4.4). The reason for the variation in the retention times of the 100 nm latexes EGDMA1c is unknown, it may be that as these injections where preformed first the column was still in the process of equilibrating to the flow pressures.

Table 4.4: Mean retention times (± 1 s) of 100 nm, 460 nm and 800 nm polystyrene latex particles on the various polyHIPE columns.

| Column | Retention Time (s) | | | | | |
|---|---|---|---|---|---|---|
| | 100 nm | | 460 nm | | 800 nm | |
| | Average | %RSD | Average | %RSD | Average | %RSD |
| BMA3c | 47 | 0.0 | 45 | 0.0 | 49 | 1.0 |
| EGDMA1c | 940 | 4.7 | 578 | 0.2 | 781 | 0.6 |
| PS-3c | Shoulder | | | | | |
| | 110 | 1.5 | 106 | 0.0 | [a] | n.a. |
| | Peak 1 | | | | | |
| | 148 | 0.6 | 144 | 0.3 | 154 | 1.6 |
| | Peak 2 | | | | | |
| | 161 | 0.5 | 156 | 0.6 | 161 | [b] |

[a] Not observed on the peaks produced by the 800 nm latex
[b] A second peak was only observed on one of the injections.

As well as the latex particles, injections of acetone (1% v/v dilution in mobile phase for BMA3c and PS-3c and 1 drop in 10 ml for EGDMA1c) were also performed between each run. The role of the acetone was to act as a low molecular weight marker for

the column and also to help keep the columns clean, as it was hoped that any remaining latex particles would be dissolved by the acetone (the polystyrene particles were not believed to be crosslinked).

While all three columns could separate the latex particles, the mechanism, or mechanisms, of the separations are not understood. None of the columns produced a linear size based separation and the elution order of the particles was not consistent between the columns (Table 4.8)

Table 4.5: Mean retention times (± 1 s) of triplicate injections of the latex particles injected into the polyHIPE column BMA3c.

| Latex Size (nm) | 100 | 460 | 800 | Acetone |
|---|---|---|---|---|
| $r_t$ (s) | 47 | 45 | 49 | 98 |

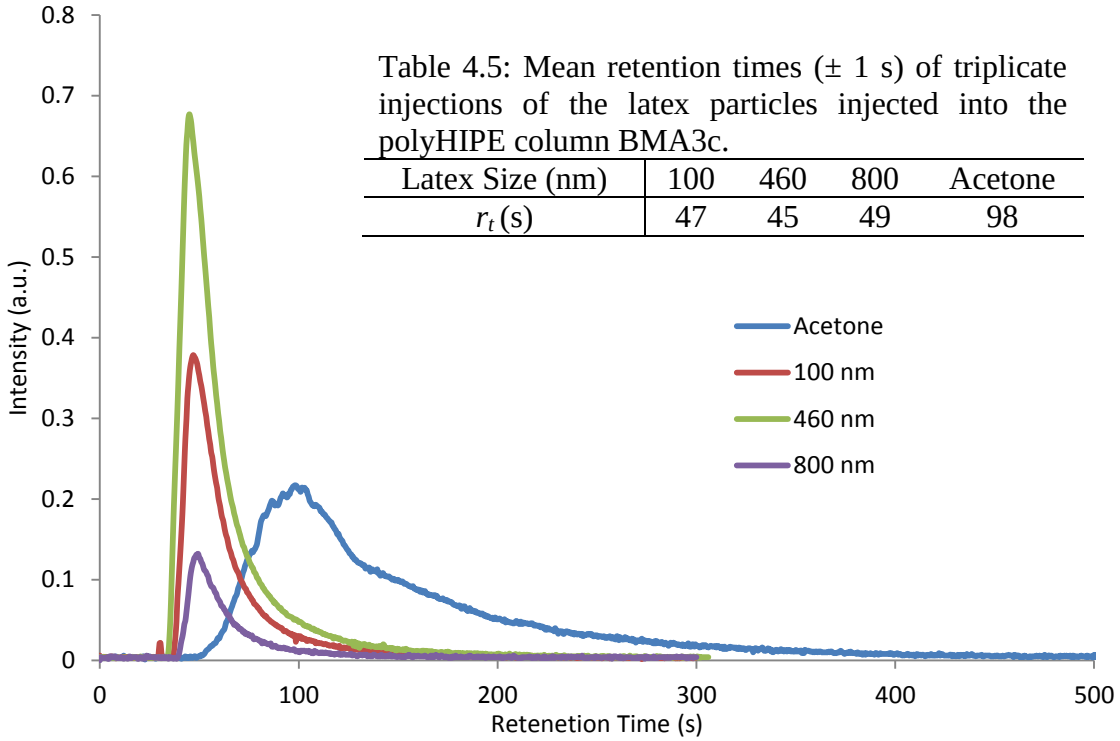


Figure 4.5: Averaged chromatograph of triplicate injections of 100 nm, 460 nm and 800 nm polystyrene latexes and an acetone marker through a HPLC column containing benzyl methacrylate/EDGMA polyHIPE as a stationary phase.

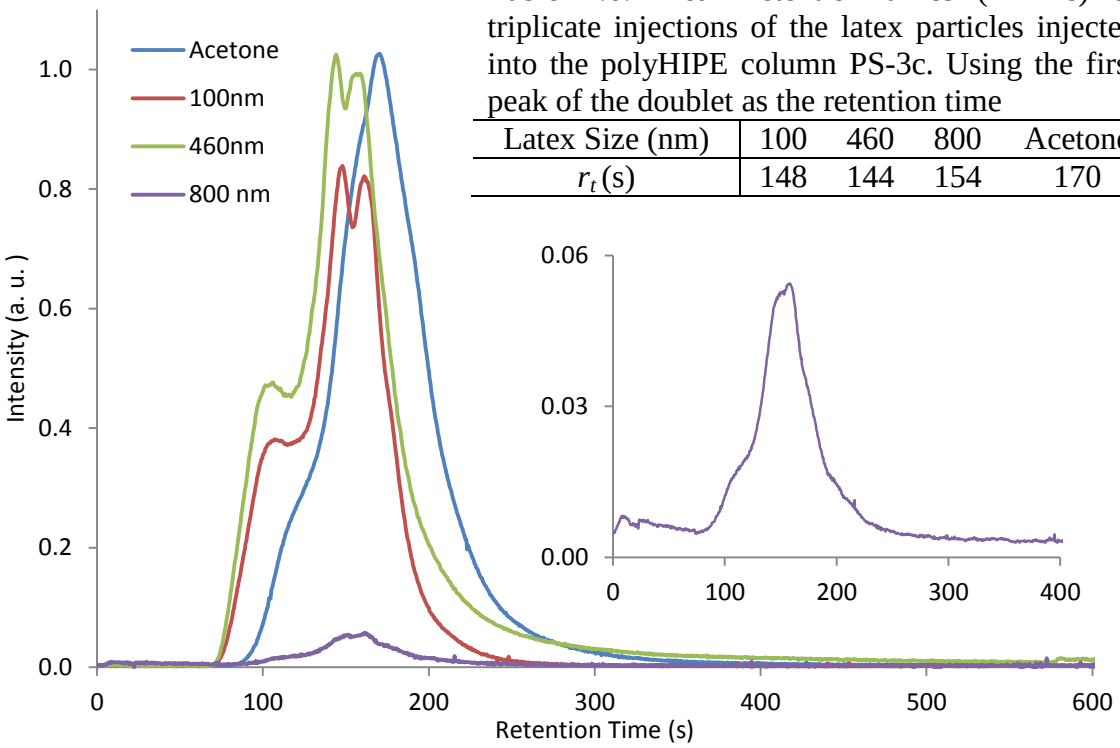


Table 4.6: Mean retention times (± 1 s) of triplicate injections of the latex particles injected into the polyHIPE column PS-3c. Using the first peak of the doublet as the retention time

| Latex Size (nm) | 100 | 460 | 800 | Acetone |
|---|---|---|---|---|
| $r_t$ (s) | 148 | 144 | 154 | 170 |

Figure 4.6: Averaged chromatograph of triplicate injections of 100 nm, 460 nm and 800 nm polystyrene latexes, as well as an acetone marker, produced by the poly(styrene-*co*-DVB) polyHIPE column PS-3C. The insert in the top right shows an enhanced view of the 800 nm peak profile.

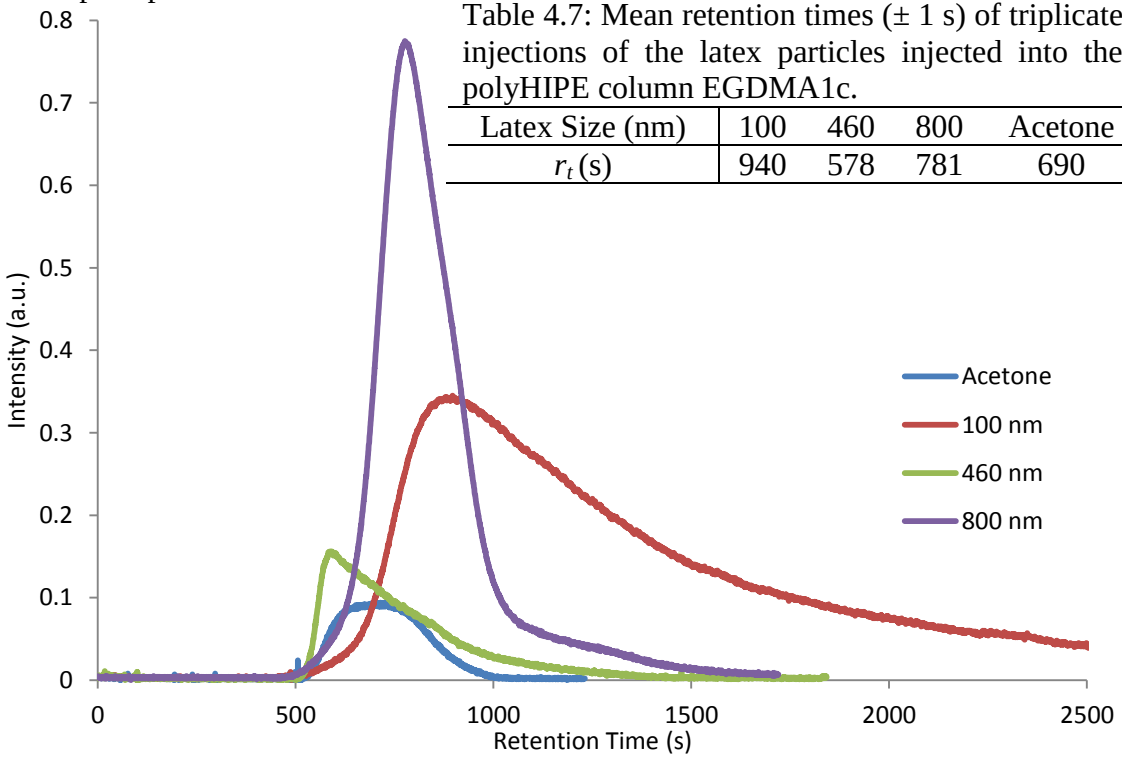


Table 4.7: Mean retention times (± 1 s) of triplicate injections of the latex particles injected into the polyHIPE column EGDMA1c.

| Latex Size (nm) | 100 | 460 | 800 | Acetone |
|---|---|---|---|---|
| $r_t$ (s) | 940 | 578 | 781 | 690 |

Figure 4.7: Averaged chromatograph of triplicate injection of 100 nm, 460 nm and 800 nm polystyrene latexes and a low concentration acetone marker (1 drop in 10 ml) on the polyHIPE column EDGMA1c. The 100 nm peak tail continues to approximately 3500 seconds but is cut off here to make the peak maximum clearer.

Table 4.8: Elution order of the polystyrene latex particles off each of the three polyHIPE columns which produced a separation.

| Column | Elution Order |
|---|---|
| BMA3c | 460 nm – 100 nm – 800 nm – Acetone |
| PS-3c | 460 nm – 100 nm – 800 nm – Acetone |
| EGDMA1c | 460 nm – Acetone – 800 nm – 100 nm |

Separations on BMA3c and PS-3c both resulted in the same elution order (460 nm – 100 nm – 800 nm - Acetone) and as can be seen in Figure 4.5 and Figure 4.6 respectively both columns had similarly poor resolution with significant overlap of chromatographic peaks. The retention time window of the particles was only 4 seconds on BMA3c and 6 seconds on PS-3c (taking the first peak of the doublet). The peak overlap was such that if a mixture of particles was injected it would be impossible to distinguish the individual peaks. Due to the obvious level of peak overlap it was not deemed meaningful to calculate the resolution.

PS-3c also produced a highly unorthodox peak shape characterised by a shoulder before the main peak, with the main peak being split into a doublet. The shoulder was visible on the chromatograph regardless of the injection identity, though it was not distinct enough to determine an associated retention time with injections of the 800 nm latex or acetone. Each individual element of the peak displayed separation and, when the retention time could be determined, the order of separation was consistent *e.g.*, the first and second peak of the doublet both eluted in the order 460 nm – 100 nm – 800 nm. As the peak shape was consistent and reproducible it is unlikely that they were caused by a poorly performed injection. The three separate elements of the peak could possibly indicate that there was more than one distinct path through the column each resulting in a different retention time. These different paths could have resulted for several different reasons *e.g.*, poor packing of the column, large poorly emulsified water droplets in the HIPE resulting a large void space in the polyHIPE column. However, as no characterisation of the polyHIPE monoliths after

the separations were performed without further investigation this only speculative at this point.

For both PS-3c and BMA3c the acetone marker eluted last, as would be expected of a size based separation based on the greater excluded volume of larger species. This could be an indication that there are two mechanisms at work within the column which operate at different size ranges, resulting in the 800 nm particles being separated by a different mechanism to the one that separated the 100 nm and 460 nm latex particles and acetone. However, to establish if this is truly the case would require further work with a wider range of particle sizes.

The peak tailing observed with both BMA3c and PS-3c suggests that there is a certain amount of on column interactions. While a degree of peak tailing is unavoidable in all forms of chromatography, the asymmetry factors of the peaks (Table 4.9) in the chromatograph produced by BMA3c are all > 2 which would be considered poor by chromatographic standards, as above this value the resolution becomes compromised.[22] The unorthodox peak shapes produced by the column PS-3c prevented a reliable calculation of the peak asymmetry factors

Table 4.9: Peak asymmetry factors ($A_s$) in the chromatographs produced by the polyHIPE columns BMA3c and EGDMA1c. The chromatographs are displayed in Figure 4.5 (BMA3c) and Figure 4.7 (EGDMA1c).

| Column | Peak Asymmetry ($A_s$) | | | |
|---|---|---|---|---|
| | 100 nm | 460 nm | 800 nm | Acetone |
| BMA3c | 5.1 | 4.5 | 4.8 | 4.4 |
| EGDMA1c | 6.2 | 6.1 | 1.7 | 1.9 |

While only minimal separation was observed with polyHIPE columns BMA3c and PS-3c, this was not the case with EGDMA1c which produced significant differences in retention time between latex particles (Figure 4.7). The differences in retention times meant that a meaningful resolution between the latex peaks could be calculated (Table 4.10).

Table 4.10: Calculated resolution between the peaks of the different latex particles on the polyHIPE column EGDMA1c, calculated from elution order.

| Column | Peak Resolution ($R_s$) | |
|---|---|---|
| | 460 nm – 800 nm | 800 nm – 100 nm |
| EGDMA1c | 0.52 | 0.22 |

Interestingly the peak shape was not consistent, with peaks produced by the 100 nm and 460 nm latexes having a different peak shape to the one produced by the 800 nm latex. The considerable peak tailing which resulted in high peak asymmetry factors (Table 4.10) suggests that a significant amount of column interactions were present for runs of the 100 nm and 460 nm particles, while the peak profile of the 800 nm particles is much closer to an ideal Gaussian function, and therefore has a much lower asymmetry factor. This suggests the 800 nm particles interacted far less with the column. This could indicate that there may be more than one separation mechanism operating within the column with the on column interactions being influenced by the size of the particles.

It is possible that with further work the peak tailing observed on all of the columns could be reduced by a fine tuning of the mobile phase to one more applicable to the individual columns, rather than one appropriated from another use.

As mentioned in the experimental section, in between repeat injections of latex particles there was an injection of dilute acetone. As well as acting as a low molecular weight marker it was also hoped to remove any particles which absorbed to the column surface. If this injection of acetone was omitted in between repeat injections of latex particles there was an accompanying decrease in the peak maxima (Figure 4.8). This is further evidence of on column interactions, with the decrease in peak maxima being attributed to increasing adsorption of latex particles on the column surface. Peak intensity could be restored on injection of acetone on to the column which it is believed dissolved the adsorbed polystyrene latex particles, which as mentioned were not believed to be cross-linked.

The presence of on-column interactions between the polyHIPE and the latex particles may also be evidenced by the long retention times. Assuming that the 90% internal phase HIPE formed a monolithic stationary phase with 90% internal free volume, a column with an i.d. of 4.6 mm and a length of 150 mm would give a volume, accessible to eluent and latex, of 2.24 $cm^3$. At a flow rate of 0.25 ml $min^{-1}$, an analyte injected onto the column would take 539 seconds to transit it, or less, if there were size-exclusion effects. For the polyHIPE monolithic column 'EGDMA1c', all values for retention time were greater than this, indicating the possibility of on-column interactions.

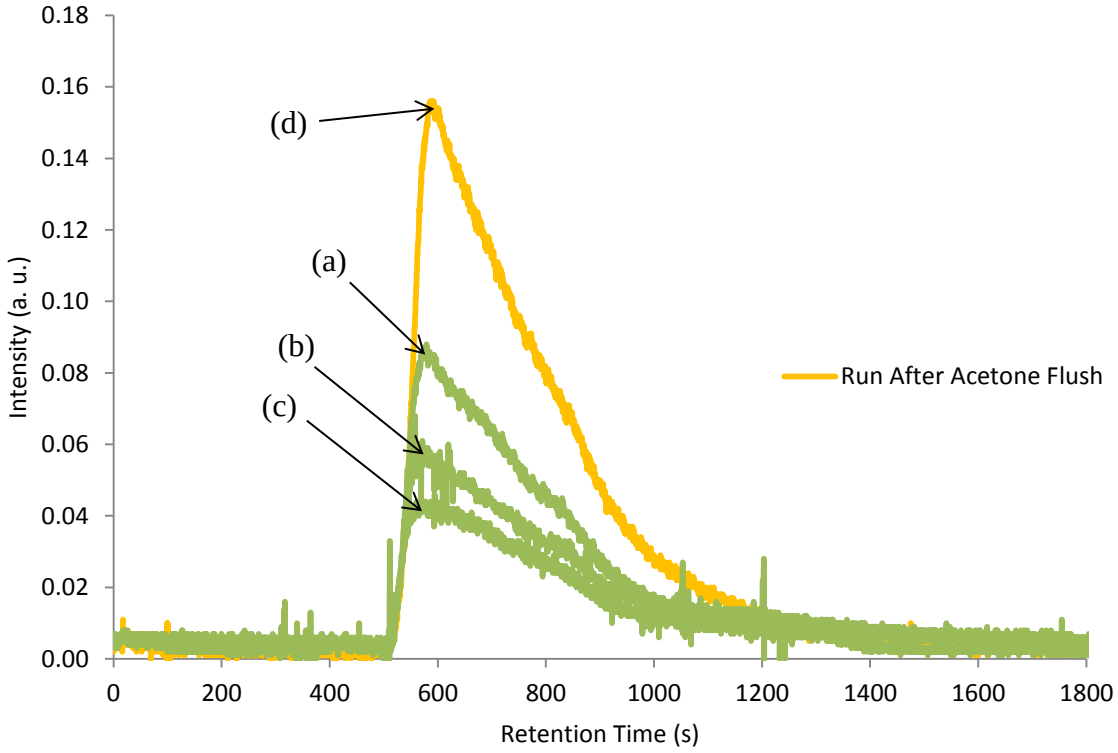


Figure 4.8: Peaks produced by repeat injections of the 460 nm polystyrene latex onto the polyHIPE column EGDMA1c without an injection of acetone in between injections. The repeat injections (green), (a) injection 1, (b) injection 2 and (c) injection 3, display a decrease in absorption intensity which was restored when the column was flushed with an injection of acetone prior to a (d) further fourth injection of latex particles (orange).

### 4.3.4 Effect of Aging on the PS-3c PolyHIPE column.

The column PS-3c was aged for 61 days and the latexes were injected again in triplicate. As before, peaks displayed a consistent shape and retention time and the three

injections were averaged to produce the chromatogram in Figure 4.9. However while consistent with each other, both the peak shape and retention times were different from the initial injections producing a chromatogram which appeared considerably different from the one shown in Figure 4.6. As with the previous injections, multiple peaks were present with each latex, as well as the acetone marker. The shoulder which had previously been observed was no longer present and a third peak appeared with a much longer retention time. There was now no separation observed between the main peaks (retentions times were within 1 second which is within the error of the measurements) though there was a separation between the third peaks with a different separation order than before (Table 4.11).

Table 4.11: Retention times of the various peaks associated with the chromatograph produced by the polyHIPE column PS-3c after aging for 61 days.

| Column | Retention Time (s) | | | |
|---|---|---|---|---|
| | 100 nm | 460 nm | 800 nm | Acetone |
| PS-3c Aged 61 Days | Peak 1 | | | |
| | 97 | 96 | 97 | 113 |
| | Peak 2 | | | |
| | None | 109 | 106 | None |
| | Peak 3 | | | |
| | 299 | 275 | 264 | 192 |

The cause of this change in chromatographic performance with age is unknown. It may have arisen from reaction of the polyHIPE with the components of the mobile phase within the column over the aging period, or, if the seal on the column was poor, from drying effects which would change the polyHIPE morphology and diameter over the aging time.

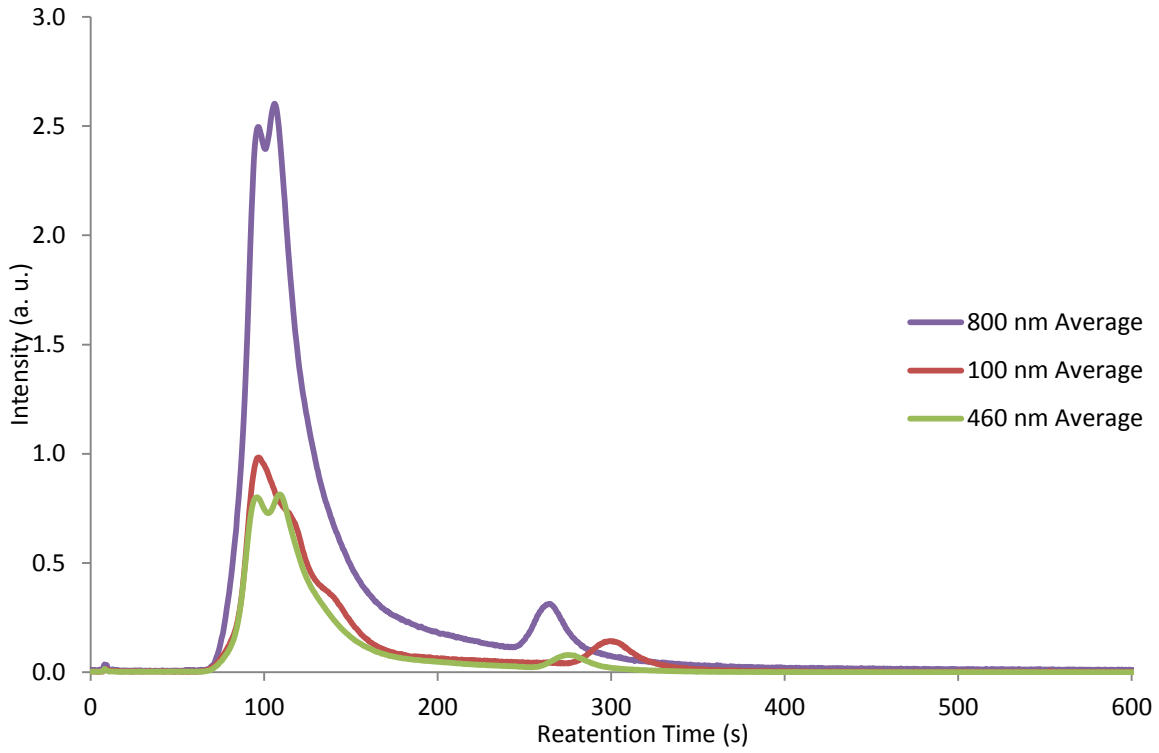


Figure 4.9: The average chromatograph of triplicate injections of 100 nm, 460 nm and 800 nm polystyrene latexes, as well as an acetone marker, onto the styrene/DVB polyHIPE column PS-3C 61 days after the initial experiments with the same latexes.

## 4.4 Conclusions

PolyHIPE columns produced from three different polymers (Poly(BuMA-co-EGDMA), poly(styrene-*co*-DVB) and polyEGDMA) have all been able to separate polymer latex particles over a wide size range (100 nm to 800 nm). However, resolution was not particularly good for the polyHIPE columns BuMA3c and PS-3c. While the resolution was somewhat better for the polyHIPE column EGDAM1c, it was compromised by significant peak tailing, which was present with all of the columns. Tailing could likely be reduced by using a mobile phase more suited to the columns.

The mechanism of separation is not understood and it is possible, particularly with EGDMA1c, that there is more than one mechanism at operation within the columns.

The polyHIPE column PS-3c column was shown to be unstable to aging, producing a very different chromatogram the original experiments after 61 days after of aging with significant differences in retention time and peak shape.

As none of the particles separated in this chapter were below 100 nm (the current European definition of a nanoparticle)[23] it was decided that further work, which is detailed in chapter 6 of this thesis, would be carried out. A new set of columns (one polyEGDMA and one poly(styrene-*co*-DVB)) was to be produced and they would be investigated to see if it was possible to separate engineered nanoparticles with diameters of less than 100 nm.

## 4.5 References

1. G. R. McGowen, M. A. Langhorst, *J. Coll. Interf. Sci.* 1982, **89**, 94-106
2. K. Tiede, A. B.A. Boxall, S. P. Tear, J. Lewis, H. David, M. Hassellöv, *Food Addit. Contam.*, 2008, **25**, 795-821
3. J. R. Lead, K. J. Wilkinson, *Environ Chem.* 2006, **3,** 159–171
4. S. C. Clear, R. V. Parthasarathy, R. K. Sura, P. P. Soo, *US Pat. Appl.*, 2004, 6 750 261
5. K. Allmer, E. Berggren, E. Erikson. A Larson, I. Porrvik, *US Pat. Appl.*, 2001, 6 290 853
6. B. C. Benicewicz, G. D. Jarvinen, D. J. Kathios, B. S. Jorgenson, *J. Radioanal. Nucl. Ch.*, 1998, **235**, 31-35
7. J. A. Tripp, T. P. Needham, E. M. Ripp, B. G. Konzman, P. J. Homnick, *React. Funt. Polym.*, 2010, **70**, 414-418
8. Z. Bhumgara, *Filtr. Separ*., 1995, **32**, 245-251
9. Y. Tunc, C. Gölgelioğlu, N. Hasirci, K. Ulubayram, A. Tuncel, *J. Chromatagor. A.*, 2010, **1217**, 1654-1659
10. Y. Tunc, C. Gölgelioğlu, A. Tuncel, K. Ulubayram, *Sepra. Sci. Technol.*, 2012, **47**, 2444-2449
11. I. Junkar, T. Koloini, P. Krajnc, D. Nemec, A. Podgornik, A. Štancar, *J. Chromatagor. A*, 2007, **1144**, 48-54
12. J. Yang, G. Yang, H. Liu, L. Bai, Q. Zhang, *J. Appl. Polym. Sci.*, 2010, **119**, 412-418
13. C. Yao, L, Qi, H. Jia, P. Xin, G. Yang, Y. Chen, *J. Mater. Chem.*, 2009, **19**,767-776
14. P. Krajnc, N. Leber, D. Štefanec, S. Kontrec, A. Podgornik, *J. Chromatogr. A*, 2005, **1065**, 69-73
15. I. Pulko, V, Smrekarm A. Podgornik, P. Krajnc, *J. Chromatagor. A*, 2011, **1218**, 2396-2401
16. N. R. Cameron, D. C. Sherrington, L. Albiston, D. P. Greogory, *Colloid Polym. Sci.*, 1996, **274**, 592-595
17. A. Menner, A. Bismarck, *Macromol. Symp.*, 2006, **242**, 19-24
18. H. Small, M. Langhorst, *Anal. Chem.*, 1982, **54**, 892A-898A
19. G. Saunders, Personal Communication
20. D. C. Prieve, P. M. Hoysan, *J. Colloid Interf. Sci.*, 1978, **64**, 201-213
21. D. Fairhurst, R. W. Lee, *Drug Devel. Deliv.*, 2011, **11**, 60-64
22. J. W. Dolan, *LCGC Asia Pacific*, 2002, **5**, 14-20
23. J. Potočnik, *Off. J. Euro. Comm.*, 2011, **L275**, 38-40

# Chapter 5

# Synthesis and Characterisation of Lanthanide Containing Polystyrene Nanoparticles by Micro-Emulsion Polymerisation for Use as Analytical Standards to be Used with Hydrodynamic and PolyHIPE Chromatography

## 5.1 Introduction

As with all areas of nano-science, interest in polymeric nanoparticles (PNPs) has expanded considerably over the last 20 years. This is due in part to their increased use in a wide variety of practical applications, such as electronics,[1] photonics,[2] adhesives,[3] coatings,[4] sensors,[5] drug delivery[6,7] and environmental technologies.[8] Due to the ease and reproducibility with which they can be manufactured and their relative stability and chemical inertness, PNPs (often referred to as latexes when present as an aqueous dispersion) are also regularly used as calibration standards for a variety of different analytical techniques [*e.g.*, Field Flow Fractionation (FFF),[9] optical particle counting,[10] Hydrodynamic Chromatography (HDC)].[11] However, because of the high ionisation energy of carbon (11.2030 eV, compared to sodium at 5.1391 eV), the main component in the particle matrix, PNPs cannot be used with separation techniques that utilise the

element-specific detection capability of Inductively-Coupled Plasma Mass Spectrometry (ICP-MS), as the element is virtually undetectable.

### 5.1.1 Aims and Objectives

The aim of the work carried out in this chapter was the development, production and characterisation of a range of well-defined, lanthanide-doped spherical PNPs. The particles were specifically intended for use analytical standards for use with HDC- and polyHIPE-ICP-MS chromatography (which is described in chapter 6), although they will retain their applicability for use with other detection techniques. Particles were to be prepared over the size range 40 – 160 nm, containing several different metals and stabilised by different surfactants (three particle sizes, three metals and two surfactant systems).

The choice of metal was based on two criteria:

1. Ionisability in an ICP-MS – the lower the ionisation energy; the greater the instrument response; the less of the element required in the particle.
2. Environmental abundance of the element – the lower the likely concentration of the element in environmental samples, the smaller the number of doped particles required for extraction efficiency experiments, *etc*

For these reasons, three elements were chosen from the Lanthanide section of the periodic table; dysprosium (Dy), gadolinium (Gd) and neodymium (Nd) the relevant properties of which are displayed in Table 5.1.

Table 5.1: Earth's crust abundance and ionisation energy of the three chosen lanthanides displayed, along with sodium for comparison to a highly abundant and readily ionisable metal

| Metal | Earth's Crust Abundance (p.p.m) | Ionisation energy (eV) |
|---|---|---|
| Neodymium | 38 | 5.5250 |
| Gadolinium | 7.7 | 6.1498 |
| Dysprosium | 6 | 5.9390 |
| Sodium | 23,000 | 5.1391 |

Regarding the choice of stabilising surfactant; Sodium dodecyl sulphate (anionic) and Pluronic-F68 (non-ionic) were chosen to allow control over the surface charge of the particles enabling the potential different charge interactions to be investigated.

Particle sizes were controlled by tailoring the amounts of surfactant and initiator to produce particles sets containing three sizes of particle (~ 160, ~80 and ~40 nm). The need for three sizes of particles was based on having a range of potential calibrants above and below the 100 nm value defined as being 'nano'.[12]

### 5.1.2 Polymer Nanoparticles: Synthesis Methods

Polymer nanoparticles are commonly defined as colloidal systems with a lower size range of 5-10 nm and an upper size range of 1000 nm, although the majority of preparation methods yield particles of 100 to 500 nm.[13,14] The term 'polymer nanoparticle' can be used to refer to any polymer nanomaterial, although it is most often used to refer specifically to polymer nanomaterials with a spherical morphology. The work detailed in this chapter only focused on the production of nano-spheres. As such, other morphologies (*e.g.*, polymer nano rods,[15] nano fibres[16] and nano cubes[17]) will not be covered in this introduction.

Spherical PNP production can be broadly separated into two methodological approaches:

1. Preparation from pre-formed polymers.
2. Polymerisation of monomers *in-situ*.

#### 5.1.2.1 Polymer Nanoparticles: Synthesis by using pre-formed polymers

Common methods of PNP production using 'pre-formed polymers' include: solvent evaporation,[18] emulsification-diffusion,[19,20] salting out,[21] nanoprecipitation,[22,23] dialysis [24]

and supercritical fluid technology.[25,26] These methods typically produce particles larger than 100 nm in diameter. As one of the aims of this work was to produce particle systems well below this size (~40 nm), these techniques were not used in any of the work presented in this chapter. They are only mentioned for completeness, if greater detail is required, the reader is recommended to read the reviews by Nagavarma *et al.*,[27] Rao and Geckeler,[28] Vauthier and Bouchemal[29] and Allouche.[30]

#### 5.1.2.2 Polymer Nanoparticles: Synthesis by using in-situ polymerisation

For the purposes of this project, the PNPs needed to meet the following criteria:

1. To easily accommodate the incorporation of ICP-MS detectable elements.
2. To cover a range of sizes below 100 nm, in order to meet the European definition of 'nano.'[12]
3. Have a zero (or as low as possible) surface charge, to minimise charge interactions within the HDC column and with other particles.

The three general approaches which can be used to produce 'tailored' PNPs from *in-situ* polymerisation are, (1) emulsion-based techniques, (2) interfacial polymerisation,[31,32] and (3) controlled/living radical interfacial polymerisation.[33,34,35] As initial work focused on the former approach, and was found to produce particles with the desired attributes, the remainder of this chapter will focus on the use of emulsion-based techniques.

##### 5.1.2.2.1 Emulsion Polymerisation

*In-situ* polymerisation within emulsion systems allows the formation of PNPs with well-defined and specifically tailored properties, and is the subject of the majority of the literature on PNPs. Different emulsion polymerisation techniques are compared in Table

5.2, and can be classified as macro-emulsion polymerisation (often referred to as 'conventional emulsion' or 'emulsion polymerisation'), mini-emulsion polymerisation, and micro-emulsion polymerisation. The latter is the technique utilised for the synthesis of the PNPs described in this chapter.

Table 5.2: Comparison of the different emulsion systems used for the polymerisation of monomers to produce PNPs. Data from refs. 28, 30 & 52.

| Property | Macro-Emulsion [a] | Mini-Emulsion | Micro-Emulsion |
|---|---|---|---|
| Thermodynamic Stability | Un-Stable | Meta-Stable | Stable |
| Stability Period [b] | Seconds-Months | Hours-Months | Indefinite |
| Typical PNP Diameter | 50-300 nm | 50-500 nm | 30-100 nm |
| Polydispersity | Low | Very Low | Very Low |
| Typical Droplet Size | 1-10 μm | 40-300 nm | 5-50 nm |

[a] Includes surfactant-free emulsion polymerisation
[b] Assuming consistent storage conditions

**5.1.2.2.2 Macro-Emulsion Polymerisation**

Macro-emulsion polymerisation is often considered the traditional method to generate PNPs, and, despite the emergence of new emulsion techniques, is still widely used. A monomer is emulsified in an aqueous/surfactant phase, forming large monomer droplets. The surfactant acts to suppresses coalescence of the monomer droplets, preventing emulsion degradation. The excess surfactant forms micelles within the aqueous phase, and small amounts of monomer diffuse from the larger droplets into them, forming monomer swollen micelles. After emulsification an initiator, usually a water soluble radical or ionic species (although radiation has been used),[36] is introduced into the system. The polymerisation mechanism and rate kinetics can be described by the Smith-Ewart-Harkins theory (Figure 5.1)[37,38] and are divided into three stages. Stage I: Due to the surface area of the monomer swollen micelles being much greater than that of the monomer droplets, initiation will typically begin within them. The rate of polymerisation increases as more and more micelles are initiated. Stage II: Monomer contained within the

micelles polymerises, and the growing chain quickly terminates, resulting in a polymer particle. At this stage the emulsion contains both monomer droplets and polymer particles. Continued polymerisation within the micelles is fed by monomer diffusing through the water phase from the large monomer droplets into the micelles. During this stage the rate of polymerisation is constant and particle growth is exclusively by micellar nucleation. Stage III: continued diffusion of monomer, from the droplets to the micelles, causes the monomer droplets to shrink. The rate of polymerisation decreases as the monomer droplets are depleted and disappear, leaving behind only polymer particles.

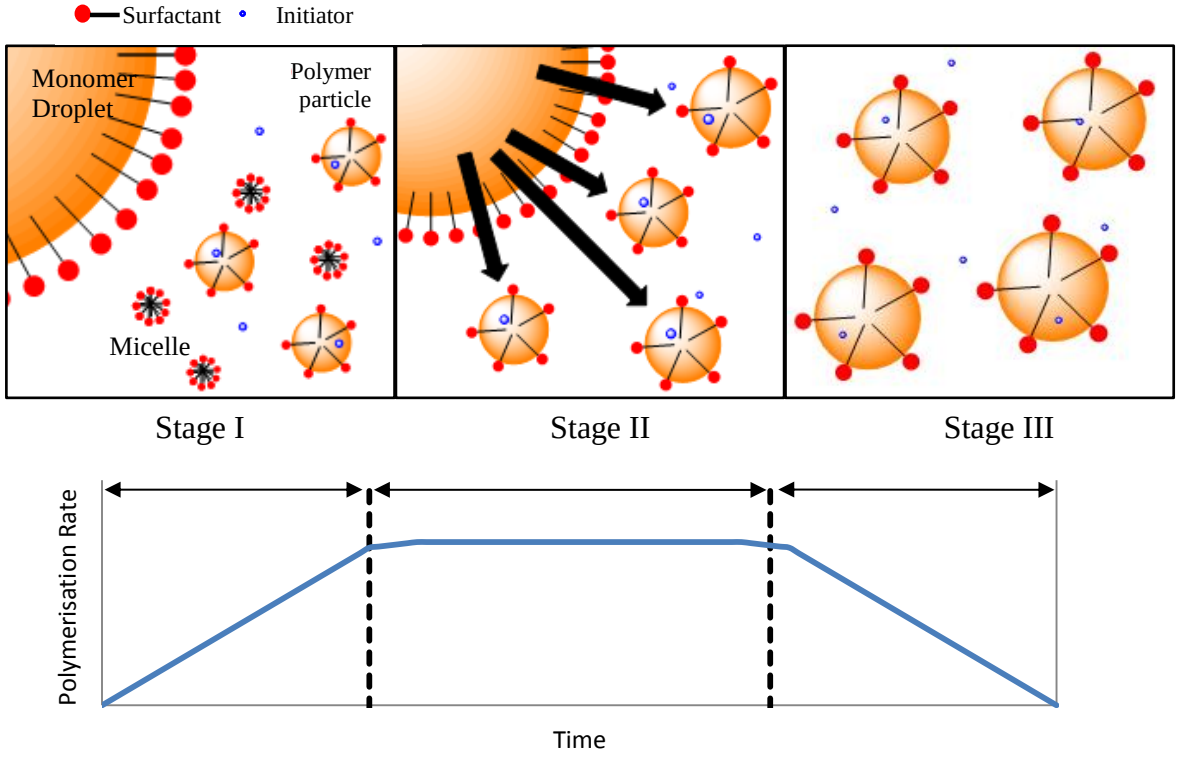


Figure 5.1: Top: Schematic diagram of the three stages of emulsion polymerisation described the Smith-Ewart-Harkins model. Bottom: rate profile of a typical emulsion polymerisation.

If the monomer has moderate water solubility, such as methyl methacrylate, or the polymerisation takes place below the critical micelle concentration of the surfactant, homogeneous nucleation of particles within the aqueous phase will also be observed.[39] The resulting particles will then originate from both homogeneous and micellar nucleation mechanisms.[40] Emulsion polymerisation has been used to synthesise many different PNPs,

such as polystyrene,[41,42] poly(methyl methacrylate)[43] and poly(alkylcyanoacrylate), amongst others.[44]

A sub-set of macro-emulsion polymerisation is 'Surfactant-Free Emulsion Polymerisation', where particles are formed without use of a surfactant. This has the advantage that it negates the often difficult, and time consuming, stage of surfactant removal. However limitations exist with respect to particle size control and production of monodisperse particles. [45]

The typical components of this method are an aqueous continuous phase, a water soluble initiator and monomers, usually vinyl or acrylic. To maintain emulsion stability, non-surfactant stabilisers are used *e.g.*, oleic acid[46] or poly(vinyl alcohol).[47] Co-solvents, such as ethanol[48] and acetone,[49] are also frequently employed. In surfactant-free systems, stabilisation of the resultant PNPs is often achieved through the use of ionisable initiators or ionic co-monomers.[28] Homogenous nucleation[50] and micellar-like nucleation[51] have both been proposed as mechanisms for particle growth in surfactant-free emulsion polymerisation.

#### 5.1.2.2.3 Mini-Emulsion Polymerisation

Emulsions can degrade by two processes:

1. Coalescence, in which dispersed droplets merge.
2. Ostwald ripening (or diffusion degradation), in which the contents of a monomer droplet gradually diffuse, through the aqueous phase, into another droplet, causing the first droplet to shrink.

In macro-emulsions the surfactant suppresses the effect of coalescence, but the emulsion can still degrade by Ostwald ripening. In mini-emulsions Ostwald ripening is reduced by the addition of a co-stabiliser (sometimes referred to as a co-surfactant),

typically a highly hydrophobic long chain alkane or alcohol, to the monomer phase.[52] To operate effectively the co-stabiliser must be highly insoluble in the continuous phase so that it cannot diffuse from one droplet to the other. This provides an osmotic pressure in the droplet counteracting the Laplace pressure which would normally drive Ostwald ripening.[53] A typical formulation for an oil-in-water (o/w) mini-emulsion polymerisation consists of an aqueous phase, containing a surfactant and the initiator, and a monomer phase, containing the hydrophobic monomer and co-stabiliser.

A further difference between macro- and mini-emulsion polymerisation is the method of mixing; whereas macro-emulsions are emulsified by mechanical mixing, mini-emulsions require high energy emulsification techniques, such as a high power ultrasound or a high pressure homogeniser. Once emulsified, polymerisation is initiated within the emulsion droplets by addition of an initiator to the aqueous phase. Though radical polymerisation is most frequently employed, other methods, such as polyaddition[54] and ionic polymerisation[55] have been used.

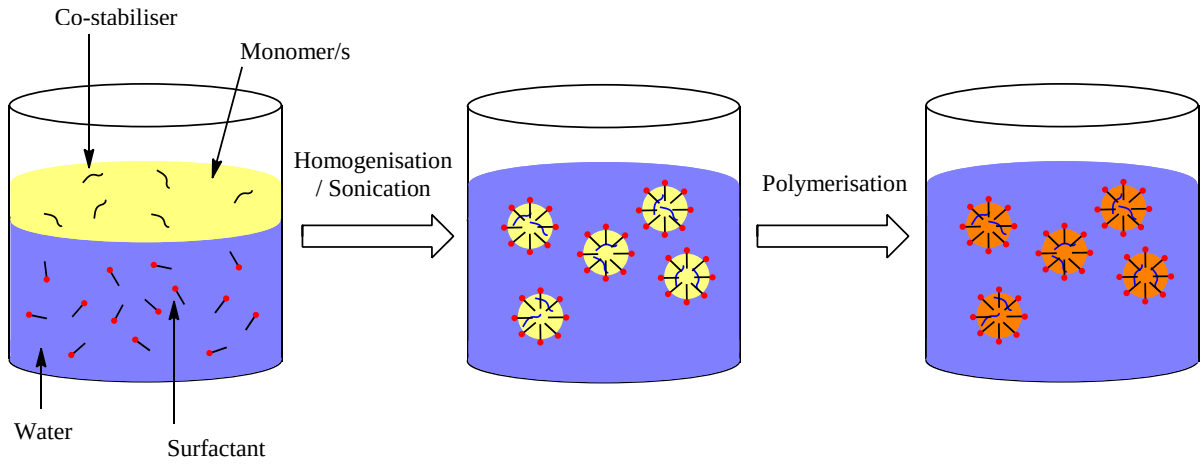


Figure 5.2: Schematic representation of an o/w mini-emulsion polymerisation.

As both Ostwald ripening and coalescence are suppressed, polymerisation is not kinetically dependent upon the diffusion of the monomer through the aqueous phase as it is

with macro-emulsion polymerisation. This means that with respect to Smith-Ewart-Harkins kinetics no stage II is present, and polymerisation is exclusively through droplet nucleation.[52] The number and size of droplets/particles remains constant throughout polymerisation, radicals enter the droplets and initiate polymerisation within, allowing each droplet to be considered an individual reactor (Figure 5.2).[30]

#### 5.1.2.2.4 Micro-Emulsion Polymerisation

Micro-emulsions are a class of thermodynamically-stable emulsions. They form spontaneously, are optically transparent and possess a near zero interfacial tension at the oil-water interface. They typically are composed of four components; a water phase, an oil phase, a surfactant and a co-surfactant (though this is not always present). The diameter of the micro-emulsion droplets is significantly less than observed in macro-emulsions, and can be as small as 5 nm. This leads to a very large interfacial area; hence micro-emulsions require large volumes of surfactant, typically 5-10% w/w.[56] However, by using a semi-continuous, or starved feed method, in which the monomer phase is added slowly or in multiple additions, it has been possible for surfactant concentrations as low as 1% w/w to be employed.[57,58,59]

For o/w micro-emulsions the co-surfactant is typically a medium chain length alcohol and in micro-emulsions stabilised with an ionic surfactant, with a single aliphatic tail (*e.g.*, CTAB), a co-surfactant is almost always utilised. However, for double-tailed ionics and some non-ionics, co-surfactants may not be required. Because the co-surfactant penetrates between the surfactant molecules at the interface, altering the packing and allowing optimum interfacial curvature thereby lowering the interfacial tension to near zero, it is often critical in dictating the micro-emulsion stability and droplet size.[60]

Micro-emulsion polymerisation is a relatively new, and still developing, approach to the production of PNPs and allows the production of PNPs of less than 50 nm (not attainable with macro-emulsion polymerisation).[56] The first reported polymerisation (of methyl methacrylate, in a globular o/w micro-emulsion system) was in 1980 by Stoffer and Bone.[61,62] With the first described micro-emulsion polymerisation of styrene reported, soon afterwards, by Atik and Thomas in 1981.[63] It is these two systems, styrene and methyl methacrylate, which are the most represented in the literature. Inverse micro-emulsion polymerisation has also been reported, first by Leong and Candau in1982,[64] however, this chapter will only focus on o/w systems.

Despite the apparent similarities of the micro- and macro-emulsion polymerisation process *i.e.*, both methods produce colloidal particles with a high molar mass, they differ kinetically. With relation to Smith-Ewart-Harkins kinetics, the stage of constant rate (corresponding to particle growth) is not present in micro-emulsion polymerisation, because particles are constantly being created throughout the process. In micro-emulsion polymerisation there are only two distinct kinetic stages:

Stage 1: Rate increases, until around 20-25% of monomer conversion, when maximum rate is reached.

Stage 2: Rate decreases with further polymerisation.

These kinetic stages are generally interpreted as particle nucleation primarily happening within stage 1 and further particle growth during stage 2.[65]

Polymerisation is, typically, initiated by a water-soluble radical species and is believed to take place by the following mechanism: Primary radicals, generated from the initiator, react with some dissolved monomer creating radical oligomers. These have an even greater hydrophobicity and are then harvested by the micro-emulsion droplets, at which point the monomer within the droplet is then initiated, beginning the formation of

particles. The newly formed latex particles continue to grow from a supply of monomer from other 'feeder' droplets until terminated by chain transfer to monomer (Figure 5.3: Schematic representation of micro-emulsion polymerisation of a monomer with a low solubility in the continuous phase. (a) Shows the un- initiated micro-emulsion, (b) shows the diffusion of monomer from monomer swollen micelles to growing particles (monomer can also be exchanged by collisions)[56] and (c) shows the final polymer latex.Figure 5.3).[66,67,68]

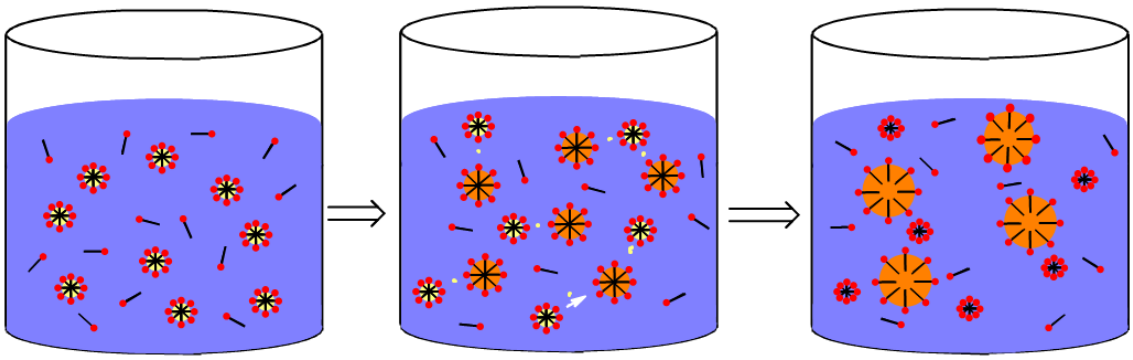


Figure 5.3: Schematic representation of micro-emulsion polymerisation of a monomer with a low solubility in the continuous phase. (a) Shows the un- initiated micro-emulsion, (b) shows the diffusion of monomer from monomer swollen micelles to growing particles (monomer can also be exchanged by collisions)[56] and (c) shows the final polymer latex.

The mechanism of polymerisation and particle formation is highly dependent upon the solubility of the monomer in the aqueous phase. For monomers with low water solubility, such as styrene, (0.031% at 25 $^{o}$C),[69] particle nuclei are generated within the emulsion droplets by capture of radicals. Particle growth then proceeds by droplet nucleation, throughout polymerisation, whereby growing particles acquire surfactant and monomer from uninitiated droplets. As the amount of monomer present in the aqueous phase is insufficient for particle nucleation homogenous nucleation is insignificant, and radicals generated in the aqueous phase are harvested by excess droplets. For systems using a monomer of non-trivial water solubility, such as methyl methacrylate (1.5% at 25

$^{o}$C),[70] there will be sufficient monomer in the aqueous phase for homogenous nucleation to occur.[71]

Micro-emulsion polymerisation will generally produce polymers with a much higher $M_w$ than conventional radical polymerisation, frequently of the order of $10^6$ Da[72,73] with molecular weights as high as 3.3 x $10^7$ Da being reported.[74] Final particle size can be controlled by the initial micro-emulsion formulation. Should a range of particle sizes be required, it is possible to achieve this by tailoring initial micro-emulsion formulation. Keeping the identity of all components the same, but varying their relative amounts, allows for the production of particles with a designed size *e.g.*, a decrease in relative initiator[75] or surfactant[76] amounts results in an increase in final particle size.

### 5.1.3 Homogenous Encapsulation of Metal Complexes within PNPs

Encapsulation of molecules within polymer nanocapsules is widely reported in the literature.[77,78] It is most commonly used in the pharmaceutical sciences for the encapsulation and delivery of drugs,[79,80] with cases of encapsulation of metal containing species such as metal oxides[81] and metal complexes[82] also reported. Homogeneous encapsulation (or dispersion) of metal complexes within the matrix of the PNPs is less common than within hollow particles; however this can be achieved with macro- and mini-emulsion polymerisation (homogenous encapsulation is less common for all materials but this chapter is only focusing on metal complexes). For the metal complex to be homogeneously encapsulated it must be soluble in the monomer phase but insoluble in the continuous phase. Therefore, when an emulsion is formed the metal complex will be located within the monomer droplets and monomer swollen micelles. Upon polymerisation, the resulting polymer particle contains the homogeneously dispersed

complex.[83] This technique has been utilised by several researchers to incorporate metal complexes in a variety of particle systems examples of which are shown in Table 5.3.

Inverse micro-emulsions have been used to encapsulate metals with inorganic nanoparticles (NPs). Cerium, europium, manganese and neodymium were encapsulated within $BaMgF_4$[84] NPs, and neodymium has been encapsulated in barium fluoride NPs[85] However, there are, as far as the author is aware, no reported cases of micro-emulsion polymerisation being applied for the homogeneous dispersion of metal complexes within PNP's.

Table 5.3: Literature examples of the use of emulsion polymerisation techniques for the homogeneous dispersion of metal complexes within PNP's. Abbreviations: PSt; Polystyrene, PMMA; Poly(methyl methacrylate), PBA; Poly(butyl acrylate), PLMA; Poly(lauryl methacrylate), PHEMA; Poly(2-hydroxyethyl methacrylate), PAA; Poly(acryl amide), PMPC; Poly(2-methacryloyloxyethyl phosphorylcholine), DVB; Divinylbenzene

| Emulsion Type | Particle Type | Metals Incorporated | Particle Size Range | Reference |
|---|---|---|---|---|
| Mini-emulsion | PSt & PMMA | Pt, Fe, Eu | 107-148[a] | 86 |
| Macro- & mini-emulsion | PSt | Pt, In, Fe, Cr, Zn | 102-374[a] | 87 |
| Mini-emulsion | PSt, PBA, PLMA & PMMA | Eu, Nd, Y, Pr, Sm, Nd | 62-167[b] | 88 |
| Inverse mini-emulsion | PHEMA | Co | 68-188[a] | 89 |
| Inverse mini-emulsion | PAA | Zn | 149-333[a] | 90 |
| Inverse mini-emulsion | PHEMA & PMPC | Ag | 132-161[a] | 91 |
| Mini-emulsion | PSt, PBA, PLMA | Gd, Al, Sm, Eu, La, Nd, Ho | 164-363[a] | 92 |
| Mini-emulsion | P(St/DVB/LMA) | Ho, Tb, Eu, Pr | 36-88[a] | 93 |
| Mini-emulsion | P(St/DVB) | Eu | 19-97[a] | 94 |
| Macro-emulsion | PSt | Eu, Tb, Ho | 162-1466[c] | 95 |

Sizing by a: by dynamic light scattering,
b: photon cross-correlation spectroscopy
c: scanning electron microscopy.

## 5.2 Experimental

### 5.2.1 Materials

Styrene (Sigma-Aldrich) was distilled under reduced pressure to remove inhibitors, and stored at −20 $^{o}$C before use. Sodium dodecyl sulphate (SDS; Fisher) and potassium persulphate (KPS; Fisher) were re-crystallised from ethanol and water, respectively, before use. Neodymium chloride hexahydrate ($NdCl_3 \cdot 6H_2O$ 99.9%; Aldrich), dysprosium chloride hexahydrate ($DyCl_3 \cdot 6H_2O$, 99.9%; Alfa Aesar), gadolinium chloride hexahydrate ($GdCl_3 \cdot 6H_2O$ 99.9%; Aldrich), neodymium acetylacetonate hydrate ($Nd(acac)_3 \cdot xH_2O$; Aldrich) chromium (III) acetylacetonate ($Cr(acac)_3$; Acros Organics), n-dodecane (Alfa Aesar), Pluronic® F-68 (Poly(ethyleneglycol)-*block*-poly(propylene glycol)-*block*-poly(ethyleneglycol) average $M_n \approx 8{,}400$; Sigma), Tween 80 (polysorbate 80; Fluka), Span 80 (sorbitan monoolate; Fluka), 1-(2-Naphthoyl)-3,3,3-trifluoroacetone (NTFA, 99%; Alfa Aesar), magnesium sulphate (Fisher), ammonia solution (35 %; Fisher), dichloromethane (DCM; Sigma-Aldrich) and 2-propanol (Sigma-Aldrich) were all used as received. De-ionised water was for all polymerisations and syntheses.

### 5.2.2 Preparation of the Lanthanide Complexes.

As preparation of the lanthanide (rare earth) complexes is already documented in the literature,[96,97] only a brief description is provided here. The amounts of lanthanide chloride and the ligand, NTFA (structure in shown in Figure 5.4), used for each complex are listed in Table 5.4. NTFA was dissolved by sonication (15 min), in a mixture of ethanol (50 ml) and ammonia solution (19 ml). The desired lanthanide chloride hexahydrate was dissolved in deionised water (10 ml) and then added, drop-wise, with stirring, to the NTFA solution. This resulted in instantaneous precipitation of the complex. The mixture was kept stirring for 24 hours in a sealed vessel.

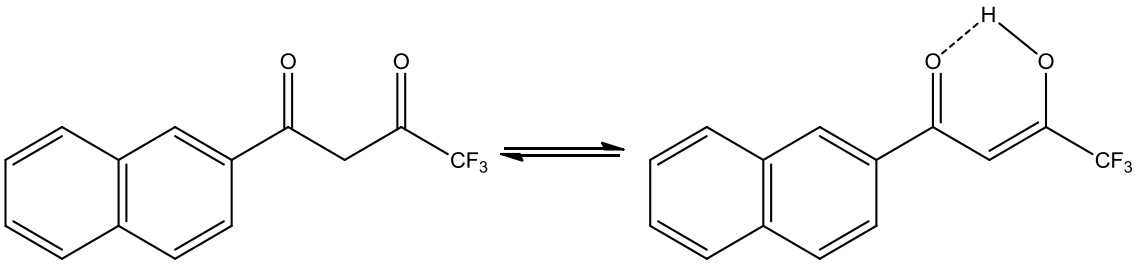


Figure 5.4: Structure of the diketone 1-(2-naphthoyl)-3,3,3-trifluoroacetone, which acts as the ligand in the described synthesis.

The product was extracted into dichloromethane (50 ml), and then washed with four aliquots (50 ml) of deionised water. The DCM layer was then dried with magnesium sulphate, and Buchner filtered. DCM was removed on a rotary evaporator to collect the final product. The resulting solid was dried overnight under vacuum at 60 $^{o}$C. The yields of each complex are reported in Table 5.4. To confirm the identity of each complex, elemental analysis was performed at the School of Chemistry, The University of Manchester, and the data is presented in Table 5.5.

Table 5.4: Yields of the Lanthanide 1-(2-Naphthoyl)-3,3,3-trifluoroacetone complex

| Rare Earth | Metal Chloride Mass (g / mmol) | Ligand Mass (g / mmol) | Complex Yield (g / mmol) | Theoretical Yield (g / mmol) | Yield (%) |
|---|---|---|---|---|---|
| Gd | 0.55 / 1.48 | 1.18 / 4.54 | 1.14 / 1.20 | 1.41 / 1.48 | 85 |
| Nd | 0.71 / 2.00 | 1.60 / 6.00 | 0.85 / 0.90 [a] | 1.88 / 2.00 | n.a.[a] |
| Dy | 0.75 / 2.00 | 1.60 / 6.00 | 1.76 / 1.84 | 1.92 / 2.00 | 92 |

[a] In isolating the product a significant amount of DCM phase was spilt.

Table 5.5: Expected and found elemental compositions of the lanthanide complexes.

| Metal Complex | Carbon (%) | | Hydrogen (%) | | Metal (%) | |
|---|---|---|---|---|---|---|
| | Expected | Found | Expected | Found | Expected | Found |
| Gd | 52.93 | 54.24 | 2.54 | 2.60 | 16.50 | 14.64 |
| Nd | 53.67 | 54.45 | 2.58 | 3.08 | 15.35 | 15.75 |
| Dy | 52.64 | 50.94 | 2.53 | 2.99 | 16.96 | 17.24 |

### 5.2.3 Synthesis of Latex Particles

#### 5.2.3.1 Synthesis of Metal Containing (Chromium/Lanthanide) Latex Particles

The exact amounts of the various emulsion components are listed in sections 1 to 4 of Table 5.6 for the chromium containing particles and in sections 7 to 9 of Table 5.6 for

the lanthanide containing particles. The synthesis of the chromium containing particles was split into four separate experiments and synthesis of the lanthanide containing particles into three batches; however the procedure for all systems was broadly the same. As such a typical procedure, taking CrSt5 as the example, is as follows: In a 4 neck round bottom flask the surfactant, SDS, (0.5 g) was dissolved in de-ionised water (45 ml)[i]. The flask was then fitted with an IKA RW20.n overhead stirrer with a PTFE paddle through the central neck. A reflux condenser and an addition funnel were attached to two of the side necks of the flask. The remaining neck was sealed with a Suba seal. The solution was then heated to70 $^{o}$C. Separately, KPS (0.1 g) was dissolved in de-ionised water (5 ml) and sealed. Both solutions where then purged with nitrogen (30 mins).

N-dodecane (0.05 g) and $Cr(acac)_3$ (0.05 g) were dissolved in styrene (5 g). The monomer phase was then placed in the addition funnel and purged with nitrogen (30 min). Once the SDS solution reached temperature (70 $^{o}$C), and all solutions had been purged with nitrogen, the monomer phase was added drop wise, via the addition funnel. Once addition of the monomer phase was complete, the initiator solution was introduced into the micro-emulsion, and polymerisation was allowed to continue (3 hours at 70 $^{o}$C). Once polymerisation was complete, the reaction mixture was allowed to cool to ambient temperature and then passed through filter paper to remove any polymer grist. Latexes were then stored at 3 $^{o}$C.

#### 5.2.3.2 Synthesis of Metal Free Latex Particles

For the metal free latex particles the exact amounts of the various micro-emulsion components are listed in Section 6 of Table 5.6. Despite the differences in emulsion

[i] For some of the lanthanide containing particle systems (the identity of which are detailed in Table 5.6), the total volume of water used in synthesis was 40 ml, not 50 ml. In these cases the surfactant solution was made up with 35 ml of water not 45 ml.

Table 5.6: Composition of emulsions used in the chapter for the synthesis of polystyrene nanoparticles.

| Sample | Metal Source (mass, g) | Styrene Mass (g) | Surfactant (mass, g) | Additive (mass, g) | Water (ml) [a] | KPS Mass (g) |
|---|---|---|---|---|---|---|
| Section1: Chromium Containing Particles: Experiment 1. Variation of Relative Water Concentration | | | | | | |
| CrSt1.25 | $Cr(acac)_3$ (0.05) | 1.25 | SDS (0.125) | n-dodecane (0.013) | 50 | 0.025 |
| CrSt2.5 | $Cr(acac)_3$ (0.05) | 2.50 | SDS (0.25) | n-dodecane (0.025) | 50 | 0.05 |
| CrSt5 | $Cr(acac)_3$ (0.05) | 5.00 | SDS (0.50) | n-dodecane (0.050) | 50 | 0.10 |
| CrSt7.5 | $Cr(acac)_3$ (0.05) | 7.50 | SDS (0.75) | n-dodecane (0.075) | 50 | 0.15 |
| CrSt10 | $Cr(acac)_3$ (0.05) | 10.00 | SDS (1.00) | n-dodecane (0.10) | 50 | 0.20 |
| Section 2: Chromium Containing Particles: Experiment 2. Variation of n-Dodecane Concentration | | | | | | |
| CrDo0% | $Cr(acac)_3$ (0.05) | 5.00 | SDS (0.5) | None | 50 | 0.10 |
| CrDo1% | $Cr(acac)_3$ (0.05) | 5.00 | SDS (0.5) | n-dodecane (0.05) | 50 | 0.10 |
| CrDo2% | $Cr(acac)_3$ (0.05) | 5.00 | SDS (0.5) | n-dodecane (0.10) | 50 | 0.10 |
| CrDo3% | $Cr(acac)_3$ (0.05) | 5.00 | SDS (0.5) | n-dodecane (0.15) | 50 | 0.10 |
| CrDo4% | $Cr(acac)_3$ (0.05) | 5.00 | SDS (0.5) | n-dodecane (0.20) | 50 | 0.10 |
| Section 3: Chromium Containing Particles: Experiment 3. Variation of KPS Concentration | | | | | | |
| CrKPS0.5 | $Cr(acac)_3$ (0.05) | 5.00 | SDS (0.5) | n-dodecane (0.05) | 50 | 0.025 |
| CrKPS1 | $Cr(acac)_3$ (0.05) | 5.00 | SDS (0.5) | n-dodecane (0.05) | 50 | 0.05 |
| CrKPS3 | $Cr(acac)_3$ (0.05) | 5.00 | SDS (0.5) | n-dodecane (0.05) | 50 | 0.15 |
| CrKPS4 | $Cr(acac)_3$ (0.05) | 5.00 | SDS (0.50) | n-dodecane (0.05) | 50 | 0.02 |
| Section 4: Chromium Containing Particles: Experiment 3. Variation of SDS Concentration | | | | | | |
| CrSDS1% | $Cr(acac)_3$ (0.05) | 5.00 | SDS (0.50) | n-dodecane (0.05) | 50 | 0.10 |
| CrSDS2.5% | $Cr(acac)_3$ (0.05) | 5.00 | SDS (0.125) | n-dodecane (0.05) | 50 | 0.10 |
| CrSDS5% | $Cr(acac)_3$ (0.05) | 5.00 | SDS (0.25) | n-dodecane (0.05) | 50 | 0.10 |
| CrSDS15% | $Cr(acac)_3$ (0.05) | 5.00 | SDS (0.75) | n-dodecane (0.05) | 50 | 0.10 |
| CrSDS20% | $Cr(acac)_3$ (0.05) | 5.00 | SDS (1.00) | n-dodecane (0.05) | 50 | 0.10 |

| Sample | Metal Source (mass, g) | Styrene Mass (g) | Surfactant (mass, g) | Additive (mass, g) | Water (ml) [a] | KPS Mass (g) |
|---|---|---|---|---|---|---|
| Section 5: Effect of Monomer Addition Rate on Final Particle Size | | | | | | |
| Cr-0.10 | $Cr(acac)_3$ (0.05) | 5.00 | SDS (0.5) | n-dodecane (0.05) | 50 | 0.10 |
| Cr-0.15 | $Cr(acac)_3$ (0.05) | 5.00 | SDS (0.5) | n-dodecane (0.05) | 50 | 0.10 |
| Cr-0.20 | $Cr(acac)_3$ (0.05) | 5.00 | SDS (0.5) | n-dodecane (0.05) | 50 | 0.10 |
| Cr-0.25 | $Cr(acac)_3$ (0.05) | 5.00 | SDS (0.5) | n-dodecane (0.05) | 50 | 0.10 |
| Cr-0.30 | $Cr(acac)_3$ (0.05) | 5.00 | SDS (0.5) | n-dodecane (0.05) | 50 | 0.10 |
| Cr-0.35 | $Cr(acac)_3$ (0.05) | 5.00 | SDS (0.5) | n-dodecane (0.05) | 50 | 0.10 |
| Cr0.40 | $Cr(acac)_3$ (0.05) | 5.00 | SDS (0.5) | n-dodecane (0.05) | 50 | 0.10 |
| Cr-0.45 | $Cr(acac)_3$ (0.05) | 5.00 | SDS (0.5) | n-dodecane (0.05) | 50 | 0.10 |
| Cr-0.50 | $Cr(acac)_3$ (0.05) | 5.00 | SDS (0.5) | n-dodecane (0.05) | 50 | 0.10 |
| Cr-Bulk | $Cr(acac)_3$ | 5.00 | SDS (0.5) | n-dodecane (0.05) | 50 | 0.10 |
| Section 6: Metal Free Particles | | | | | | |
| Tween5% | None | 5.00 | Tween (0.25) | Span 80 (0.05) | 50 | 0.10 |
| Tween10% | None | 5.00 | Tween (0.50) | Span 80 (0.05) | 50 | 0.10 |
| Tween20% | None | 5.00 | Tween (1.00) | Span 80 (0.05) | 50 | 0.10 |
| Tween30% | None | 5.00 | Tween (1.50) | Span 80 (0.05) | 50 | 0.10 |
| Plu5% | None | 5.00 | Pluronic F68 (0.25) | n-dodecane (0.05) | 50 | 0.10 |
| Plu10% | None | 5.00 | Pluronic F68 (0.50) | n-dodecane (0.05) | 50 | 0.10 |
| Plu20% | None | 5.00 | Pluronic F68 (1.00) | n-dodecane (0.05) | 50 | 0.10 |
| Plu30% | None | 5.00 | Pluronic F68 (1.50) | n-dodecane (0.05) | 50 | 0.10 |
| La 11 | None | 5.00 | SDS (0.50) | n-dodecane (0.05) | 50 | 0.10 |
| Section 7: Pluronic F68 Stabilised Lanthanide Containing particles (Batch 1) | | | | | | |
| NdPlu-1 | $Nd(NFTA)_3$ (0.10) | 5.00 | Pluronic F68 (0.125) | n-dodecane (0.05) | 40 | 0.025 |
| NdPlu-2 | $Nd(NFTA)_3$ (0.10) | 5.00 | Pluronic F68 (0.50) | n-dodecane (0.05) | 50 | 0.10 |
| NdPlu-3 | $Nd(NFTA)_3$ (0.10) | 5.00 | Pluronic F68 (1.50) | n-dodecane (0.05) | 50 | 0.25 |
| GdPlu-1 | $Gd(NFTA)_3$ (0.10) | 5.00 | Pluronic F68 (0.125) | n-dodecane (0.05) | 40 | 0.025 |
| GdPlu-2 | $Gd(NFTA)_3$ (0.10) | 5.00 | Pluronic F68 (0.50) | n-dodecane (0.05) | 50 | 0.10 |
| GdPlu-3 | $Gd(NFTA)_3$ (0.10) | 5.00 | Pluronic F68 (1.50) | n-dodecane (0.05) | 50 | 0.25 |
| DyPlu-1 | $Dy(NFTA)_3$ (0.10) | 5.00 | Pluronic F68 (0.125) | n-dodecane (0.05) | 40 | 0.025 |
| DyPlu-2 | $Dy(NFTA)_3$ (0.10) | 5.00 | Pluronic F68 (0.50) | n-dodecane (0.06) | 50 | 0.10 |
| DyPlu-3 | $Dy(NFTA)_3$ (0.10) | 5.00 | Pluronic F68 (1.50) | n-dodecane (0.05) | 50 | 0.25 |

| Sample | Metal Source (mass, g) | Styrene Mass (g) | Surfactant (mass, g) | Additive (mass, g) | Water (ml) [a] | KPS Mass (g) |
|---|---|---|---|---|---|---|
| Section 8: Pluronic F68 Stabilised Lanthanide Containing Particles (Batch 2) | | | | | | |
| NdPlu-21 | $Nd(NFTA)_3$ (0.10) | 5.00 | Pluronic F68 (0.125) | n-dodecane (0.05) | 40 | 0.025 |
| NdPlu-22 | $Nd(NFTA)_3$ (0.10) | 5.00 | Pluronic F68 (0.50) | n-dodecane (0.05) | 50 | 0.10 |
| NdPlu-23 | $Nd(NFTA)_3$ (0.10) | 5.00 | Pluronic F68 (1.50) | n-dodecane (0.05) | 50 | 0.25 |
| GdPlu-21 | $Gd(NFTA)_3$ (0.10) | 5.00 | Pluronic F68 (0.125) | n-dodecane (0.05) | 40 | 0.025 |
| GdPlu-22 | $Gd(NFTA)_3$ (0.10) | 5.00 | Pluronic F68 (0.50) | n-dodecane (0.05) | 50 | 0.10 |
| GdPlu-23 | $Gd(NFTA)_3$ (0.10) | 5.00 | Pluronic F68 (1.50) | n-dodecane (0.05) | 50 | 0.25 |
| DyPlu-21 | $Dy(NFTA)_3$ (0.10) | 5.00 | Pluronic F68 (0.125) | n-dodecane (0.05) | 40 | 0.025 |
| DyPlu-22 | $Dy(NFTA)_3$ (0.10) | 5.00 | Pluronic F68 (0.50) | n-dodecane (0.05) | 50 | 0.10 |
| DyPlu-23 | $Dy(NFTA)_3$ (0.10) | 5.00 | Pluronic F68 (1.50) | n-dodecane (0.05) | 50 | 0.25 |
| LaPlu-21 | None | 5.00 | Pluronic F68 (0.125) | n-dodecane (0.05) | 40 | 0.025 |
| LaPlu-22 | None | 5.00 | Pluronic F68 (0.50) | n-dodecane (0.05) | 50 | 0.10 |
| LaPlu-23 | None | 5.00 | Pluronic F68 (1.50) | n-dodecane (0.05) | 50 | 0.25 |
| Section 9: SDS Stabilised Lanthanide Containing Particles (Batch 3) | | | | | | |
| NdSDS-1 | $Nd(NFTA)_3$ (0.05) | 5.00 | SDS (0.125) | n-dodecane (0.05) | 40 | 0.025 |
| NdSDS-2 | $Nd(NFTA)_3$ (0.05) | 5.00 | SDS (0.50) | n-dodecane (0.05) | 50 | 0.10 |
| NdSDS-3 | $Nd(NFTA)_3$ (0.05) | 5.00 | SDS (1.50) | n-dodecane (0.05) | 50 | 0.25 |
| GdSDS-1 | $Gd(NFTA)_3$ (0.05) | 5.00 | SDS (0.125) | n-dodecane (0.05) | 40 | 0.025 |
| GdSDS-2 | $Gd(NFTA)_3$ (0.05) | 5.00 | SDS (0.50) | n-dodecane (0.05) | 50 | 0.10 |
| GdSDS-3 | $Gd(NFTA)_3$ (0.05) | 5.00 | SDS (1.50) | n-dodecane (0.05) | 50 | 0.25 |
| DySDS-1 | $Dy(NFTA)_3$ (0.05) | 5.00 | SDS (0.125) | n-dodecane (0.05) | 40 | 0.025 |
| DySDS-2 | $Gd(NFTA)_3$ (0.05) | 5.00 | SDS (0.50) | n-dodecane (0.05) | 50 | 0.10 |
| DySDS-3 | $Gd(NFTA)_3$ (0.05) | 5.00 | SDS (1.50) | n-dodecane (0.05) | 50 | 0.25 |

[a] Samples synthesized with 40ml of water in the external phase where made to up to 50 ml post synthesis to keep latex solid concentration consistent with other samples

composition, *i.e.* the absence of $Cr(acac)_3$, and the varied identity of the surfactant and co-surfactant, the polymerisation procedure was identical to the one followed for synthesis of the chromium containing particles. As such the procedure will not be repeated here, and section 5.2.3.1 should be referred to for reference.

### 5.2.3.3 Varied Monomer Addition Rate Synthesis of Chromium Containing Latex.

KPS (0.1 g) and SDS (0.5 g) were dissolved in de-ionised water (50 ml) in a 4 neck round-bottom flask. An IKA RW20.n overhead stirrer with a PTFE paddle was fitted through the central neck. A reflux condenser was attached to one of the side necks of the flask, and the remaining necks were sealed with Suba seals. The solution was heated (70 $^{o}$C) and purged with nitrogen (30 mins). $Cr(acac)_3$ (0.05 g) and n-dodecane (0.05 g) were dissolved in styrene (5 g) and then purged with nitrogen (30 min). The solution was then introduced into the round-bottom flask, containing the SDS/KPS solution, at addition rates from 0.1 ml min$^{-1}$ to 0.5 ml min$^{-1}$, (0.05 ml min$^{-1}$ increments), and one bulk addition. This was done by means of a syringe pump (Model '22', Harvard Apparatus) through one of the side necks, with slow stirring (100 rpm).

Once addition was complete the final emulsion composition was supposed to be the same in all cases, and identical to CrSt5. However, the syringe pump would often not fully inject the monomer phase and on average 0.3 g of solution remained within the syringe. This resulted in an average styrene addition of 4.706 g, an average n-dodecane addition of 0.047 g and an average $Cr(acac)_3$ addition of 0.047 g. Theses quantities were used for the bulk the addition to allow comparison of results.

After the last of the monomer phase was added, polymerisation was left to proceed under nitrogen atmosphere (3 hours at 70 $^{o}$C). Once polymerisation was complete the

reaction mixture was allowed to cool to ambient temperature and then passed through filter paper to remove any polymer grist. Latexes were then stored at 3 $^{o}$C.

### 5.2.4 Dialysis

Prior to final characterisation, the lanthanide containing batches of latex particles were 'cleaned' of excess surfactant and KPS by dialysis. A sample of latex (10 ml) was placed in a regenerated cellulose membrane (molecular weight cut off 12000-14000) (Scientific Laboratory Supplies, UK) and dialysed against deionised water (1000 ml for 48 hours). Dialysis water was changed seven times with the first change being made after 2 hours.

ICP-MS analysis of the potassium content of the dialysis water showed that by 50 hours and six changes, the levels of potassium in the water were the same as in a control sample of fresh de-ionised water (Figure 5.5), meaning that dialysis had 'cleaned' the latexes to maximum possible level.

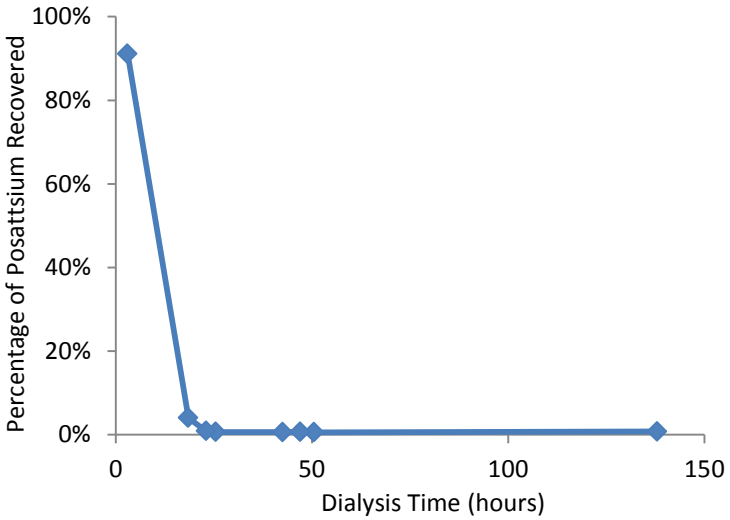


Figure 5.5: ICP-MS analysis of potassium content of the dialysis water used to 'clean' latex particles with each change, expressed as a % of total potassium recovered

### 5.2.5 Particle Characterisation

#### 5.2.5.1 Dynamic Light Scattering

For all particle systems produced, the z-average ($D_z$), intensity-average ($D_I$), number-average ($D_n$) and volume-average ($D_v$) diameters were determined by Dynamic light scattering (DLS), performed with a Zetasizer Nano ZS (Malvern Instruments, UK) with a maximum 5mW He-Ne laser, of 633nm wavelength, at 25 $^{o}$C. Latex samples were diluted to at least 10 % v/v with deionised water before analysis. This was necessary to ensure that any remaining surfactant was below its critical micelle concentration (cmc) preventing a secondary peak, corresponding to surfactant micelles, appearing in the measurement data. Measurements were performed a minimum of three times with the value reported corresponding to the average of the measurements.

It is important to note here that it was unknown what effect the complex would have upon the final refractive index (RI) of the latex particles. While this will not influence the values of $D_z$ and $D_I$, values of $D_v$ and $D_n$, generated by DLS, require knowledge of the material (RI). It was hoped that the low complex content, below 1 % w/w. would only have a minimal effect upon the final particle RI. Therefore the RI of polystyrene (1.59) was used

The dispersity of the particles was also determined by DLS, and was expressed in two ways. Firstly, the polydispersity index (PDI) elucidated by the Malvern software. This is determined from $D_z$ and can be expressed by equation 5.1:

$$\mathrm{PDI} = \frac{\sigma^2}{{D_z}^2} \qquad \text{(Eq. 5.1)}$$

where $\sigma$ is the standard deviation of $D_z$.

PDI is a dimensionless value between 0 and 1, which is scaled such that values ≥ 0.07 are considered highly monodisperse and values > of 0.05 are rarely seen.[98]

Secondly, dispersity was also expressed by $D_v/D_n$ ($D_v$=$D_w$ assuming the particles have an equal density regardless of size)[75] in which values close to 1 are highly monodisperse.

#### 5.2.5.2 Transmission electron microscopy

Transmission electron microscopy (TEM) was performed at the Institute for Materials Research at the University of Leeds with a Tecnai TF20 field emission gun (FEG)-TEM (TEI, USA) operating at 200 kV. Samples were prepared by placing a drop of latex (diluted to 50 % v/v in deionised water) onto copper grids coated in a holey carbon film (Agar Scientific). The $D_w$ was also calculated for the particles using the density of polystyrene (1.05 g $cm^{-3}$) as the density of the particles (again assuming that the complex would only have a minimal effect of particles mass). This allowed a calculation of particle dispersity from $D_w/D_n$. This metric however was only used to complement the dispersity obtained from other methods as due to the low number of measurements compared the other analytical techniques it will be of less accuracy.

#### 5.2.5.3 Differential Centrifugal Sedimentation

Differential Centrifugal Sedimentation (DCS) measurements were carried out at the Food and Environment Agency (fera), York, using a CPS DC24000-UHR instrument (AnalytikLtd, UK). Instrument settings were outlined in user manual but with the following gradient; 8%-2%; 1.6 ml per gradient step; and 24,000 rpm spin speed. For particles <60 nm, a sedimentation path with a lower thickness was created by injecting 1.4 ml per gradient step. Sample injection volume was 50 $\mu$l, with sample dilution between 0.5 and 5% v/v, dependent on individual sample turbidity. The instrument was calibrated using

522 nm latex particles (AnalytikLtd), with an injection volume of 100 $\mu$l. As with DLS and TEM the density of the particles was taken as that of polystyrene (1.05 g $cm^{-3}$)

#### 5.2.5.4 HDC-ICP-MS

Details for setting-up the HDC-ICP-MS for NP analysis is described elsewhere,[99] but in the work presented here, the samples were diluted to 1% v/v in mobile phase. Injection volume was 20 $\mu$l, with the ICP-MS monitoring 157, 158, 160, 161, 162, 163, 164 and 197 isotopes. Size calibration was performed using gold nanoparticle standard (BBI, UK) at 5, 20, 50 and 150 nm. It is important to note that uncertainty in the values quoted for the smaller particles is significant, as a slight shift in column conditions would result in a significant shift in the 'measured' size. Also the 150nm gold-NP standard was very polydisperse, making the upper end of the calibration slightly dubious.

#### 5.2.5.5 Zeta Potential

The zeta potentials ($\zeta$) of the particles were measured with a Zetasizer Nano ZS (Malvern Instruments, UK) at 25 $^{o}$C. A sample of latex (0.1 ml) was diluted in deionised water (0.9 ml), and injected into a disposable zeta cell. Analysis was repeated three times, at constant voltage, the reported value corresponding to the average of the measurements.

#### 5.2.5.6 Solids Content of the Latexes

Solid content of the latexes was determined by gravimetric analysis after dialysis (which was assumed to have removed any residual species from the latex dispersion). A latex sample of known mass was dried in air for 72 hours. The mass of the residue was then measured and converted to percentage of the original sample mass.

#### 5.2.5.7 Lanthanide Content of Latexes

The lanthanide content of the latex particles was determined at fera by the following method: 100$\mu$l of latex was mixed with 2ml of 4:1 nitric:hydrochloric acid in a TFM tube. The sample was then microwave digested (20 minutes at 240°C and 80 bar) in an UltraWAVE microwave digester (Milestone, USA). The sample was then diluted and analysed using a 7700 series ICP-MS (Agilent, UK) in 'no gas' mode. Results were calculated against a set of standards covering three orders of magnitude and recovery was determined by using a spiked reagent blank and a spiked sample. Rhodium was used as an internal standard and the limit of detection was calculated from the standard deviation of three reagent blanks.

## 5.3 Results and Discussion

Before embarking on the synthesis of the lanthanide-containing particles, a set of polystyrene latex particles containing $Cr(acac)_3$ were synthesised to demonstrate proof-of-principle that metals could be encapsulated within latex particles, using micro-emulsion polymerisation. These initial experiments also provided data which was used to determine the conditions for production of the lanthanide containing particles over the desired (40 nm to 160 nm) size range. In addition to this, chromium complexes are more readily available and, also, less expensive than lanthanides, representing a cheaper option for investigating various procedures.

### 5.3.1 $Cr(acac)_3$ Containing Polystyrene Particles

Initially the emulsions appeared translucent with a purple hue, which can be attributed to the $Cr(acac)_3$. As the polymerisation progressed the micro-emulsions became

increasingly turbid, due to particle formation, until the end of the reaction when stable opaque latexes was formed, with the purple hue still present (Figure 5.6).

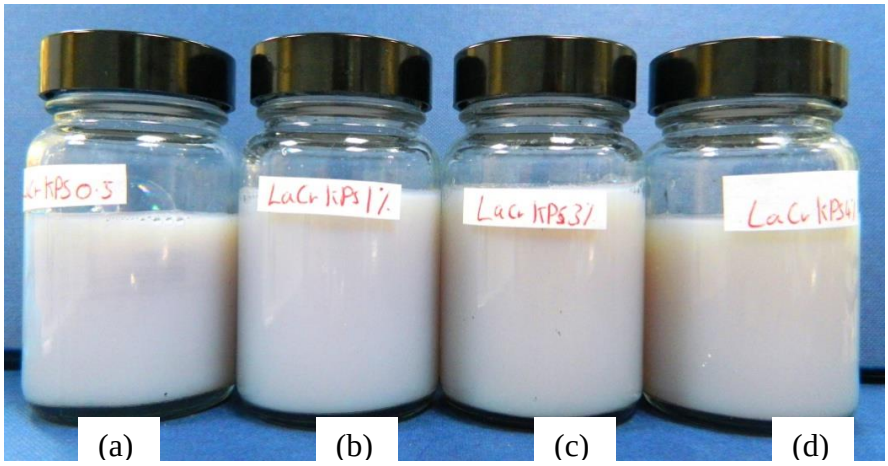


Figure 5.6: Polystyrene particles synthesised with varying initiator concentrations; (a) 0.5 % (CrKPS0.5), (b) 1 % (CrKPS1), (c) 3 % (CrKPS3), and (d) 4 % (CrKPS4) w/w with respect to styrene. The purple hue results from the $Cr(acac)_3$ dispersed throughout the particles

### 5.3.1.1 Effects of Emulsion Composition.

To study the effect of emulsion composition upon final particle size, and polydispersity, the synthesis of the chromium containing particles was divided into four separate experiments. Each experiment saw the concentration of one of the emulsion components varied with respect to styrene, with all other components' relative concentrations remaining constant:

Experiment 1: water content from 500 % to 4000 % v/w with respect to styrene.

Experiment 2: n-dodecane content from 0% to 4 % w/w with respect to styrene.

Experiment 3: KPS concentration from 0.5 % to 4 % w/w with respect to styrene.

Experiment 4: SDS concentration from 1 % to 20 % w/w with respect to styrene.

To aid clarity, sections 5.3.1.1.1 to 5.3.1.1.4 present the results of each experiment, followed by a discussion of these results in section 5.3.1.1.5.

#### 5.3.1.1.1 Experiment 1: Effect of Relative Water Content upon Final Particle Size

As the 4-neck round-bottom flask, used as the reaction vessel, had to be made bespoke, it was not possible to increase the physical volume of water in the reaction over the required range. Therefore, to vary the relative water concentration by the appropriate amounts the water volume was kept at 50 ml and the quantities of the other components were varied accordingly (see section 1of Table 5.6 for exact compositions).

The data presented in Table 5.7 and in Figure 5.7(a) shows that the relative water content of the micro-emulsion has no discernible upon the final particles size. The mean $D_z$ of the particle systems was 41 nm, with a relative standard deviation (RSD) of 1.3 %. This non-dependence of particle size on water concentration is further borne out by the values of $D_I$, $D_v$ and $D_n$, all of which have < 3 nm spread, with an RSD 1.2 %, 1.9 % and 3.4 % respectively.

Table 5.7: The effect of the relative water concentration (with respect to styrene) in the micro-emulsion formulation on final particle size, and PDI, measured by DLS. Water volume was kept constant, at 50 ml and other components where varied, keeping their concentration, with respect to styrene, constant; SDS 10% w/w, KPS 2% w/w, n-dodecane 1% w/w and $Cr(acac)_3$ 1% w/w.

| Sample | Styrene Mass (g) | Water Concentration (% wrt. styrene) | $D_z$ (nm) | $D_I$ (nm) | $D_v$ (nm) | $D_n$ (nm) | PDI | $D_v/D_n$ |
|---|---|---|---|---|---|---|---|---|
| CrSt2.5 | 1.25 | 4000 | 41 | 43 | 38 | 35 | 0.05 | 1.11 |
| CrSt5 | 2.50 | 2000 | 40 | 42 | 36 | 32 | 0.06 | 1.15 |
| CrSt7.5 | 5.00 | 1000 | 41 | 44 | 37 | 32 | 0.07 | 1.15 |
| CrSt10 | 7.50 | 667 | 41 | 42 | 38 | 34 | 0.07 | 1.11 |
| CrSt20 | 10.00 | 500 | 41 | 43 | 37 | 33 | 0.08 | 1.12 |

The values of PDI and $D_v/D_n$, (highest PDI value, displayed by CrSt20, was only 0.08) indicated that highly monodisperse particles had been produced. The data in Table 5.7 and Figure 5.7(b) shows that a decrease in relative water concentration was accompanied by an increase in the PDI. It is, however, not clear if this is a genuine

relationship or a coincidental trend as the change is small and is not mirrored in the $D_v/D_n$ values.

#### 5.3.1.1.2 Experiment 2: Effect of n-Dodecane Content upon Final Particle Size.

The data presented in Table 5.8 and in plots (c) and (d) of Figure 5.7, show that the concentration of n-dodecane in the micro-emulsion has no apparent effect upon the final particle size or dispersity. All formulations produced particles of similar size (average diameter was 42 nm with an RSD of 3.2 %), with similarly high levels of monodispersity (all values of PDI were $\geq 0.08$)

Table 5.8: The effect of n-dodecane concentration (with respect to styrene) in the micro-emulsion formulation on final particle size, and PDI, measured by DLS. All other components were constant; styrene 5 g, water 50 ml, SDS 0.5 g, KPS 0.1 g and $Cr(acac)_3$ 0.05 g.

| Sample | n-dodecane mass (g) | n-dodecane Conc. (%) | $D_z$ (nm) | $D_I$ (nm) | $D_v$ (nm) | $D_n$ (nm) | PDI | $D_v/D_n$ |
|---|---|---|---|---|---|---|---|---|
| CrDo0% | 0.00 | 0 | 41 | 44 | 38 | 33 | 0.06 | 1.17 |
| CrSt10% | 0.05 | 1 | 41 | 44 | 37 | 32 | 0.07 | 1.15 |
| CrDo2% | 0.10 | 2 | 44 | 46 | 41 | 36 | 0.06 | 1.13 |
| CrDo3% | 0.15 | 3 | 41 | 44 | 37 | 32 | 0.08 | 1.16 |
| CrDo4% | 0.20 | 4 | 40 | 44 | 36 | 31 | 0.08 | 1.17 |

#### 5.3.1.1.3 Experiment 3: Effect of Initiator (KPS) Content upon Final Particle Size.

Table 5.9 and Figure 5.7(e), shows the final particle size is influenced by the KPS concentration in the micro-emulsion. An eight fold increase in KPS concentration resulted in a 10 nm reduction in $D_z$. Table 5.9 and Figure 5.7(f) shows KPS content in the micro-emulsion had no discernible effect upon the monodispersity. All particle systems displayed high levels of mono-dispersity with values of PDI and $D_v/D_n$ all $\geq 0.09$ and $\geq 1.15$ respectively.

Table 5.9: The effect of the KPS concentration (wrt. styrene) in the initial micro-emulsion formulation on final particle size and PDI, measured by DLS. All other components were constant; Styrene 5 g, water 50 ml, SDS 0.5 g, n-dodecane 0.05 g and $Cr(acac)_3$ 0.05 g

| Sample | KPS Mass (g) | KPS conc. (%) | $D_z$ (nm) | $D_I$ (nm) | $D_v$ (nm) | $D_n$ (nm) | PDI | $D_v/D_n$ |
|---|---|---|---|---|---|---|---|---|
| CrKPS0.5 | 0.025 | 0.5 | 48 | 50 | 44 | 40 | 0.09 | 1.11 |
| CrKPS1 | 0.05 | 1 | 44 | 47 | 41 | 37 | 0.07 | 1.12 |
| CrSt5 | 0.10 | 2 | 41 | 44 | 37 | 32 | 0.07 | 1.15 |
| CrKPS3 | 0.15 | 3 | 39 | 41 | 36 | 31 | 0.06 | 1.14 |
| CrKPS4 | 0.20 | 4 | 38 | 40 | 35 | 31 | 0.07 | 1.12 |

#### 5.3.1.1.4 Experiment 4: Effect of SDS Content upon Final Particle Size.

Table 5.10 and Figure 5.7 (g) show an inverse relationship between the SDS concentration and the final particle size. An eight fold increase in SDS concentration resulted in a decrease in $D_z$ of 22 nm. This relationship was also evident in the $D_I$, $D_v$ and $D_n$ values.

Low PDI ($\geq 0.09$), and $D_v/D_n$ ($\geq 1.20$) indicated that highly monodisperse particles were formed, irrespective of the SDS concentration.

Table 5.10: Effect of the SDS concentration (wrt. styrene) in the micro-emulsion formulation on final particle size and PDI, measured by DLS. Styrene, 5 g, and all other components were constant; water, 50 ml, KPS, 0.1 g, n-dodecane, 0.05 g, and $Cr(acac)_3$, 0.05 g.

| Sample | SDS Mass (g) | SDS conc. w/w (%) | $D_z$ (nm) | $D_I$ (nm) | $D_v$ (nm) | $D_n$ (nm) | PDI | $D_v/D_n$ |
|---|---|---|---|---|---|---|---|---|
| CrSDS1% | 0.05 | 1 | Micro-emulsion did not form | | | | | |
| CrSDS2.5% | 0.125 | 2.5 | 56 | 59 | 52 | 46 | 0.07 | 1.13 |
| CrSDS5% | 0.25 | 5 | 47 | 49 | 45 | 41 | 0.09 | 1.10 |
| CrSt5 | 0.50 | 10 | 41 | 44 | 37 | 32 | 0.07 | 1.15 |
| CrSDS15% | 0.75 | 15 | 34 | 37 | 30 | 26 | 0.08 | 1.17 |
| CrSDS20% | 1.00 | 20 | 34 | 37 | 30 | 25 | 0.08 | 1.20 |

#### 5.3.1.1.5 Discussion of Experiments 1-4.

Experiment 1 (section 5.3.1.1.1) revealed that an increase in the relative water concentration was accompanied by a corresponding decrease in the PDI of the particles. However as the decrease was small (easily being accounted for by the error inherent in the

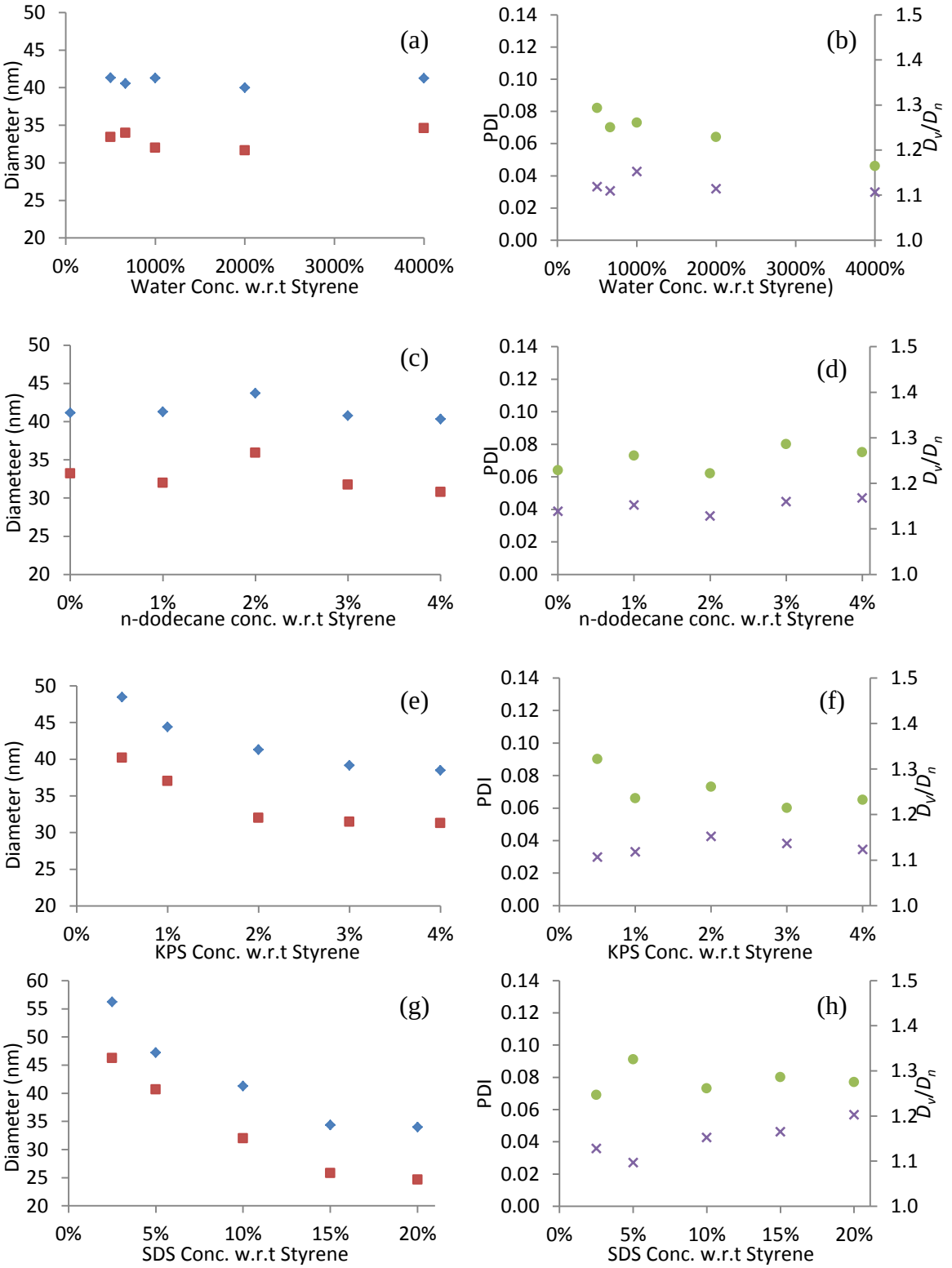


Figure 5.7: The effects of varying (a) and (b): the water concentration v/w, (c) and (d): the n-dodecane w/w concentration, (e) and (f): the KPS w/w concentration, and (g) and (h): the SDS w/v concentration (in all cases wrt. Styrene) of the micro-emulsion on the $D_z$ (◆), $D_n$ (■), PDI (●) (all measured by DLS) and $D_v/D_n$ (X) of $Cr(acac)_3$ containing polystyrene particles produced by micro-emulsion polymerisation. In all cases, with the exception of the varied component, other factors *i.e.* SDS, KPS, n-dodecane and $Cr(acac)_3$ concentrations with respect to styrene were kept constant.

measurements), and the same trend was not observed for the values of $D_v/D_n$, it is most likely that the trend in coincidental rather than genuine. If it is a genuine relationship it may be as result of dilution of the micro-emulsion reducing droplet/droplet interactions however it would not be reasonable to speculate further at this time.

Experiment 1 also showed no apparent relationship between final particle size and the relative water concentration of the micro-emulsion. This may be explained by the near insolubility of styrene in water (0.031 % at 25 $^{o}$C).[69] Styrene, unlike monomers, such as methyl methacrylate, with a non-negligible solubility in water (1.5 % at 25 $^{o}$C),[82] will only lose a trivial amount of monomer to dissolution in the aqueous phase. Therefore, even in micro-emulsion systems formed with large volumes of water there was no significant decrease in the amount of monomer requiring solubilisation by the surfactant. As the styrene to SDS ratio was maintained in all systems the monomer droplet size was likely unchanged by variation in relative water concentration. While there are several mechanisms that define the final particle size it is known that the initial droplet size of the micro-emulsion has a significant effect on the particle size.[100,101,102] The low solubility of styrene also means that even with high water content in the micro-emulsion homogenous nucleation is never likely to be a significant, and competing, process of particle formation.

While medium-chain alcohols are typically used as co-surfactants in micro-emulsion polymerisation they do have some disadvantages; they can negatively affect the stability of the micro-emulsion during polymerisation, as they are non-solvents for the resulting polymer.[56] In partitioning between the interfacial film and the continuous phase they complicate the dilution process when determining particle size.[66] Alcohols can also act as chain-transfer agents, affecting the final polymer molecular weight.[103] Initially, it was hoped that n-dodecane (which has previously been used in micro-emulsion polymerisation[75]) could act as a co-surfactant without exhibiting the drawbacks of

alcohols. However, with retrospective consideration it is likely that due to the high hydrophobicity of n-dodecane it will not act as a co-surfactant (0.0037 mg $l^{-1}$ water solubility at 25$^{o}$C).[104] Rather it will locate wholly within the styrene phase and not interact with the interface having little effect on droplet/particle formation. This is evidenced by the results from experiment 2 (section 5.3.1.1.2.) which revealed no correlation between the concentration of n-dodecane in the micro-emulsion and the final particles size (even when no n-dodecane was present, CrDo0%). While n-dodecane has been used as an osmotic agent (countering the Laplace pressure of the droplet)[105,106] to aid stabilisation of certain emulsion systems, it is unlikely that it will act in such a way in here as micro-emulsions will have a very low Laplace pressure due the near zero interfacial tension of the droplets

As can be seen in plots (e) and (g) of Figure 5.7, the concentration of both KPS (experiment 3; section 5.3.1.1.3) and SDS (experiment 4; section 5.3.1.1.4) in the micro-emulsion have a similar effect upon the final particle size. Due to the similarity it was possible to express the relation of both by equation 5.2:

$$D_z = a\frac{1}{[C]^x} \qquad \text{(Eq. 5.2)}$$

where [$C$] represents the concentration of either SDS or KPS, $a$ and $x$ are constants which are specific to either SDS or KPS. From the collected data, $a$=22.3 and $x$=0.12 for KPS concentration, and for SDS concentration $a$=26.6 and $x$=0.25. This shows that though both have a similar effect on particle size, the effect of the SDS concentration is more significant.

The dependence of final particle size upon the KPS concentration in the initial micro-emulsion formulation has previously been observed by Kong and co-workers[75] among many others. There are several potential mechanisms operating during polymerisation which can be used to explain this behaviour. Firstly, the persulphate portion of KPS thermally decomposes into two ionic radicals, $S_2O_8^{2+} \rightarrow SO_4^{\bullet-}$. It is these radicals

which are responsible for initiation by reacting with the small amounts of styrene in the aqueous phase. This forms a sulphate terminated styrene radical which will react with other styrene molecules forming oligomers with even greater insolubility in water. These oligomers, which will diffuse into the styrene droplets, can be considered as having a structure analogous to a single tail (the styrene units) anionic (the sulphate anion) surfactant. Once in the droplet they will most likely locate with the sulphate anion at the interface acting as an additional stabiliser for droplets.[102]An increase in the amount of KPS will lead to a corresponding increase in sulphate radical anions. This then will produce more of these stabiliser oligomers allowing for the formation of smaller droplets and, as mentioned earlier, smaller droplets can lead to smaller final particles.[100,101] Secondly, during stage 1, or the nucleation period, of polymerisation, the increased radical content of the micro-emulsion leads to a larger number of droplets being initiated in turn leading to a greater number of particle nucleation sites.[107] In stage 2 the remaining monomer contained in the uninitiated droplets will more readily diffuse through the aqueous phase into the initiated droplets to feed particle growth, rather than generate new particles.[75] Therefore, the remaining monomer has to be distributed over a greater number of initiated droplets, which will yield a smaller average particle size.

Regarding the decreasing final particle size with increasing SDS concentration in the micro-emulsion, the greater the amount of SDS present in the micro-emulsion, the larger the interfacial area that can be stabilised. This allows for the formation of smaller droplets, which, as discussed, can lead to smaller particles.[100,101,102]

The effect of both KPS and SDS concentration in the micro-emulsion on final particle size is shown by plots (e) and (g) in Figure 5.7 to be non-liner. Moraes and co-workers have also noted this relationship for SDS, as well as for the surfactant Dowfax 2A1.[76] In their work they propose that as surfactant concentration is increased droplets will

initially become smaller, however, due to physical limits on surfactant packing droplet size cannot decrease continuously. At high surfactant concentrations the surfactant can no longer form spherical micelles and will instead form rod like-structures.[108] This limits the number of micelles as well as reducing the surface area for a given number of micelles preventing smaller particles being formed.

### 5.3.1.2 Effect of Monomer Addition Rate on Final Particle Size

It has been reported that by utilising a gradual monomer feed into the aqueous phase during polymerisation, in what is termed semi-continuous micro-emulsion polymerisation, that the final particle size can be influenced.[109,110] To investigate if the monomer feed rate could be used for particle size control, another batch of test particles containing $Cr(acac)_3$ was produced.

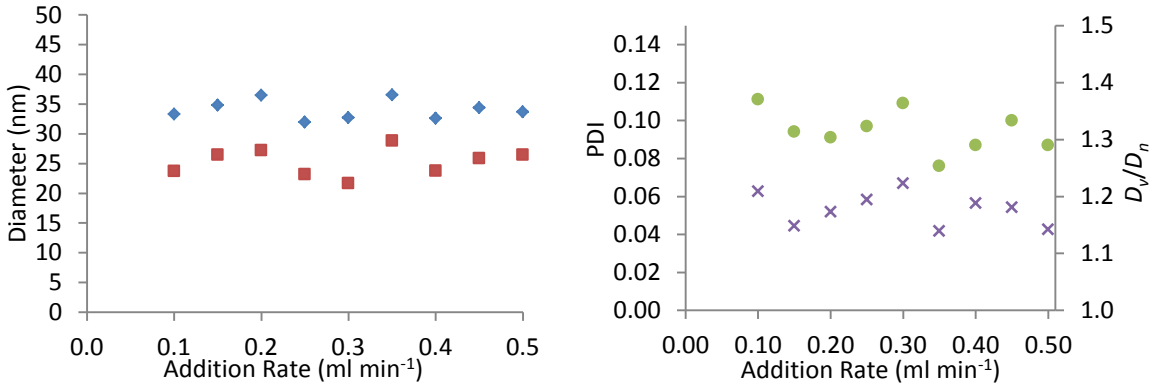


Figure 5.8: Effect of the monomer addition rate into the micro-emulsion on the z-average diameter (◆) the number-average diameter (■), as well as dispersity, both from DLS (●) and as expressed as $D_v/D_n$ (X).

It had been expected that the rate of monomer addition would have influenced the final particle size. However, the particles sizes measured by DLS and displayed in Table 5.11 and Figure 5.8, show that this was not the case with particles of a similar size being produced irrespective of monomer phase addition rate. With even the bulk addition producing similar sized particles. Put simply, the principal of semi-continuous, micro-emulsion polymerisation is to starve the system of monomer creating a significant excess

of initiator and allowing the formation of smaller particles.[111] At the slowest addition rate of 0.1 ml min$^{-1}$ all the monomer phase would have been added within 46 minutes.[i] KPS has a dissociation rate constant of 9.23 x 10$^{-6}$ s$^{-1}$ at 70 $^{o}$C,[112] and this can be related to the half-life of an initiator by

$$t_{1/2} = ln2/k_d \quad \text{(Eq. 5.2)}$$

where $t_{1/2}$ is the initiator half-life and $k_d$ is the dissociation rate constant of the initiator. This gives a half-life of ≈ 29 hours 50 minutes at 70 $^{o}$C. As addition of the monomer phase was completed in considerably less time than one half-life of KPS the polymerisation was never under monomer starved conditions and was always in monomer excess. As such the addition rates used here would not be expected to influence final particle size.

Table 5.11: Effect of monomer addition rate upon the final particle size and polydispersity.

| Sample | Addition Rate (ml min$^{-1}$) | $D_z$ (nm) | $D_I$ (nm) | $D_v$ (nm) | $D_n$ (nm) | PDI | $D_v/D_n$ |
|---|---|---|---|---|---|---|---|
| Cr-0.10 | 0.10 | 33 | 37 | 29 | 24 | 0.11 | 1.21 |
| Cr-0.15 | 0.15 | 35 | 37 | 30 | 26 | 0.09 | 1.15 |
| Cr-0.20 | 0.20 | 36 | 39 | 32 | 27 | 0.09 | 1.17 |
| Cr-0.25 | 0.25 | 32 | 35 | 28 | 23 | 0.10 | 1.19 |
| Cr-0.30 | 0.30 | 33 | 37 | 27 | 22 | 0.11 | 1.22 |
| Cr-0.35 | 0.35 | 37 | 38 | 33 | 29 | 0.08 | 1.14 |
| Cr0.40 | 0.40 | 33 | 35 | 28 | 24 | 0.09 | 1.19 |
| Cr-0.45 | 0.45 | 34 | 38 | 31 | 26 | 0.10 | 1.18 |
| Cr-0.50 | 0.50 | 34 | 36 | 30 | 26 | 0.09 | 1.14 |
| Cr-Bulk | Bulk | 36 | 38 | 33 | 29 | 0.08 | 1.11 |
| Average | N/A | 34 | 37 | 30 | 26 | 0.09 | 1.17 |
| %RSD | N/A | 4.9 | 3.6 | 7.2 | 9.8 | 13.1 | 2.9 |

However, the particles had an average $D_z$ of 34 nm, which is 7 nm smaller than CrSt5 ($D_z$ = 41 nm). The difference can be attributed to the problems encountered with the syringe pump. On average, 0.3 g of monomer solution was found to remain in the syringe post injection. This means that on average only 4.71 g of styrene was added the aqueous

[i] Styrene has a density on 0.91 g cm$^{-3}$ meaning that the 5 g of monomer phase had a volume of 4.46 ml meaning at 0.1 ml min$^{-1}$ addition would have taken 45.5 min.

phase compared to the 5 g used in the production of CrSt5. This would have led to an increased SDS/styrene and KPS/styrene ratio which, as shown in sections 5.3.1.1.3 and 5.3.1.1.4, results in a decreased particle size. This is supported by the fact that Cr-Bulk displays a $D_z$ value of 36 nm, similar to the samples produced with a controlled rate of monomer feed, not CtSt5. For Cr-Bulk, the monomer phase was introduced to the reaction in a single addition and the incomplete addition was accounted for by reducing the amounts of styrene, n-dodecane and $Cr(acac)_3$.

The values for PDI, between 0.7 and 0.11, indicate high levels of monodispersity, comparable to the particles from section 5.3.1.1

#### 5.3.1.3 Synthesis of Polystyrene Latex Particles Using Non-Ionic Surfactants

As has been shown in the preceding sections, particle size can be tailored by variation of the SDS concentration in the micro-emulsion. However, the use of SDS was only able to produce particles over a 22 nm size range, from $D_z$ 34 nm to 56 nm, which barely covers any of the 40 nm to 160 nm size range desired for analytical calibrants. In an attempt to increase the particle size range, two other surfactants, Tween 80 and Pluronic F68, were investigated. A further advantage to using these surfactants is that, because both are non-ionic, unlike SDS, stabilisation of the resulting particles is by steric forces instead of electrostatic. The outcome of this is that neither surfactant will contribute to particle surface charge, which is particularly relevant for the particles intended use for HDC-ICP-MS analytical standards. Particle velocity through the HDC column bed has been shown to be sensitive to electrostatic interactions between the particle and the column packing, as well as physical size.[11,113,114] This effect can be negated by use of a mobile phase with a low ionic strength, which effectively renders these interactions inconsequential.[115]

However, ideal calibrants would still possess a near zero surface charge, to minimise even small charge-based effects and to allow use in a variety of mobile phases.

Particles were produced over a range of surfactant concentrations (5 % to 30 % w/w with respect to styrene), and did not contain $Cr(acac)_3$. The sizes and polydispersity were measured by DLS and are displayed in Table 5.12 and Table 5.13.

As can be seen in Figure 5.9 (a) and (c), both Tween 80 and Pluronic F68 demonstrate the expected inverse relationship between particle size and surfactant concentration. As explained in section 5.3.1.1.4, this is due to the larger volume of surfactant being able to stabilise a greater interfacial area, allowing more monomer droplets. The linear decrease in size is attributed to the limits of surfactant packing, causing non-spherical micellar structures to form at high surfactant concentrations.[76]

Both surfactants were able to produce particles over a greater size range than SDS. The $D_z$ range using Tween 80 was 71 nm (from 127to 198 nm) and 63 nm (from 62 to 125 nm) using Pluronic F68.

Pluronic F68 was also able to produce particles with a greater degree of mono-dispersity than Tween 80 with PDI values between 0.04 and 0.02, ($D_v/D_n$ between 1.10 and 1.05). This compared favourably to the dispersity of the chromium containing particles produced using SDS discussed in the previous sections.

Both Tween 80 and Pluronic F68 particle systems initially seemed stable, however after aging for 7 months Tween10% and Tween5% displayed clearly visible aggregates, forming a thick layer of solids on the bottom of the container which would not re-disperse with manual agitation. The equivalent Pluronic F68 particle systems, Plu10% and Plu5% showed some signs of aggregation but they would easily re-disperse (Figure 5.10).

Table 5.12: The effect of Tween 80 concentration (with respect to styrene) in the micro-emulsion formulation, on the final particle size and dispersity, measured by DLS.

| Sample | Tween 80 (g) | Tween 80 conc. w/w (%) | $D_z$ (nm) | $D_I$ (nm) | $D_v$ (nm) | $D_n$ (nm) | PDI | $D_v/D_n$ |
|---|---|---|---|---|---|---|---|---|
| Tween5% | 0.25 | 5 | 198 | 211 | 211 | 174 | 0.06 | 1.21 |
| Tween10% | 0.50 | 10 | 173 | 184 | 181 | 145 | 0.07 | 1.25 |
| Tween20% | 1.00 | 15 | 131 | 150 | 126 | 84 | 0.14 | 1.49 |
| Tween30% | 1.50 | 20 | 127 | 137 | 126 | 103 | 0.09 | 1.23 |

Table 5.13: The effect of Pluronic F68 concentration (with respect to styrene) in the micro-emulsion formulation upon the final particle size and dispersity, measured by DLS.

| Sample | Pluronic F68 (g) | Pluronic F68 conc. w/w (%) | $D_z$ (nm) | $D_I$ (nm) | $D_v$ (nm) | $D_n$ (nm) | PDI | $D_v/D_n$ |
|---|---|---|---|---|---|---|---|---|
| Plu5% | 0.25 | 5 | 125 | 128 | 123 | 112 | 0.04 | 1.10 |
| Plu10% | 0.50 | 10 | 78 | 81 | 76 | 71 | 0.03 | 1.07 |
| Plu20% | 1.00 | 15 | 66 | 67 | 64 | 60 | 0.02 | 1.06 |
| Plu30% | 1.50 | 20 | 62 | 63 | 60 | 57 | 0.02 | 1.05 |

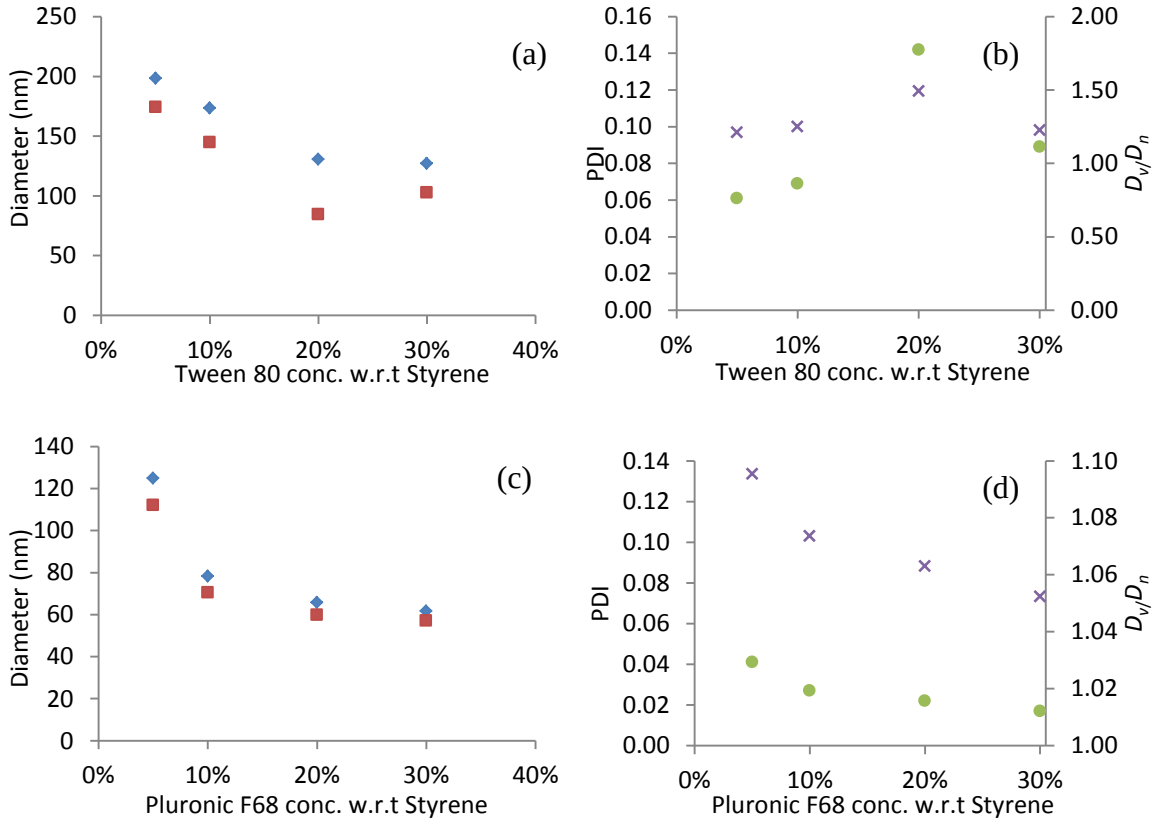


Figure 5.9: Effect of Tween 80 concentration (wrt. styrene) in the micro-emulsion on (a) the particle $D_z$ (■) and $D_n$ (●) and (b) the particle PDI (◆) and $D_v/D_n$ (X). Also shown is the effect of Pluronic F68 concentration (wrt. styrene) in the micro-emulsion on (c) the particle $D_z$ (■) and $D_n$ (●) and (b) the particle PDI (◆) and $D_v/D_n$ (X). All measured by DLS.

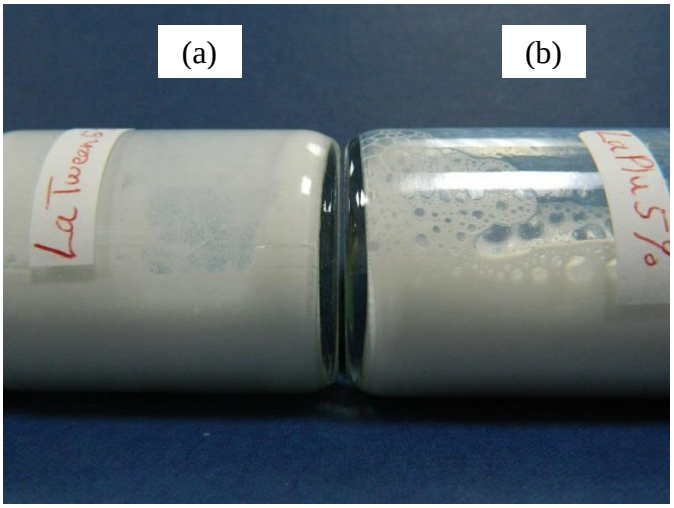


Figure 5.10: Contrasting stability of the latex particles stabilised with (a) Tween 80 and (b) Pluronic F68. (a) Shows Tween5% displaying the thick layer of aggregates formed at the bottom of the container, and on the sides after approximately 7 months whereas none can be seen in Plu5% (b).

Table 5.14: Size and dispersity of polystyrene particles produced by micro-emulsion polymerisation using different surfactants. Aside from surfactant identity all other components of the micro-emulsion were identical.

| Sample | Surfactant | | | $D_z$ (nm) | $D_I$ (nm) | $D_v$ (nm) | $D_n$ (nm) | PDI | $D_v/D_n$ |
|---|---|---|---|---|---|---|---|---|---|
| | | HLB[a] | cmc [b] | | | | | | |
| La11 | SDS | 40 | 7-10 | 41 | 44 | 39 | 35 | 0.07 | 1.11 |
| Plu10% | Pluronic F68 | 29 | 0.04 | 78 | 81 | 76 | 71 | 0.03 | 1.07 |
| Tween10% | Tween 80 | 15 | 0.012 | 173 | 184 | 181 | 145 | 0.07 | 1.25 |

[a] In mM $l^{-1}$, with values taken from reference [116]
[b] In water at 20 – 25 $^{o}$C

To allow a comparison with of Tween 80 and Pluronic F68 and latex particles were produced using SDS as the surfactant and omitting $Cr(acac)_3$. Aside from surfactant identity the composition of La11, Plu10% and Tween10% was identical and the comparative data is displayed in Table 5.14.

As all surfactants were at concentrations above their respective cmc a possible explanation for the difference in sizes can be rationalised via application of the hydrophilic-lipophilic balance (HLB) concept (outlined in chapter 1). When the HLB number of a surfactant ≈ 10 the o/w interface has zero curvature, as the HLB number of the surfactant increases o/w emulsions can from with increased curvature at the interface.[117]

Increased interfacial curvature allows smaller oil droplets to form, and though several competing mechanisms influence the final particle size it is known that smaller droplets can result in smaller particles.[118,119,120,121] Therefore, since a surfactant with a higher HLB will result in smaller droplets it would be expected to yield smaller particles,[122] and this is what was observed with the three surfactants used. The surfactant with the highest HLB number, SDS (HLB=40), produces the smallest particles and the lowest, Tween 80 (HLB=15), produces the largest particles

Comparison of La11 and CrSt5 (detailed in Table 5.14 and Table 5.10 respectively) shows similar particles size (difference in $D_z$ = 1.4 nm) with both systems also displaying high monodispersity. This implies that $Cr(acac)_3$, does not affect the emulsion and subsequent particle nucleation. This could be due to hydrophobicity of $Cr(acac)_3$ which will likely locate in the styrene rich phase of the micro-emulsion, at the centre of the droplets, and not interact with the interfacial region.[123]

The greater stability and monodispersity of particles produced using Pluronic F68, as well the fact that the size range over which particles could be produced was wholly within the desired 40 – 160 nm size range it was decided that Pluronic F68 would be used as the surfactant for the synthesis of the lanthanide containing particles.

The particles produced using Tween 80 all had particle sizes over 100 nm, this is larger than would normally be expected by micro-emulsion polymerisation.[28] It is possible that instead of a micro-emulsion polymerisation particles were in fact produced by conventional macro-emulsion polymerisation. It had been considered that this may have potentially happened in emulsions with low surfactant contents *i.e.*, Plu5% and CrSDS2.5% and, as such, low mechanical stirring was continued throughout polymerisation. This may have facilitated the formation of a macro-emulsion allowing the formation of particles. As the aim of the work was the production of latex particles of

certain sizes, and the experimental procedures achieved this, it was decided that to better make use of time, this would not be investigated further. Though, outside the confines of this project, it would be of interest for further work.

It is worth mentioning here that the emulsion itself was never investigated. As the experimental methods were similar to other procedures with a restricted monomer feed reported in the literature[75,76] it was assumed that micro-emulsion polymerisation was being used. An attempt was made to investigate the emulsion structure by DLS but the data returned was poor meaning the no inferences could be made. There was some visual evidence observed during the polymerisation that the system may have been a Winsor type I emulsion but further investigation would be required. However as the synthetic procedure resulted in particles of the desired sizes it was decided that to better make use to time that it would not be investigated further and attention would be focused on the aims of the project.

### 5.3.2 Lanthanide (Nd, Dy and Gd) Containing Polystyrene Particles

Initially lanthanide acetylacetonate hexahydrates, were used as the lanthanide source to mirror $Cr(acac)_2$. However poor solubility in styrene, even after dehydrating at 100 $^{o}$C under vacuum, discounted these. Therefore complexes of dysprosium, neodymium and gadolinium, which had been shown to have solubility in styrene[93] were synthesised, using NTFA as the ligand. The generic structure of the resulting lanthanide complexes is displayed in Figure 5.11.

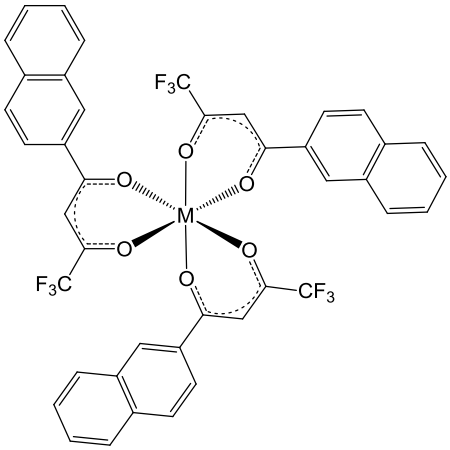


Figure 5.11: Structure of the lanthanide containing complex, where M represents the lanthanide metal centre (neodymium, dysprosium or gadolinium).

Three batches of particles were synthesised named batch one, batch two and batch three. The particles of batch one and batch two were stabilised by Pluronic F68 and particles of batch three were stabilised by SDS. Each batch contained several sets of particles with each set containing a different metal, as well as a set of non-doped particles in batch two. Within each set they were particles three different sizes, which were termed small, medium and large. This range of sizes was achieved by tailoring surfactant and KPS concentration of the micro-emulsion to produce the particle of the desired size sizes. While both batch one and batch three particles were produced using 0.05g of the lanthanide complex the particles of batch two were different in that they contained 0.1 g of the lanthanide complex. The exact compositions of the emulsions are given in sections 7 – 9 of Table 5.6. The size and dispersity of the particles was measured by DLS and the data is displayed in Table 5.15 (batch 1), Table 5.16 (batch 2) and Table 5.17 (batch 3). Surfactant concentrations of 30 %, 10 % and 2.5 % (all w/w with respect to styrene) and KPS concentrations of 4 %, 2% and 0.5 % (all w/w with respect to styrene) were used for the small, medium and large particles respectively (the exact micro-emulsion compositions are listed in Table 5.6). The reasons for the effect of surfactant and KPS concentration on particle size have already been discussed in previous sections.

The final latexes displayed a yellow/green hue, which, like the purple hue observed in the $Cr(acac)_3$ containing particles, can be attributed to the lanthanide complex, all of which were coloured on the yellow/green spectrum.

As was to be expected from section 5.3.1.3 the Pluronic F68 systems displayed higher levels of mono-dispersity (no PDI value of greater than 0.04) than the SDS stabilised systems. The SDS systems themselves, however, also displayed high mono-dispersity (greatest PDI value was 0.08). The intensity particle size distribution (measured by DLS), in Figure 5.12 to Figure 5.14, highlights the narrow size distribution of the particles.

Also as expected Pluronic F68 produced larger particles that covered a greater size range than the SDS stabilised equivalents. The greatest size difference amongst any of the Pluronic F68 set was 163 nm (58 nm to 221 nm) between NdPlu-21 and NdPlu-23, whereas the greatest size difference observed in any of the SDS stabilised set was 43 nm (from 35 nm to 79 nm) between GdSDS-1 and GdSDS-2. All the Pluronic F68 systems particle sets (batch 1 and batch 2) all covered, or were close to covering, the desired 40-160 nm range (Table 5.15 to Table 5.17).

Table 5.15: Size, and dispersity, of the lanthanide containing polystyrene particles of batch one[a] before dialysis.

| Sample | Metal Complex | $D_z$ (nm) | $D_I$ (nm) | $D_v$ (nm) | $D_n$ (nm) | PDI | $D_v/D_n$ |
|---|---|---|---|---|---|---|---|
| NdPlu-1 | Nd | 178 | 181 | 182 | 172 | 0.01 | 1.06 |
| NdPlu-2 | Nd | 65 | 67 | 63 | 59 | 0.03 | 1.06 |
| NdPlu-3 | Nd | 61 | 63 | 59 | 56 | 0.02 | 1.06 |
| GdPlu-1 | Gd | 164 | 169 | 169 | 153 | 0.03 | 1.10 |
| GdPlu-2 | Gd | 80 | 81 | 79 | 75 | 0.02 | 1.04 |
| GdPlu-3 | Gd | 56 | 57 | 55 | 52 | 0.02 | 1.05 |
| DyPlu-1 | Dy | 154 | 155 | 155 | 149 | 0.02 | 1.04 |
| DyPlu-2 | Dy | 54 | 56 | 52 | 49 | 0.02 | 1.07 |
| DyPlu-3 | Dy | 40 | 41 | 38 | 36 | 0.04 | 1.07 |

[a] Batch one particles were produced using Pluronic F68 as the surfactant and 0.05 g of lanthanide complex dissolved in the styrene phase. Other components were the same as the batch two and three particle systems, exact compositions can be found in Table 5.6.

Table 5.16: Size, and dispersity, of the lanthanide containing polystyrene particles of batch two[a] before dialysis.

| Sample | Metal Complex | $D_z$ (nm) | $D_I$ (nm) | $D_v$ (nm) | $D_n$ (nm) | PDI | $D_v/D_n$ |
|---|---|---|---|---|---|---|---|
| NdPlu-21 | Nd | 221 | 225 | 226 | 212 | 0.01 | 1.04 |
| NdPlu-22 | Nd | 71 | 73 | 69 | 65 | 0.02 | 1.08 |
| NdPlu-23 | Nd | 58 | 59 | 55 | 52 | 0.04 | 1.08 |
| GdPlu-21 | Gd | 142 | 142 | 141 | 137 | 0.02 | 1.03 |
| GdPlu-22 | Gd | 77 | 79 | 76 | 72 | 0.01 | 1.05 |
| GdPlu-23 | Gd | 57 | 58 | 55 | 52 | 0.02 | 1.06 |
| DyPlu-21 | Dy | 162 | 164 | 164 | 158 | 0.03 | 1.06 |
| DyPlu-22 | Dy | 78 | 80 | 75 | 70 | 0.02 | 1.06 |
| DyPlu-23 | Dy | 52 | 54 | 50 | 46 | 0.04 | 1.07 |
| Plu-21 | None | 144 | 146 | 145 | 138 | 0.01 | 1.05 |
| Plu-22 | None | 75 | 76 | 72 | 68 | 0.03 | 1.06 |
| Plu-23 | None | 49 | 50 | 47 | 43 | 0.04 | 1.08 |

[a] Batch one particles were produced using Pluronic F68 as the surfactant and, when used, 0.1 g of lanthanide complex dissolved in the styrene phase. Other components were the same as the batch one and three particle systems, exact compositions can be found in Table 5.6

Table 5.17: Size, and dispersity, of the lanthanide containing polystyrene particles of batch three[a] before dialysis.

| Sample | Metal Complex | $D_z$ (nm) | $D_I$ (nm) | $D_v$ (nm) | $D_n$ (nm) | PDI | $D_v/D_n$ |
|---|---|---|---|---|---|---|---|
| NdSDS-1 | Nd | 60 | 63 | 55 | 49 | 0.05 | 1.13 |
| NdSDS-2 | Nd | 48 | 49 | 45 | 41 | 0.04 | 1.09 |
| NdSDS-3 | Nd | 34 | 36 | 32 | 29 | 0.06 | 1.12 |
| GdSDS-1 | Gd | 78 | 84 | 68 | 54 | 0.08 | 1.28 |
| GdSDS-2 | Gd | 48 | 50 | 46 | 42 | 0.04 | 1.09 |
| GdSDS-3 | Gd | 35 | 37 | 32 | 28 | 0.06 | 1.14 |
| DySDS-1 | Dy | 68 | 71 | 63 | 57 | 0.05 | 1.12 |
| DySDS-2 | Dy | 49 | 50 | 46 | 42 | 0.05 | 1.08 |
| DySDS-3 | Dy | 33 | 36 | 30 | 26 | 0.06 | 1.15 |

[a] Batch three particles were produced using SDS as the surfactant and 0.05 g of lanthanide complex dissolved in the styrene phase. Other components were the same as the batch one and two particle systems, exact compositions can be found in Table 5.6

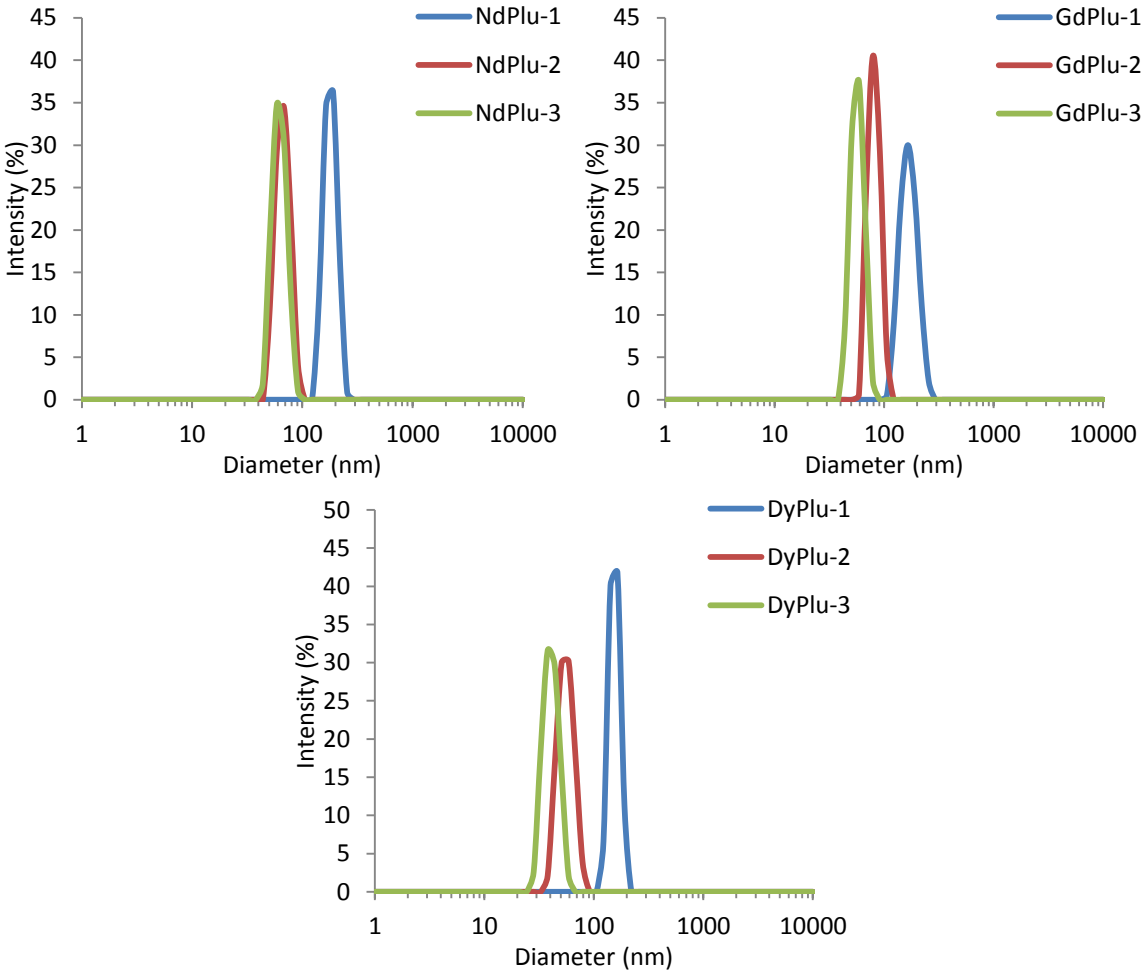


Figure 5.12: Intensity particle size distributions measured by DLS of the batch one (Pluronic F68 stabilised) particle sets.

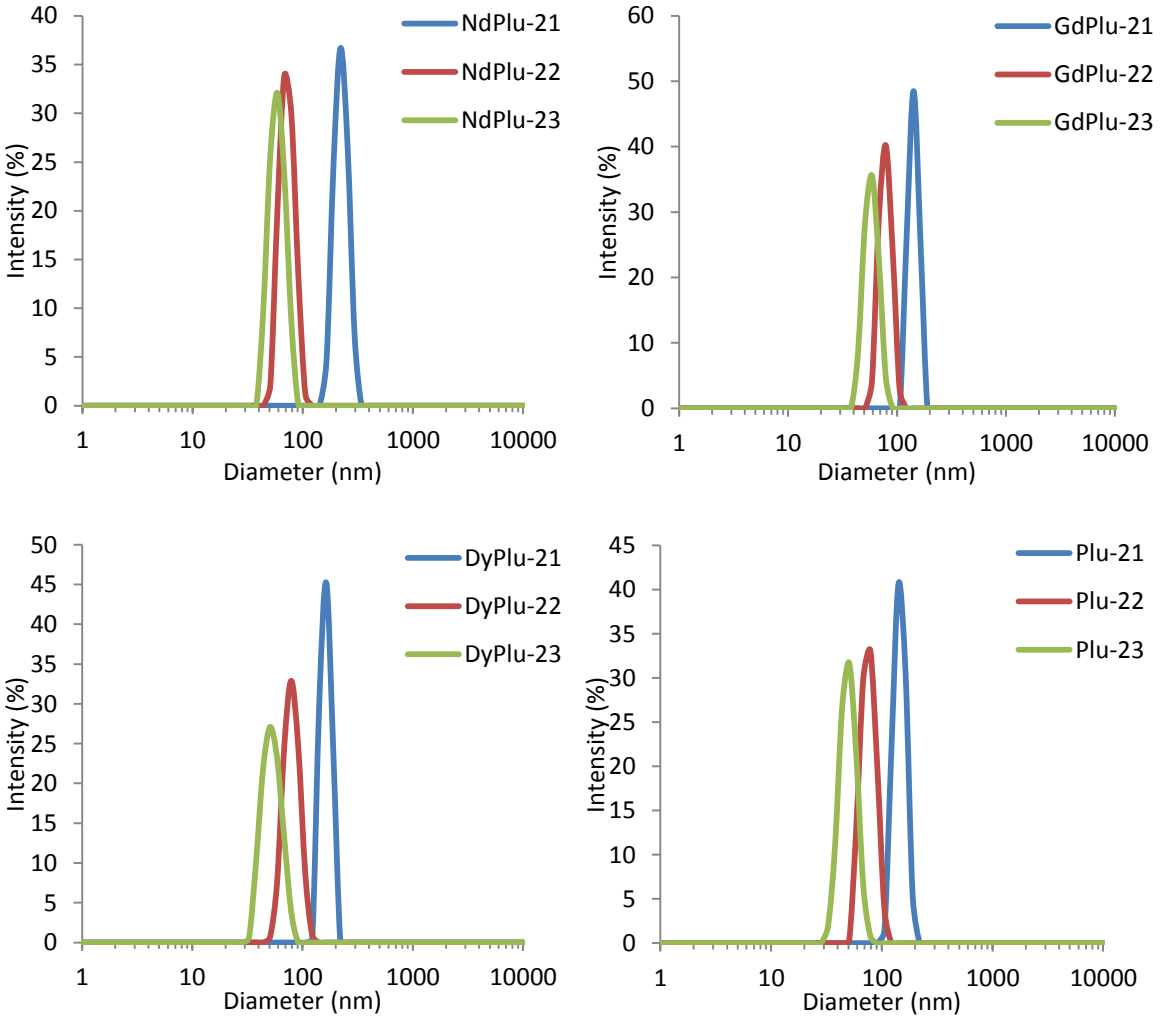


Figure 5.13: Intensity particle size distribution measured by DLS of the batch two (Pluronic F68 stabilised) lanthanide containing particle sets.

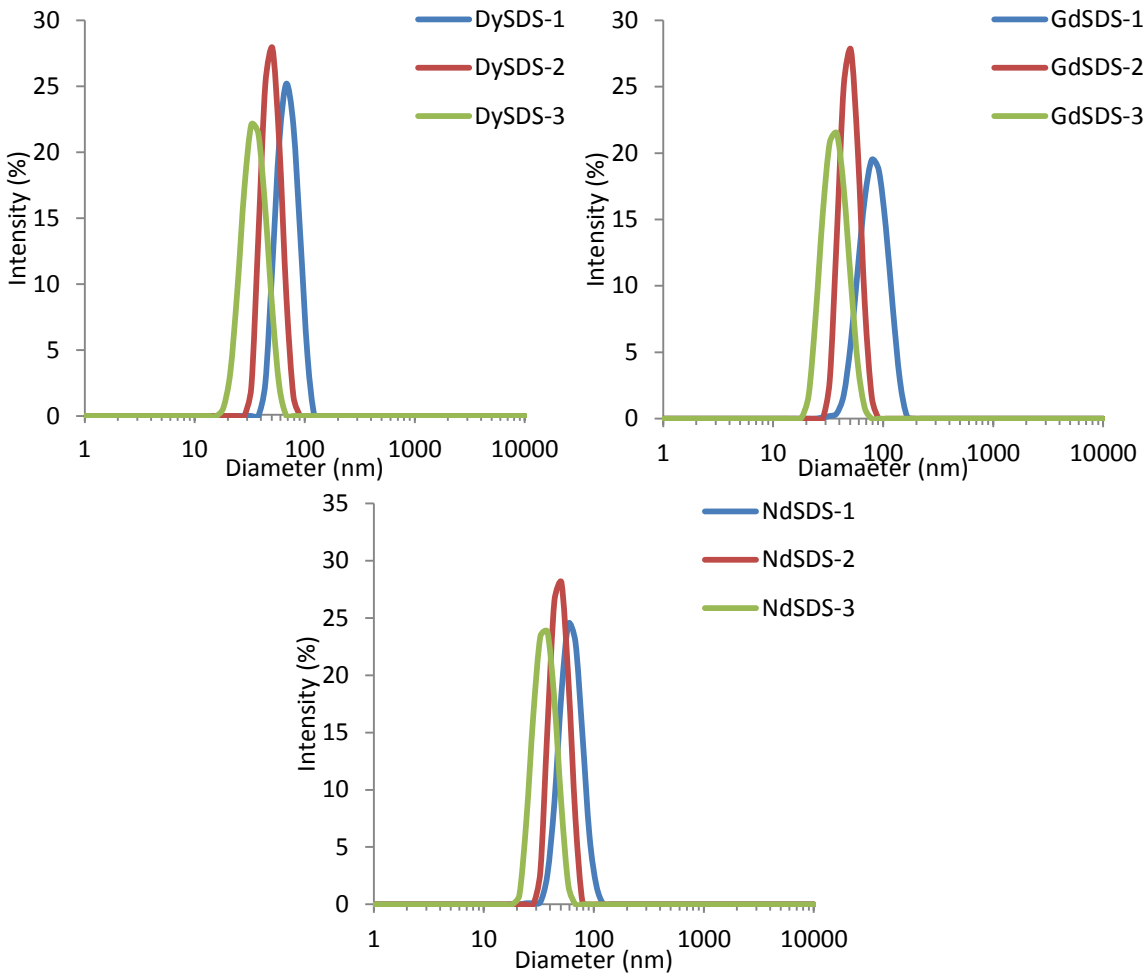


Figure 5.14: Intensity particle size distribution measured by DLS of batch three (SDS stabilised) particle sets.

In all particle sets, the large particles were > 100 nm in diameter. As mentioned earlier, this is greater than would be expected with micro-emulsion polymerisation. It is possible that due to the low surfactant concentrations used for the production of the large particles, they were instead produced by macro - rather than micro - emulsion polymerisation. However, since particles of the desired size had ultimately been produced, attention was turned to the characterisation of the particles rather than investigation to the emulsion properties.

Curiously, the presence, and identity of the lanthanide complex appears to have some influence on the final particle size. The three different particle sizes – small, medium

and large – each had their own corresponding micro-emulsion composition (compositions are defined in sections 7 to 9 of Table 5.6). Therefore, within a batch, the only difference in micro-emulsion formulation between the particles sets was the identity, or presence, of the lanthanide complex. As it was the only difference in synthesis it must be this which caused size variation between the sets the containing different lanthanides within batches. Further evidence for this comes from comparison of the batch 1 and batch 2 particles sizes. To aid detection by ICP-MS the amount of lanthanide complex in the monomer phase of the batch 2 particles was doubled (from 0.05 g to 0.1 g) from the corresponding batch 1 formulations. If the lanthanide complex did not influence the final particle size, then similar sizes would be expected between comparable particle sets in batch 1 and batch 2. However, as can be seen by comparison of Table 5.15 and Table 5.16, this is not the case. The explanation for the influence of the lanthanide complex on particle size is unclear and would benefit from further investigation.

#### 5.3.2.1 Dialysis and Further Analysis of Pluronic F68 Stabilised Particle Systems.

As the batch 1 and batch 2 particles better covered the desired size range and the SDS stabilised particles of batch 3 did not, it was decided that only they would be investigated further. Before further investigation however they were dialysed against de-ionised water to ‘clean’ them of KPS and any excess surfactant and unreacted styrene.

After dialysis the particle sizes and dispersity were re-measured by DLS (see Figure 5.15 and Figure 5.16). A comparison of the $D_z$ pre-dialysis with the $D_z$ post-dialysis (displayed in Table 5.18, for batch 1, and in Table 5.19, for batch 2) shows that, apart from NdPlu-21 which saw a 13.3 % change in $D_z$, dialysis appears to have had little effect upon the particle sizes. Aside from the aforementioned NdPlu-21, the change in $D_z$ post- dialysis was $\leq$ 5.9%. There were some increases observed in PDI after dialysis but, aside from

DyPlu-23, all values remained ≥ 0.1 indicating high levels of monodispersity, as can be seen in the intensity particle size distributions in Figure 5.15 (batch 1) and Figure 5.16 (batch 2).

Table 5.18: Comparison of the z-average diameter and polydispersity index, obtained by DLS, of the batch 1 polystyrene latex particles before and after dialysis

| Batch 1 Particle Systems | Lanthanide Present | Before Dialysis | | After Dialysis | | $D_z$ % Change |
|---|---|---|---|---|---|---|
| | | $D_z$ (nm) | PDI | $D_z$ (nm) | PDI | |
| NdPlu-1 | Nd | 178 | 0.01 | 175 | 0.02 | 3.1 |
| NdPlu-2 | Nd | 65 | 0.03 | 63 | 0.09 | 2.1 |
| NdPlu-3 | Nd | 61 | 0.02 | 57 | 0.07 | 4.5 |
| GdPlu-1 | Gd | 164 | 0.03 | 159 | 0.02 | 5.0 |
| GdPlu-2 | Gd | 80 | 0.02 | 81 | 0.01 | 1.2 |
| GdPlu-3 | Gd | 56 | 0.02 | 56 | 0.09 | 0.2 |
| DyPlu-1 | Dy | 154 | 0.02 | 152 | 0.01 | 1.4 |
| DyPlu-2 | DY | 54 | 0.03 | 54 | 0.15 | 1.3 |
| DyPlu-3 | Dy | 40 | 0.04 | 40 | 0.15 | 1.7 |

Table 5.19: Comparison of the z-average diameter and the polydispersity index, obtained by DLS, before and after dialysis against de-ionised water for 50 hours of all batch 2 polystyrene latex particle systems.

| Batch 2 Particle System | Lanthanide Present | Before Dialysis | | After Dialysis | | $D_z$ % Change |
|---|---|---|---|---|---|---|
| | | $D_z$ (nm) | PDI | $D_z$ (nm) | PDI | |
| NdPlu-21 | Nd | 220 | 0.03 | 193 | 0.03 | 13.3 |
| NdPlu-22 | Nd | 71 | 0.02 | 69 | 0.09 | 2.8 |
| NdPlu-23 | Nd | 58 | 0.04 | 57 | 0.04 | 1.4 |
| GdPlu-21 | Gd | 142 | 0.02 | 144 | 0.02 | 1.8 |
| GdPlu-22 | Gd | 77 | 0.01 | 79 | 0.06 | 1.9 |
| GdPlu-23 | Gd | 57 | 0.02 | 58 | 0.06 | 2.3 |
| DyPlu-21 | Dy | 162 | 0.01 | 155 | 0.02 | 4.3 |
| DyPlu-22 | Dy | 78 | 0.02 | 79 | 0.05 | 0.5 |
| DyPlu-23 | Dy | 52 | 0.04 | 52 | 0.09 | 0.0 |
| Plu-21 | None | 144 | 0.01 | 148 | 0.01 | 2.8 |
| Plu-22 | None | 75 | 0.03 | 79 | 0.09 | 5.9 |
| Plu-23 | None | 49 | 0.04 | 49 | 0.10 | 0.7 |

Table 5.20: Comparison of the different sizing techniques used to measure the dysprosium and gadolinium containing particle sets from batch 1

| Batch1 Particle System | Lanthanide Present | Diameter (nm) Measured By | | | | | | | | | |
|---|---|---|---|---|---|---|---|---|---|---|---|
| | | DLS | | | | DCS | | | TEM | | |
| | | $D_z$ | $D_v$ | $D_n$ | PDI | $D_w$ | $D_n$ | $D_w/D_n$ | $D_w$ | $D_n$ | $D_w/D_n$ |
| GdPlu-1 | Gd | 159 | 161 | 155 | 0.02 | 148 | 147 | 1.02 | 123 | 123 | 1.00 |
| GdPlu-2 | Gd | 81 | 80 | 77 | 0.01 | 75 | 72 | 1.04 | 64 | 64 | 1.01 |
| GdPlu-3 | Gd | 56 | 52 | 49 | 0.09 | 53 | 52 | 1.02 | 35 | 35 | 1.01 |
| DyPlu-1 | Dy | 152 | 154 | 147 | 0.01 | 133 | 131 | 1.02 | 125 | 125 | 1.00 |
| DyPlu-2 | Dy | 54 | 46 | 39 | 0.15 | 51 | 51 | 1.01 | 32 | 32 | 1.01 |
| DyPlu-3 | Dy | 40 | 35 | 30 | 0.15 | [a] | [a] | [a] | 27 | 27 | 1.01 |

[a] Particle diameter was below the measurement limit of the centrifuge.

Table 5.21: Comparison of the different sizing techniques used to measure the dysprosium and gadolinium containing particle sets from batch 2 as well as the batch 2 un-doped particle set.

| Batch 2 Particle System | Lanthanide Present | Diameter (nm) Measured By | | | | | | | | | | |
|---|---|---|---|---|---|---|---|---|---|---|---|---|
| | | DLS | | | | DCS | | | TEM | | | HDC-ICP-MS |
| | | $D_z$ | $D_v$ | $D_n$ | PDI | $D_w$ | $D_n$ | $D_w/D_n$ | $D_w$ | $D_n$ | $D_w/D_n$ | |
| GdPlu-21 | Gd | 144 | 145 | 138 | 0.02 | 126 | 122 | 1.03 | 107 | 107 | 1.00 | 138 |
| GdPlu-22 | Gd | 79 | 74 | 68 | 0.06 | 71 | 69 | 1.03 | 56 | 55 | 1.01 | 68 |
| GdPlu-23 | Gd | 58 | 55 | 50 | 0.06 | 53 | 52 | 1.02 | 36 | 35 | 1.01 | 53 |
| DyPlu-21 | Dy | 155 | 157 | 149 | 0.02 | 134 | 132 | 1.01 | 117 | 117 | 1.00 | 145 |
| DyPlu-22 | Dy | 78 | 75 | 71 | 0.05 | 69 | 68 | 1.02 | 54 | 54 | 1.00 | 68 |
| DyPlu-23 | Dy | 52 | 48 | 45 | 0.09 | 49 | 48 | 1.01 | 33 | 33 | 1.01 | 49 |
| Plu-21 | None | 148 | 149 | 143 | 0.01 | 126 | 125 | 1.01 | 113 | 113 | 1.00 | – |
| Plu-22 | None | 79 | 73 | 63 | 0.09 | 68 | 65 | 1.04 | 50 | 50 | 1.01 | – |
| Plu-23 | None | 49 | 41 | 35 | 0.10 | 42 | [a] | [a] | 27 | 26 | 1.02 | – |

[a] The measurement limit of the centrifuge was 40 nm as such the peak was unable to return to the baseline which prevented the software extrapolating a $D_n$ value and dispersity. However for a peak maximum was present allowing determination of a value of $D_w$.

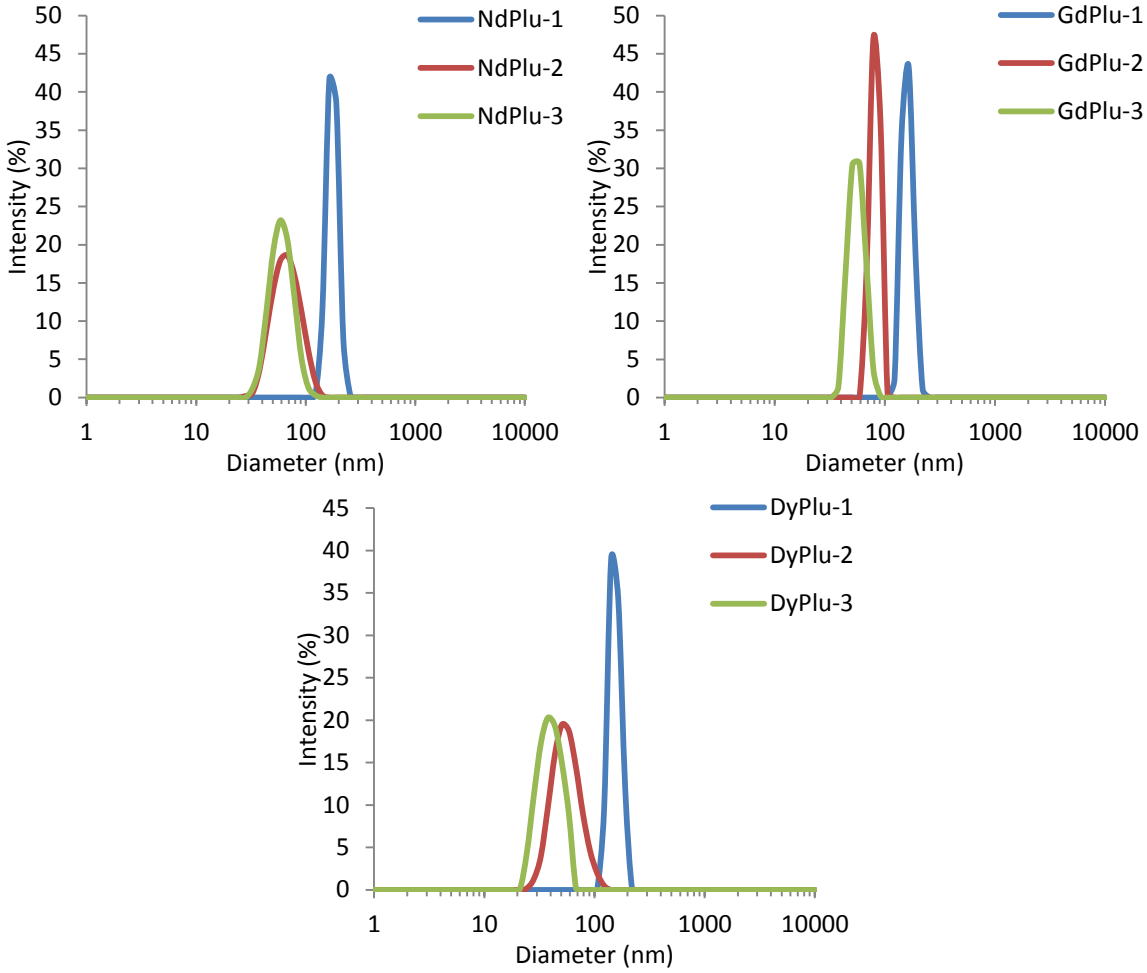


Figure 5.15: Intensity particle size distribution measured by DLS of the batch 2 particle sets after dialysis against distilled water for 50 hours.

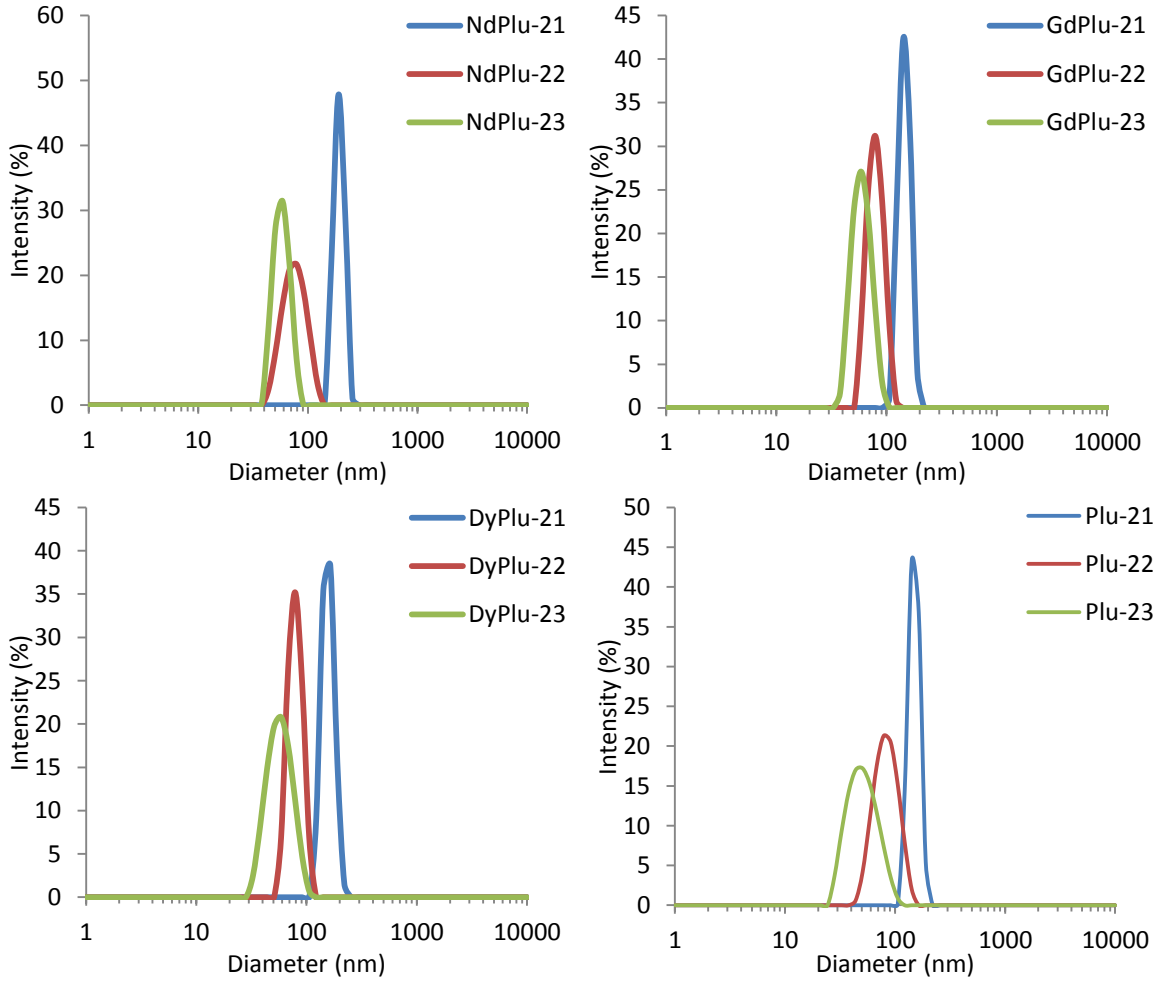


Figure 5.16: Intensity particle size distribution measured by DLS for batch 2 particle sets systems after dialysis against distilled water for 50 hours

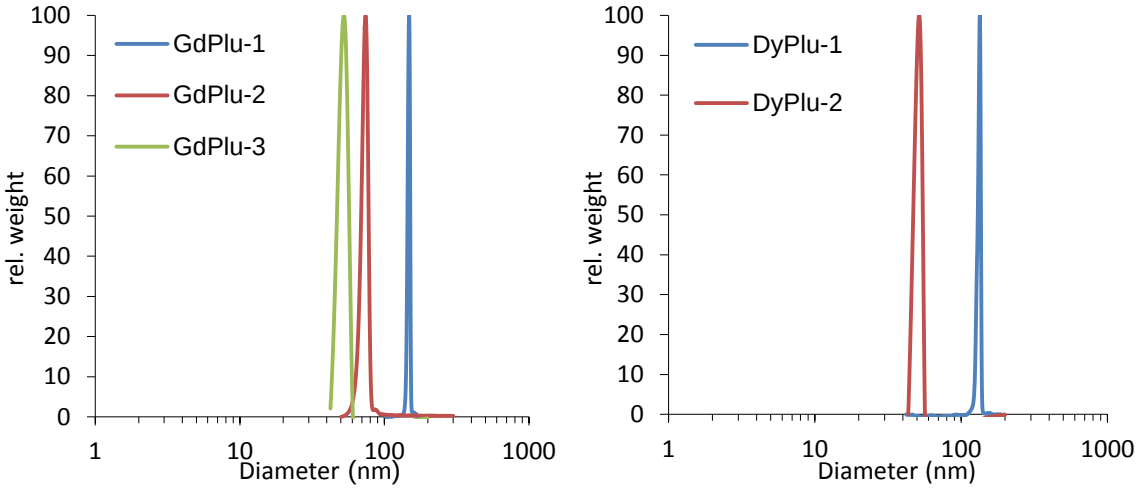


Figure 5.17: Weight particle size distributions (measured by DSC) of; (a) the dysprosium continuing particles and (b) the gadolinium containing particles of batch 1 The small dysprosium containing particles (DyPlu-3) were below than the detection limit of the centrifuge, which is why they are not displayed.

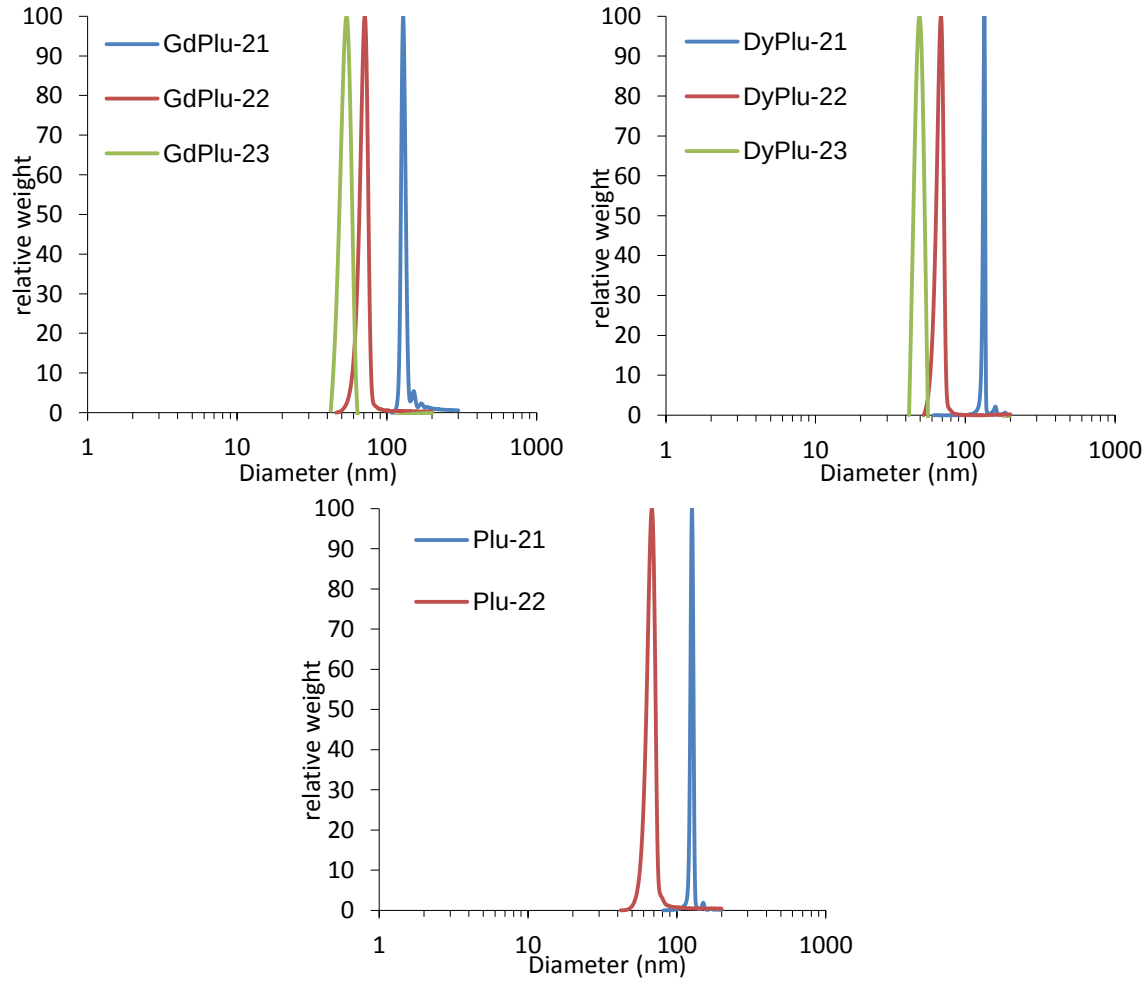


Figure 5.18: Weight diameter size distributions (measured by DSC) of; (a) dysprosium containing particles, (b) the gadolinium containing particles and (c) the non-doped particles from batch 2. The small non-doped particles (Plu-23) were below than the detection limit of the centrifuge which is why they are not shown.

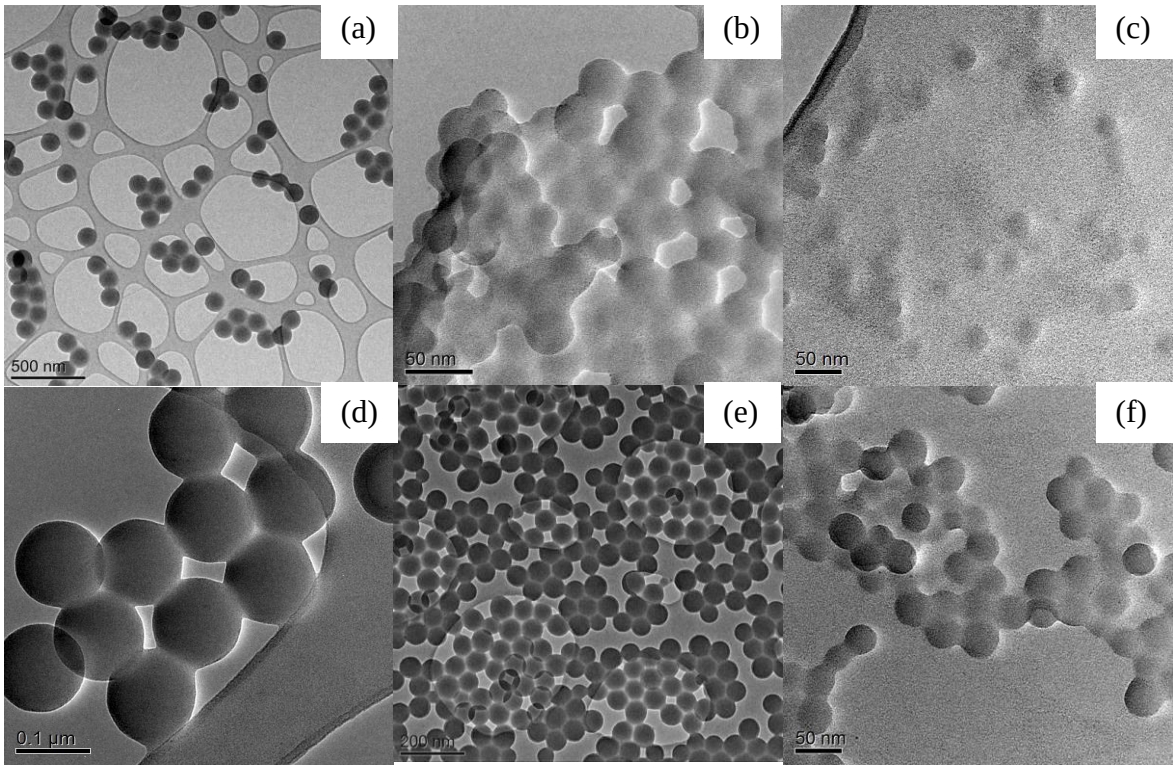


Figure 5.19: TEM images of the batch 1 latex particles. On the top row are the dysprosium containing latex particles; (a) DyPlu-1, (b) DyPlu-2 and (c) DyPlu-3. On the middle are the gadolinium containing particles; (d) GdPlu-1, (e) GdPlu-2 and (f) GdPlu-3.

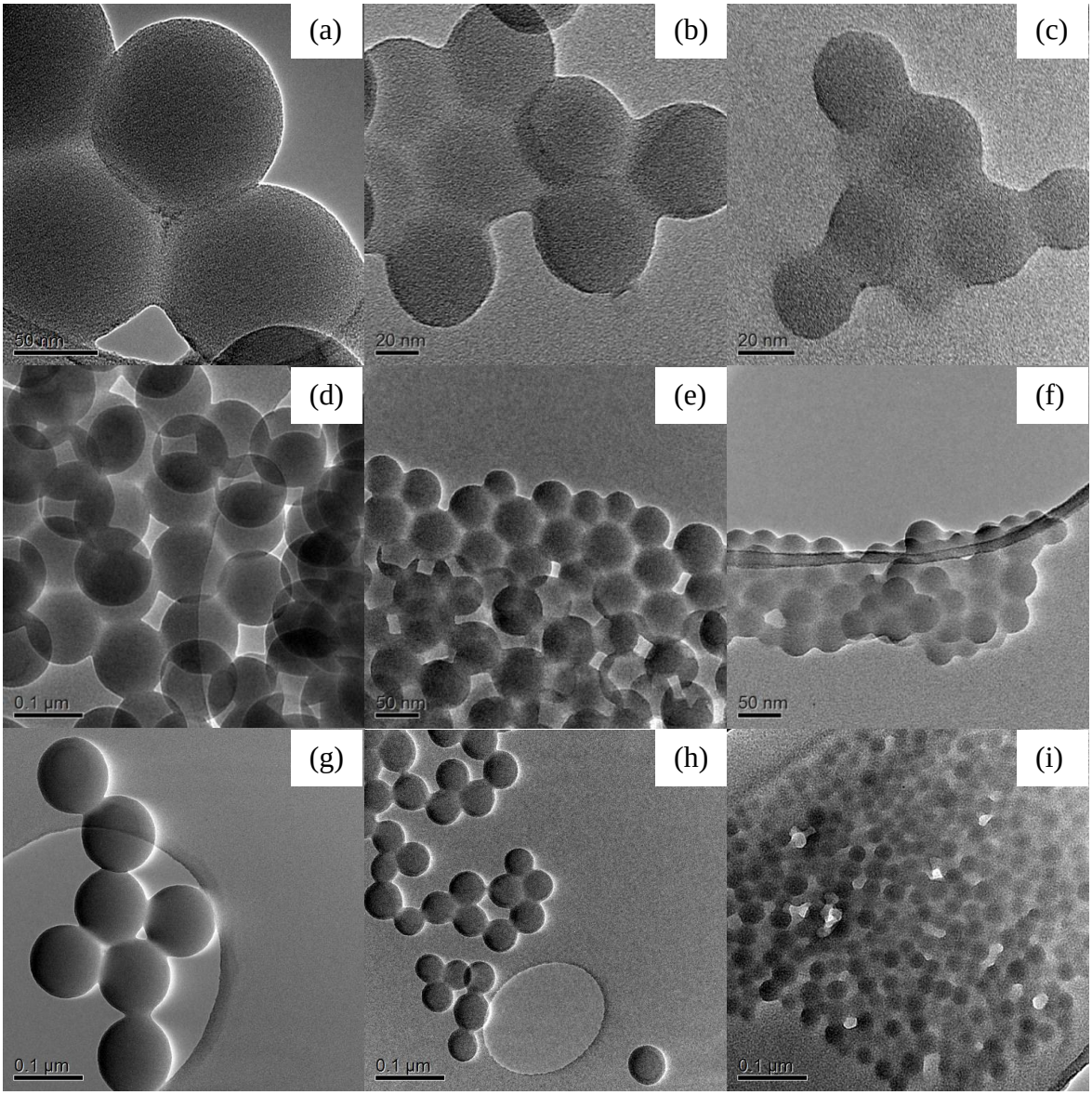


Figure 5.20: TEM images of the batch 2 latex particles. On the top row are the dysprosium containing latex particles; (a) DyPlu-21, (b) DyPlu-22 and (c) DyPlu-23. On the middle row are the gadolinium containing particles; (d) GdPlu-21, (e) GdPlu-22 and (f) GdPlu-23. On the bottom row are the non-doped latex particles; (g) Plu-21, (h) Plu-22 and (i) Plu-23.

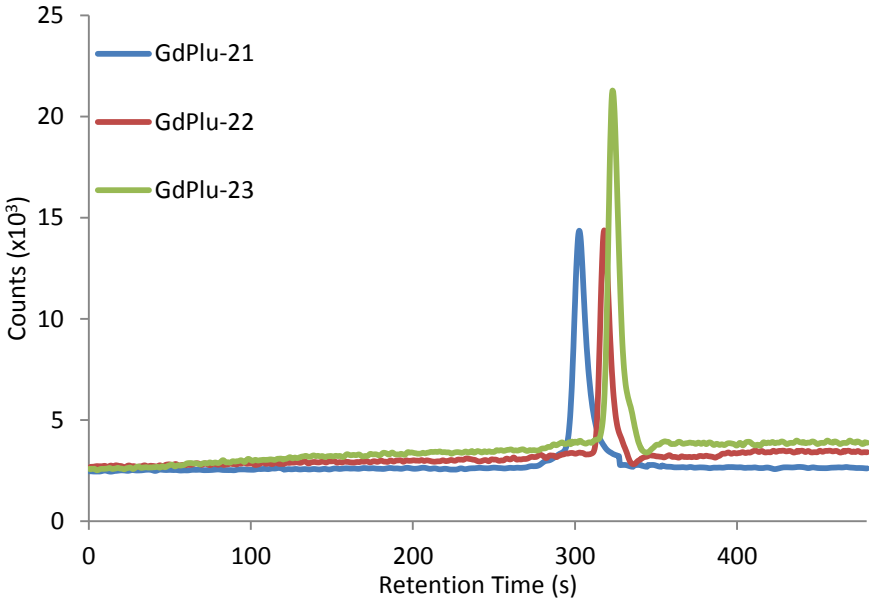


Figure 5.21: Representative HDC-ICP-MS chromatogram of the batch 2 gadolinium containing latex particles

As the gadolinium and dysprosium contacting particles of both batches better covered the desired 40 – 160 nm size range they were singled out for further analysis. As well as sizing by DLS they were also sized by DCS (batch 1 Figure 5.17 and batch 2 Figure 5.18) and TEM (batch 1 Figure 5.19 and batch 2 Figure 5.20). The un-doped latex particles from batch 2 were also analysed by DCS and TEM for comparative purposes. To see if the particles could be used with HDC-ICP-MS as was desired the batch 2 dysprosium and gadolinium doped particles were also injected on a HDC-ICP-MS system and detected by means of the lanthanide present within the particle (Figure 5.21). The sizing data is presented in Table 5.20 for the particles of batch 1 and in  for the particles of batch 2

As can be seen from Table 5.20 and  for the small and medium particles a set there was good agreement between the values of $D_v$ returned by DLS, DCS and the HDC-ICP-MS data (difference ≤ 10 %). However, whereas there was good agreement between the $D_v$ measured by DLS and the HDC-ICP-MS data for the large particles of the set (again ≤ 10 %) the $D_n$ measured by DLS was consistently 14-15 % larger than measured by DSC. The reason for this is unknown and cannot be explained at this juncture. DCS analysis also

confirmed the high monodispersity of the particle systems with no value of $D_w/D_n$ greater than 1.04

As discussed earlier detection of the particles by HDC-ICP-MS was made possible by the inclusion of the lanthanide complex. The fact that particle sizes measured by HDC-ICP-MS agree with the other sizing methodologies (particularly DLS), which would only have detected the latex particles, is evidence that the lanthanide complex ended up, as desired, within the particles.

TEM (Batch 1, Figure 5.19 and batch 2, Figure 5.20) showed that particles were of the desired spherical morphology. However, the $D_n$ values of particles measured by TEM were consistently, and significantly, less than the values obtained by DLS and DCS. For example, all values of $D_n$ measured by TEM were 20-30 % less than those measured by DLS. This difference was attributed to the inability of TEM to visualise the surfactant sheath present at the particle surface, whereas both DLS and DCS (which report the hydrodynamic diameter of the particles in dispersion), account for the presence of the surfactant. Pluronic F68 is a non-ionic tri-block co-polymer consisting of a central hydrophobic block of poly(propylene oxide) attached to a pair poly(ethylene oxide) hydrophilic tails. These poly(ethylene oxide) chains each have 76 repeat units ($M_r \approx 3340$ each, total $M_r \approx 6680$ approximately 80% of the total $M_r$ of Pluronic F68).[124] These tails locate at the particle surface, and extend into the dispersion medium, thereby increasing the hydrodynamic diameter.

As well as control of size another desirable characteristic of the particles was control of the surface charge, which was investigated by measurement of their zeta potential ($\zeta$). While not identical, zeta potential is closely related to surface charge, with larger values for the zeta potential representing a greater surface charge. A value of ±35 mVis used to separate highly charged surfaces from those with a low surface charge.[125] As

can be seen from Table 5.22, the particle surface charge was significantly influenced by the choice of surfactant. Particles stabilised by the anionic surfactant SDS (utilising a charge stabilisation mechanism) gave high $\zeta$ values (-37 to -39) whereas those stabilised by the non-ionic surfactant Pluronic F68 (utilising a steric stabilisation mechanism) gave low $\zeta$ values (-3 to -6)

Table 5.22: Comparison of the zeta potentials of the two sets of particles containing gadolinium, one of which was charge stabilised by the anionic surfactant SDS and the other steric stabilised by the non-ionic surfactant Pluronic F68

| Surfactant Used | Zeta Potential (mV) | | |
|---|---|---|---|
| | Large | Medium | Small |
| SDS | -38[c] | -37[b] | -39[a] |
| Pluronic F68 | -3[d] | -4[e] | -6[f] |

Sample i.d [a.] GdSDS-3, [b.] GdSDS-2, [c.] GdSDS-3,
[d.] Gd Plu-21, [e.] GdPlu-22, [f.] GdPlu-23

The residual surface charge present on the particles stabilised by Pluronic F68 was assumed to be a result of the sulphate anions attached to the end of the polymer chains as a consequence of initiation by a sulphate radical anion. As mentioned earlier it is reasonable to assume that these ionic chain-ends would have located at the droplet/water interface during polymerisation resulting in a surface charge to the particles. As can be seen from Table 5.22 with for the Pluronic F68 stabilised particles the zeta potential is greater the smaller the particle. This change while small fits with the synthetic procedure in which larger amounts of KPS were used to produce the smaller particles. A larger amount of KPS will result in a larger number sulphate terminated polymer chains meaning a higher surface charge on the particles, and therefore a higher zeta potential.

With the exception of NdPlu-23 the solid content of the latexes was significantly lower than expected (Table 5.23), with the lowest solids content being observed in the large particles of the set. This can be attributed to formation of a mass of bulk-phase polymer, which was observed to have aggregated on the nitrogen purge needle and stirrer paddle during polymerisation. This mass appeared larger in the micro-emulsion systems

used for the synthesis of the large particles, which were probably more prone to aggregation due the low surfactant content of the micro-emulsions. As mentioned NdPlu-3 was the exception with a solids content of 11.2 % (which was close to the 12.0 % maximum expected)[i] which can be explained by the minimal aggregation of polymer which was observed during the synthesis of NdPlu-23. Why this was the case for this system and no other is not clear though the solids content of NdPlu-23 does suggest that the majority of the surfactant in the micro-emulsion remains attached to the particles and is not removed by dialysis.

The lanthanide content of the particles was found to be inversely related to particle size (Table 5.23 and Figure 5.22 (b)) with the large particles of a set having either a similar amount to what was expected (PluDy-21), or significantly more (PluGd-21 and PluNd-22). As the final location of the complex is unknown, little speculation can be made regarding this observation at this time and will likely benefit from further investigation.

Table 5.23: Solid content and lanthanide content of polystyrene latex particles stabilised by Pluronic F68.

| Sample | Measured (% wt.) | | Lanthanide Content (wt.%) |
|---|---|---|---|
| | Measured | Maximum Estimate | |
| NdPlu-21 | 1.8 | 9.6 | 0.39[c] |
| NdPlu-22 | 5.8 | 10.2 | 0.20[c] |
| NdPlu-23 | 11.2 | 12.0 | 0.18[c] |
| GdPlu-21 | 3.3 | 9.6 | 0.37[b] |
| GdPlu-22 | 6.4 | 10.2 | 0.23[b] |
| GdPlu-23 | 6.7 | 12.0 | 0.15[b] |
| DyPlu-21 | 1.2 | 9.6 | 0.30[a] |
| DyPlu-22 | 6.6 | 10.2 | 0.12[a] |
| DyPlu-23 | 7.3 | 12.0 | 0.10[a] |
| Plu-21 | 7.1 | 9.3 | n.a. |
| Plu-22 | 6.6 | 10.1 | n.a. |
| Plu-23 | 5.7 | 11.9 | n.a. |

[a] Expected Lanthanide content 0.34 wt %, [b] Expected Lanthanide content 0.29 wt %
[c] Expected Lanthanide content 0.31 wt %

[i] The maximum expected solids content assumed 100 % monomer conversion and that all the surfactant, lanthanide complex, n-dodecane and sulphate groups of the KPS were present either in the particles on the surface.

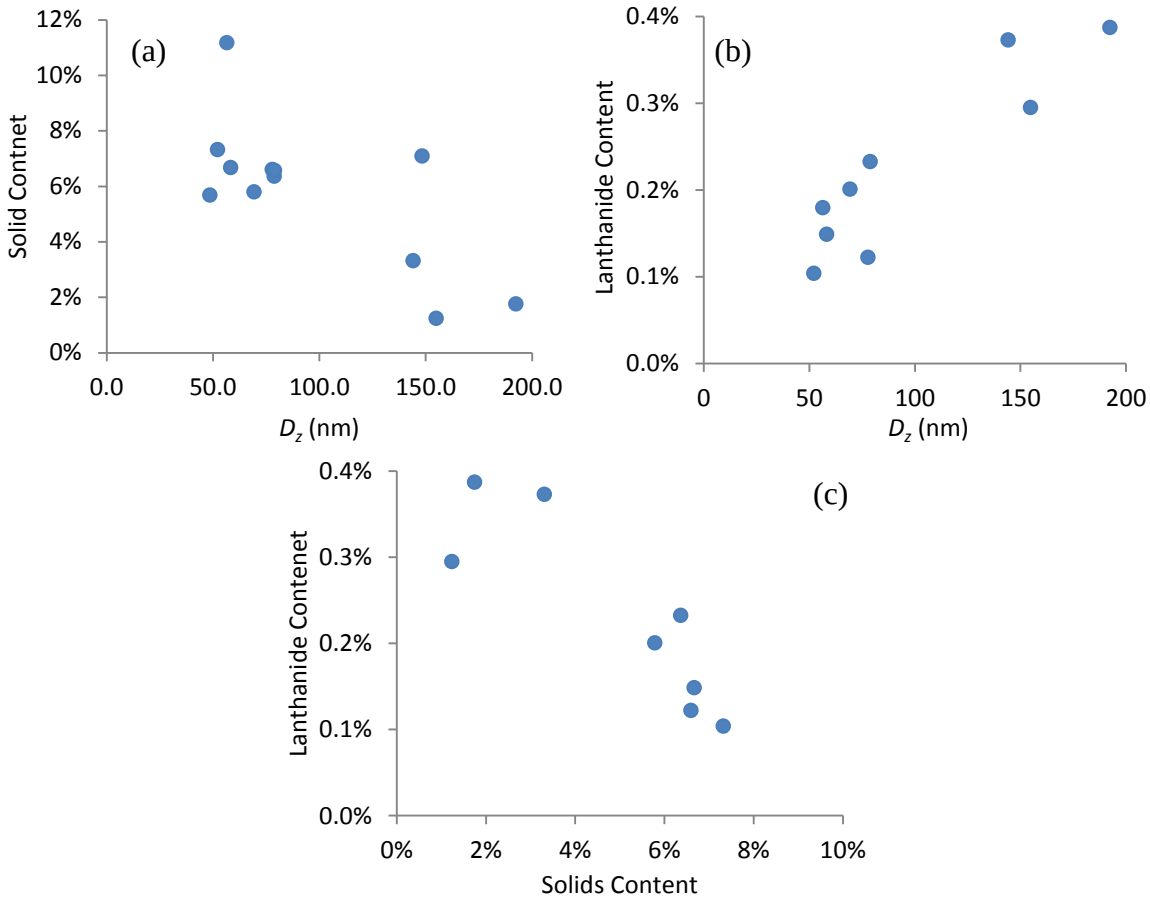


Figure 5.22: (a) the solids content of the lanthanide particles as a function of particles size ($D_z$) and the lanthanide content of the polystyrene particles as a function of (b) the solids content of the corresponding latex and (c) the particle size ($D_z$) as measured by DLS.

## 5.4 Conclusions

This chapter has shown that it is possible to homogeneously encapsulate both chromium and lanthanide complexes within polystyrene nanoparticles by o/w micro-emulsion polymerisation. For successful encapsulation it is imperative that the complex has good monomer solubility and poor water solubility. Both ionic (SDS) and non-ionic (Pluronic F68) surfactants can be employed to this end and surfactant choice also allows control of the particle surface charge. This, as far as the author is aware, is the first documented case of encapsulation of metal complexes in PNPs using micro-emulsion polymerisation. Previous examples where metal complexes have been homogenously

encapsulated within PNPs have utilised mini-emulsion polymerisation or conventional macro-emulsion polymerisation.

Pluronic F68 was found to significantly affect the reported size of the particles by different measurement techniques e.*g.*, the 20-30 % discrepancy in diameter between DLS and TEM, that can be attributed to the surfactant corona, which is invisible to TEM.

The Dy(NTFA)3 and Gd(NTFA)3 containing particles were singled out as the most promising candidates for use as calibrants on the HDC-ICP-MS system and initial investigation showed a good response with that technique. As such, further investigation of these particles within a HDC-ICP-MS system is planned separate to the work carried out in this thesis.

Dialysis appeared to be a promising method for 'cleaning' the particles; however the effect this will have on the stability is unknown; because of this it is recommended that particles only be dialysed immediately prior to use and any storage of particles post dialysis should be kept to a minimum.

The larger lanthanide containing particles were found to have significantly lower than expected solids contents. This was attributed significant bulk aggregation of polymer due to the lower stability of the micro-emulsion because of the low surfactant content. Lanthanide content of the particles was found to be dependent of the final particles size the reason for which is unknown at this time and my benefit from further investigation.

## 5.5 References


1. E. Fisslthaler, A. Blümel, K. Landfester, U. Scherf, E. J. W. List, *Soft Matter*, 2008, **4**, 2448-2453
2. Y. Hu, J. Wang, H. Wang, Q. Wang, J. Zhu, Y. Yang, *Langmuir*, 2012, **12**, 17186-17192
3. A. C.Taylor in *Handbook of Adhesion Technology*, ed. L. F. M. da Silva, A. Öchsner, R. D. Adams, Springer, Heidelberg, 2011, ch. 55, pp. 1437-1462
4. P. Samyn, G. Schoukens, H. Van de Abbeele, L. Vonck, D. Stanssens, *J. Coat. Technol. Res.*, 2011, **8**, 363-373
5. Y. Wang, Z. Wu, Z. Liu, *Anal. Chem.*, 2013, **85**, 258-264
6. J.M. Chan, P. M. Valencia, L. Zhang, R. Langer, O. C. Farokhazd, *Method. Mol. Biol.*, 2010, **624**, 163-175
7. J. Panyam, V. Labhasetwar, *Adv. Drug Deliver. Rev.*, 2012, **64**, 61-67
8. J. Y. Kim, J. Wainaina, J. H. Kim, J. K. Shim, *J. Nanosci. Nanotechnol.*,2007, **11**, 4000-4004
9. M. H. Moon, S. Lee, *J. Microcolumn Seperations*, 1997, **9**, 565-570
10. R. Xu, in *Particle Size Characterization: Light Scattering Methods*, Kluwer, Dordrecht, 2000, ch. 4, pp. 182-222
11. H. Small, M. Langhorst, *Anal. Chem.*, 1982, **54**, 892A-898A
12. J. Potočnik, *Off. J. Euro. Comm.*, 2011, **L275**, 38-40
13. D. Quintanar-Guerrero, E. Allermann, H. Fessi, E. Doelker, *Drug Dev. Ind. Pharm.* 1998, **24**, 1113-1128
14. P. Couvreur, Crit. Rev. Ther. Drug. Carr. Syst., 1988, **5**, 1-20
15. L. Xue, A. Kovalev, F. Thöle, G. T. Rengarajan, M. Steinhart, S. N. Gorb, *Langmuir*, 2012, **28**, 10781-10788
16. J. Pal, S. Sanwaria, R. Srivastava, B. Nandan, A. Horechyy, M. Stamm, H. Chen *J. Mater. Chem.*, 2012, **22**, 25102-25107
17. M. Hu, S. Ishihara, K Ariga, M. Imura, Y. Yamauchi, *Chem.-Eur. J.*, 2013, **19**. 1882-1885
18. J. W. Vanderhoff, M. S. El-Aasser, J. Ugelstad, *US Pat. Appl.*, **1979**, 4 177 177
19. J. C. Leroux, J. C. Allémann, E. Doelker, *Eur. J. Pharm. Biopharm.*, 1995, **41**, 14-18
20. D. Quintanar-Guerrero, E. Allémann, H. Fessi, E. Doelker, *Int. J. Pharm.* 1995, **143**, 133-141
21. C. Bindschaedler, R. Gurny, E. Doelker, *US Pat. Appl.*, **1990**, 4 968 350
22. H. Fessi, F. Puisieux, J. P. Devissaguet, *Eur. Pat. Appl.*,**1986**, 274 961
23. H. Fessi, F. Puisieux, J. P. Devissaguet, N. Ammoury, S. Benita, *Int. J. Pharm.*, 1989, **55**, R1-R4
24. S. Horing, T. Heinze, C. R. Becer, U. S. Schubert, *J. Mater. Chem.*, 2009, **19**, 3838-3840
25. P. York, *Pharm. Sci. Technol. Today*, 1999, **2**, 430-440
26. Y. P. Sun, M. J. Mezani, P. Pathak, L. Qu, *Chemistry*, 2005, **11**, 1366-137
27. B. V. N. Nagavarma, K. S. Y. Hemant, A. Ayaz, L. S. Vasudha, H. G. Shivakumar, *Asian J. Pharm. Clin. Res.* 2012, **5**, 16-23
28. J. P. Rao, K. E. Geckeler, *Prog. Polym. Sci.* 2011, **36**, 887-913
29. C. Vauthier, K. Bouchemal, *Pharm. Res.*, 2009, **26**, 1025-1058
30. J. Allouche in *Nanomaterials: A Danger or a Promise?*, ed. R. Brayner, F. Fiévet, T. Coradin, Springer-Verlang, London, 2013, ch. 2, pp. 27-74
31. K. Hirech, S. Payan, G. Carnelle, L. Brujes, J. Legrand, *Powder Technol.*, 2003, **130**, 324-330
32. U. Sree, Y. Yamamoto, B. Deore, H. Shiigi, T. Nagaoka, *Synth. Met*., 2002, **131**, 161-165
33. C. Dire, S. Magnet, L. Couvreur, B. Charleux, *Macromolecules*, 2009, **42**, 95-103
34. W. Li, K. Matyjaszewski, K. Albrecht, M. Moller, *Macromolecules, 2009*, **42**, 8228-8233
35. J. Rieger, W. Zhang, F. Soffelbach, B. Charleux, *Macromolecules*, 2010, **43**, 6302-6310
36. C. Costa, A. F. Santos, M. Fortuny, P. H. H. Araujo, C. Sayer, *Mater. Sci. Eng. C*, 2009, **29**, 415-419
37. W. V. Smith, R. H. Ewart, *J. Chem. Phys.*, 1948, **16**, 592-599
38. W. D. Harkins, *J. Am. Chem. Soc.*, 1947, **69**, 1428-1444
39. M. Nomura, H. Tobita, K. Suzuki, *Adv. Polym. Sci.*, 2005, **175**, 1-128
40. C. Chern, C. Li, *Polymer*, 2000, **41**, 4473-4481

41. S. Lu, R. Qu, J. Forcada, *Mater. Lett.*, 2009, **63**, 770-772
42. J. Gao, C. Wu, *Langmuir*, 2005, **21**, 782-785
43. X. Cheng, M. Chen, S. Zhou, L. Wu, *J. Polym. Sci. Part A Polym. Chem.*, 2006, **44**, 3807-3816
44. J. Nicolas, P. Couvreur, *Nanomed. Nanobiotechnol.*, 2009, **1**, 111-127
45. G. Zhang, A. Niu, S. Peng, M. Jiang, Y. Tu, M. Li, C. Wu, *Acc. Chem. Res.*, 2001, **34**, 249-256
46. G. Liu, P. Liu,*Colloid. Surf. A*, 2010, **354**, 377-381
47. S. T. Camli, F. Buyukserin, O. Balci, G. G. Budak, *Colloid Polym. Sci.*, 2009, **287**, 745-749
48. S. Han, K. Lee, S. E. Shim, P. J. Saikia, S. Choe, *Macromol. Res.*, 2007, **15**, 403-411
49. N. Ozturka, N. Bereli, S. Akgola, S. Denizlib, *Colloid. Surf. B*, 2008, **67**, 14-19
50. F. K. Hansen, J. Ugelstad, *J. Polym. Sci. A Polym. Chem.*, 1979, **17**, 3047-3067
51. A. R. Goodall, M. C. Wilkinson, J. Hearn, *J. Polym. Sci. Polymn. Chem. Ed.*, 1977, **15**, 2193-2218
52. F. J. Schork, G. W. Poehelin, S. Wang, J. Reimers, J. Rodrigues, C. Samer, *Colloid. Surf. A*, 1999, **153**, 39-45
53. C. K. Weiss, K. Landfester, *Adv. Polym. Sci.*, 2010, **233**, 185-236
54. C. Li, W. Wu, T. Don, *J. Polym. Sci. Part A Polym. Chem.*, 2005, **43**, 4870-4881
55. C. Maitre, F. Ganchaud, O. Ferreira, J. F. Lutz, Y. Paintoux, P. Hémery, *Macromolecules*, 2000, **33**, 7730-7736
56. F. M. Pavel, *J. Disper. Sci. Technol.*, 2004, **25**, 1-16
57. M. R. Ferrick, J. Murtagh, J. K. Thomas, *Macormolecules*, 1989, **22**, 1515-1517
58. J. X. Xu, K. S. Siow, M. K. Wong, L. M. Gan, *Colloid Polym. Sci.*, 2001, **279**, 879-886
59. J. X. Xu, C. H. Chew, K. S. Siow, M. K. Wong, L. M. Gan, *Langmuir*, 1999, 15, 8067-8071
60. E. J. Acosta, A. S. Bhakta, *J. Surfactants Deterg.*, 2009, **12**, 7-19
61. J. O. Stoffer, T. Bone, *J. Disper. Sci. Technol.*, 1980, **1**, 37-54
62. J. O. Stoffer, T. Bone, *J. Polym. Sci. Polym. Chem.* 1980, **18**, 2641-2648
63. S. S. Atik, K. J. Thomas, *J. Am. Chem. Soc.*, 1981, **103**, 4279-4280
64. Y. S. Leong, F. Candau, *J. Phys. Chem.*, 1982, **86**, 2269-2271
65. C. Yong, L. Gan, *Adv. Ploym. Sci.*, 2005, **178**, 257-298
66. J.S. Guo, E. D. Sudol, J. W. Vanderhoff, M.S. El-Aasser, *J. Polym. Sci .Pol. Chem.*, 1992, **30**, 691-702
67. J. E. Puig, V. H. Pérez-Luna, M. Pérez-Gonzáez, E. R. Macias, B. E. Rodriguez, E. W. Kaler, *Colloid. Polym. Sci.*, 1993, **271**, 114-123
68. C-S. Chern, H-J. Tang, *J. Appl. Polym. Sci.*, 2005, **97**, 2005-2013
69. United States Environmental Protection Agency, *OPPT Chemical Fact Sheets (Styrene) Fact Sheet: Support Document*, 1994, **EPA 749-F-95-019a**
70. United States Environmental Protection Agency, OPPT Chemical Fact Sheets (Methyl Methacrylate) Fact Sheet: Support Document, 1994, **EPA 749-F-94-014a**
71. E. Mendizabal, J. Flores, J. E. Puig, I. Katime, F. Lopez-Serrano, J. Alvarez, *Macromol. Chem. Phys.*, 2000, **201**, 1259-1265
72. C. C. Co, P. Cotts, S. Burauer, R. deVries, E. W. Kaler, *Macromolecules*, 2001, **34**, 3245-3254
73. D. Kukulj, T. P. Davis, R. G. Gilbert, *Macromolecules*,1998, **31**, 994-999
74. L. M. Gan, C. H. Chew, J. H. Lim, K. C. Lee, L. H. Gan, *Colloid Polym. Sci.*, 1994, **272**, 1082-1089
75. X. Kong, Q. Wu, W. Hu, Z. Wang, *J. Polym. Sci. Part A. Polym. Chem.*, 2008, **46**, 4522-4528
76. R. P. Moraes, R. A. Hutchinson, T. F. L. McKenna, *J. Polym. Sci. A.*, 2010, **48**, 48-54
77. W. Meier, *Chem. Soc. Rev.*, 2000, **29**, 295-303
78. T. A. F. P. Doll, S. Raman, R. Dey, P. Buckhard, *J. R. Soc. Interface*, 2013, **10**, 20120740
79. Y. Wang, Y. Yan, J. Cui, L. Hosta-Rigau, J. K. Heath, E. C. Nice, F. Caruso, *Adv. Mater.*, 2010, **22**, 4293-4297
80. J. Nicolas, S. Mura, D. Brambilla, N. Mackiewicz, P. Couvreur, *Chem. Soc. Rev.*, 2013, **42**, 1147-1235
81. J. Möller, M. Cebi, M. A. Schroer, M. Paulus, P. Degen, C. J. Sahle, D. C. Wieland, S. Leick, A. Nyrow, H. Rehage, M. Tolan, *Phys. Chem. Chem. Phys.*, 2011, **13**, 20354-20360
82. S. Bontha, A. V. Kabanov, T. K. Bronich, *J. Control. Release*, 2006, **114**, 163-174

83. K. Landfester, *Angew. Chem. Int. Ed.*, 2009, **48**, 4488-4507
84. S. Janssens, G. V. M. Williams, D. Clarke, *J. Lumin.*, 2013, **134**, 277-283
85. C. M. Bender, C. Pollock, *Chem. Mater.*, 2000, **12**, 1969-1976
86. N. Vogel, C. P. Hauser, K. Schuller, K. Landfester, C. K. Weiss, *Macromol. Chem. Phys.*, 2010, **211**, 1355-1368
87. E. Schreiber, U. Ziener, A. Manzke, A. Plettl, P. Ziemann, K. Landfester, *Chem. Mater.*, 2009, **21**, 1750-1760
88. C. P. Hauser, Christoph, D. T. Thielemann, M. Adlung, C. Wickleder, P. W. Roesky, C. K. Weiss, K. Landfester, *Macromol. Chem. Phys.*, 2011, **212**, 286-296
89. Z. Cao, Z. Wang, C. Herrmann, U. Ziener, K. Landfester, *Langmuir*, 2010, **26**, 7054-7061
90. E. Kobitskya, D. Ekinci, A. Manzke, A. Plettl, U. Wiedwald, P. Ziemann, J. Biskupek, U. Kaiser, U. Ziener, K. Landfester, *Macromolecules*, 2010, **43**, 3294-3305
91. A. V. Fuchs, C. Walter, K. Landfester, U. Ziener, *Langmuir*, 2012, **28**, 4974-4983
92. L. P. Ramírez, M. Antonietti, K. Landfester, *Macromol. Chem. Phys.*, 2006, **207**, 160-165
93. C. Vancaeyzeele, O. Ornatsky, V. Baranov, L. Shen, A. Abdelrahman, M. A. Winnik, *J. Am. Chem. Soc.*, 2007, **129**, 13653-13660
94. J. Desbiens, B. Bergeron, M. Patry, A. M. Ritcey, *J. Colloid Interf. Sci.*, 2012, **376**, 12-19
95. S. C. Thickett, A. I. Abdelrahman, O. Ornatsky, D. Bandura, V. Baranov, M. A. Winnik, *J. Anal. At. Spectrom.*, 2010, **25**, 269-281
96. L. R. Melby, E. Abramson, J. C. Caris, N. J. Rose, *J. Am. Chem. Soc.*, 1964, **86**, 5117-5125s
97. C. Vancaeyzeele, O Ornatsky, V. Baranov, L. Shen, A. Abdelrahman, M. A. Winnik, *J. Am. Chem. Soc.*, 2007, **129**¸13653-13660
98. *Dynamic Light Scattering Common Terms Defined*, 2011, Malvern Instruments Inform White Paper
99. K. Tiede, A. B. A. Boxall, D. Tiede, S. P Tear, H. David, J. Lewis. *J. Anal. At. Spectrom.*, 2009, **24**, 964-97
100. J. Chen, F. Q. Wu, *Surf. Eng.*, 2012, **28**, 225-229
101. M. Antonietti, W. Bremser, D. Muschenborn, C. Rosenauer, C. B. Schupp, *Macromolecules*, 1991, **24**, 6636-6643
102. J. Gao, C. Wu, *Langmuir*, 2005, **21**, 782-785
103. F. Candau in *Polymerization in Organized Media*, ed. C. M. Paleos, Gordon and Breach Science Publishers, Philadelphia, 1992, ch. 4, pp. 215-283
104. Sciencelab.com, *Dodecane MSDS*, 2013, http://tinyurl.com/n5s29dw, accessed 23/5/2013
105. Y. Chen, H. R. Liu, Z. C. Zhang, S. J. Wang, *Eur. Polym. J.*, 2007, **43**, 2928-2934
106. J. Texter in *Recations and Synthesis in Surfactant Systems*, ed. J. Texter, Marcel Decker Inc., New York, 2001, ch. 29, pp. 557-608
107. J. S. Guo, M. S. El-Aasser, J. W. Vanderhoff, *J. Polym. Sci. A*, 1989, **27**, 691-710
108. R. Franklin, M. Hoey, R. Premachandran in *Chemistry in the oil industry VII: Performance in a challenging environment*, ed. T. Balson, H. A. Craddock, J. Dunlop, H. Frampton, G. Payne, P. Reid, Royal Society of Chemistry, Cambridge, 2002, pp. 96-106
109. M. S. A. Palma, *Indian J. Chem. Techn.*, 2007, **14**, 515-222
110. Y. Chen, F. Jahnzad, S. Sajjadi, *Langmuir*, 2013, **29**, 5650-5658
111. A. G. Ramierez, R. G. Lopez, K. Tauer, *Macromolecules*, 2004, **37**, 2738-2747
112. S-C. Hsu, T-M. Don, W-Y. Chiu, *Polym. Degrad. Stabil.*, 2002, **75**, 73-83
113. G. Saunders, Personal Communication
114. D. C. Prieve, P. M. Hoysan, *J. Colloid Interf. Sci.*, 1978, **64**, 201-213
115. H. Small, *J. Colloid Interf. Sci.*, 1974, **48**, 147-161
116. Sigma-Aldrich, *Detergent Properties and Applications*, accesses online at http://tinyurl.com/q4v9d9k on 19th July 2013
117. J. Israelachvilli, *Colloid. Surface. A*, 1994, **91**, 1-8
118. C. Stubenrauch, T. Wielpütz, T. Scottmann, C. Roychowdhury, F. J. DiSalvo, *Collod. Surface. A*, 2008, **317**, 328-338

119. A. Zielińska-Jurek, J. Reszczyńska, E. Grabowska, A. Zaleska in *Microemulsions – An Introduction to Properties and Applications*, ed. R. Najjar, InTech, Rijeka, 2012, ch. 12, pp. 231-250
120. M. Anderson, J. Pedersen, J. Skov, A. E. C. Palmqvist, *Langmuir*, 2005, **21**, 11387-11396
121. M. R. Housaindokht, A. N. Pour, *Solid State Sci.*, 2012, **14**, 622-625
122. S. J. Douglas, I. Illium, S. S. Davis, *J. Colloid Interf. Sci.*, 1985, **103**, 154-163
123. R. A. Mackay in *Recations and Synthesis in Surfactant Systems*, ed. J. Texter, Marcel Decker Inc., New York, 2001, ch. 16, pp. 373-383
124. *Martindale: The complete drug reference*, ed. S. C. Sweetman, Pharmaceutical Press, London, **2011**; Vol. A
125. Z. Zhang, D. Law, G. Lan, in *Technologies for Active Food Ingredients and Food Processin*, ed. N. J. Zuidan, V. A. Nedović, Springer: London, 2010; Ch. 4, pp 101-126

# Chapter 6

# Application PolyHIPE Chromatography with ICP-MS detection for the Separation of Engineered Nanoparticles.

## 6.1 Introduction

Previously, in chapter 4, polyHIPE columns produced from poly(styrene-*co*-DVB), poly(BMA-*co*-EGDMA) and polyEGDMA had been shown to be capable of separating engineered nanoparticles over the size range 100 nm – 800 nm. However, as the current European definition of a nanoparticle is any material of one dimension under 100 nm[1] none of the particles separated in chapter 4 met this criterion. Therefore, in this chapter a new set of polyHIPE columns were investigated for the separation of engineered nanoparticles below 100 nm.

### 6.1.1 Aims and Objectives

The aim of the work detailed in this chapter was the separation of different sized engineered nanoparticles with diameters below 100 nm using polyHIPE-ICP-MS liquid chromatography.

It was postulated that polyHIPEs with smaller cages and windows would have a greater chance of separating smaller particles. To that end two new polyHIPE columns

were prepared, one poly(styrene-*co*-DVB) and one poly(EGDMA), with increased shear during the mixing stage compared to the polyHIPEs produced in chapter 3.

Once the polyHIPE columns had been produced they were attached to an inductively coupled plasma mass spectrometer (ICP-MS) to provide element specific detection. This required the selection of particles which contained elements with a low natural abundance, *i.e.*, gold nanoparticles and the dysprosium containing particles detailed in chapter 5 of this thesis.

## 6.2 Experimental

### 6.2.1 Chemicals

Styrene (Sigma-Aldrich) and divinylbenzene (DVB; Aldrich) were distilled under reduced pressure to remove inhibitors and then stored at -20 $^{o}$C until used. Ethyleneglycol dimethacrylate (EGDMA; Alfa Aesar) was passed through an alumina column (Brockmann activity I), to remove inhibitors, and then through a 0.45 μm HDPE filter (Millipore) and used immediately. Calcium chloride (anhydrous; Fisher), Pluronic® L-121 *(*Poly(ethyleneglycol)-*block*-poly(propylene glycol)-*block*-poly(ethyleneglycol), average $M_n$ ~4,400; Aldrich)**,** potassium persulphate (KPS; Fisher), 2-propanol (Aldrich), SPAN$^{TM}$ 80 (sorbitane monooleate; Fluka) and N,N,N',N'-tetramethylethylenediamine (TMEDA; Sigma-Aldrich) were all used as received.

### 6.2.2 Polymerisations

The HIPE compositions, initiator system and polymerisation conditions are listed Table 6.1 below. The general procedure for the production of the polyHIPEs was virtually identical to the method used and detailed in chapter 3 section 3.2.1.3 and, as such, it will not be repeated here. There where however two differences; washing of the final polyHIPE

monoliths was by soxhlet extraction with 2-propanol rather than with ethanol and most importantly the mixing was performed at 1200 rpm rather than 460 rpm to generate higher shear.

Table 6.1: HIPE compositions and polymerisation conditions used for the synthesis of the polyHIPEs descried in this chapter.

| PolyHIPE | Monomers | Surfactant | Initiator System | Internal Phase Volume | Polymerisation Conditions |
|---|---|---|---|---|---|
| EGDMA21c [a] & EGDMA23M [b] | EGDMA (4 ml) | Pluronic L121 (1.2 ml) | KPS/ TMEDA [c] | 36 ml | 72 hrs @ room temp. |
| PS-11c [a] & PS13M [b] | Styrene (1.4 ml) DVB (0.6 ml) | Span 80 (0.6 g) | KPS [d] | 18 ml | 48 hrs @ 65 $^{o}$C |

[a] Polymerised within an empty stainless steel HPLC column (i.d. 4.6 mm, length 150 mm).
[b] Polymerised within a glass mould
[c] KPS/TMEDA acts as a redox initiator system with TMEDA being added just prior to the end of mixing
[d] KPS initiates by thermal degradation of the persulphate hence the need for elevated temperatures of polymerisation.

Once the HIPEs had been formed they were split between a glass mould and an empty stainless HPLC column (Supleco, Germany). Both vessels were sealed and polymerisation undertaken within. HPLC columns were sealed without frits[i] so as to allow the transit of analytes greater the 0.46 $\mu$m, though these were not used in this chapter.

Once polymerisation was complete the monolithic polyHIPE columns to be used for chromatography were pumped through with 2-propanol at a flow rate of 0.1 ml min$^{-1}$ overnight followed by a flow of deionised water, also at a flow rate of 0.1 ml min$^{-1}$ for approximately 6 hours using the same HPLC system described in chapter 3 section 3.2.1.3.

[i] While columns where prepared without frits the end fittings of the column were described as zero dead volume so it was hoped that the absence of frits would not leave a dead volume that would adversely influence the column performance.

### 6.2.3 Structural Characterisation of the PolyHIPEs

Samples were first sputter coated with gold/palladium and scanning electron microscopy (SEM) was carried out on a Phillips XL30 FEG SEM at the School of Materials at the University of Manchester.

The average diameters and the size distributions were calculated by manual measurement of a large number of entities (≥ 200 measurements) using software designed for the measurement of nanoparticles. Once the average diameter of the cages had been determined a statistical correction was applied by multiplying the average value measured from SEM by $2/(3^{1/2})$. (The explanation for the statistical correction is given in reference [2] and section A1.1 of appendix 1.)

### 6.2.4 Chromatography

#### 6.2.4.1 Equipment

Chromatography experiments were performed on a HPLC system built from a HPLC pump (model 307 Gilson, UK), a manually driven injector valve (model 9125 Rheodyne, USA) with a 20 $\mu$l sample loop. The flow rates of the mobile phase in the system were dependent on the column and are displayed in Table 6.2. For the polyHIPE column EGDMA21c the flow rate was lower than the natural aspiration rate of the nebuliser; to compensate a post column make up flow of mobile phase at 0.1 ml $min^{-1}$ was provided by means of a peristaltic pump (Miniplus-2, Gilson, UK).

Table 6.2: Flow rates of mobile used for each of the columns

| Column | Flow Rate (ml $min^{-1}$) |
|---|---|
| PS-11C | 0.30 |
| EGDMA21C | 0.15 [a] |
| PL-PSDA Type-1 HDC | 1.70 |

[a] A peristaltic pump supplied post column make up flow of mobile phase at 0.1 ml $min^{-1}$ to compensate for the natural aspiration rate of the nebuliser (0.24 ml $min^{-1}$)

Detection was by means of an ICP-MS (model 7500 Agilent, UK), the instrument parameters are detailed in Table 6.3. Data was acquired on a PC and processed on the ChemStation software (Agilent, USA).

Table 6.3: Instrumental set up of the ICP-MS

| Parameter | Setting |
|---|---|
| RF Power | 1550 W |
| Nebuliser Identity | Agilent Micromist Nebuliser |
| Nebuliser Gas Flow | |
| Carrier Gas | 0.75 L $min^{-1}$ |
| Make up Gas | 0.34 L $min^{-1}$ |
| Sample Depth | 8 mm |
| Isotopes Monitored | $^{109}Ag$ or $^{162}Dy$, $^{163}Dy$, $^{164}Dy$ |

Figure 6.1: Picture of the chromatography ICP-MS system.

### 6.2.4.2 Separations

Separations were achieved using the polyHIPE columns described above and, for comparison, a commercially obtained HDC column (separation range 5-300 nm) (PL-PSDA Type-1 Agilent, UK). The mobile phase was a propriety aqueous eluent concentrate (Agilent, UK) which was diluted to the manufacturer specifications before use. The exact composition of the mobile phase is unknown, however, several components are identified in the MSDS; sodium azide (presumably as a biocide), sodium dodecyl sulphate (an

anionic surfactant), and ethoxylated dodecane-1-ol (presumably acting as a non-ionic surfactant).[3]

Separations were performed on dysprosium doped polystyrene latexes DyPlu-23 ($D_z$ 52 nm and PDI 0.09 measured by DLS), DyPlu-22 ($D_z$ 78 nm and PDI 0.05 measured by DLS) and DyPlu-21 ($D_z$ 155 nm and PDI 0.02 measured by DLS) (the synthesis and characterisation of which is described in chapter 5 of this thesis) and also on commercially obtained gold nanoparticles of mean diameters 5 nm, 10 nm and 20 nm (BBI Group, UK). Particles were diluted to 1.25 % v/v in mobile phase before injection.

Peak asymmetry factors and column resolution were calculated for each column from the chromatographs by the equations detailed in sections Al.3 and Al.4 of appendix 1.

## 6.3 Results and Discussion

As was expected from the work described in chapter 3, both monomer systems formed stable HIPEs which presented as white liquids with an oily appearance. The viscosity of the HIPEs was markedly increased compared to the HIPEs produced in chapter 3, instead of vicious liquids they now resembled a thick paste. This was attributed to the increased shear during mixing (the HIPE was mixed at 1200 rpm compared to 450 rpm in chapter 3) which formed HIPEs with a smaller average droplet size. This will result in greater levels of interfacial tension in the HIPEs, causing a corresponding increase in viscosity.[4] The reduced droplet size of the HIPEs compared to those produced in chapter 3 was evidenced by SEM analysis of the polyHIPEs (discussed in further detail in section 6.3.3) which showed that the polyHIPEs had significantly smaller cages and windows than those produced in chapter 3, indicating that smaller droplets were indeed present in the HIPE (Figure 6.5 to Figure 6.9.and Table 6.10 and Table 6.11).

When the 2-propanol/water mixture was pumped through the polyHIPE columns it initially eluted murky white, which over time became clear. This was taken as an indication that the polyHIPE column had been successfully washed.

### 6.3.1 Chromatographic Performance of PolyHIPE columns

In the first stage of the work the dysprosium containing polystyrene latex particles DyPlu-23, DyPlu-22 and DyPlu-21 (sized by DLS at 52, 78 and 155 nm respectively) were separately injected on to the polyHIPE EDGMA21c. Ideally the column would have been able to separate the particles DyPlu-23 and DyPlu-22, (which were both under 100 nm, matching the European definition of nanoparticles1) but it was unable to produce a separation, with no discernable difference in retention times. The column was, however, able to produce a separation for DyPlu-23 and DyPlu-21 (Figure 6.2 and Table 6.4) with consistent retention times and peak shapes over triplicate injections. The stepped nature of the peaks was a result of the discrepancy between the flow rate of the mobile phase (0.15 ml $min^{-1}$) and the natural aspiration rate of the nebuliser (0.24 ml $min^{-1}$) resulting in a pulsing in the flow at the nebuliser. While this was made up post column with a flow of mobile phase from a peristaltic pump at 0.1 ml $min^{-1}$ it was not able to completely eliminate the effect.

Despite the separation the calculated resolution (0.06) of the column (Table 6.5) was poor which, along with the significant peak overlap in the chromatograph (Figure 6.2), indicates that the column would not be able to resolve discrete peaks for a mixture of particles with a difference in size of 100 nm or less.

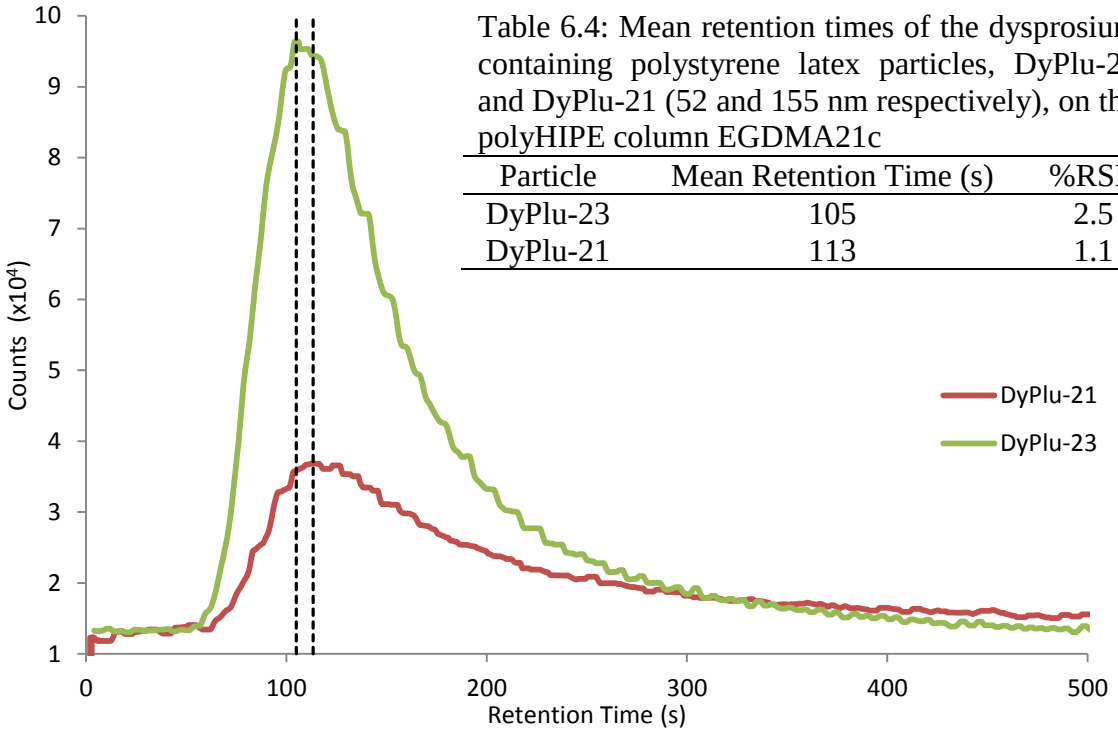


Table 6.4: Mean retention times of the dysprosium containing polystyrene latex particles, DyPlu-23 and DyPlu-21 (52 and 155 nm respectively), on the polyHIPE column EGDMA21c

| Particle | Mean Retention Time (s) | %RSD |
|---|---|---|
| DyPlu-23 | 105 | 2.5 |
| DyPlu-21 | 113 | 1.1 |

Figure 6.2: Chromatograph of the dysprosium doped polystyrene latex particles, DyPlu-21 (155 nm) and DyPlu-23 (52 nm), on the polyHIPE column EGDMA21c. The hashed lines represent the retention times of the analytes.

Further work into elucidating the flow rate which gives the optimum (minimum) peak width would help improve the resolution of the column (flow rate onto the column was deliberately kept low to minimise the backpressure as the stability of the column was unknown). It would not however be a simple case of an increased flow rate resulting in an increased resolution. While there should be no contribution from mass transfer of the analyte from mobile to stationary phase (the C term in the van Deemter equation (Eq. 6.1)), there will still be eddy-diffusion (the A term) and longitudinal diffusion (the B term) effects, both of which are to some extent influenced by flow rate.

$$H = A + {}^{B}/_{u} + Cu \qquad \text{(Eq. 6.1)}$$

Where; $H$ = Plate height

$A$ = The Eddy-diffusion parameter, associated with channeling in non-ideal packing in m

$B$ = longitudinal diffusion coefficient of the eluting analytes resulting in dispersion in $m^2\ s^{-1}$

$C$ = mass transfer coefficient of the analyte from the mobile to stationary phase in s

$u$ = linear velocity in $m\ s^{-1}$

As well as poor resolution, the significant peak tailing, which resulted in high peak asymmetry factors (Table 6.5), suggests the presence of on column interactions. Peak asymmetry could almost certainly be reduced by development of a suitable mobile phase rather than using one designed for HDC, which may not have been the most effective at limiting the on column interactions (particularly electrostatic) between the analytes and the stationary phase. Reducing the peak asymmetry would also help improve the resolution of column.

Table 6.5: Resolution and peak symmetry factors for the separation of the dysprosium containing polystyrene latex particles on the polyHIPE column EGDMA21c.

| Column | Resolution | Peak Asymmetry Factor | |
|---|---|---|---|
| | | DyPlu-23 (52 nm) | DyPlu-21 (155 nm) |
| EGDMA21c | 0.06 | 4.1 | 5.7 |

The second stage of this work was to attempt to repeat the separation of the dysprosium containing polystyrene latex particles with the polyHIPE column PS-11c. However, after the first injection of the DyPlu-23, the particles were retained on the column and the back pressures began to rise. To remove the particle, and allow further injections, the column was then gently back-flowed. Removal of the particles was established by monitoring the ion $M_z$ 162 (associated with dysprosium) content of the eluent back-flow using the ICP-MS until the levels had returned to background. Since it had been established that even the smallest dysprosium continuing latex particles were too large to transit the column, commercially obtained gold nanoparticles of three sizes (5 nm,

10 nm and 20 nm) were injected onto the column to investigate if PS-11c could affect a separation.

PS-11c was able to successfully separate the 5 nm and 10 nm gold particles, with consistent retention times over triplicate injections, (Table 6.6), producing the chromatograph displayed in (Figure 6.3). However, after injection of the 20 nm gold particles onto the column the particles were retained and the back pressure began to increase, indicating that the column had a very narrow operating size range

Table 6.6: Mean Retention times of 5 nm and 10 nm gold nanoparticles on the polyHIPE column PS-11c.

| Particle | Mean Retention Time (s) | %RSD |
|---|---|---|
| Gold 5 nm | 348 | 1.5 |
| Gold 10 nm | 489 | 1.4 |

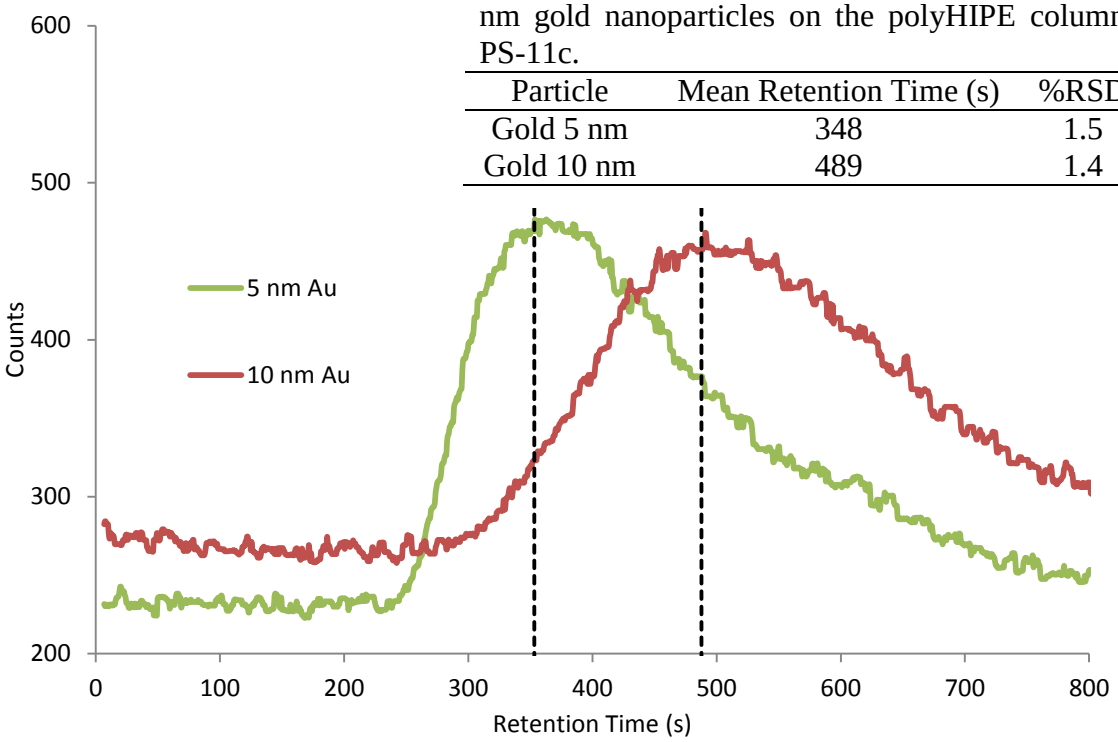


Figure 6.3: Chromatographs of gold nanoparticles (5 nm and 10 nm) produced by the polyHIPE column PS-11c. The hashed lines represent the mean retention times of the triplicate injections.

Table 6.7: Resolution and peak asymmetry factors of the 5 and 10 nm gold particles on the polyHIPE column PS-11c

| Column | Resolution | Peak Asymmetry Factor | |
|---|---|---|---|
| | | 5 nm Gold | 10 nm Gold |
| PS-11c | 0.31 | 3.7 | 2.2 (est) |

Unlike the polyHIPE column EGDMA21c, there was a significant difference in retention times between the particles injected onto PS-11c. However, despite these significant differences in the retention time, the considerable peak width which caused significant peak overlap resulted in a less than ideal resolution (0.31) (Table 6.7). However, as there was no overlap of the peak maxima it is possible that a resolution of peaks could be achieved for mixtures of the 5 nm and 10 nm gold particles. The broad peaks are likely as a result of the column and not the dispersity of the gold particles which have a coefficient of variation of (also known as the %RSD) of < 15%.[5]

The peak asymmetry factor had to be estimated for the 10 nm gold particles as measurement was terminated before the peak had returned to the base line. While less than on EGDMA21c, peak asymmetry was still greater than ideal for both peaks, again indicating on column interactions. As with EGDMA21c the resolution and peak asymmetry of PS-11c could potentially be improved by development of a bespoke mobile phase and investigation into optimising flow rates along with other aspects of the chromatography set up.

While the elution order was the same for both columns the mechanism is unknown would require further investigation to be elucidated. As the smaller particles elute before the larger particles on both columns is not a mechanism based upon excluded volume, as with SEC of HDC, which would see the larger particles elute before the smaller one.

### 6.3.2 Comparison with HDC

To compare how the polyHIPE columns performed against a commercially available size separation technique, the gold and dysprosium containing particles were also injected onto a commercially available PL-PSDA Type-1 HDC column which was fitted into the same chromatography setup as the polyHIPE columns. HDC was able to separate

the dysprosium latex particles considerably better than the polyHIPE column EGDMA21c (Figure 6.4), with a resolution between DyPlu-23 and DyPlu-21 of 1.21 (which is approaching baseline resolution at 1.5)[6] compared to the resolution of 0.06 on EGDMA21c. It was also able to resolve the DyPlu-23 and DyPlu-22 particles (resolution 0.30); though it is unlikely that for a mixture separate peaks would be obtained.

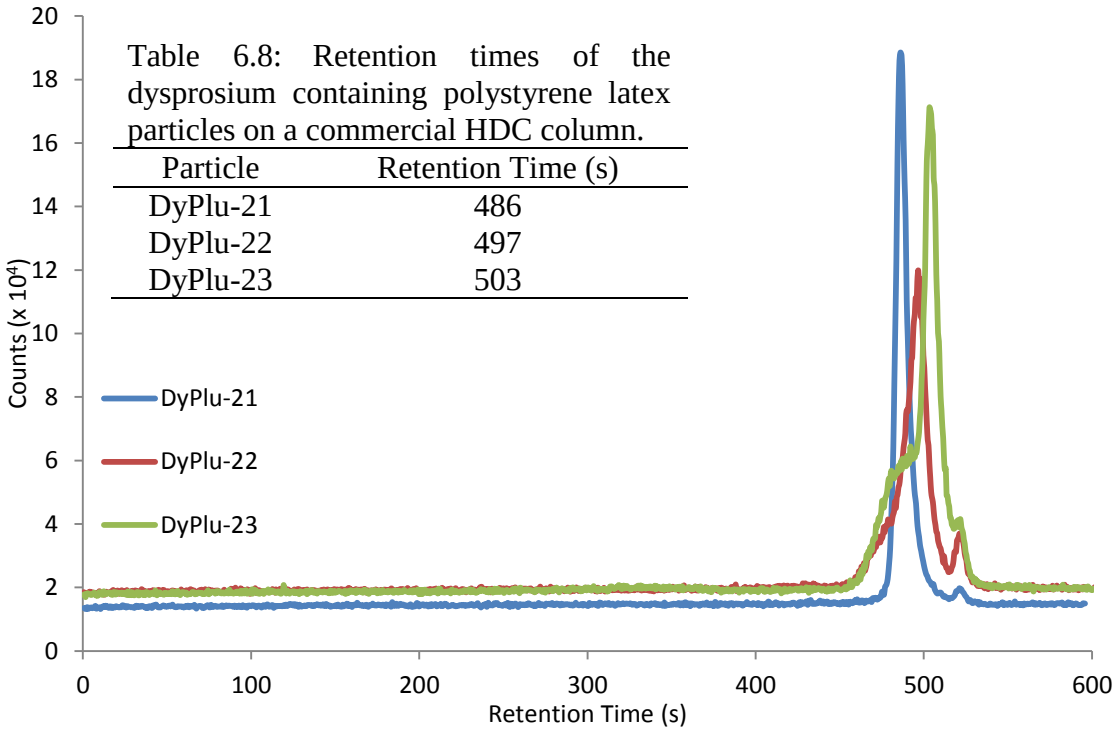


Table 6.8: Retention times of the dysprosium containing polystyrene latex particles on a commercial HDC column.

| Particle | Retention Time (s) |
|---|---|
| DyPlu-21 | 486 |
| DyPlu-22 | 497 |
| DyPlu-23 | 503 |

Figure 6.4: Chromatographs of the dysprosium containing polystyrene particles separated on a commercial PL-PSDA HDC column. Particle sizes measured by DLS were DyPlu-21 $D_z$ = 155 nm, DyPlu-22 $D_z$ = 78 nm and DyPlu-23 $D_z$ =52 nm.

Table 6.9: Resolution of the dysprosium containing polystyrene latex particles, DyPlu-21, DyPlu-22 and DyPlu-23 (measured by DLS 155 nm, 78 nm and 155 nm respectively), on a PL-PSDA type 1 HDC column.

| Column | Resolution | | |
|---|---|---|---|
| | DyPlu-21/ DyPlu-22 | DyPlu-22/ DyPlu-23 | DyPlu-21/DyPlu23 |
| HDC | 0.77 | 0.30 | 1.21 |

While HDC did outperform EGDMA21c for the separation of the dysprosium containing particles the polyHIPE column PS-11c outperformed HDC for the separation of the 5 and 10 nm gold particles. HDC was unable to resolve the gold particles, producing similar retention times for each particle whereas, as discussed earlier, the polyHIPE

column PS-11c was able to separate the 5 and 10 nm gold particles with resolution of 0.31 between the two particles. The polyHIPE column PS-11c was, however, limited in its operating size range with the 20 nm gold particles being retained on the column implying that it would be unable to separate particles much above 20 nm.

While the resolution of the particles DyPlu-21 and DyPlu-23 on the polyHIPE column EGDMA21c was poorer than on the HDC, the column dimensions were significantly smaller. The polyHIPE column EGDMA21c had internal dimensions of 150 mm x 4.6 mm, whereas the HDC column is comprised of two columns in series each with internal dimensions of 400mm x 7.5 mm. Resolution of the polyHIPE column could potentially be improved by scale up of the column to a similar size to the HDC column. While a theoretical resolution cannot be calculated with any reasonable degree of accuracy due to several unknowns about the columns, some comments can be made on the potential effects of a column scale up. No significant effects on the resolution would be expected from the increase in column i.d. Assuming that the same linear velocity was used (*i.e.* a ratio of $(4.6^2) / (7.5^2)$ meaning that 0.15 ml $min^{-1}$ would become 0.40 $ml^{-1}$) the peaks would be expected to elute at the same time. There may be some effects from the column wall which can be influenced by i.d.; *e.g.* "tracking" between the stationary phase and the wall (resulting in fronting of the peak), or drag (resulting in tailing). The column wall also supports the polyHIPE so there will be differences in the stability of the monolith.

By increasing the column length one would expect to observe an increase in retention time corresponding to the increased length, *i.e.* PluDy-23 which had a retention time of 105 s on the 150 mm long column EGDMA21c would have an expected retention time of 560 s on an 800 mm long polyHIPE column of the same stationary phase. Also, with increased column length the extra volume in the system (tubing, detector cell etc.) will be less significant. For two columns of the same stationary phase a longer column will

have a greater number of theoretical plates. Since as the greater the number of theoretical plates the closer the peak will resemble an ideal Gaussian curve, a longer column would be expected to have a greater resolution. However, because in longer columns there will be greater diffusion of the analytes, which will result in greater peak broadening, it does not necessarily follow that resolution will be increased.

### 6.3.3 Effect of Chromatography on PolyHIPEs Structure.

To assess what effect the separations had had, if any, on the polyHIPE structure, SEM was performed on the polyHIPE stationary phase of the monolithic columns after separations. As it was not possible to perform SEM on the polyHIPEs used for chromatography before the separations, a freestanding monolith which had been prepared from the same HIPE and under the same conditions as the polyHIPE monolithic columns was also examined by SEM. The assumption being that the internal structure of the freestanding monoliths would be equivalent to the internal structure of the polyHIPE monolithic columns before the chromatography experiments had taken place.

Table 6.10: Mean cage diameter and mean window diameter of the polyEGDMA polyHIPEs measured by SEM. Both polyHIPEs were prepared from the same HIPE under the same conditions. The SEM was performed on the monolithic column EDGMA21c after the chromatography experiments had been performed.

| PolyHIPE | Type | Mean Cage Diameter ($\mu$m) | | Mean Window Diameter ($\mu$m) | |
|---|---|---|---|---|---|
| | | $\bar{D}_n$ | %RSD | $\bar{d}_n$ | %RSD |
| EGDMA21c | Column | 1.1 | 36 | 0.2 | 57 |
| EGDMA23M | Monolith | 1.1 | 50 | 0.2 | 50 |

Table 6.11: Mean window diameter of the poly(styrene-*co*-DVB) polyHIPEs measured by SEM. Both polyHIPEs were prepared from the same HIPE under the same conditions. The SEM was performed on the monolithic column PS-11C after the chromatography experiments had been performed polyHIPEs.

| PolyHIPE | Type | Window Diameter ($\mu$m) | |
|---|---|---|---|
| | | $\bar{d}_n$ | %RSD |
| PS-11C | Column | 0.6 | 37 |
| PS13-M | Monolith | 0.6 | 42 |

The SEM showed that the internal structure of the polyHIPEs was similar for both the monolithic column (post separation) and the freestanding monolith of both the polyEGDMA (Figure 6.5) and poly(styrene-*co*-DVB) (Figure 6.8) polyHIPEs, as were the average size of the cages and windows (Table 6.10 and Table 6.11) and the corresponding size distributions (Figure 6.6, Figure 6.7 and Figure 6.9). This suggests that, at least in the short term, the polyHIPE structure is robust enough to withstand the pressures associated with the eluent flow, and chemically inert enough not be affected by the chemical composition of the mobile phase or the presence of the particles.

In both cases the cages of the polyHIPEs were less well defined than the polyHIPEs produced from similar HIPE compositions and polymerised under identical conditions described in chapter 3 (compare Figure 3.9 and Figure 3.14, chapter 3, to Figure 6.5 and Figure 6.8). The consequence of this was that the cages of poly(styrene-*co*-DVB) poly HIPEs were so poorly defined that it was not possible to calculate an average diameter. The lack of definition of the cages can be attributed to the more open nature of the polyHIPE. This greater openness is likely resulted from a decreased droplet size due to increased shear of mixing. In any emulsion for the same volume of internal phase a smaller average droplet size will produce a greater interfacial area. In a HIPE this will lead to a thinner average thickness of the film interfacial film in-between droplets. Since a thinner film will be more likely to rupture a greater number of windows will form will result more open cage, which, as a result, will be less well defined.[7]

SEM of the polyHIPE columns gave no indication of particles on the column surfaces. However, they may not have been visible at the magnification used, particularly with the 5 and 10 nm gold particles. They would also be further masked by sputter coating of the samples.

It had been postulated that smaller cages and smaller windows in the polyHIPE structure would result in a better chance of particle separation. The rationale was that smaller cages will result in less volume inactive in separation and smaller windows will result in greater selectivity between analytes of different sizes; in an analogous way to using narrower diameter capillaries in capillary HDC will improve separation efficiency and resolution. While there are a variety of different ways to produce smaller cages/windows in polyHIPEs (increased surfactant concentration *etc*.)[8] higher shear mixing was employed for this work as it did not require any change to HIPE composition from the work detailed in chapter 3. By comparing the SEM images of the polyHIPEs in this chapter (Figure 6.5 and Figure 6.8) to those of similar polyHIPEs produced in chapter 3 (Figure 3.10 and Figure 3.15) it can be seen that the use of higher shear mixing produced polyHIPEs with cages/windows that are considerably smaller than those produced in chapter 3 (Table 6.12). This can be attributed to the increased shear of mixing (1200 rpm compared to 450 rpm) forming smaller droplets in the HIPE, in turn templating smaller cages and windows in the resulting polyHIPE. As mentioned earlier, these smaller droplets also result in greater interfacial tension in the HIPE systems which leads to the increased viscosity of these HIPEs[2] compared to those described in chapter 3.

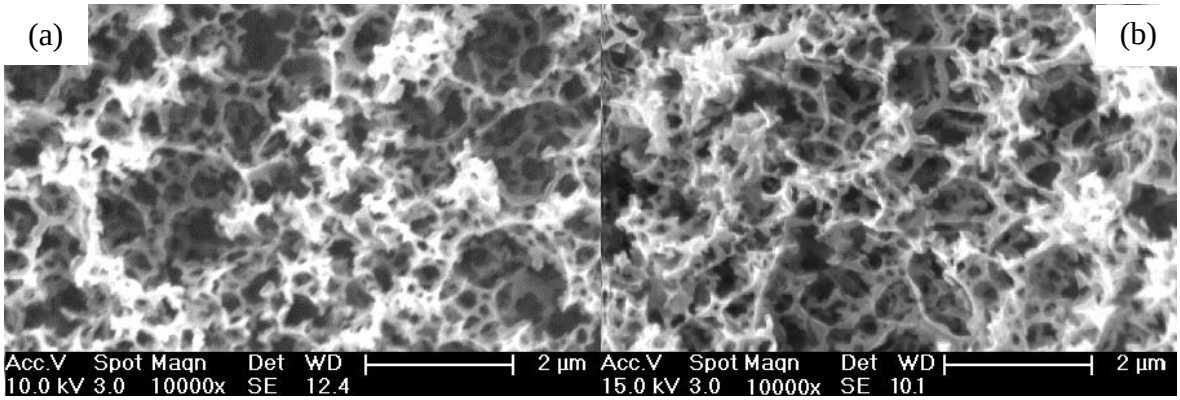


Figure 6.5: SEM images of (a) the polyHIPE monolith EGDMA23M which was not exposed to a chromatographic flow and prepared in a glass mould and (b) the polyHIPE monolith EGDMA21C which had been removed from the chromatographic system after separations.

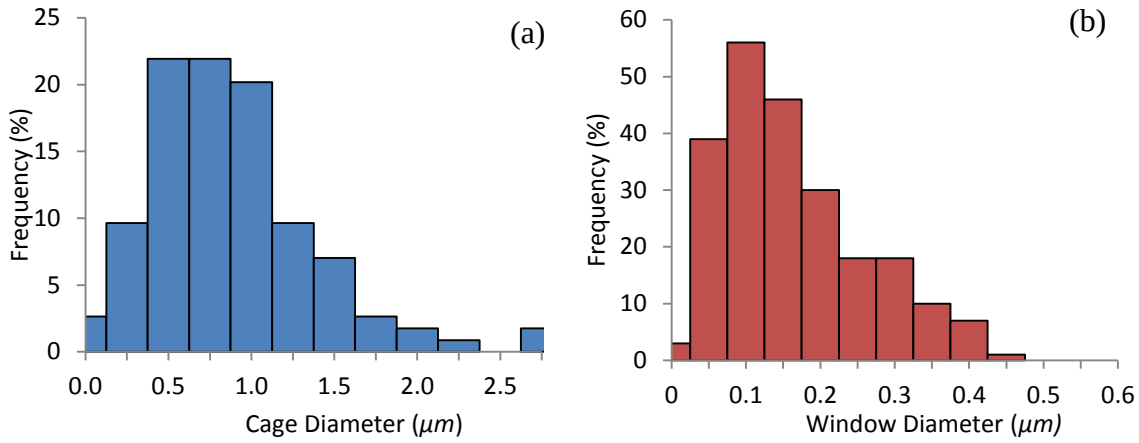


Figure 6.6: Size distributions, determined by SEM, of the (a) cage and (b) window diameters of the polyHIPE monolith EGDMA23M.

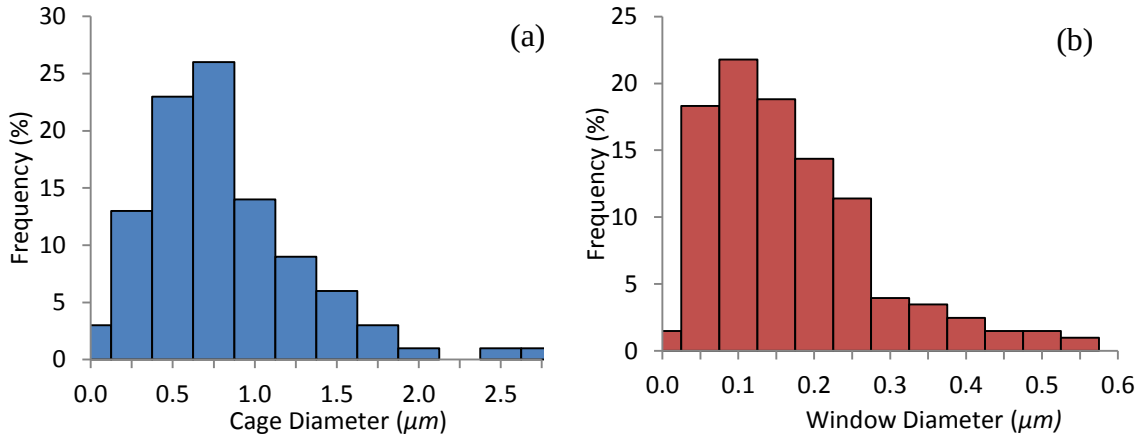


Figure 6.7: Size distributions, determined by SEM, of the (a) cage and (b) window diameters of the polyHIPE monolith EGDMA21c after separations.

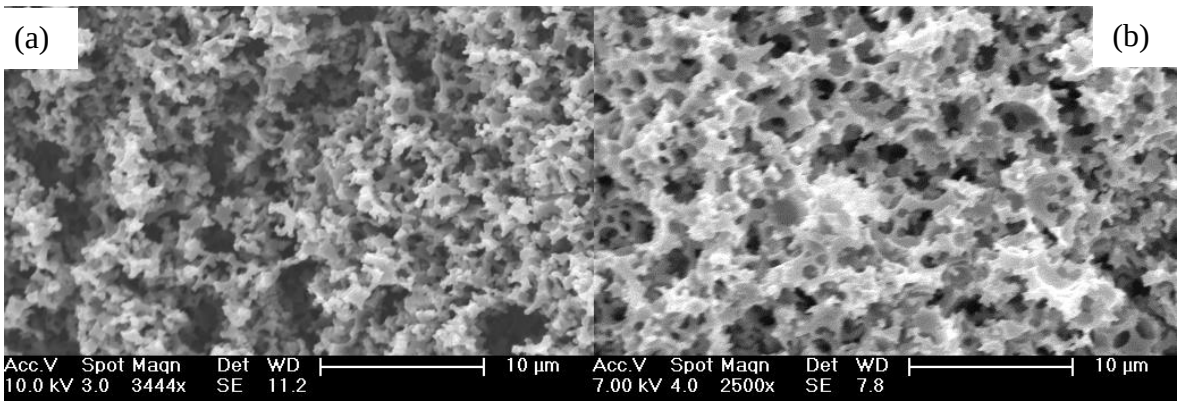


Figure 6.8: SEM images of (a) the polyHIPE monolith PS13-M which was not exposed to a chromatographic flow and prepared in a glass mould and (b) the polyHIPE monolith PS-11c which had been removed from the chromatographic system after separations.

(a) (b)

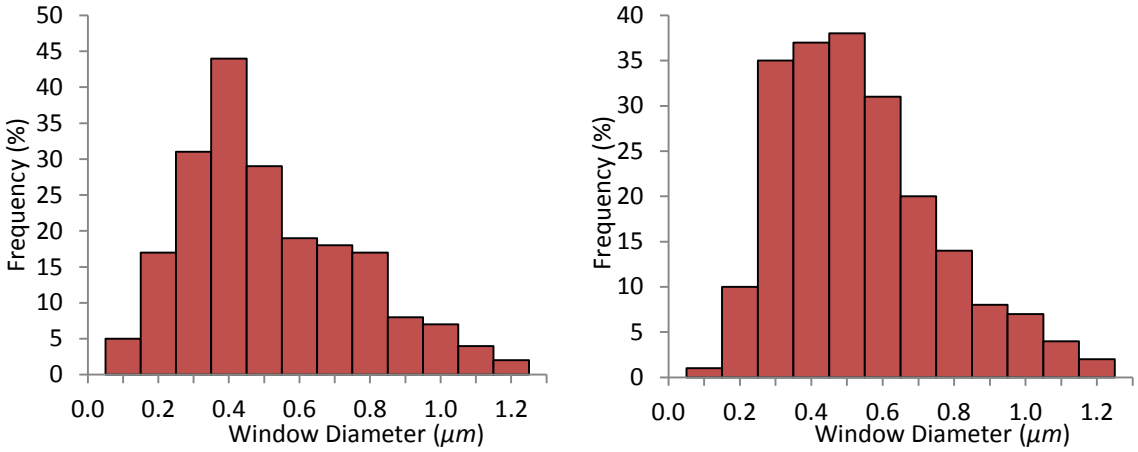


Figure 6.9: Size distributions, determined by SEM, of the windows of the polyHIPEs (a) PS-11c (after separations) and (b) PS13M .

Table 6.12: Comparison of the mean cage diameter and mean windows diameters of the polyHIPEs produced in this chapter (mixed at 1200 rpm) to those produced in chapter 3 (mixed at 450 rpm).

| PolyHIPE | Displayed in Figure.. | Mean Cage Diameter ($\mu$m) | | Mean Window Diameter ($\mu$m) | |
|---|---|---|---|---|---|
| | | $\bar{D}_n$ | %RSD | $\bar{d}_n$ | %RSD |
| EGDMA21c | Figure 6.5 | 1.1 | 36 | 0.2 | 57 |
| EGDMA23M | Figure 6.5 | 1.1 | 50 | 0.2 | 50 |
| EGDMA1 | Figure 3.14 | 2.2 | 35 | 0.4 | 45 |
| PS-11C[a] | Figure 6.8 | n.a | n.a | 0.6 | 37 |
| PS13-M[a] | Figure 6.8 | n.a | n.a | 0.6 | 42 |
| PS-3 | Figure 3.9 | 13.0 | 39 | 1.7 | 54 |

## 6.4 Conclusions

Two different polyHIPE columns, one poly(styrene-*co*-DVB) and one polyEGDMA, have been shown to be capable of separating engineered nanoparticles, ostensibly based upon size. The poly(styrene-*co*-DVB) polyHIPE was able to produce a resolution with particles of a narrow size range (5 and 10 nm gold particles) and in this respect it outperforms HDC which under normal operating conditions cannot resolve particles over this size range.

The elution order of particles off both columns was the same, with smaller particles eluting first. The mechanism behind the separation is unknown and without further work to generate more evidence the mechanism cannot be speculated upon at this juncture.

Comparison of SEM images of the polyHIPEs after separations to a polyHIPE monolith produced from the same HIPE and polymerised under identical conditions shows similar micro-scale structures with comparable size distributions for the polyHIPE cages and windows. This indicates that, in the short term at least, the polyHIPE columns are stable and the internal structure is not altered by chromatography.

While resolution of the particles on the column EGDMA21c and the peak asymmetry on both columns is not ideal, the author believes that both of these could be improved by further work optimising the chromatographic conditions (injection volumes, flow rates etc.) as well as developing a bespoke mobile phase for the columns.

## 6.5 References

1. J. Potočnik, *Off. J. Euro. Comm.*, 2011, **L275**, 38-40
2. A. Barbette, N. R. Cameron, *Macromolecules*, 2004, **37**, 3188-3204
3. Agilent Technologies, PL-PSDA Materials Safety Data Sheet, 2012
4. Y. Otsubo, P. K. Prund'homme, *Rheol. Acta*, 1994, **33**, 303-306
5 BBI Gold Nanoparticle Datasheets, http://tinyurl.com/n5ck9cn, accessed 27/7/2013
6. J. W. Dolan, *LCGC Asia Pacific*, 2002, **5**, 14-20
7. N. Cameron, *Polymer*, 2005, **46**, 1439-1449
8. I. Pulko, P. Krajnc, *Macromol. Rapid. Commum.*, 2012, **33**, 1731-1746

# Chapter 7

# Concussions and Recommendations for Further Work

## 7.1 Conclusions

As stated in the introduction (chapter 1) the two primary aims of this thesis were:

1. To produce a chromatographic column from high internal phase emulsion (HIPE) templated materials capable of size separating engineered nanoparticles in aqueous media.
2. To produce a series of highly monodisperse polymer nanoparticles, containing a low natural abundance element, over a 40 -160 nm size range, with a potential use as analytical standards.

The work carried out it this thesis has successfully met both of these aims. It has been shown that polyHIPE monoliths produced from poly(styrene-*co*-divinylbenzene), poly(ethyleneglycol dimethacrylate) have the ability to act as a stationary phase for the aqueous chromatography of engineered nanoparticles (chapter 6) as well as submicron particles (chapter 4). As mentioned in the introduction to chapter 4, polyHIPE columns have previously be used for the separation of proteins however, as far as the author is aware, there are no reported cases in the literature of polyHIPE columns being used for a size separation.

In this work a poly(styrene-*co*-divinybenzene) polyHIPE column was shown to outperform the current separation technique of hydrodynamic chromatography (HDC) when it came to the separation of small gold particles of 5 nm and 10 nm. The polyHIPE column was able to separate these particles when they cannot normally be resolved by HDC.

The separation mechanism does appear to be based on size, as analytes were all of a similar chemical identity and only differed in size. However, the mechanism is as yet not understood. It is possible that they may be multiple mechanisms at work can be seen by the separations in chapter 4. It appears to have also shown that the effective separation range of the polyHIPEs could be influenced by the synthetic procedure (*i.e.*, for a poly(styrene-*co*-divinylbenzene) polyHIPE column produced from a HIPE of similar composition and polymerised under identical conditions (*i.e.*, styrene/divinylbenzene ratio surfactant concentration, internal phase composition and content and polymerisation conditions) by increasing the shear during the mixing stage is was possible to produce a polyHIPE column that could separate particles with a difference of only 5 nm, which before had produced a small separation between 100 and 460 nm particles.

Micro-emulsion polymerisation was successfully used to encapsulate a lanthanide containing complex with polystyrene nano-particles covering a size range of 40 -160 nm (however, it is not clear if the larger particles were truly prepared by micro-emulsion polymerisation). Characterisation by a variety of techniques (*i.e.*, dynamic light scattering, transition election microscopy, differential centrifugal sedimentation and HDC) all confirmed that even after dialysis particles had good levels of monodispersity. Analysis by HDC coupled to an inductively coupled plasma mass spectrometer (ICP-MS) showed that the lanthanides were associated with the particles at levels easily detectable by ICP-MS.

The choice of surfactant was also used to control the surface charge of the particles, which gives the potential for the particles to be used over a wide range of ionic strengths.

While SiHIPE materials were not deemed appropriate for investigation as a stationary phase due the physical properties (*e.g.*, shrinkage during synthesis and brittleness) it has been shown that porosity of these materials can be controlled by both surfactant choice and the inclusion of either iron (III) chloride or copper (I) chloride. Use of surfactant was able to increase micro-porosity which manifested as a rise in in surface area from 132 to 383 $m^2$ $g^{-1}$. By a combination both surfactant and iron (III) chloride or copper (I) chloride it was possible to increase the surface area further to 745 $m^2$ $g^{-1}$ and 767 $m^2$ $g^{-1}$, respectively. The BET isotherms of SiHIPE materials showed some evidence of the evolution of mesoporosity.

## 7.2 Recommendations for Further Work

The recommendations for further work are split between two aims; the first set of recommendations relating to the polyHIPE columns and the second set relate to the lanthanide containing particles.

### 7.2.1 Further Work Recommendations for the PolyHIPE Columns

While it has been shown that the polyHIPE columns can separate submicron and nanoparticles, there is still significant work to be done establishing the mechanism of the separation and improving column performance. During this work, a proprietary mobile phase was used that had been designed for use with hydrodynamic chromatography. It is very probable that column performance could be improved by development of bespoke mobile phase which would be appropriate for the individual column. Due to time restraints minimal attention was paid to fully investigating the optimal chromatography set-up. It is

likely that optimisation of the set up (*e.g.*, flow rates, column lengths, injection volumes and on column pressures) would allow improvements in chromatography.

It is also likely that the stationary phase would have had a surface charge resulting from the presence of the sulphate anionic groups left over from initiation. By use of an oil soluble non-ionic initiator, the surface charge could be reduced (surface charge would not be eliminated as materials will develop a spontaneous surface charge when in contact with water).

To this end it would be useful to take the knowledge gained in this work and produce a set of columns by a range of synthetic conditions to control their properties (controlled pore sizes, surface charge *etc.*). This set of columns could then be investigated with a range of mobile phases under array of chromatographic conditions with particles covering a wide size range to establish the optimum chromatographic performance.

### 7.2.2 Further Work Recommendations for the Polystyrene Latex Particles

Further work with the latex particles would focus on their intended use as retention time markers and internal standards for analytical techniques such as in HDC-ICP-MS for analysis of real world samples *e.g.*, soils and sewage sludge [work which is already being undertaken by researchers at the food and environment agency (fera)].

As mentioned, the final location of the complex was not fully understood, the particles had varying amounts of complex encapsulated apparently dependent on size. Further investigation determining location and behaviour of the complex during synthesis could potentially lead to the ability to control the levels of doping in the particles. This could enable use of the particles with elemental techniques with a lower sensitivity than ICP-MS *e.g.*, EDX. It could also be possible to produce particles with multi-element doping at controlled levels. These multi-element doped particles would have greater

potential as internal makers and internal standards and they would be detectable even when the samples contained a contaminant which was same as one of the metals in the particle. This could also be combined with a more thorough investigation of the emulsion properties to accurately establish the method of polymerisation.

# Appendix 1: Calculations

Calculations used in multiple chapters are included here.

## A1.1 Statistical Correction Applied to Poly/SiHIPE cage Measurements

The explanation for this statistical correction was originally outlined by Barbetta and Cameron[1] and is included here for ease of reference.

Simple mean average cage diameters determined from SEM micrographs will be an underestimation of the real value. This is because sectioning means measurements of the cage diameter can be made at any random distance from the cage centre. To account for this a statistical correction can be applied to value to provide a more accurate measurement.

This can be achieved by evaluating the average of the ratio *R/r* where *R* is the equatorial radius of the cage and *r* is the radius of the cage a distance *h* from the centre (Figure A.1)

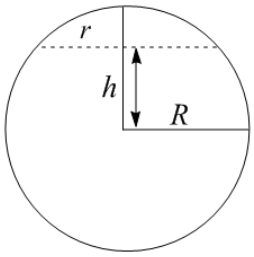


Figure A.1

As *h* is related to *r* by

$$h = R^2 - r^2 \qquad \text{(Eq. A1 1)}$$

As the probability of sectioning of the cage measurement is the same for all values of *h*, the average probability value for *h* is *R*/2. If this is replaced in Eq. A.1 this becomes *R/r* =

($2/3^{1/2}$) therefore multiplication of the measured average cage diameter by $2/3^{1/2}$ gives a better value for the average diameter of the cages.

**A1.2 Openness of the Poly/SiHIPEs**

The openness of can be estimated from the following equations propsed by Pulko and Krajnc: [2]

$$O = \frac{Surface\ Area\ of\ Cage\ Windows}{Surface\ Area\ of\ Cages} = \frac{S_w}{S_c} \quad \text{(Eq. A1.2)}$$

$$O = \frac{N\pi\left(d/2\right)^2}{\pi D^2} = \frac{N\left(d/2\right)^2}{D^2} = \frac{Nd^2}{4D^2} \quad \text{(Eq. A1.3)}$$

$$N = \frac{4n}{\sqrt{3}} \quad \text{(Eq. A1.4)}$$

where: $O$ = openness of the polyHIPEs

$N$= Estimated average number of windows

$n$= Average number of visible windows per cage

$d_a$= area average window diameter

$D_a$= area average cage diameter

As openness is the ratio open surface area to closed surface area the surface area average diameter of both the cages and windows was considered to be the most appropriate metric for the cage and window diameters.

**A1.3 Calculation of Resolution**

Resolution of the peaks was calculated from the following equation:

$$R_s = \frac{2(r_{tB} - r_{tA})}{1.7(W_{1/2A} - W_{1/2B})} \quad \text{(Eq. A1.5)}$$

Where: $R_s$ = resolution, which is a dimensionless parameter.

$A$ and $B$ are the two peaks.

$r_t$ = retention time in seconds.

$W_{1/2}$ = the width at half height of the peak in seconds.

### A1.4 Calculation of the Peak Asymmetry Factor

The peak asymmetry factor was calculated from the following equation:

$$A_s = {}^{b}/_{a} \qquad \text{(Eq. A1. 6)}$$

Where: $A_s$ = the dimensionless peak symmetry factor.

$a$ = the width of the front half of the peak at 10 % height in seconds.

$b$ = the width of the back half of the peak at 10 % height in seconds.

Values of $A_s$ > 2.0 are considered poor, as above this value the resolution becomes compromised, with values of < 1.5 considered ideal.[3]

### A1.5 References

1. A. Barbette, N. R. Cameron, *Macromolecules*, 2004, **37**, 3188-3204
2. I. Pulko, P. Krajnc, *Macromol. Rapid Commun.*, 2012, **33**, 1731-1746
3. J. W. Dolan, *LCGC Asia Pacific*, 2002, **5**, 14-20

# Appendix 2: PolyHIPE Characterisation Data from Chapter 3

Table A2.1: Complete cage, window and openness data for the polyHIPEs produced in chapter 3. Measured by SEM

| Monolith | Average Cage Diameter ($\mu$m) | | | | | | Average Window Diameter ($\mu$m) | | | | Average Number of Windows ($N$) | Openness % |
|---|---|---|---|---|---|---|---|---|---|---|---|---|
| | $D_n$ | %RSD | $D_A$ | %RSD | $D_V$ | %RSD | $d_n$ | %RSD | $d_a$ | %RSD | | |
| PS-3 | 13.0 | 39 | 13.1 | 96 | 14.2 | 113 | 2.0 | 55 | 2.3 | 106 | 48 | 37 |
| HEMA75 | 3.3 | 27 | 3.4 | 74 | 3.5 | 95 | 0.9 | 41 | 1.1 | 85 | 5 | 14 |
| HEMA85 | 3.1 | 24 | 3.2 | 68 | 3.3 | 89 | 1.3 | 32 | 1.5 | 100 | 10 | 57 |
| HEMA90 | [a] | [a] | [a] | [a] | [a] | [a] | 1.1 | 41 | 1.4 | 106 | [b] | – |
| BuA1 | 9.1 | 26 | 9.5 | 77 | 9.9 | 96 | 1.1 | 50 | 1.4 | 97 | 15 | 8 |
| MMA1 | [a] | [a] | [a] | [a] | [a] | [a] | 0.2 | 44 | 0.2 | 100 | [b] | – |
| HPMA1 | 2.1 | 33 | 2.3 | 92 | 2.4 | 120 | 0.5 | 40 | 0.6 | 89 | 18 | 34 |
| EGDMA1 | 2.2 | 35 | 2.3 | 84 | 2.4 | 103 | 0.3 | 45 | 0.4 | 95 | 31 | 35 |
| GMA3 | [a] | [a] | [a] | [a] | [a] | [a] | 0.4 | 58 | 0.5 | 113 | [b] | – |
| BMA3 | 4.2 | 42 | 4.4 | 96 | 5.0 | 116 | 0.5 | 62 | 0.6 | 127 | [b] | – |
| BuMA1 | 3.6 | 26 | 3.7 | 73 | 3.8 | 94 | 0.5 | 62 | 0.6 | 112 | 33 | 24 |

[a] cages were to poorly defined for an average value to be calculated.
[b] The windows of BuMA were not discrete and ran into each other. It was still possible to determine an average size and distribution, but, due to the interconnected nature of the windows, openness would be inaccurate.

Table A2.2: Porosity to Water Data for the PolyHIPEs Produced in Chapter 3. Measurements of polyHIPE dimensions are to ±0.005 cm

| Monolith | Dry Mass (g) | Dry Diameter (cm) | Dry Height (cm) | Dry Diameter Central Hole (cm) [a] | Wet Mass (g) | Dry Volume ($cm^3$) | Wet Diameter. ($cm^3$) | Wet Height (cm) | Wet Diameter of Central (cm) [a] | Wet Volume ($cm^3$) | Water Absorbed (ml) | Porosity to Water |
|---|---|---|---|---|---|---|---|---|---|---|---|---|
| PS-3 | 0.4178 | 1.30 | 1.35 | – | 1.62 | 1.79 | 1.30 | 1.35 | – | 1.79 | 1.20 | 67 |
| VE1 | 0.0226 | 0.70 | 0.50 | – | 0.09 | 0.10 | 0.70 | 0.50 | – | 0.19 | 0.07 | 34 |
| HEMA75 | 1.0683 | 1.55 | 2.40 | – | 7.09 | 4.53 | 1.85 | 2.80 | – | 7.53 | 6.02 | 80 |
| HEMA85 | 0.2846 | 1.25 | 1.70 | – | 3.27 | 2.09 | 1.45 | 1.95 | – | 3.22 | 2.99 | 93 |
| StHE | 0.1616 | 0.45 | 2.00 | – | 0.37 | 0.32 | 0.50 | 2.10 | – | 0.41 | 0.23 | 52 |
| BuA1 | 0.3524 | 1.20 | 3.25 | – | 0.54 | 3.68 | 1.20 | 3.25 | – | 3.68 | 0.19 | 5 |
| MMA1 | 0.4438 | 1.65 | 1.60 | 0.50 | 6.55 | 3.11 | 2.05 | 2.40 | 0.65 | 7.13 | 6.11 | 86 |
| HPMA1 | 2.1027 | 2.10 | 4.60 | 0.60 | 12.89 | 14.63 | 2.30 | 4.90 | 0.65 | 18.73 | 10.79 | 58 |
| EDGMA1 | 2.6272 | 2.30 | 6.00 | 0.65 | 16.53 | 22.94 | 2.30 | 6.00 | 0.65 | 22.94 | 13.90 | 61 |
| GMA3 | 0.3993 | 1.10 | 1.90 | – | 1.94 | 1.81 | 1.10 | 1.90 | – | 1.81 | 1.54 | 85 |
| BMA3 | 0.1795 | 1.35 | 1.05 | – | 0.31 | 1.50 | 1.35 | 1.05 | – | 1.50 | 0.13 | 9 |
| BuMA1 | 0.4723 | 1.40 | 2.60 | – | 1.46 | 4.00 | 1.40 | 2.60 | – | 4.00 | 0.9 | 25 |

[a] Some polyHIPEs were produced with a central hole due to the shape of the mould used.

Table A2.3: Completer Shrinkage Data for the polyHIPE produced in Chapter 3

| Monolith | Average Diameter after drying (mm) (± 0.5 mm) | Original Diameter (mm) | Change in Diameter (mm) (± 0.5 mm) | Shrinkage (%) |
|---|---|---|---|---|
| PS-3 | 14.0 | 15.0 | 1.0 | 7 |
| VE1 | 7.5 | 8.5 | 1.0 | 12 |
| HEMA75 | 17.0 | 19.0 | 2.0 | 11 |
| HEMA85 | 10.5 | 14.5 | 4.0 | 28 |
| HEMA90 | 8.0 | 14.5 | 6.5 | 45 |
| StHE | 4.5 | 8.5 | 4.0 | 47 |
| BuA1 | 12.0 | 12.0 | 0.0 | 0 |
| MMA1 | 16.5 | 23.0 | 6.5 | 28 |
| HPMA1 | 21.0 | 23.0 | 2.0 | 9 |
| EGDMA1 | 23.0 | 23.0 | 0.0 | 0 |
| GMA3 | 19.0 | 23.0 | 4.0 | 17 |
| BMA3 | 22.0 | 23.0 | 1.0 | 4 |
| BuMA1 | 23.0 | 23.0 | 0.0 | 0 |